

Lakehead University

An investigation of saccharide complexation by aqueous oxoacids. Can oxoacids mediate AI-2 quorum sensing in bacteria?

By

Bradley Vis

A Thesis Submitted to the Faculty of Graduate Studies

In Partial Fulfillment of the Requirements for the

Degree of Master of Science

Department of Chemistry

Thunder Bay, Ontario, Canada

© 2012

Lakehead

UNIVERSITY

OFFICE OF GRADUATE STUDIES

NAME OF STUDENT: Bradley Vis

DEGREE AWARDED: Master of Science

ACADEMIC UNIT: Department of Chemistry

TITLE OF THESIS: An investigation of saccharide complexation by aqueous oxoacids. Can oxoacids mediate AI-2 quorum sensing in bacteria?

This thesis has been prepared
under my supervision
and the candidate has complied
with the Master's regulations.



Signature of Supervisor

21 SEP 2012

Date

Abstract

The goal of this investigation was to determine whether it is plausible for bacterial AI-2 quorum sensing to be selectively regulated by environmentally available oxoacids. In particular, we investigated the ability of H_2CO_3 and H_4SiO_4 to bind molecules structurally analogous to the AI-2 signaling compound (a hydration product of (4S)-4,5-dihydroxy-2,3-pentanedione, S-DPD) which is known to be bound to H_3BO_3 in the AI-2 receptor site of *V. harveyi*.

We report the first ever evidence of mono- and di-ester linked complexes formed spontaneously between carbonic acid and aqueous polyhydroxy hydrocarbons, providing support for the hypothesis that a complex between H_2CO_3 and some S-DPD derivative regulates AI-2 quorum sensing in *S. gordonii*. The carbonate centre in these novel complexes retains three-fold coordination. Additionally, we compared the binding affinity of silicic acid to that of boric acid and carbonic acid to several different alcohols and saccharides, and determined that the formation constants generally increase as $\text{H}_2\text{CO}_3 < \text{H}_4\text{SiO}_4 < \text{H}_3\text{BO}_3$. It seems entirely plausible, therefore, that silicic acid could modulate AI-2 quorum sensing in Si-rich environments such as soil solutions.

Finally, we determined that stannic acid is also complexed by a range of polyhydroxy hydrocarbons in aqueous solution and characterized the structures of many of the resulting *mono*-, *bis*- and *tris*-ligand complexes.

Acknowledgements

First and foremost, I would like to thank Dr. Stephen Kinrade for his guidance and expertise during the course of this research. I would also like to thank my committee members, Drs. Robert Mawhinney and Greg Pyle, for their advice throughout this project. I also wish to thank Drs. Andres Mae and Zezhang T. Wen for graciously supplying me with strains of the *Pectobacterium carotovorum* and *Streptococcus mutans*. Additionally, I would like thank the LU Instrumentation Lab for ICP-AES analysis and generous allocation of NMR time, the Biorefining Research Institute for loan of their 96-well UV-Vis spectrophotometer; Mr. Michael Moore (Biology Department) for access to the biological safety hood, and the LU Chemistry Department for supplying many resources. I would like to thank Mr. Bill Dew as well, for teaching me the ways of a microbiologist. Finally, I would like to thank the past and present members of Dr. Kinrade's lab, for always keeping the time spent in the lab interesting.

Contents

Abstract.....	ii
Acknowledgements.....	iii
Contents.....	iv
List of Tables.....	vii
List of Figures.....	ix
Abbreviations.....	xv
Symbols.....	xv
Prologue.....	1
Chapter 1 – INTRODUCTION.....	2
1.1 AI-2 based quorum sensing.....	2
1. <u>Three genera of bacteria that employ AI-2 quorum sensing</u>	5
A. <i>Vibrio harveyi</i> – Marine bacterium.....	6
B. <i>Streptococci</i> – Oral bacteria.....	6
C. <i>Pectobacterium carotovorum</i> – Soil bacterium.....	6
1.2 Aqueous ester complexes of inorganic oxoacids.....	7
A. Borate complexes.....	7
B. Carbonate complexes.....	8
C. Silicate complexes.....	8
D. Stannate complexes.....	9
Chapter 2 - EXPERIMENTAL.....	10
2.1 Labware and chemical reagents.....	10
2.2 Analytical Instrumentation.....	11
2.3 Bacterial culturing and characterization.....	12
2.3.1 <i>Vibrio harveyi</i>	12
2.3.2 <i>Streptococci</i>	13
2.3.3 <i>Pectobacterium carotovorum</i>	14
2.3.4 Genetic expression.....	14

Chapter 3. RESULTS AND DISCUSSION	16
3.1 Effect of inorganic oxoacids on AI-2 quorum sensing	16
3.1.1 Determination of appropriate conditions for bacterial growth	16
3.1.2 <i>Vibrio harveyi</i> – bioluminescence as a marker of quorum sensing	19
3.1.3 <i>Streptococci</i> and <i>Pectobacterium</i> – biofilm formation as a marker for quorum sensing.....	19
3.1.4 Gene expression analysis.....	21
3.2 Aqueous ester complexes of inorganic oxo-acids.....	21
3.2.1 <u>Borate-saccharide complexes</u>	21
A. Formation constants of the borate-saccharide complexes.....	24
3.2.2 <u>Carbonate-saccharide complexes</u>	27
A. Simple alcohols	27
B. Acyclic polyols	31
C. Sugar acids.....	37
D. Furanoidic vicinal <i>cis</i> -diols.....	42
E. Formation constants of the carbonate-saccharide complexes.....	50
3.2.3 <u>Silicate-saccharide complexes</u>	52
A. Formation constants of the silicate-saccharide complexes.....	54
3.2.4 <u>Stannate-saccharide complexes</u>	57
A. Complexes of alcohols.....	57
B. Complexes of furanoidic vicinal <i>cis</i> -diols.....	65
C. Complexes of acyclic polyols.....	76
D. Formation constants of the stannate-saccharide complexes.....	88
3.2.5 <u>Comparison of saccharide complex formation constants for boric acid, carbonic acid and silicic acid</u>	90
A. <i>Mono</i> -ligand mono-ester complexes.....	90
B. <i>Mono</i> -ligand di-ester complexes.....	91
C. <i>Bis</i> -ligand oxoacid complexes.....	92

Conclusions	<u>93</u>
Future work.....	<u>93</u>
References	<u>94</u>
Appendix I. A study on the interactions between carbonic acid and amino containing buffers...	<u>98</u>
Appendix II. A study on increasing the stability of Al-2 in alkaline environments.....	<u>104</u>
Appendix III. A study on silicon in an artificial cell environment.....	<u>106</u>
Appendix IV. A study on silicon-saccharide equilibrium in the presence of co-solvent.....	<u>110</u>
Appendix V. A study on the interaction between silicic acid and furanoidic vicinal <i>trans</i> -diols...	<u>112</u>
Appendix VI. Solutions used for determination of formation constants for borate-ligand complexes.....	<u>114</u>
Appendix VII. Solutions used for determination of formation constants for carbonate-ligand complexes.....	<u>127</u>
Appendix VIII. Solutions used for determination of formation constants for silicate-ligand complexes	<u>134</u>
Appendix IX. Solutions used for determination of formation constants for stannate-ligand complexes.....	<u>147</u>

List of Tables

Table 1.1. Average Average abundances of boron, silicon, tin and inorganic carbon in different environments.

Table 3.1. Borate-saccharide species investigated in this study

Table 3.2. Formation constants for borate-furanoidic *cis*-diol complexes at 5 and 25 °C

Table 3.3. Formation constants for borate-polyol complexes at 5 and 25 °C

Table 3.4. Formation constants for the complexes between boric acid and the *S*-DPD derivatives at 25 °C, determined from the data reported by Semmelhack *et al.*^[37]

Table 3.5. Representative ¹³C NMR peak assignment of carbonate complexes with simple alcohols

Table 3.6. Representative ¹³C NMR peak assignment of carbonate complexes with aliphatic polyhydroxy molecules

Table 3.7. Representative ¹³C NMR peak assignment of carbonate complexes with sugar acids

Table 3.8. Representative ¹³C NMR peak assignment of carbonate complexes with furanoidic vicinal *cis*-diols

Table 3.9. Formation constants for carbonate-furanoidic *cis*-diol complexes at 5 and 25 °C

Table 3.10. Formation constants for carbonate-polyol complexes at 5 °C

Table 3.11. Representative silicate complexes with polyhydroxy molecules and the corresponding ²⁹Si NMR chemical shift ranges.

Table 3.12. Formation constants for silicate-furanoidic *cis*-diol complexes at 5 °C

Table 3.13. Formation constants for silicate-polyol complexes at 5 °C.

Table 3.14. Stannate complexes with alcohols

Table 3.15. Stannate complexes with furanoidic vicinal *cis*-diols (*cis*-1,2-cyclopentanediol, 1,4-anhydroerythritol, cytidine)

Table 3.16. Stannate complexes with aliphatic polyhydroxy molecules (threitol, erythritol, xylitol, adonitol, mannitol)

Table 3.17. Formation constants for stannate-furanoidic *cis*-diol complexes at 5 °C

Table 3.18. Formation constants for stannate-polyol complexes at 5 °C.

Table 3.19. Comparison of the formation constants from the literature and this study.

Table 3.20. Representative formation constants for mono-ester complexes with carbonic acid and silicic acid at 5 °C

Table 3.21. Representative formation constants for di-ester *mono*-ligand complexes with boric acid and carbonic acid at 5 °C

Table 3.22 Representative formation constants for di-ester *bis*-ligand complexes with boric acid and silicic acid at 5 °C

Table 4.1. Representative ¹³C NMR peak assignment of carbonate complexes with amino containing buffers

Table 4.2. The concentration of silicate oligomers present in silicate solutions with and without agarose gels.

Table 4.3. The concentration of silicate species present in silicate solutions with and without agarose gels.

Table 4.4. The concentration of silicate species present in silicate solutions with and without n-propanol.

List of Figures

Figure 1.1. The Al-2 family of interconverting molecules (herein referred to as S-DPD derivatives) and the S-THMF-borate complex; after Miller *et al.*^[11]

Figure 1.2. The a) growth and b) luminescence of wild-type *Vibrio harveyi* in oxoacid medium and in media treated with 1 mM H₃BO₃ or H₄SiO₄; after Noroozi *et al.*^[16]

Figure 1.3. Biofilm production by *Pectobacterium carotovorum* in untreated medium and media treated with 1 mM H₂CO₃, H₃BO₃ or H₄SiO₄; after Dew *et al.*^[19] The y-axis represents extent of biofilm formation by measuring the optical density of crystal violet that absorbed into the biofilm, relative to that for bacteria-free medium.

Figure 1.4. Proposed structure of the carbonate ester of R-THMF; after McKenzie *et al.*^[3]

Figure 1.5. Structure of pentaoxosilicon *bis*-(diolato)-hydroxo and hexaioxosilicon *tris*-(diolato) complexes formed in aqueous alkaline solution between silicic acid and 1,4-anhydroerythritol.^[14]

Figure 1.6. Proposed structure of the di-ester *mono*-ligand stannate-polyhydroxy molecule complex; after Mbabazi *et al.*^[71]

Figure 3.1. Growth of *Vibrio harveyi* BB120 (wild-type) in PC, PMP, PFA, PP and borosilicate flasks a) when they were new or b) after they had undergone six cleaning and autoclaving cycles.

Figure 3.2. Extraction efficiency for B and Si as a function of pH from solutions containing a) 2.5 mmol kg⁻¹ boric acid, b) 1 mmol kg⁻¹ silicic acid or c) 2.5 mmol kg⁻¹ boric acid and 1 mmol kg⁻¹ silicic acid upon addition of Amberlite IRA-743 (0.5 g in 25 mL) and agitating for 24 h

Figure 3.3. Biofilm production by *S. mutans* in untreated medium and media treated with H₂CO₃, H₃BO₃ or H₄SiO₄. The y-axis represents extent of biofilm formation by measuring the optical density of crystal violet that absorbed into the biofilm, relative to that for bacteria-free medium.

Figure 3.4. Biofilm production by *S. gordonii* in untreated medium and media treated with H₂CO₃, H₃BO₃ or H₄SiO₄. The y-axis represents extent of biofilm formation by measuring the optical density of crystal violet that absorbed into the biofilm, relative to that for bacteria-free medium.

Figure 3.5. Boron-11 NMR spectrum (160.33 MHz) of an aqueous solution containing 0.092 mol kg⁻¹ H₃BO₃, 0.490 mol kg⁻¹ phosphoric acid and 0.159 mol kg⁻¹ 1,4-anhydroerythritol at pH = 7.39 and 25 °C. The regions corresponding to the principal borate species are shown.

Figure 3.6. Carbon-13 DOSY NMR spectrum (125.67 MHz) of a solution containing approximately 1 mol kg⁻¹ H₃BO₃ and 3 mol kg⁻¹ D-arabitol at pH 10.5 and 25 °C

Figure 3.7. Carbon-13 NMR spectrum (125.67 MHz) of an aqueous solution containing 0.13 mol kg⁻¹ Na₂¹³CO₃ and 3.9 mol kg⁻¹ methanol at pH 10.9 and 25 °C.

Figure 3.8. Carbon-13 NMR spectra of the solution represented in Figure 3.7, acquired at a) 25 °C and b) 5 °C.

Figure 3.9. Dynamic equilibrium between the hydrogen bonded states of **CM_{Monof}**.

Figure 3.10. Carbon-13 NMR spectrum of an aqueous solution containing 0.12 mol kg⁻¹ Na₂¹³CO₃ and 13 mol kg⁻¹ ethane-1,2-diol at pH 11.1 and 25 °C

Figure 3.11. Carbon-13 NMR spectrum of an aqueous solution containing 0.13 mol kg⁻¹ Na₂¹³CO₃ and 1.5 mol kg⁻¹ L-threitol at pH 11.2 and 5 °C

Figure 3.12. Carbon-13 NMR spectrum of an aqueous solution containing 0.031 mol kg⁻¹ Na₂¹³CO₃ and 3.8 mol kg⁻¹ butane-1,2,4-triol at 25 °C

Figure 3.13. Carbon-13 NMR spectrum of an aqueous solution containing 0.13 mol kg⁻¹ Na₂¹³CO₃ and 1.5 mol kg⁻¹ *meso*-erythritol at pH 11.2 and 5 °C

Figure 3.14. Carbon-13 NMR spectrum of an aqueous solution containing 0.058 mol kg⁻¹ Na₂¹³CO₃ and 6.9 mol kg⁻¹ xylitol at pH 10.3 and 25 °C.

Figure 3.15. Carbon-13 NMR spectrum of an aqueous solution containing 0.044 mol kg⁻¹ Na₂¹³CO₃ and 1.8 mol kg⁻¹ adonitol at pH 8.7 and 5 °C.

Figure 3.16. Concentration of the **CX_{Monof}** complexes vs pH at 25 °C

Figure 3.17. Carbon-13 NMR spectrum of an aqueous solution containing 0.056 mol kg⁻¹ Na₂¹³CO₃ and 2.0 mol kg⁻¹ gluconic acid at pH 9.6 and 25 °C.

Figure 3.18. Carbon-13 NMR spectrum of the gluconic acid containing solution represented in Figure 3.17 a) with and b) without gated ¹H-decoupling.

Figure 3.19. Carbon-13 NMR spectrum of an aqueous solution containing 0.25 mol kg⁻¹ Na₂¹³CO₃ and 1.5 mol kg⁻¹ glucoheptonic acid at pH 10.4 and 25 °C.

Figure 3.20. Carbon-13 NMR spectrum of an aqueous solution containing 0.057 mol kg⁻¹ Na₂¹³CO₃ and 1.4 mol kg⁻¹ glucoheptonic acid at pH 10.1 and 25 °C a) with and b) without gated ¹H-decoupling

Figure 3.21. Carbon-13 NMR spectrum of an aqueous solution containing 0.050 mol kg⁻¹ Na₂¹³CO₃ and 2.3 mol kg⁻¹ L-tartaric acid at pH 10.3 and 25 °C.

Figure 3.22. Carbon-13 NMR spectrum of an aqueous solution containing 0.042 mol kg⁻¹ Na₂¹³CO₃ and 1.5 mol kg⁻¹ *cis*-1,2-cyclopentanediol at pH 10.5 and 25 °C

Figure 3.23. Carbon-13 NMR spectrum (125.67 MHz) of an aqueous solution containing 0.27 mol kg⁻¹ Na₂¹³CO₃ and 4.0 mol kg⁻¹ 1,4-anhydroerythritol at 5 °C

Figure 3.24. A revised version of the carbonate-THMF complex proposed by McKenzie *et al.*^[13] to account for enhanced AI-2 quorum sensing in *Vibrio harveyi*.

Figure 3.25. Carbon-13 NMR spectrum of an aqueous solution containing 0.044 mol kg⁻¹ Na₂¹³CO₃ and 0.72 mol kg⁻¹ cytidine at pH 9.1 and 5 °C.

Figure 3.26. Carbon-13 NMR spectrum of an aqueous solution containing 0.030 mol kg⁻¹ Na₂¹³CO₃ and 0.88 mol kg⁻¹ adenosine triphosphate at pH 7.2 and 25 °C

Figure 3.27. Carbon-13 NMR spectrum of an aqueous solution containing 0.24 mol kg⁻¹ Na₂¹³CO₃, 0.96 mol kg⁻¹ tris buffer and 4.0 mol kg⁻¹ D-ribose at pH 7 and 5 °C.

Figure 3.28. Carbon-13 NMR spectrum of an aqueous solution containing 0.044 mol kg⁻¹ Na₂¹³CO₃ and 2.0 mol kg⁻¹ D-fructose at pH 9.6 and 5 °C

Figure 3.29. Carbon-13 NMR spectrum of an aqueous solution containing 0.051 mol kg⁻¹ Na₂¹³CO₃ and 3.9 x 10⁻³ mol kg⁻¹ D-ribose at pH 7.0 and 5 °C.

Figure 3.30. Tin-119 NMR spectra (186.35 MHz) of an aqueous solution containing 0.22 mol kg⁻¹ Sn, 3.4 mol kg⁻¹ methanol, 3.1 mol kg⁻¹ TMAOH and 0.83 mol kg⁻¹ HCl at 5 °C. The expanded region is shown a) with and b) without gated ¹H-decoupling.

Figure 3.31. ¹¹⁹Sn {¹H} NMR spectrum of an aqueous solution containing 0.21 mol kg⁻¹ Sn, 6.6 mol kg⁻¹ ethanol, 2.9 mol kg⁻¹ TMAOH and 0.77 mol kg⁻¹ HCl at 5 °C.

Figure 3.32. ¹¹⁹Sn {¹H} NMR spectra at 21 °C of the aqueous solutions containing a) 0.18 mol kg⁻¹ Sn, 0.31 mol kg⁻¹ ethane-1,2-diol, 2.3 mol kg⁻¹ TMAOH and 1.8 mol kg⁻¹ HCl at 5 °C, and b) 0.19 mol kg⁻¹ Sn, 0.95 mol kg⁻¹ ethane-1,2-diol, 2.4 mol kg⁻¹ TMAOH and 2.2 mol kg⁻¹ HCl

Figure 3.33. ¹¹⁹Sn NMR spectrum of the ethane-1,2-diol containing solution represented in Figure 3.32b, a) with and b) without gated ¹H-decoupling

Figure 3.34. ¹¹⁹Sn NMR spectrum of the ethane-1,2-diol containing solution represented in Figure 3.32b, a) with and b) without gated ¹H-decoupling

Figure 3.35. ¹¹⁹Sn {¹H} NMR spectrum of an aqueous solution containing 0.22 mol kg⁻¹ Sn, 0.65 mol kg⁻¹ propane-1,2-diol, 3.1 mol kg⁻¹ TMAOH and 0.82 mol kg⁻¹ HCl at 5 °C. The expanded region is shown with a) with and b) without gated ¹H-decoupling.

Figure 3.36. ¹¹⁹Sn NMR spectrum of the ethane-1,2-diol solution represented in Figure 3.32b a) with and b) without gated ¹H-decoupling.

Figure 3.37. ¹¹⁹Sn {¹H} NMR spectra at 21 °C of aqueous solutions containing a) 0.18 mol kg⁻¹ Sn, 0.13 mol kg⁻¹ *cis*-1,2-cyclopentanediol, 2.2 mol kg⁻¹ TMAOH and 0.67 mol kg⁻¹ HCl, and b) 0.23 mol kg⁻¹ Sn, 0.68 mol kg⁻¹ *cis*-1,2-cyclopentanediol, 2.1 mol kg⁻¹ TMAOH and 0.89 mol kg⁻¹ HCl.

Figure 3.38. ¹¹⁹Sn NMR spectrum of the cyclopentanediol containing solution represented in Figure 3.37c, a) with and b) without gated ¹H-decoupling.

Figure 3.39. ^{119}Sn NMR spectrum of the cyclopentanediol containing solution represented in Figure 3.37c, a) with and b) without gated ^1H -decoupling

Figure 3.40. The four possible diastereomers of the *bis*-ligand complex between stannic acid and *cis*-1,2-cyclopentanediol.

Figure 3.41. ^{119}Sn NMR spectrum of the cyclopentanediol containing solution represented in Figure 3.37c, a) with and b) without gated ^1H -decoupling.

Figure 3.42. The two possible diastereomers of the *tris*-ligand complex between stannic acid and *cis*-1,2-cyclopentanediol.

Figure 3.43. ^{119}Sn NMR spectrum of the cyclopentanediol containing solution represented in Figure 3.37c, a) with and b) without gated ^1H -decoupling

Figure 3.44. ^{119}Sn $\{^1\text{H}\}$ NMR spectrum at 21 °C of an aqueous solution containing 0.41 mol kg $^{-1}$ Sn, 0.40 mol kg $^{-1}$ 1,4-anhydroerythritol, 3.8 mol kg $^{-1}$ TMAOH and 1.6 mol kg $^{-1}$ HCl.

Figure 3.45. ^{119}Sn NMR spectrum of the 1,4-anhydroerythritol containing solution represented in Figure 3.44 a) with and b) without gated ^1H -decoupling

Figure 3.46. ^{119}Sn NMR spectrum of the 1,4-anhydroerythritol containing solution represented in Figure 3.44 a) with and b) without gated ^1H -decoupling.

Figure 3.47. ^{119}Sn NMR spectrum of the 1,4-anhydroerythritol containing solution represented in Figure 3.44 a) with and b) without gated ^1H -decoupling

Figure 3.48. ^{119}Sn $\{^1\text{H}\}$ NMR spectrum at 5 °C of an aqueous solution containing 0.22 mol kg $^{-1}$ Sn, 0.43 mol kg $^{-1}$ cytidine, 3.1 mol kg $^{-1}$ mol kg $^{-1}$ TMAOH and 0.83 mol kg $^{-1}$ HCl

Figure 3.49. ^{119}Sn NMR spectrum of the cytidine containing solution represented in Figure 3.48 a) with and b) without gated ^1H -decoupling.

Figure 3.50. ^{119}Sn NMR spectrum of the cytidine containing solution represented in Figure 3.48 a) with and b) without gated ^1H -decoupling

Figure 3.51. ^{119}Sn NMR spectrum of the cytidine containing solution represented in Figure 3.48 a) with and b) without gated ^1H -decoupling.

Figure 3.52. ^{119}Sn $\{^1\text{H}\}$ NMR spectra at 5 °C of the aqueous solutions containing a) 0.20 mol kg $^{-1}$ Sn, 0.21 mol kg $^{-1}$ L-threitol, 2.5 mol kg $^{-1}$ TMAOH and 0.76 mol kg $^{-1}$ HCl, and b) 0.21 mol kg $^{-1}$ Sn, 0.79 mol kg $^{-1}$ L-threitol, 2.7 mol kg $^{-1}$ mol kg $^{-1}$ TMAOH and 0.80 mol kg $^{-1}$ HCl.

Figure 3.53. ^{119}Sn NMR spectrum of the threitol containing solution represented in Figure 3.52a, a) with and b) without gated ^1H -decoupling.

Figure 3.54. ^{119}Sn NMR spectrum of the threitol containing solution represented in Figure 3.52a, a) with and b) without gated ^1H -decoupling.

Figure 3.55. ^{119}Sn NMR spectrum of the threitol containing solution represented in Figure 3.52a, a) with and b) without gated ^1H -decoupling.

Figure 3.56. ^{119}Sn NMR spectrum of the threitol containing solution represented in Figure 3.52a, a) with and b) without gated ^1H -decoupling.

Figure 3.57. ^{119}Sn NMR spectrum of the threitol containing solution represented in Figure 3.52a, a) with and b) without gated ^1H -decoupling.

Figure 3.58. ^{119}Sn $\{^1\text{H}\}$ NMR spectra at 5 °C of aqueous solutions containing 0.23 mol kg $^{-1}$ Sn, 2.9 mol kg $^{-1}$ TMAOH and 0.9 mol kg $^{-1}$ HCl and a) 0.11 mol kg $^{-1}$ erythritol, b) 0.24 mol kg $^{-1}$ erythritol or c) 0.79 mol kg $^{-1}$ erythritol.

Figure 3.59. ^{119}Sn NMR spectrum of the erythritol containing solution represented in Figure 3.58b, a) with and b) without gated ^1H -decoupling

Figure 3.60. ^{119}Sn NMR spectrum of the erythritol containing solution represented in Figure 3.58b, a) with and b) without gated ^1H -decoupling

Figure 3.61. ^{119}Sn $\{^1\text{H}\}$ NMR spectra of the erythritol containing solutions represented in Figure 3.58 b and c.

Figure 3.62. ^{119}Sn NMR spectrum of the erythritol containing solution represented in Figure 3.58a, a) with and b) without gated ^1H -decoupling

Figure 3.63. ^{119}Sn NMR spectrum of the erythritol containing solution represented in Figure 3.58a, a) with and b) without gated ^1H -decoupling.

Figure 3.64. ^{119}Sn NMR spectra at 5 °C of aqueous solutions containing 0.2 mol kg $^{-1}$ Sn, 3 mol kg $^{-1}$ TMAOH, 0.8 mol kg $^{-1}$ HCL and 0.6 mol kg $^{-1}$ xylitol (a), adonitol (b) or mannitol (c)

Figure 4.1. Carbon-13 NMR spectrum of an aqueous solution containing 0.069 mol kg $^{-1}$ Na $_2$ $^{13}\text{CO}_3$ and 0.744 mol kg $^{-1}$ tris buffer at pH 7.0 and 5 °C

Figure 4.2. Carbon-13 NMR spectra of aqueous solutions containing 0.05 mol kg $^{-1}$ Na $_2$ $^{13}\text{CO}_3$ and 0.744 mol kg $^{-1}$ tris buffer at different pH values and 25 °C

Figure 4.3. Concentration of the proposed carbamide complexes vs pH at 25 °C

Figure 4.4. Concentration of the CTR $_{\text{Monot}}$ complex vs pH at 25 °C

Figure 4.5. Carbon-13 NMR spectrum (125.67 MHz) of an aqueous solution containing 0.073 mol kg $^{-1}$ Na $_2$ $^{13}\text{CO}_3$ and 1.007 mol kg $^{-1}$ ammonium chloride at pH 9.98 acquired at a) 5 °C and b) 21 °C.

Figure 4.6. Expanded regions of ^1H NMR spectra of a sample containing 1 mol kg $^{-1}$ Si, 4 mmol kg $^{-1}$ B and 4 mmol kg $^{-1}$ D-ribose at a) t = 0, b) t = 5 days and c) t = 12 days

Figure 4.7. Silicon-29 NMR spectra (at 99.28 MHz) of a samples containing 1.54 mol kg^{-1} Si, 1.54 mol kg^{-1} OH, 1.62 mol kg^{-1} arabitol and 7.57% wt n-propano

Figure 4.8. Silicon-29 NMR spectrum (at 99.28 MHz) of a sample containing 1.04 mol kg^{-1} ^{29}Si , 1.04 mol kg^{-1} OH⁻ and 3.06 mol kg^{-1} *trans*-1,2-cyclopentenediol.

Abbreviations

AI-2	autoinducer-2
NMR	nuclear magnetic resonance
ICP-AES	inductively coupled plasma atomic emission spectrometry
DDW	deionized distilled water
FEP	fluorinated ethylene-propylene
PFA	perfluoroalkoxy
LDPE	low density polyethylene
PC	polycarbonate
PP	polypropylene
PMP	polymethylpentene

Symbols

δ	NMR chemical shift
J	nuclear spin-spin coupling constant
K	equilibrium constant
β	formation constant

Prologue

Bacteria control their cellular activities in response to local population density. They do this by releasing chemical compounds into the environment that are subsequently perceived by other bacteria, a process that has come to be described as “quorum sensing”. One of the most important signal compounds is autoinducer-2 (AI-2), which collectively represents the hydration products of (4*S*)-4,5-dihydroxy-2,3-pentanedione (*S*-DPD), together with ester complexes they form with boric or carbonic acids. Although nearly half of all sequenced bacteria contain the gene responsible for *S*-DPD production, different species of bacteria are thought to recognize different structural derivatives of this compound. Recognizing that silicic acid, H_4SiO_4 , is also capable of binding several furanoidic vicinal *cis*-diols such as the *S*-DPD hydration products, we began this project by posing the following questions:

- Have the bacterial AI-2 receptors evolved in response to a species’ particular chemical environment and, specifically, to the inorganic oxoacids dominating its habitat?
- How do the three oxoacids mentioned above compare in their AI-2 binding characteristics?
- Does silicic acid either mediate or interfere with well-characterized AI-2 quorum sensing pathways?
- Could novel strategies for interference of AI-2 quorum sensing be developed from such knowledge?

CHAPTER 1. INTRODUCTION

1.1 AI-2 based quorum sensing

Quorum sensing is the process by which bacteria regulate communal functions in response to their cellular density.^[1] Chemical messengers, also termed autoinducers, are responsible for this intercellular communication and are produced throughout the lifetime of the bacteria.^[2, 3] Only when a threshold cellular density or “quorum” of the bacteria is attained do the chemical messengers reach a concentration that the receptor protein recognizes, resulting in the initiation of a communal function.^[1] Since the initial discovery of quorum sensing in *Vibrio fischeri* in 1970, a range of autoinducers have been identified, including certain acylated homoserine lactones, oligopeptides, and small sugar molecules.^[1, 4]

In the marine bacterium *Vibrio harveyi*, multiple chemical messengers have been identified, all of which regulate the genes encoding for bioluminescence.^[1, 5, 6] The second chemical messenger uncovered, thus named autoinducer-2 (AI-2), was identified as a borate ester of S-(2S,4S)-2-methyl-2,3,3,4-tetrahydroxytetrahydrofuran (S-THMF), one of five hydrated forms of (4S)-4,5-dihydroxy-2,3-pentanedione (S-DPD) that is produced through the luxS enzyme (Figure 1.1).^[5-8] When *V. harveyi* is deprived of boric acid, which is abundant in the marine environment, AI-2 dependent quorum sensing activity is significantly decreased.^[7]

AI-2 quorum sensing has now been identified in many species of bacteria; the gene corresponding to the AI-2 production enzyme is conserved in 35 of 89 sequenced bacterial genomes.^[9] Moreover, AI-2 has been shown to mediate both *inter*- and *intra*-species communication.^[10] Different species of bacteria, however, appear to recognize different S-DPD derivatives. For example, *Salmonella typhimurium* only recognizes the R-THMF form (Figure 1.1) and the presence of boric acid *decreases* its AI-2 activity.^[11]

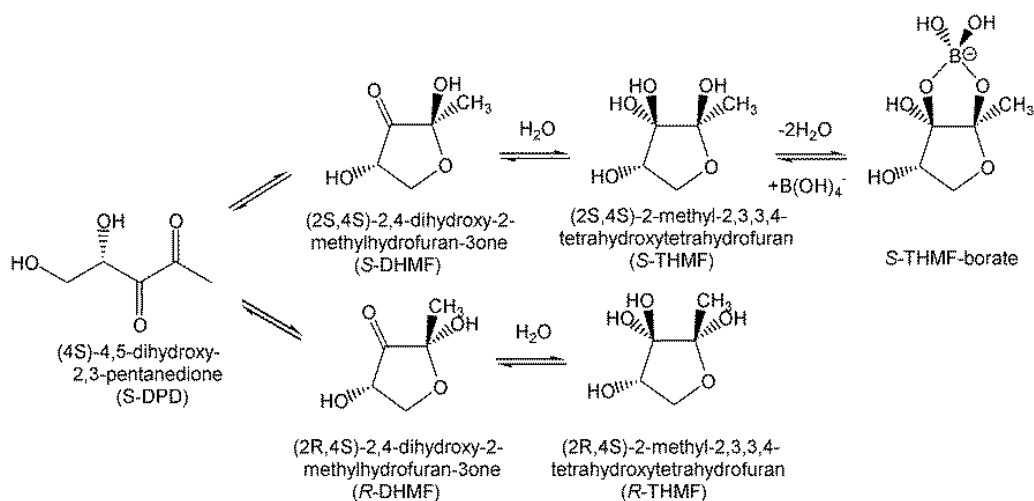


Figure 1.1. The AI-2 family of interconverting molecules (herein referred to as S-DPD derivatives) and the S-THMF-borate complex, collectively referred to as the AI-2 pool; after Miller *et al.*^[11] and Galloway *et al.*^[12]

Carbonic acid has been reported to increase biofilm production in the oral bacterium *Streptococcus gordonii*.^[13] Two mechanisms have been proposed for the role of this particular oxoacid, which dominates the oral cavity environment. It was initially thought to increase the amount of S-DPD produced.^[13] However, McKenzie *et al.* later suggested that carbonic acid binds S-THMF in a fashion analogous to boric acid, thereby enhancing its binding affinity to the receptor protein.^[14] As evidence they demonstrated that luminescence of *V. harveyi* was enhanced by H₂CO₃ addition, although the effect was less than half that of H₃BO₃.

As silicic acid is well known to form di-ester complexes with furanoidic vicinal *cis*-diol molecules analogous to *R*- and *S*-THMF (Figure 1.1)^[15, 16], we set out to determine if silicic acid could also modulate AI-2 quorum sensing. Preliminary studies in this laboratory have demonstrated that *V. harveyi* bacteria grown in Si-treated medium exhibit greater bioluminescence than those grown in an oxoacid-free control medium (Figure 1.2b), although the enhancement was roughly half that caused by boric acid.^[17] These results would suggest that silicic acid might indeed regulate AI-2 quorum sensing, especially in Si-rich soil solutions. In the plant pathogen *Pectobacterium carotovorum*, plant virulence and biofilm formation are known to be regulated by AI-2 quorum sensing.^[18, 19] Preliminary work conducted with this species indicated that biofilm production is increased by the addition of H₂CO₃, H₃BO₃ and especially H₄SiO₄ (Figure 1.3).^[20]

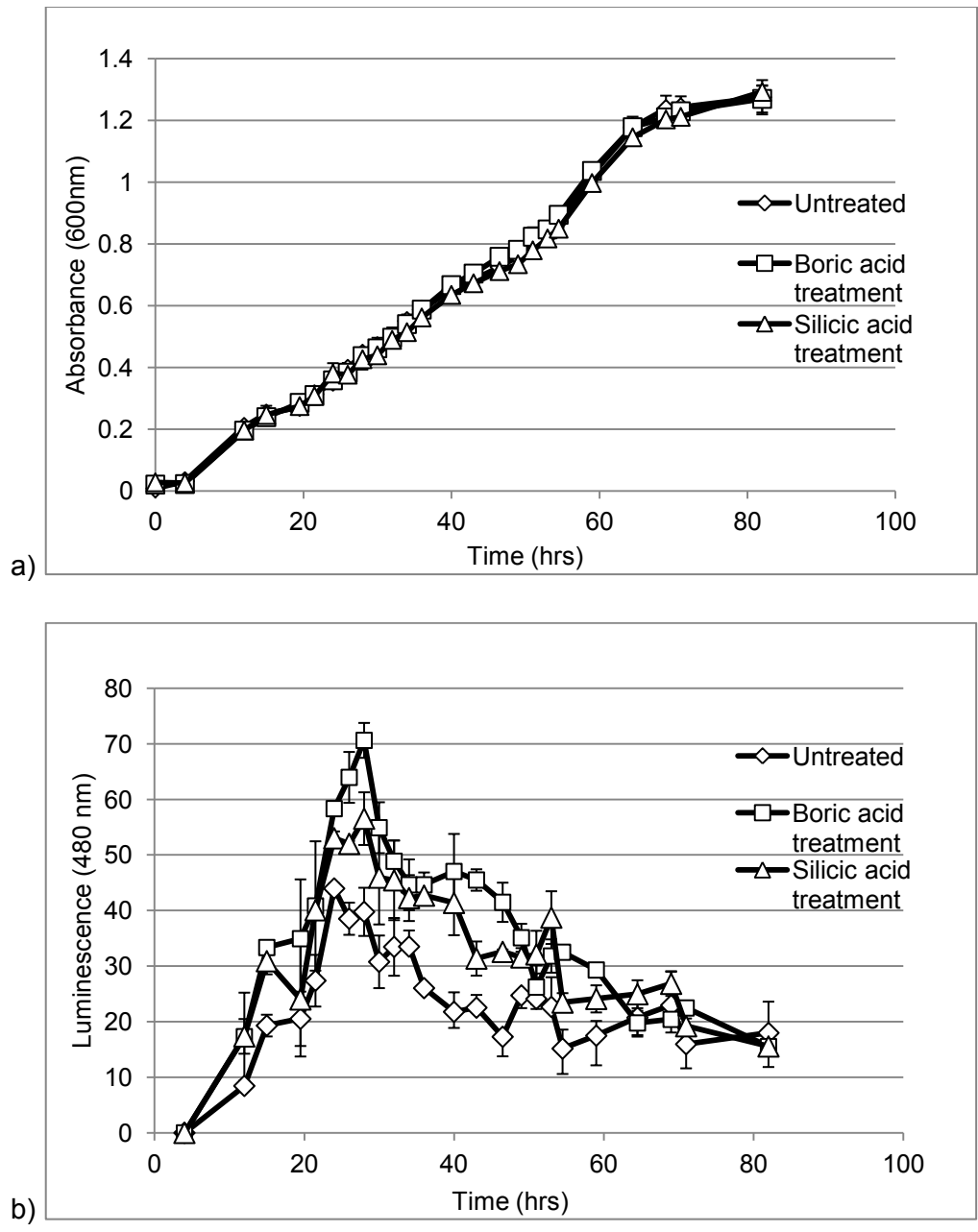


Figure 1.2. The a) growth and b) luminescence of wild-type *Vibrio harveyi* in untreated medium and in media treated with 1 mM H_3BO_3 or H_4SiO_4 ; after Noroozi.^[17]

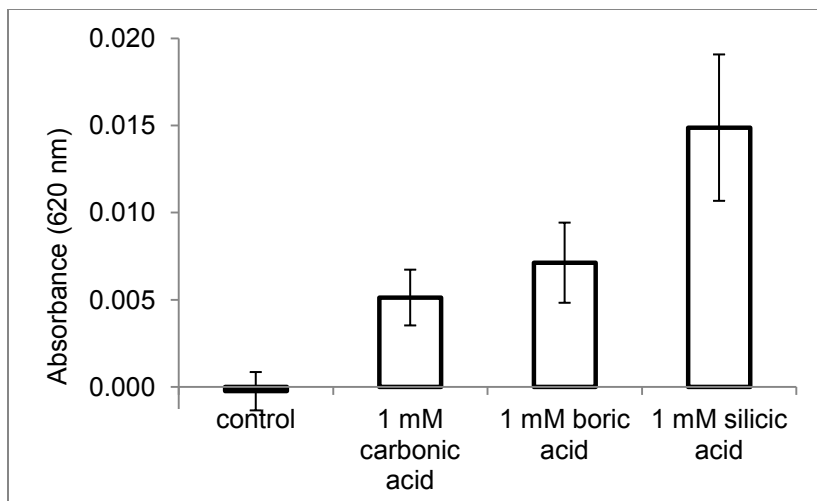


Figure 1.3. Biofilm production by *Pectobacterium carotovorum* in untreated medium and media treated with 1 mM H_2CO_3 , H_3BO_3 or H_4SiO_4 ; after Dew *et al.*^[20] The y-axis represents extent of biofilm formation by measuring the optical density of crystal violet that absorbed into the biofilm, relative to that for bacteria-free medium (method is described in Section 2.3).

The overriding goal of this investigation was to determine whether it is plausible for AI-2 quorum sensing in different species of bacteria to be selectively regulated (that is, either promoted or inhibited) by the presence of particular oxoacids in the local environment.

1.2 The effect of oxoacids on AI-2 quorum sensing activity

The first approach that we considered towards addressing this question was to investigate oxoacid effects on quorum sensing activity in bacteria which inhabit environments that are characteristically rich in H_3BO_3 , H_2CO_3 or H_4SiO_4 . Species were selected on the basis of two criteria:

- a) AI-2 quorum sensing has been previously shown to regulate one or more cellular functions.
- b) One or more strains are available in which S-DPD production is either suppressed or eliminated.

A. *Vibrio harveyi* – Marine bacterium (*i.e.*, H₃BO₃-rich environment)

The Bassler group at Princeton University is largely responsible for characterizing the complete AI-2 quorum sensing pathway in *V. harveyi* (Figure 1.4). When quorum is reached, the borate ester of S-THMF is recognized by the receptor, LuxP, and a signal is passed through multiple proteins that eventually regulates the luciferase structural operon, luxCDABE.^[21] *V. harveyi* also contains an AI-1 quorum sensing system, which converges with the AI-2 pathway at the LuxU protein and regulates the same target genes.^[21] Strains have been developed which are incapable of producing AI-1 or AI-2 owing to insertions of transposons into the genome.^[6] In the strain that is unable to produce AI-1, bioluminescence occurs in the presence of boric acid, carbonic acid or molecules that are structurally analogous to S-THMF, thus demonstrating that the receptor does not solely recognize the borate ester of S-THMF.^[14, 22-25]

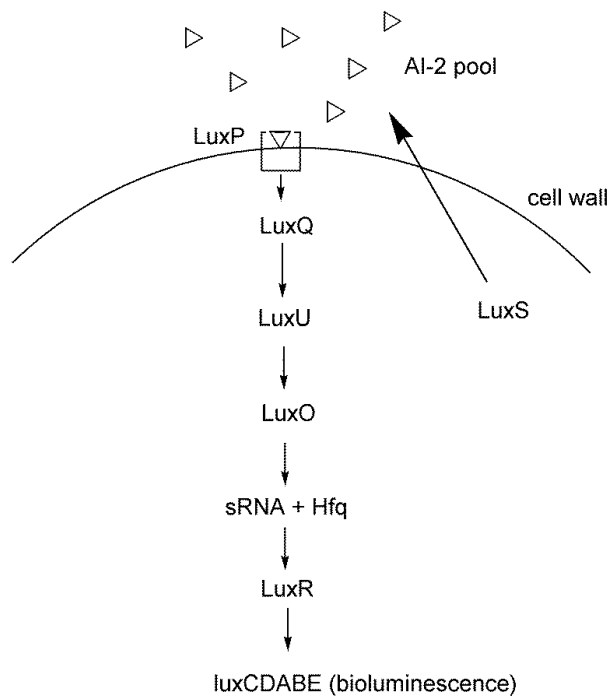


Figure 1.4. The AI-2 quorum sensing pathway of *V. harveyi*; after Freeman *et al.*^[26] S-DPD is produced by LuxS, undergoes cyclization and hydration (Figure 1.1), and then is transported out of the cell.

B. *Streptococci* – Oral bacteria (*i.e.*, H₂CO₃-rich environment)

In the oral bacterium *S. gordonii*, AI-2 quorum sensing is known to regulate genes that encode for glucosyltransferase, tagatose 1,6-diphosphate aldolase and exo-β-D-fructosidase, all of which contribute to biofilm production.^[10, 13] It has been reported that the extent of biofilm formation is increased in the presence of carbonic acid, which is present in high concentrations due to its equilibrium with carbon dioxide.^[27] The S-DPD derivative recognized by the protein receptor is as yet unknown. The biofilm production in *Streptococcus mutans* is also partially regulated by AI-2 quorum sensing.^[28-30] In a strain incapable of producing S-DPD, biofilm production is decreased but not eliminated entirely.^[28] As with *S. gordonii*, the S-DPD derivative recognized by the protein receptor is unknown.

C. *Pectobacterium carotovorum* – Soil bacterium (*i.e.*, H₄SiO₄-rich environment)

AI-2 quorum sensing was found to regulate virulence in *P. carotovorum* (formerly known as *Erwinia carotovora*).^[18, 19] The generation of pectate lyase, polygalacturonase, and therefore biofilm production decreased in a strain in which the production of S-DPD is suppressed.^[18] No evidence has been reported regarding the particular S-DPD derivative that is involved in the AI-2 signalling process.

1.3 Aqueous ester complexes of inorganic oxoacids

The second approach we considered towards addressing whether AI-2 quorum sensing is modulated by inorganic oxoacids was to investigate the binding affinity of H₃BO₃, H₂CO₃ and H₄SiO₄ to molecules which are structurally analogous to S-DPD derivatives. We also investigated the binding affinity of stannic acid, another group 14 oxoacid.

A. Borate complexes

Boron can be found throughout the Earth's hydrosphere, but is particularly abundant in the oceans as shown in Table 1.1. It is known to be an essential nutrient for a number of organisms^[31-33] and, most notably, is responsible for cross-linking pectic polysaccharides in plant cell walls.^[31] Hydroxyl containing molecules have been shown to form both mono- and di-ester complexes with boric acid.^[34-38] The boron centre has a four-fold coordination in the resulting species.^[35, 37]

Semmelhack *et al.* identified many borate-THMF complexes in addition to the borate-ester of S-THMF found in the *V. harveyi* receptor protein (Figure 1.1).^[39] Using ¹¹B NMR spectroscopy, they identified the formation of *mono*-ligand borate, *bis*-ligand borate and *mono*-ligand dimeric borate complexes.^[39] Boron binds strongly to the *cis*-diol groups on both the *R*- and *S*-THMF derivatives of S-DPD.

Table 1.1. Average abundances of boron, silicon, tin and inorganic carbon in different environments.

	Average abundance (ppm)				
	Earth's crust	Sea water	Stream water	Soil solution	Human blood
B	8.7 ^[40]	4 - 5 ^[41]	0.01 ^[42]	0.002 - 0.2 ^[43]	< 0.05 ^[44]
C*	200 ^[45]	28 ^[46]	11 - 18 ^[47]	13 - 150 ^[48]	250 ^[49]
Si	270000 ^[40]	2 ^[50]	3-5 ^[50]	2-14 ^[50]	3.9 ^[51]
Sn	2.2 ^[40]	< 0.5 ^[52]	< 0.00001 ^[52]	<0.0002 ^[52]	< 0.0000003 ^[52]

*inorganic carbon

B. Carbonate complexes

Inorganic carbon can be found in most biological aqueous environments (Table 1.1) as it is in equilibrium with carbon dioxide.^[27] Although it has been proposed that carbonic acid binds S-THMF in a fashion analogous to that of boric acid (Figure 1.5),^[14] no direct chemical evidence has ever been reported of an ester linkage forming spontaneously between carbonic acid and a polyhydroxy hydrocarbon molecule in aqueous solution.

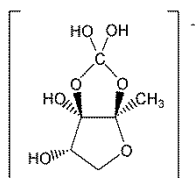


Figure 1.5. Proposed structure of the carbonate ester of S-THMF.^[14]

C. Silicate complexes

Silicon is also found throughout Earth's hydrosphere (Table 1.1). Although it has been shown to be essential in some primitive organisms (fungi, lichens and algae) and beneficial to higher plants (wheat, grass and rice),^[53-58] the underlying mechanisms are almost completely unknown.^[59]

Silicon is sparingly soluble (< 2 mM) in water at pH < 9, where it exists primarily as silicic acid.^[60] As alkalinity is increased, the solubility rises and silicic acid undergoes deprotonation and condensation to form oligomeric silicate species. The addition of simple alcohols to highly alkaline silicate solutions results in the formation of alkoxy-substituted silicate complexes, in which the silicon centre has four-fold coordination.^[61] Addition of aliphatic molecules containing four or more adjacent hydroxyl groups (e.g. threitol, xylitol)^[62-65] or furanoidic vicinal *cis*-diol molecules (e.g., ribose) results in the formation of pentaoxosilicon *bis*-(diolato)-hydroxo and hexaoxosilicon *tris*-(diolato) complexes (Figure 1.6).^[15, 16, 66] The stability of these complexes increase when the ligands contain electron withdrawing functional groups, so much so that even pentaoxosilicon *bis*-(diolato)-hydroxo complexes with gluconic acid are detected at pH 7.^[16, 67]

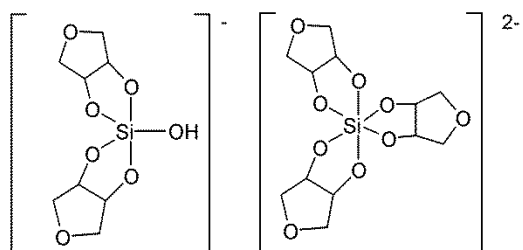


Figure 1.6. Structure of pentaosilicon *bis*-(diolato)-hydroxo and hexaosilicon *tris*-(diolato) complexes formed in aqueous alkaline solution between silicic acid and 1,4-anhydroerythritol.^[15]

D. Stannate complexes

Tin is much less abundant in the Earth's hydrosphere (Table 1.1) and has little known biological significance. Inorganic tin is toxic to many microorganisms, and there have been limited reports that it is essential in rats.^[68, 69] Mbabazi and coworkers used conductimetric analysis to demonstrate that aqueous stannic acid is able to form di-ester *mono*-ligand complexes with polyhydroxy hydrocarbons, including mannitol and D-fructose, under alkaline conditions (Figure 1.7).^[70-73] However, the structure of these complexes was not determined.

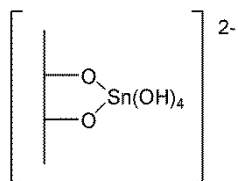


Figure 1.7. Proposed structure of the di-ester *mono*-ligand stannate-polyhydroxy molecule complex; after Mbabazi *et al.*^[73]

CHAPTER 2. EXPERIMENTAL

2.1 Labware and chemical reagents

Type I (18 Mohm cm) distilled/deionized water (DDW; Barnstead E-pure) was used throughout this investigation. When employed to make solutions for NMR analysis, it was supplemented with ca. 15 wt% $^2\text{H}_2\text{O}$ (Cambridge Isotopes, 99.98%) in order to provide a field frequency lock. The concentrations of boron and silicon in the DDW and $^2\text{H}_2\text{O}$ were below the detection limits (0.1 ug L^{-1} and 1.4 ug L^{-1} , respectively) of inductively coupled plasma atomic emission spectrometry analysis (ICP-AES; see section 2.2).

All new plastic labware (Nalgene, VWR) was rinsed with dichloromethane and acetone to remove silicone, except for that made of polycarbonate which is incompatible with these solvents. Subsequent cleaning entailed successive soakings in 10% nitric acid, 10% hydrochloric acid, and DDW. Sterile polycarbonate cultureware (Fisher) was used as received. Glass NMR tubes were rinsed with dichloromethane and acetone, followed by soap and DDW washing.

Two tests were conducted to determine which culture flasks would be most appropriate for investigating the effects of oxoacid treatments on bacteria. In the first test, 0.1 mol L^{-1} phosphate buffer (pH 7.4 at $25 \text{ }^\circ\text{C}$) was added to new and well-used borosilicate flasks (125 mL), autoclaved at $121 \text{ }^\circ\text{C}$ for 1 h, and analyzed for leached B and Si content by ICP-AES. In the second test, growth of wild-type *V. harveyi* was monitored (as described in section 2.3.1) in new, freshly-cleaned, flasks manufactured from borosilicate glass, polyfluoroalkoxy (PFA), polycarbonate (PC), polypropylene (PP) or polymethylpentene (PMP). After the flasks were cleaned and subjected to six complete cycles of sterilization and autoclaving with DDW for 1.5 h at $121 \text{ }^\circ\text{C}$, a second *V. harveyi* growth experiment was conducted to investigate the durability of the flasks.

An additional test was conducted to determine whether Amberlite IRA-743 (Sigma Aldrich), a resin designed to sequester boron from aqueous media,^[74] has a comparable ability to remove silicic acid under different pH conditions. Concentrated stocks of boric acid or silicic acid (ca. 0.5 mol kg^{-1}) were diluted to 2.6 and 1.0 mmol kg^{-1} , respectively, in 0.1 mol kg^{-1} phosphate buffer at pH 2.18, 6.78 or 12.35 ($25 \text{ }^\circ\text{C}$). The solutions were tumbled at $70 \text{ }^\circ\text{C}$ for 16

h and allowed to cool. Amberlite IRA-743 was then added at levels of 1, 2 or 4 wt%, and the solutions were tumbled for 24 h at room temperature before being decanted into clean bottles and submitted for ICP-AES analysis.

Stock solutions of sodium, potassium and tetramethylammonium hydroxide were prepared by dissolving the corresponding solid (Sigma Aldrich, 99.999%) in DDW. The solutions were titrated against potassium hydrogen phthalate (dissolved in freshly boiled DDW) using a phenolphthalein indicator.

Borate solutions were prepared by dissolving H_3BO_3 (Sigma Aldrich, 99.995%) in phosphate buffer. Similarly, carbonate solutions were prepared by dissolving $\text{Na}_2^{13}\text{CO}_3$ (Sigma Aldrich, 99 atom% ^{13}C) directly in DDW or buffer. Alkaline silicate solutions were prepared by tumbling oven dried amorphous SiO_2 , from hydrolysis of SiCl_4 (Sigma Aldrich, 99.998%), in aqueous NaOH or KOH for a minimum of 16 h at 70 °C. Those which were ^{29}Si -enriched were prepared by dissolving $^{29}\text{SiO}_2$ (Isotonics, 99.35 atom% ^{29}Si) in aqueous KOH in a PTFE-lined pressure vessel at 170 °C for a minimum of 24 h. Alkaline stannate solutions were prepared by dissolving Sn metal or SnCl_2 (Sigma Aldrich, >99%) in concentrated HCl, and then adding aqueous tetramethylammonium hydroxide (as quaternary ammonium ions serve to stabilize stannate solutions^[75]).

Alcohols and saccharides (all from Sigma Aldrich, > 95%) were dissolved at room temperature directly in prepared borate, carbonate, silicate and stannate solutions. The description of the solutions, including composition and concentrations of each species, used in the determination of the formation constants can be found in Appendices VI - IX.

2.2 Analytical Instrumentation

Aqueous boron and silicon concentrations were measured with a Varian Vista Pro CCD ICP-AES spectrophotometer.

All NMR spectra were acquired with a Varian Inova 500 spectrometer, using one-pulse (90°) detection, gated ^1H -decoupling (when required) and a recycle period of 3 s (^{11}B), 4 s (^{13}C), 40 s (^{29}Si) or 15 s (^{119}Sn). Chemical shifts were reported with respect to boric acid for ^{11}B , tetramethylsilane (indirectly via the solvent) for ^{13}C , silicic acid for ^{29}Si and tetramethylstannane (indirectly via stannic acid) for ^{119}Sn . Glass NMR tubes were used throughout, but lined with Teflon FEP in the case of borate and silicate solutions to prevent contamination.

pH measurements were conducted using an Orion Ross combination semi-micro pH electrode at 25.0 or 5.0 °C (± 0.2 °C, in a thermostating bath), following a two point calibration using appropriate buffers.

2.3 Bacteria culturing and characterization

2.3.1 *Vibrio harveyi*

V. harveyi BB120 (wildtype), BB170 (luxN::tn5Kan), and MM32 (luxN::Cm, luxS::Tn5Kan) were acquired from Cedarlane and maintained in complex growth medium (14.1 mmol L⁻¹ Na₂HPO₄, 7.3 mmol L⁻¹ KH₂PO₄, 3.8 mmol L⁻¹ (NH₄)₂HPO₄, 0.8 mmol L⁻¹ MgSO₄, 0.5% wt/vol tryptone, 0.05% wt/vol yeast extract, 513.3 mmol L⁻¹ NaCl, 23.9 mmol L⁻¹ MOPS buffer, 21.7 mmol L⁻¹ glycerol; Fisher and Sigma Aldrich) adjusted to pH 7.4 using *ca.* 10% NaOH and HCl.^[76] This “oxoacid free” medium contained undetectable boron and silicon by ICP-AES, but inevitably contained low levels of carbonic acid owing to dissolution of atmospheric CO_{2(g)}. Boric acid or silicic acid from concentrated stocks was added prior to pH adjustment and final dilution. Carbonic acid was added after the medium was sterilized (to prevent loss on heating) through a sterile 0.22 µm syringe filter. The bacteria were grown at 30 \pm 2 °C, and growth was monitored at 600 nm, using a Genesis 10 UV spectrophotometer and oxoacid free medium as a blank.

Bioluminescence experiments were conducted using two different methods. In the first, the preparatory bacteria (grown overnight) were centrifuged down, washed 3 times with phosphate-buffered saline (PBS, pH 7.4 at 25 °C) and diluted to an absorbance of 0.3 (at 600 nm) using PBS as a blank. 10 µL of this mixture was added along with 190 µL of oxoacid-specific complex growth medium (as above) to each well of a 96-well, black walled microplate. The bacteria were then grown at 30 \pm 2 °C, and the absorbance and luminescence measured every 2 h using a Spectramax 190 µL UV-vis (Molecular Devices) without (for absorbance) and with (for luminescence) the incident radiation blocked. Oxoacid free medium was employed as a blank. In the second method, the bacteria were grown in 50 mL of oxoacid-specific growth medium and transferred either to a black walled microplate or a 1 mL cuvette for the luminescent measurements. A LS 50B Luminescence Spectrophotometer (Perkin Elmer) was employed for the 1 mL cuvette luminescence measurements. Again, oxoacid free medium was used as the blank.

2.3.2 Streptococci

Wild-type *S. gordonii* was acquired from Cedarlane and maintained in oxoacid free brain-heart infusion (BHI) medium (ATCC) that was adjusted to pH 7.0 with *ca.* 10% NaOH and HCl. *S. mutans* UA159 (wildtype) and TW26D (*luxS* deletional mutant) were generously supplied by Dr. Z.T. Wen and were maintained in similar medium.^[29]

Biofilm assay medium, containing 58 mmol L⁻¹ K₂HPO₄, 15 mmol L⁻¹ KH₂PO₄, 10 mmol L⁻¹ (NH₄)₂SO₄, 35 mmol L⁻¹ NaCl, 0.2% wt/vol casamino acids, 44 mmol L⁻¹ D-glucose and 0.1 mmol L⁻¹ MnCl₂ · 4H₂O, was adjusted to pH 7.0 with *ca.* 10% KOH and HCl.^[77] After sterilization, amino acids and vitamins were added through a sterile 0.22 µm syringe filter so as to yield 0.04 mM nicotinic acid, 0.1 mmol L⁻¹ pyridoxine HCl, 0.01 mmol L⁻¹ pantothenic acid, 1 mmol L⁻¹ riboflavin, 0.3 mmol L⁻¹ thiamine HCl, 0.05 mmol L⁻¹ D-biotin, 4 mmol L⁻¹ L-glutamic acid, 1 mmol L⁻¹ L-arginine, 1.3 mmol L⁻¹ L-cysteine, 0.1 mmol L⁻¹ L-tryptophan and 2 mmol L⁻¹ MgSO₄.^[77] The individual oxoacids (prepared in a phosphate buffer) were also added after sterilization through a 0.22 µm syringe filter. An equivalent volume of phosphate buffer was added in the case of the oxoacid free control medium. Biofilm assays were performed according to Wen *et al.*^[30] In short, the preparatory bacteria (grown overnight in BHI media) was centrifuged down, washed three times with PBS (pH 7.4), and diluted with PBS to an absorbance of 1.0 at 600 nm (using PBS as a blank). Each well of a sterile, polystyrene, flat-bottom microplate containing 190 µL of the oxoacid-specific biofilm media was spiked with 10 µL of the diluted bacteria solution, followed by 24 h of growth at 36 ± 2 °C in an aerobic environment. After growth, the bacteria were removed from the wells by rinsing 3 times with DDW. After drying for 10 min, 300 µL of a 0.2% crystal violet solution was added to each well followed by 10 min incubation. The crystal violet solution was then decanted, the wells rinsed 3 times with DDW, and the plate was allowed to dry for 10 min. 200 µL of anhydrous ethanol was added to each well, and followed by a 10 min incubation at the end of which the plate was aggressively agitated for one minute. 150 µL of the resulting solution was then transferred to a new microplate and the absorbance was measured at 600 nm. A well containing bacteria-free biofilm medium that underwent the complete biofilm assay was employed as a blank.

2.3.3 *Pectobacterium carotovorum*

P. carotovorum SCC3193 (wildtype) and SCC6023 (luxS suppressed strain), generously supplied by Dr. A. Mae, were maintained in oxoacid-free lysogeny broth (LB, 1% wt/vol tryptone, 1% wt/vol NaCl and 0.5% wt/vol yeast extract) that was adjusted to pH 7.4 with NaOH and HCl.^[18]

The medium primarily used in the biofilm assays was modified M63 minimal medium – containing 43 mmol L⁻¹ NaCl, 22 mmol L⁻¹ KH₂PO₄, 40 mmol L⁻¹ K₂HPO₄, 15 mmol L⁻¹ (NH₄)₂SO₄, 1.8 μmol L⁻¹ FeSO₄, 4 mmol L⁻¹ MgSO₄, 10 mmol L⁻¹ thiamine HCl, 0.1% wt/vol peptone, and 0.05% wt/vol yeast extract – adjusted to pH 7.4 with ca. 10% NaOH and HCl.^[78] Other media used in this investigation included lysogeny broth, M63 and modified M63 with a reduced concentration of peptone and yeast extract. Biofilm assays were conducted as previously stated, using the respective nutrient-rich and biofilm media.

2.3.4 Gene expression

The isolation of RNA from the bacteria was done using an extraction protocol derived from a method developed by Chomczynski and Sacchi in 1987.^[79] In short, concentrated bacteria solutions were placed in a 1.5 mL microcentrifuge tube with 1 mL TRIzol LS (Invitrogen). The cells were broken by passing them through a pipette tip multiple times, followed by incubation on ice for 10 min. After centrifugation at 13000 rpm for 10 min at 4 °C, the supernatant was transferred to a new microcentrifuge tube and left to incubate at room temperature for 5 min. 200 μL of cold CHCl₃ was added to the supernatant and the solution was thoroughly mixed, incubated at room temperature for 3 min, and centrifuged for 15 min. The upper phase was transferred to a new microcentrifuge tube along with 500 μL cold isopropanol and, after mixing and incubation at room temperature for 10 min, the solution was centrifuged for another 30 min. The pellet was then washed with 75% ETOH, allowed to dry, and dissolved in nuclease free water. The RNA was quantified by measuring the absorbance at 260 and 280 nm and its quality determined using formaldehyde gels.

The reverse-transcriptase quantitative polymerase chain reaction (RT-Q-PCR) was performed using a method derived from Heid *et al.*^[80] In short, residual DNA was destroyed by adding 1 μL of both DNase and DNase 10x buffer to 1 μg of RNA dissolved in 8 μL of nuclease free H₂O. After incubation for 10 min at room temperature, 1 μL of 25 mM EDTA was added to

the solution followed by incubation at 65 °C for 10 min. After the solution was placed on ice for 2 min, 1 µL of both random hexamer primer and 10 mM dNTPs was added and the resulting solution incubated at 65 °C for 5 min. Immediately thereafter, the solution was placed on ice for 10 min followed by the addition of 4 µL 5x FS buffer, 2 µL 0.1 M DDT, 0.3 µL reverse transcriptase and 1 µL RNase inhibitor. After these additions, the sample was incubated at 42 °C for 60 min and 70 °C for 15 min. 2 µL of the resulting solution was transferred to a solution containing 10 µL 2x PCR master mix, 1 µL of 100 µM forward and reverse primers, and 6 µL nuclease free H₂O. The PCR reaction was run by initially heating the solution to 95 °C for 5 min, followed by 40 cycles of 95 °C for 40 s, 58 °C for 40 s and 72 °C for 40 s. Fluorescence was recorded after each cycle using a SYBR Green flouroprobe. All of the RT-Q-PCR reagents were acquired from BioRad.

CHAPTER 3. RESULTS AND DISCUSSION

3.1 Effect of inorganic oxoacids on AI-2 quorum sensing

Before we could investigate the effects of inorganic oxoacids on AI-2 quorum sensing, experimental issues needed to be addressed regarding the materials from which culture flasks are manufactured and their potential for contaminating the growth media. In preliminary studies, bacteria were grown in flasks made of PMP so as to eliminate any chance of extraneous B and Si leaching out from borosilicate glass. Growth rates were not reproducible between experiments, however, and we postulated that plasticizers and/or other soluble organic compounds could be leaching from the PMP flasks and inhibiting growth.^[17, 81]

3.1.1 Determination of appropriate conditions for bacterial growth

The first step taken in our present investigation, therefore, was to determine whether borosilicate glassware is indeed a significant source of oxoacid contamination. Dilute phosphate pH 7.4 buffer containing no detectable B or Si was employed as a proxy for the growth medium. After being autoclaved in borosilicate flasks at 121 °C for 60 min, it contained 0.02-0.06 mmol L⁻¹ B and 0.07-0.24 mmol L⁻¹ Si. (The higher levels were obtained from well-used flasks, presumably owing to an increase in surface area with wear.^[82, 83]) Borosilicate flasks were therefore shown to be inappropriate for investigating the effects of boric acid and silicic acid on bacterial cultures.

Next, we investigated growth of *V. harveyi* in flasks made from PP, PC and PFA as well as in borosilicate flasks which were used as a positive control. Experiments were conducted both with new flasks, following an initial wash, and flasks which had been subjected to multiple cleaning/autoclaving cycles. New PC and PFA flasks yielded growth curves that were indistinguishable from those obtained with borosilicate, whereas growth was clearly inhibited in PP and extremely inhibited in PMP (Figure 3.1a). However, after six cleaning cycles only the PFA and borosilicate flasks yielded healthy growth curves (Figure 3.1b). As a consequence, PFA flasks were chosen for use in all further experiments with bacteria cultures. No effort was

made in the current study to determine those agents responsible for growth inhibition of *V. harveyi*, although we note that organic leachates have been reported for PC, PMP and PP,^[84-86] including several which are bioactive.^[87]

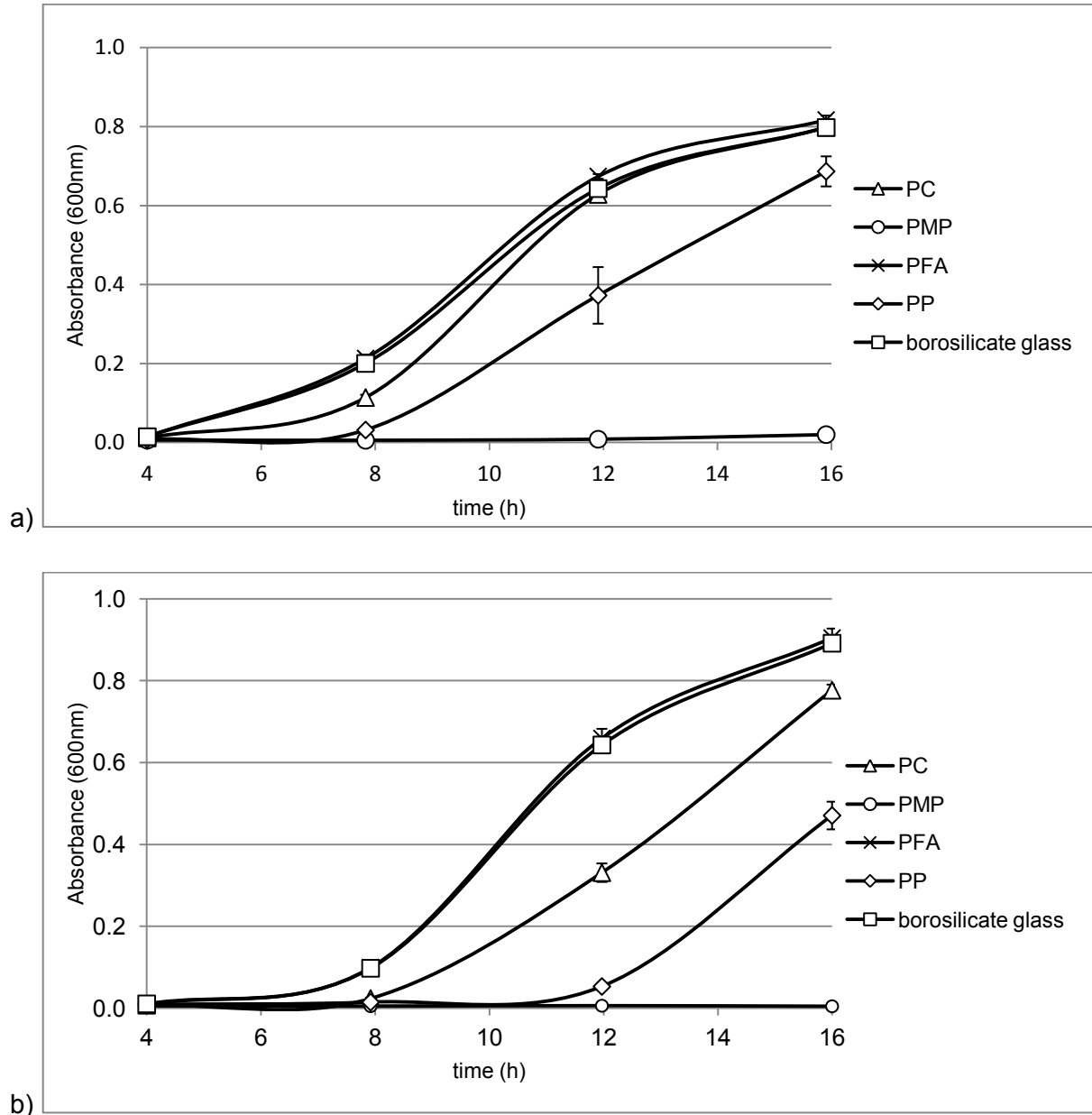


Figure 3.1. Growth of *V. harveyi* BB120 (wild-type) in PC, PMP, PFA, PP and borosilicate flasks a) when they were new or b) after they had undergone six cleaning and autoclaving cycles.

Amberlite IRA-742, a resin functionalized with long-chain polyhydroxy alkanes, is commonly used to remove traces of boron from biological growth media.^[74, 88-90] Here we investigated whether it might have a comparable ability to extract silicon. Figure 3.2 shows the percent extraction of boron and silicon from aqueous solutions containing a) 2.5 mmol kg⁻¹ H₃BO₃, b) 1 mmol kg⁻¹ H₄SiO₄, or c) 2.5 mmol kg⁻¹ H₃BO₃ & 1 mmol kg⁻¹ H₄SiO₄. The resin was nearly 100% effective for removing boric acid from neutral and alkaline solutions, but less than 50% effective under acidic conditions (Figure 3.2a). These results are consistent with previous reports.^[74] By contrast, virtually no silicic acid extraction was observed under neutral or acidic conditions and only about 50% under alkaline conditions (Figure 3.2b). The latter value was halved in the presence of boric acid, owing to its demonstrably superior binding affinity for polyols compared with silicic acid.^[65] Due to its ineffectiveness at removing silicon, from neutral solutions especially, Amberlite received no further use in the present studies. Background levels of B and Si were below detection limits in any case.

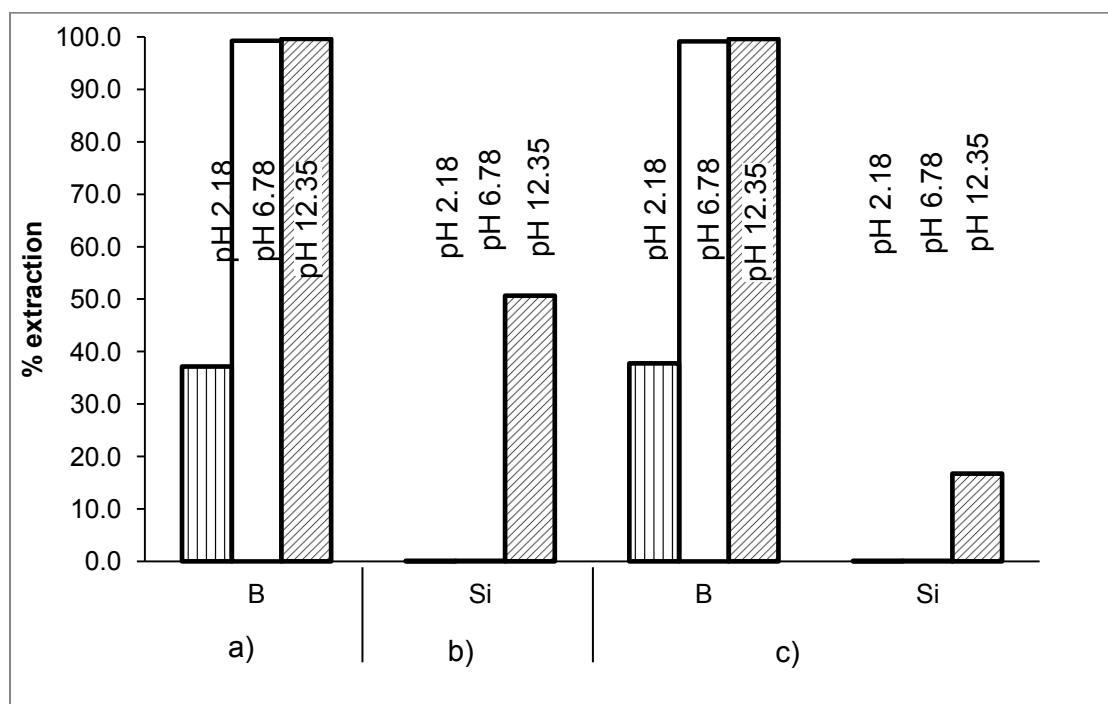


Figure 3.2. Extraction efficiency for B and Si as a function of pH from solutions containing a) 2.5 mmol kg⁻¹ H₃BO₃, b) 1 mmol kg⁻¹ H₄SiO₄ or c) 2.5 mmol kg⁻¹ H₃BO₃ & 1 mmol kg⁻¹ H₄SiO₄ upon addition of Amberlite IRA-743 (0.5 g in 25 mL) and agitating for 24 h. Addition of further Amberlite resulted in negligible increases in extraction efficiency.

3.1.2 *Vibrio harveyi* – bioluminescence as a marker of quorum sensing

Preliminary work in this laboratory indicated that silicic acid increases the luminescence activity of *V. harveyi* over that observed in oxoacid-free control media.^[17] However, the bacteria in that study were grown in PMP flasks and thus exhibited inhibited growth (Figure 1.2a; see above).^[81] We therefore repeated the experiments, but instead cultured the bacteria in PFA flasks. Unfortunately, the uncertainty of the bioluminescence measurements performed with the LS 50B Luminescence Spectrophotometer (with horizontally-oriented photodetector) was extremely large, greatly exceeding differences between the mean luminescence values obtained for the various oxoacid treatments. We suspected that the large uncertainty was due to cell sedimentation occurring in the cuvette during the measurements. We therefore repeated the experiment using a Spectramax 190 μ L UV-vis spectrophotometer (incident radiation blocked; vertically-oriented photodetector), but met with similarly high levels of experimental uncertainty. It was decided to postpone further bioluminescence experiments until we had access to a purpose-built bioluminescence spectrometer.

3.1.3 *Streptococci* and *Pectobacterium* – biofilm formation as a marker for quorum sensing

Next we investigated the effect of oxoacid addition on AI-2 mediated biofilm production by two different species of *Streptococci*, *S. mutans* and *S. gordonii*. The latter species has been reported to increase biofilm production in the presence of carbonic acid.^[13] Surprisingly, we detected no differences in the extent of biofilm formation for either *S. mutans* or *S. gordonii*, when cultured in untreated medium and media treated with H_2CO_3 , H_3BO_3 or H_4SiO_4 (Figures 3.3 and 3.4). It was therefore apparent that our assay method did not have the required sensitivity to detect carbonic acid's documented influence on AI-2 quorum sensing activity in *S. gordonii*.

Similarly, we set out to investigate the effects of oxoacid addition on AI-2 mediated biofilm production by *P. carotovorum*. All attempts at inducing biofilm production by this species were unsuccessful, despite the use of modified M63 and other types of minimal media that have been reported to induce biofilm formation.^[78]

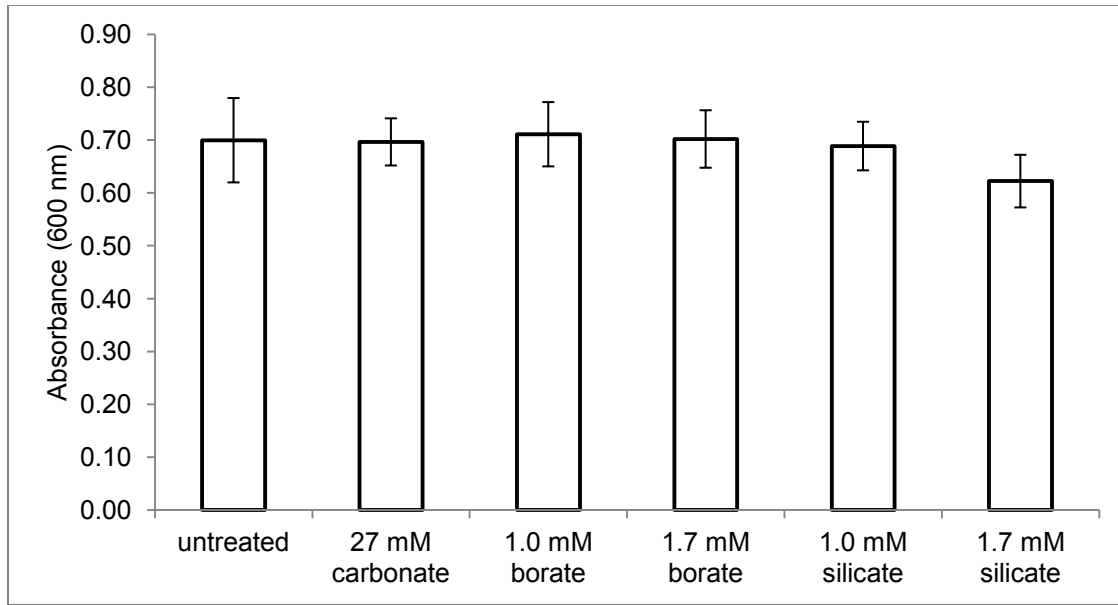


Figure 3.3. Biofilm production by *S. mutans* in untreated medium and media treated with H_2CO_3 , H_3BO_3 or H_4SiO_4 . The y-axis represents extent of biofilm formation by measuring the optical density of crystal violet that absorbed into the biofilm, relative to that for bacteria-free medium. There was a minimum of 6 replicates for each treatment.

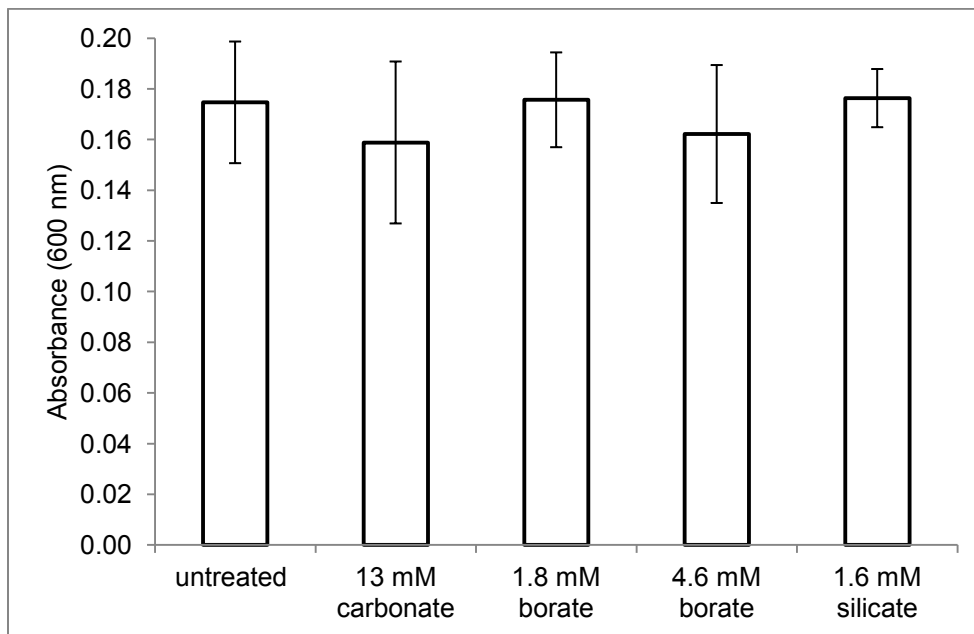


Figure 3.4. Biofilm production by *S. gordonii* in untreated medium and media treated with H_2CO_3 , H_3BO_3 or H_4SiO_4 . The y-axis represents extent of biofilm formation by measuring the optical density of crystal violet that absorbed into the biofilm, relative to that for bacteria-free medium. There was a minimum of 6 replicates for each treatment.

3.1.4 Gene expression analyses

In addition to seeking evidence of bacterial AI-2 activity at the macroscopic level (bioluminescence and biofilm production), we looked for evidence at the molecular level through application of RT-Q-PCR. RNA was extracted in good yields from all the bacteria strains as determined through absorbance at 260 and 280 nm ($> 1000 \text{ ng}/\mu\text{L}$), but we could detect no bands in the formaldehyde gels. RT-Q-PCR was performed nonetheless, but no intact RNA was evident.

In summary, we were unable to determine the influence of inorganic oxoacids on AI-2 quorum sensing using the research infrastructure that was immediately available to us. Given the enticing results obtained from both the preliminary investigations and the chemical binding studies reported below, there is obvious merit in returning to this work in the future.

3.2 Aqueous ester complexes of inorganic oxoacids

To address the chemical feasibility of oxoacids, such as H_2CO_3 , H_4SiO_4 and H_4SnO_4 , affecting AI-2 quorum sensing in the same manner as H_3BO_3 , we compared their ability to form ester complexes with polyhydroxy hydrocarbons in aqueous solution. As noted above, McKenzie *et al.* proposed that carbonic acid forms a di-ester linked S-THMF complex, analogous to that formed by boric acid (Figure 1.4), to account for the apparent ability of carbonate ions to promote quorum sensing in *S. gordonii*.^[14] There is no reported evidence, however, of carbonic acid spontaneously forming ester-linked complexes with aqueous alcohols or saccharides. Nor is there compelling evidence to support stannic acid forming such complexes. By contrast, silicic acid has been shown to bind a wide range of saccharides, including furanoidic vicinal *cis*-diol molecules analogous to THMF.^[15] Below, each oxoacid is considered in turn.

3.2.1 Borate-saccharide complexes

Although borate-saccharide complexation equilibria have been well characterized in the past,^[34-37] the formation constants were typically reported with borate anion as the reactant and, therefore, cover a limited pH range and are not readily comparable to those of other oxoacid systems. In the present study, all complexation equilibria are represented with the fully protonated oxoacid as reactant. The four representative aliphatic polyhydroxy (“polyol”) molecules (threitol, erythritol, xylitol, adonitol) and four representative furanoidic vicinal *cis*-diol molecules (*cis*-1,2-cyclopentanediol, 1,4-anhydroerythritol, D-fructose, cytidine) we selected as ligands are shown in Table 3.1. We limited our study to solutions with borate-to-ligand molar ratio $\leq 0.5:1$, to avoid complexes that contain multiple borate centres (which are not biologically significant and whose ^{11}B NMR peaks are extremely difficult to resolve). We also avoided solutions with $\text{pH} > 8$ so that there was always an NMR signal corresponding to boric acid. These precautions ensured that our equilibrium constants were as accurate as possible. The types of complexes that were characterized are shown in Table 3.2 and a representative ^{11}B NMR spectrum is shown in Figure 3.5.

Table 3.1. Representative ligands selected for determination of formation constants for this study

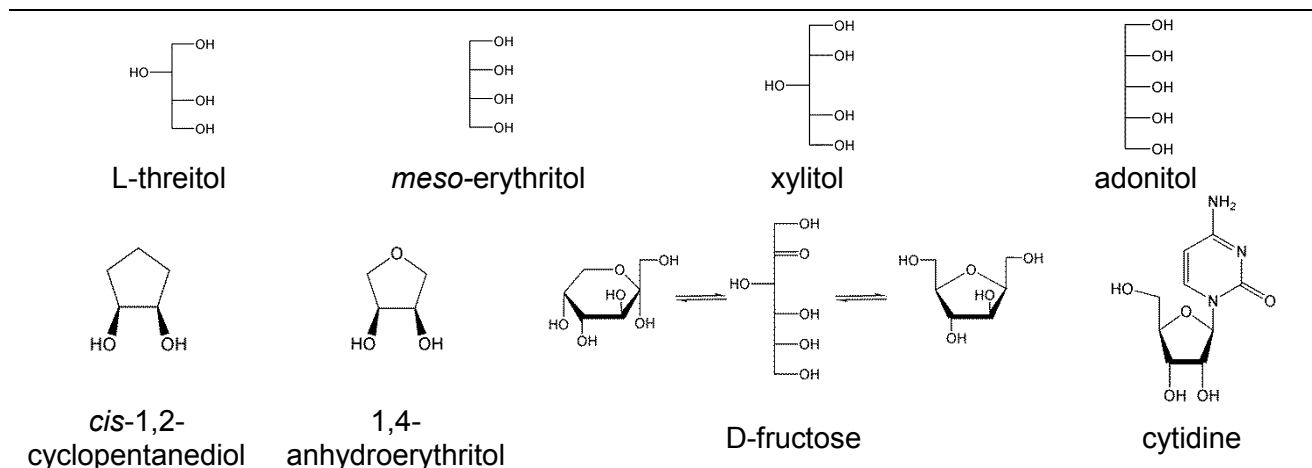


Table 3.2. Borate-saccharide species investigated in this study.

Notation	Structure	^{11}B NMR chemical shift range /ppm ^a
borate <i>mono</i> -saccharide complex (BS_{Mono})		-11 to -16
borate <i>bis</i> -saccharide complex (BS_{Bis})		-5 to -11

^a Relative to the boric acid signal at 0 ppm.

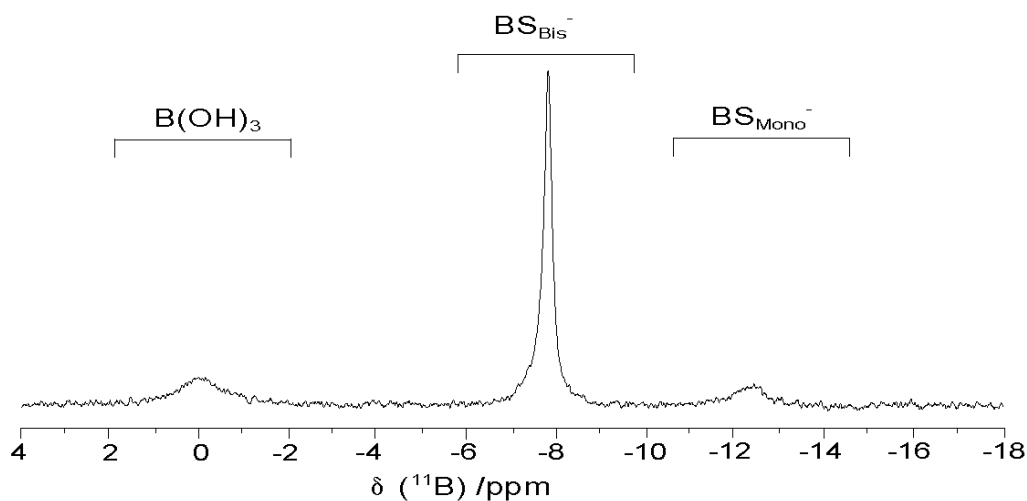


Figure 3.5. Boron-11 NMR spectrum (160.33 MHz) of an aqueous solution containing $0.092 \text{ mol kg}^{-1} \text{ H}_3\text{BO}_3$, 0.49 mol kg^{-1} phosphoric acid and 0.16 mol kg^{-1} 1,4-anhydroerythritol at $\text{pH} = 7.39$ and $25 \text{ }^\circ\text{C}$. The regions corresponding to the principal borate species are shown.

Diffusion-ordered spectroscopy (DOSY) was employed to aid in assigning the ^{13}C NMR spectrum for a solution containing boric acid and the acyclic polyol arabitol. The DOSY spectrum revealed a distinct separation between the signals corresponding to the *bis*-ligand borate complexes and those corresponding to free ligand, owing to the differences in diffusion rate (Figure 3.6). Therefore, DOSY was determined to be helpful for characterizing oxoacid-ligand complexes.

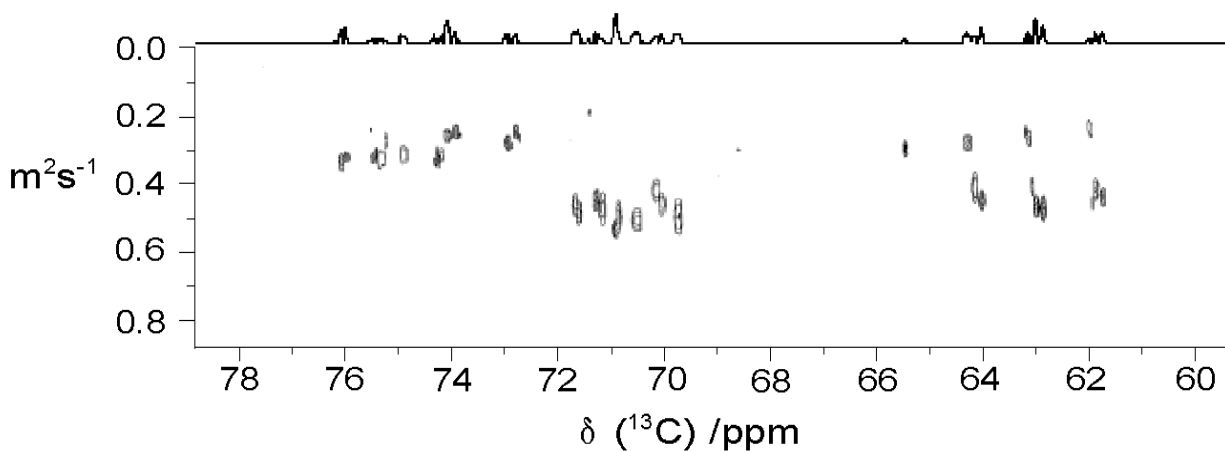
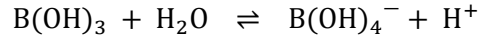


Figure 3.6. Carbon-13 DOSY NMR spectrum (125.67 MHz) of a solution containing approximately $1 \text{ mol kg}^{-1} \text{H}_3\text{BO}_3$ and $3 \text{ mol kg}^{-1} \text{D-arabitol}$ at pH 10.5 and 25°C . Five bipolar pulsed field gradient stimulated sequence (BPPSTE) spectra of 4000 transients each were measured using a 0.2 s diffusion delay and a 0.01 ms field gradient pulse with FG strength ranging from 0.2 to 6.8 T m^{-1} .

A. Formation constants of the borate-saccharide complexes

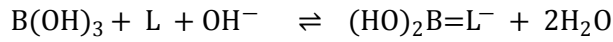
Boric acid deprotonation results in an increase in the coordination number of boron



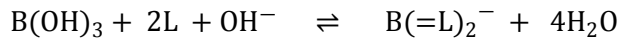
$$K_a = \frac{[\text{B(OH)}_4^-][\text{H}^+]}{[\text{B(OH)}_3]} = 10^{-9.40}$$

Ideal solution conditions are assumed, *i.e.*, $\gamma = 1$, for all of the equilibria in the present study.

Formation constants for borate complexes are therefore given by:



$${}^B\beta_{\text{Mono}} = \frac{[(\text{HO})_2\text{B}=\text{L}^-]}{[\text{B(OH)}_3][\text{L}][\text{OH}^-]} = \frac{[(\text{HO})_2\text{B}=\text{L}^-][\text{H}^+]}{[\text{B(OH)}_3][\text{L}]K_w}$$



$${}^B\beta_{\text{Bis}} = \frac{[\text{B}(=\text{L})_2^-]}{[\text{B(OH)}_3][\text{L}]^2[\text{OH}^-]} = \frac{[\text{B}(=\text{L})_2^-][\text{H}^+]}{[\text{B(OH)}_3][\text{L}]^2K_w}$$

where L represents ligand, “=L” represents a di-ester ligand linkage and $K_w = [\text{H}^+][\text{OH}^-]$. The formation constants are denoted with β (instead of K) as they represent all possible isomers of a given complex. The superscript denotes the oxoacid and the subscript represents the type of complex.

The concentrations of B(OH)_3 , $(\text{HO})_2\text{B}=\text{L}^-$, $\text{B}(=\text{L})_2^-$ and, indirectly, free saccharide ligand were determined through integration of the ^{11}B NMR spectra. The concentration of H^+ was determined from pH measurements. The solutions contained approximately $0.1 \text{ mol kg}^{-1} \text{ H}_3\text{BO}_3$, $0.25 \text{ mol kg}^{-1} \text{ L}$ and 0.5 mol kg^{-1} phosphate buffer, resulting in an ionic strength (I) of approximately 0.5. Interpolating the data reported by Hawkes, the water dissociation constant (pK_w) at this I was determined to be 13.88 ± 0.05 at $25 \text{ }^\circ\text{C}$ and 14.6 ± 0.1 at $5 \text{ }^\circ\text{C}$.^[91] The boric acid ionization constant (pK_a) was reported by van den Berg *et al.* at $25 \text{ }^\circ\text{C}$ and $I = \text{ca. } 0.2$.^[34] A complete description of the solutions used can be found in Appendix VI.

Table 3.3 shows the formation constants calculated for borate-furanoidic *cis*-diol complexes at 25 and 5 °C. There is a correlation between the formation constants and the presence of an oxygen heteroatom on the ligand. All of the ligands with a furan ring (1,4-anhydroerythritol, D-fructose, cytidine) had a greater formation constant than that of a cyclopentane ring (*cis*-1,2-cyclopentanediol). The presence of electron withdrawing functional groups on D-fructose and cytidine did not increase the binding affinity further from that of 1,4-anhydroerythritol. The binding coefficients for all the ligands were approximately one order of magnitude higher at 5 °C than at 25 °C.

Table 3.4 shows the formation constants for the borate-polyol complexes at 25 and 5 °C. The ligands containing *threo*-dihydroxy functionality (threitol and xylitol) tended to have slightly higher binding affinities than those containing only *erythro* functionality (erythritol and adonitol). There was also an increase in formation constants (1 to 2 orders of magnitude) when the chain length of the ligand was increased. As with the furanoidic diols, the binding affinities increased by approximately one order of magnitude when temperature was decreased from 25 to 5 °C.

Table 3.3. Formation constants for borate-furanoidic *cis*-diol complexes at 5 and 25 °C.

		<i>cis</i> -1,2-cyclopentanediol	1,4-anhydroerythritol	D-fructose	cytidine
$\log {}^B\beta_{\text{Mono}}$	5 °C	7.1 ± 0.4	8.9 ± 0.3	8.8 ± 0.2	8.5 ± 0.4
	25 °C	5.5 ± 0.4	7.7 ± 0.2	7.8 ± 0.2	7.4 ± 0.4
$\log {}^B\beta_{\text{Bis}}$	5 °C	9.9 ± 0.2	11.4 ± 0.2	10.8 ± 0.2	10.7 ± 0.2
	25 °C	8.7 ± 0.4	10.3 ± 0.4	9.8 ± 0.2	9.6 ± 0.2

Table 3.4. Formation constants for borate-polyol complexes at 5 and 25 °C

		threitol	erythritol	xylitol	adonitol
$\log {}^B\beta_{\text{Mono}}$	5 °C	6.8 ± 0.4	6.7 ± 0.5	8.4 ± 0.5	7.8 ± 0.5
	25 °C	6.0 ± 0.5	4.9 ± 0.5	7.2 ± 0.5	6.9 ± 0.5
$\log {}^B\beta_{\text{Bis}}$	5 °C	8.6 ± 0.8	8.1 ± 0.3	10.9 ± 0.3	8.8 ± 0.6
	25 °C	7.9 ± 0.9	7.0 ± 0.3	10.0 ± 0.4	7.6 ± 0.3

The approximate formation constants for the complexes between boron and S-DPD derivatives were determined using the data reported by Semmelhack *et al.*^[39] There is large uncertainty associated with these values, as only approximate solution conditions were supplied.^[39] The published ¹¹B NMR spectra of solutions containing 5 or 15 mM boric acid and 15 mM S-DPD were digitized and the area under each signal was determined. All the borate complexes were pooled in order to calculate the formation constants shown in Table 3.5. These values exceed those of all the borate-furanoidic *cis*-diol complexes by about 2 to 3 orders of magnitude (Table 3.3), presumably owing to the presence of multiple binding sites on both *R*- and *S*-THMF.

Table 3.5. Formation constants for the complexes between boric acid and the S-DPD derivatives at 25 °C, determined from the data reported by Semmelhack *et al.*^[39]

S-DPD derivatives	
$\log {}^B\beta_{\text{Mono}}$	9.2 ± 1.3
$\log {}^B\beta_{\text{Bis}}$	12.8 ± 1.4

3.2.2 Carbonate-saccharide complexes

As noted above, no experimental evidence has ever been reported of carbonic acid spontaneously forming ester-linked complexes with polyhydroxy hydrocarbons in aqueous solution, let alone the type of structure that McKenzie *et al.* proposed (Figure 1.4) to account for enhanced bioluminescence activity in *V. harveyi*.^[14] We designed a series of experiments to determine whether or not such interactions actually do occur. Carbon-13 NMR spectroscopy was used to monitor the status of isotopically enriched (99 atom% ¹³C) carbonic acid following its addition to solutions containing a wide variety of potential ligands, ranging from simple alcohols and polyols to structural analogues of THMF.

A. Simple alcohols.

Figure 3.7 shows the ¹³C NMR spectrum of a solution containing 0.13 mol kg⁻¹ Na₂¹³CO₃ and 3.9 mol kg⁻¹ methanol at pH = 10.9. There was a previously unreported signal at 160.0 ppm, which was split into a quartet with $J(^{13}\text{C}, ^1\text{H}) = 3.8$ Hz. Given the characteristic magnitude of this coupling and the fact that the hydroxyl protons on carbonic acid rapidly exchange with water, this splitting must arise from three-bond coupling with the methyl group protons. This signal is therefore assigned to the ester-linked species denoted in Table 3.6 as **CM_{Mono†}**, and represents the first ever reported evidence of a carbonate-alcohol complex. Its close proximity to the free carbonic acid signal would suggest that the carbonate carbon maintains its three-fold coordination. As corroboration, we note that ¹³C NMR chemical shifts reported for polymeric orthocarbonates (polymers containing 4-coordinate carbonate C(OR)₄ centres) range from 120 to 153 ppm.^[92-96] Even at exceptionally high concentrations of methanol, there was no evidence found of a *bis*-ligand carbonate complex. Upon cooling the solution from 25 °C to 5 °C, the quartet signal resolved into two overlapping quartets of equal intensity (Figure 3.8), indicating that a dynamic equilibrium exists between two hydrogen-bonded states of the carbonate-alcohol complex (Figure 3.9). Comparable hydrogen bonding states in aqueous solution have been reported.^[97, 98]

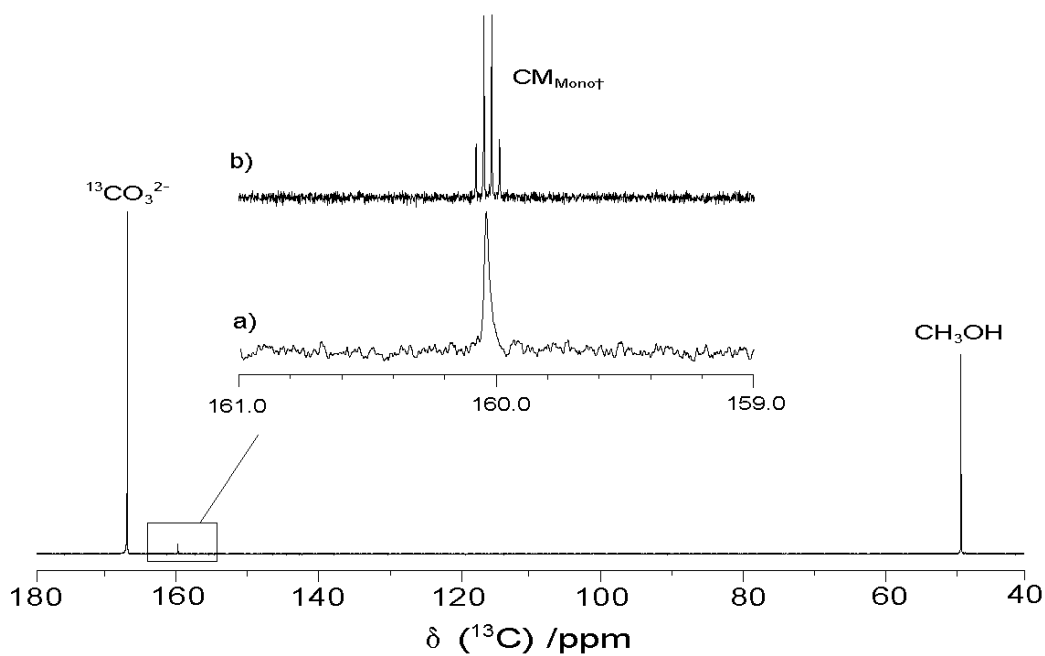


Figure 3.7. Carbon-13 NMR spectrum (125.67 MHz) of an aqueous solution containing $0.13 \text{ mol kg}^{-1} \text{ Na}_2^{13}\text{CO}_3$ and 3.9 mol kg^{-1} methanol at pH 10.9 and $25 \text{ }^\circ\text{C}$. The expanded region is shown a) with and b) without gated ^1H decoupling.

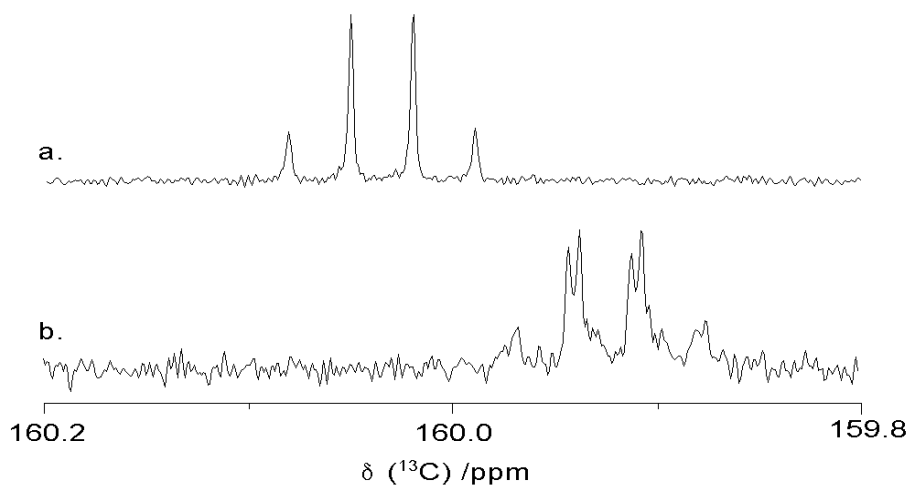


Figure 3.8. Carbon-13 NMR spectra of the solution represented in Figure 3.7, acquired without gated ^1H decoupling at a) $25 \text{ }^\circ\text{C}$ and b) $5 \text{ }^\circ\text{C}$.



Figure 3.9. Dynamic equilibrium between the hydrogen bonded states of **CM_{MonoT}**.

Figure 3.10 shows the ^{13}C NMR spectrum of a solution containing 0.12 mol kg^{-1} $\text{Na}_2^{13}\text{CO}_3$ and 13 mol kg^{-1} ethane-1,2-diol at pH 11.1. The signal to low frequency of the free carbonic acid signal corresponds to mono-ester complex **CG_{MonoT}** (Table 3.6), analogous to that observed for methanol. It was split into a triplet from long distance scalar coupling to the ligand $-\text{CH}_2-$ protons. There was no evidence a di-ester complex between carbonate and ethane-1,2-diol.

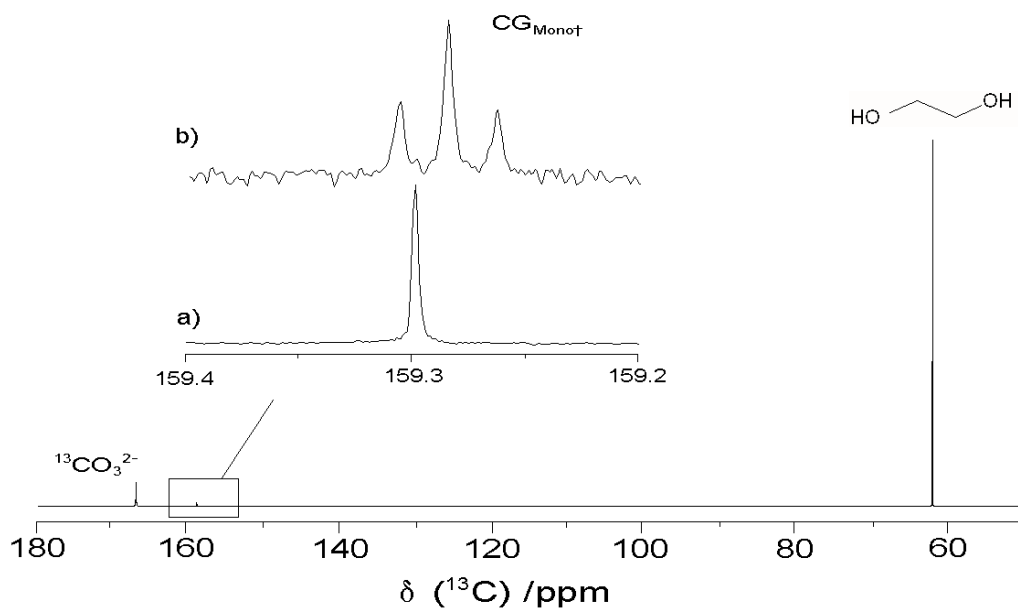
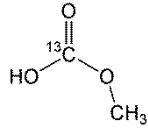
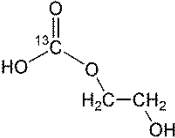


Figure 3.10. Carbon-13 NMR spectrum of an aqueous solution containing 0.12 mol kg^{-1} $\text{Na}_2^{13}\text{CO}_3$ and 13 mol kg^{-1} ethane-1,2-diol at pH 11.1 and $25 \text{ }^\circ\text{C}$. The expanded region is shown a) with and b) without gated ^1H decoupling.

Table 3.6. Representative ^{13}C NMR peak assignments for carbonate complexes of simple alcohols^a.

Alcohol	Structure	Notation ^b	$^3J(^{13}\text{C}, ^1\text{H})$ coupling of ^{13}C NMR carbonate signal (/Hz) ^c
methanol		CM_{Mono†}	3.8 (q)
ethane-1,2-diol		CG_{Mono†}	2.7 (t)

^a Representative chemical shifts were not included due to their large dependency on pH ^b The symbol † denotes a mono-ester linkage between the carbonate centre and ligand, M = methanol and G = ethane-1,2-diol. ^c Multiplicity represented by t (triplet) or q (quartet).

B. Acyclic polyols

Next we continued our investigation of carbonate-alcohol complex formation through the use of several representative aliphatic polyhydroxy molecules (polyols, Table 3.1), including those employed in previous studies of boric acid and silicic acid.^[36, 64] To promote complex formation, we maximized the polyol concentration in solution. Once again, a number of novel carbonate ester complexes were discovered (Table 3.7).

Figure 3.11 shows the ^{13}C NMR spectrum of a solution containing 0.13 mol kg^{-1} $\text{Na}_2^{13}\text{CO}_3$ and 1.5 mol kg^{-1} L-threitol at pH 11.2. The doublet at 158.7 ppm corresponds to mono-ester complex **CT_{Mono2†}** (Table 3.7), in which carbonic acid is bound to the C₂ hydroxyl group of threitol. The signal at 159.1 ppm is split into a triplet and therefore corresponds either to a di-ester complex in which carbonic acid is bound to the C₂ and C₃ hydroxyl groups or to a mono-ester complex involving a terminal hydroxyl group. To determine the true identity of this signal we acquired the ^{13}C NMR spectrum of an analogous solution containing the less symmetrical butane-1,2,4-triol in place of threitol (Figure 3.12). Three signals were detected down-frequency of the free carbonic acid peak, showing very clearly that carbonic acid forms

mono-ester complexes with each hydroxyl group on the ligand, denoted as $\text{CB}_{\text{Mono}1\ddagger}$, $\text{CB}_{\text{Mono}2\ddagger}$ and $\text{CB}_{\text{Mono}4\ddagger}$ in Table 3.7. Accordingly, the triplet resonance at 159.1 ppm in Figure 3.9 corresponds to the mono-ester threitol complex, $\text{CT}_{\text{Mono}1\ddagger}$ (Table 3.7).

Table 3.7. Representative ^{13}C NMR peak assignments for carbonate complexes of aliphatic polyhydroxy molecules^a

Polyol	Structure	Notation ^b	$^3J(^{13}\text{C}, ^1\text{H})$ coupling of ^{13}C NMR carbonate signal (/Hz) ^c
L-threitol		$\text{CT}_{\text{Mono}1\ddagger}$ $\text{CT}_{\text{Mono}2\ddagger}$	2.5 (t) 4.1 (d)
butane-1,2,4-triol ^d		$\text{CB}_{\text{Mono}1\ddagger}$ $\text{CB}_{\text{Mono}2\ddagger}$ $\text{CB}_{\text{Mono}4\ddagger}$	2.9 (t) 3.4 (d) 2.6 (t)
erythritol		$\text{CE}_{\text{Mono}1\ddagger}$ $\text{CE}_{\text{Mono}2\ddagger}$	2.4 (t) 3.6 (d)
xylitol		$\text{CX}_{\text{Mono}1\ddagger}$ $\text{CX}_{\text{Mono}2\ddagger}$ $\text{CX}_{\text{Mono}3\ddagger}$	2.6 (t) 3.8 (d) 4.1 (d)
adonitol		$\text{CA}_{\text{Mono}1\ddagger}$ $\text{CA}_{\text{Mono}2\ddagger}$ $\text{CA}_{\text{Mono}3\ddagger}$	2.5 (t) 3.6 (d) 4.0 (d)

^a Representative chemical shifts were not included due to their large dependency on pH ^b The symbol † denotes a mono-ester linkage between the carbonate centre and ligand. T = threitol, E = erythritol, X = xylitol and A = adonitol. ^c Peak multiplicity is represented by t (triplet) or d (doublet). ^d The racemic form of the ligand was used.

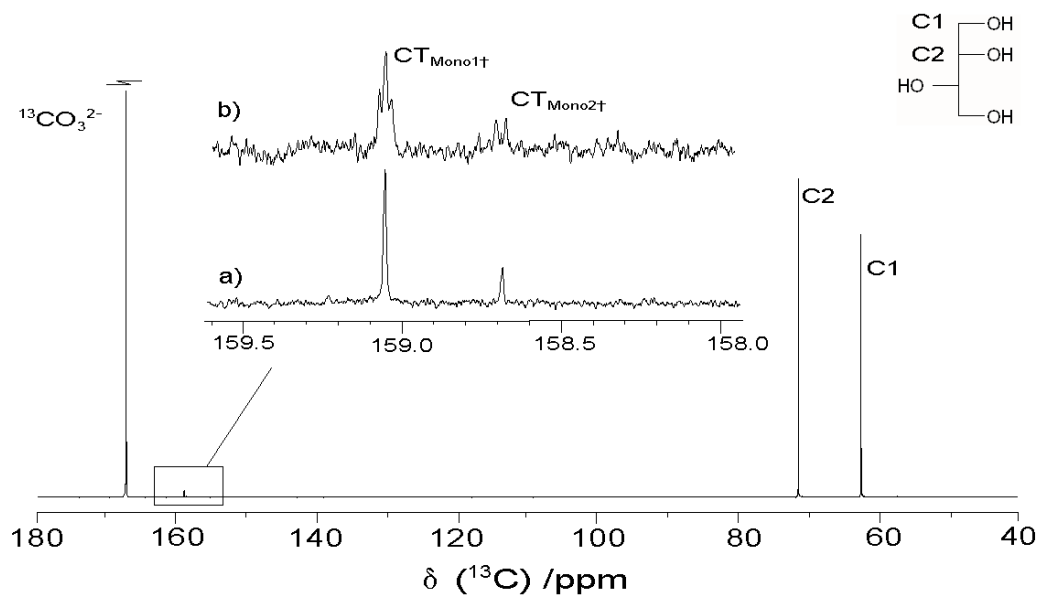


Figure 3.11. Carbon-13 NMR spectrum of an aqueous solution containing 0.13 mol kg^{-1} $\text{Na}_2^{13}\text{CO}_3$ and 1.5 mol kg^{-1} L-threitol at pH 11.2 and $5 \text{ }^\circ\text{C}$. The expanded region is shown a) with and b) without gated ^1H decoupling.

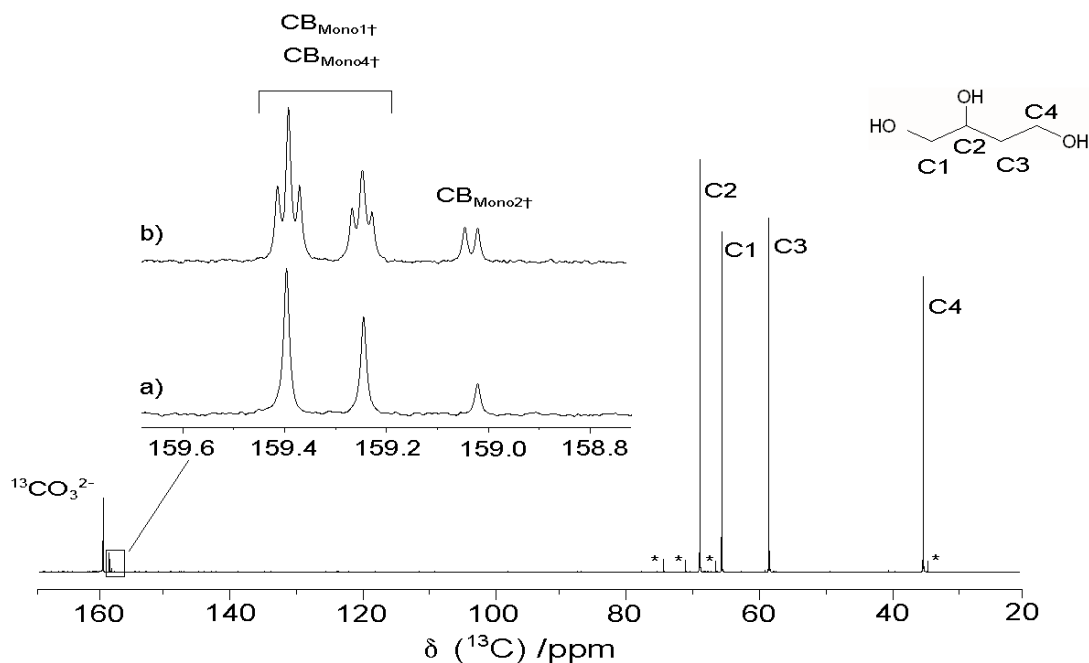


Figure 3.12. Carbon-13 NMR spectrum of an aqueous solution containing $0.031 \text{ mol kg}^{-1}$ $\text{Na}_2^{13}\text{CO}_3$ and 3.8 mol kg^{-1} butane-1,2,4-triol at $25 \text{ }^\circ\text{C}$. The expanded region is shown a) with and b) without gated ^1H decoupling. Impurities from the ligand source are denoted with asterisks.

Figure 3.13 shows the ^{13}C NMR spectrum of a solution containing 0.13 mol kg^{-1} $\text{Na}_2^{13}\text{CO}_3$ and 1.5 mol kg^{-1} *meso*-erythritol at pH 11.2. The signals at 159.3 and 158.4 ppm correspond to mono-ester complexes $\text{CE}_{\text{Mono1}\uparrow}$ and $\text{CE}_{\text{Mono2}\uparrow}$ (Table 3.7). The signals were split into a triplet and a doublet from long distance scalar coupling to the ligand protons. Polyols with *threo*-dihydroxy functionality were previously determined to form di-ester linkages with boron and silicon more readily than those lacking this functionality.^[36, 64] Therefore, if carbonate was binding the polyols through di-ester linkages, the concentration ratio between the two signals would likely change between threitol and erythritol. As the concentration ratio remains constant, we are certain that the triplets in Figure 3.11 and 3.13 correspond to mono-ester complexes.

The ^{13}C NMR spectrum of a solution containing $0.058 \text{ mol kg}^{-1}$ $\text{Na}_2^{13}\text{CO}_3$ and 6.9 mol kg^{-1} xylitol at pH 10.3 is shown in Figure 3.14. The signals at 158.6, 158.8 and 159.1 ppm correspond to mono-ester complexes between carbonic acid and the C_1 , C_2 , or C_3 hydroxyl group on xylitol, denoted as $\text{CX}_{\text{Mono1}\uparrow}$, $\text{CX}_{\text{Mono2}\uparrow}$ and $\text{CX}_{\text{Mono3}\uparrow}$ (Table 3.7). The triplet resonance at 159.1 ppm can clearly be assigned to $\text{CX}_{\text{Mono1}\uparrow}$. The doublet at 158.6 ppm is twice the intensity of the doublet at 158.8 ppm, enabling them to be assigned to $\text{CX}_{\text{Mono2}\uparrow}$ and $\text{CX}_{\text{Mono3}\uparrow}$, respectively.

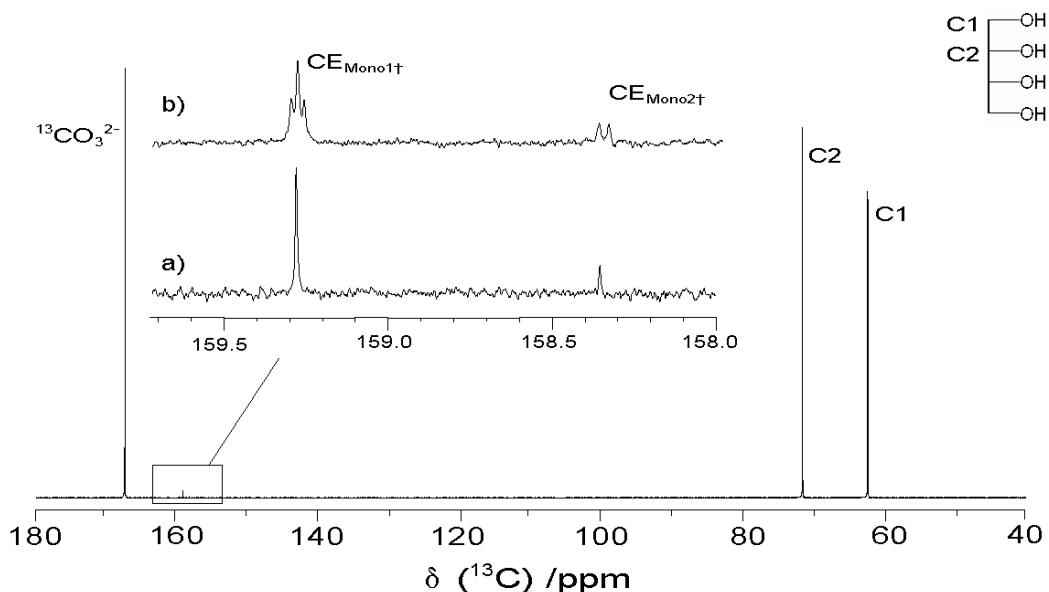


Figure 3.13. Carbon-13 NMR spectrum of an aqueous solution containing 0.13 mol kg^{-1} $\text{Na}_2^{13}\text{CO}_3$ and 1.5 mol kg^{-1} *meso*-erythritol at pH 11.2 and $5 \text{ }^\circ\text{C}$. The expanded region is shown a) with and b) without gated ^1H decoupling.

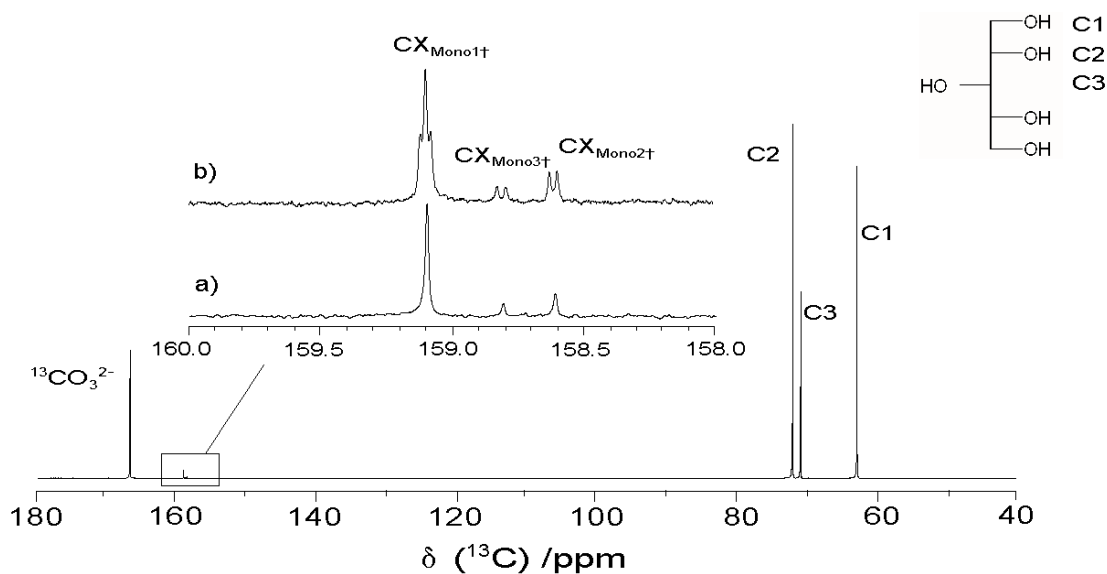


Figure 3.14. Carbon-13 NMR spectrum of an aqueous solution containing $0.058 \text{ mol kg}^{-1}$ $\text{Na}_2^{13}\text{CO}_3$ and 6.9 mol kg^{-1} xylitol at pH 10.3 and $25 \text{ }^\circ\text{C}$. The expanded region is shown a) with and b) without gated ^1H decoupling.

Figure 3.15 shows the ^{13}C NMR spectrum of a solution containing $0.044 \text{ mol kg}^{-1}$ $\text{Na}_2^{13}\text{CO}_3$ and 1.8 mol kg^{-1} adonitol at pH 8.7. The signals down-frequency of the free carbonic acid signal correspond to three mono-ester complexes, denoted as $\text{CA}_{\text{Mono}1\ddagger}$, $\text{CA}_{\text{Mono}2\ddagger}$ and $\text{CA}_{\text{Mono}3\ddagger}$ (Table 3.7), that are analogous to the carbonate-xylitol species.

In order to study the effect of pH on complex formation, a buffer was required that reacts neither with carbonic acid nor with the saccharides. Several common biological buffers were evaluated (Appendix I), but only phosphoric acid was found to be compatible with this particular chemical system. With it we investigated the effect of pH on the carbonate-xylitol species to determine under which conditions carbonate complexes form. Figure 3.16 shows that the concentration of the carbonate-xylitol mono-ester complexes, $\text{CX}_{\text{Mono}\ddagger}$, decrease with an increase in pH. This trend is also present in a similar investigation conducted with tris buffer (Appendix I), in which no complexation occurred above pH 11.8. Therefore, subsequent solutions were prepared having $\text{pH} < 11$.

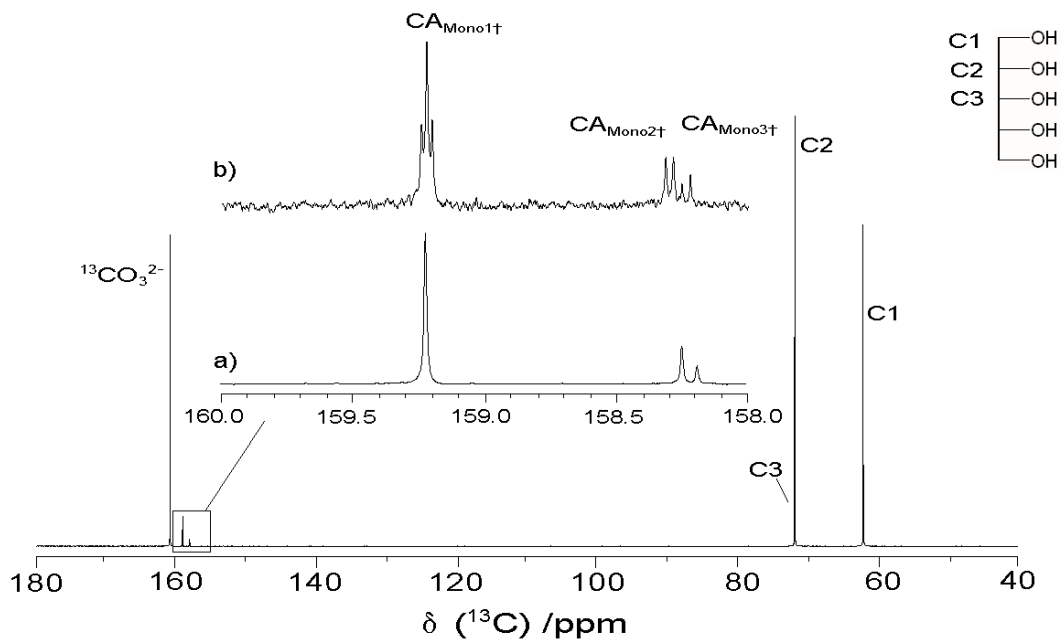


Figure 3.15. Carbon-13 NMR spectrum of an aqueous solution containing $0.044 \text{ mol kg}^{-1}$ $\text{Na}_2^{13}\text{CO}_3$ and 1.8 mol kg^{-1} adonitol at pH 8.7 and 5°C . The expanded region is shown a) with and b) without gated ^1H decoupling.

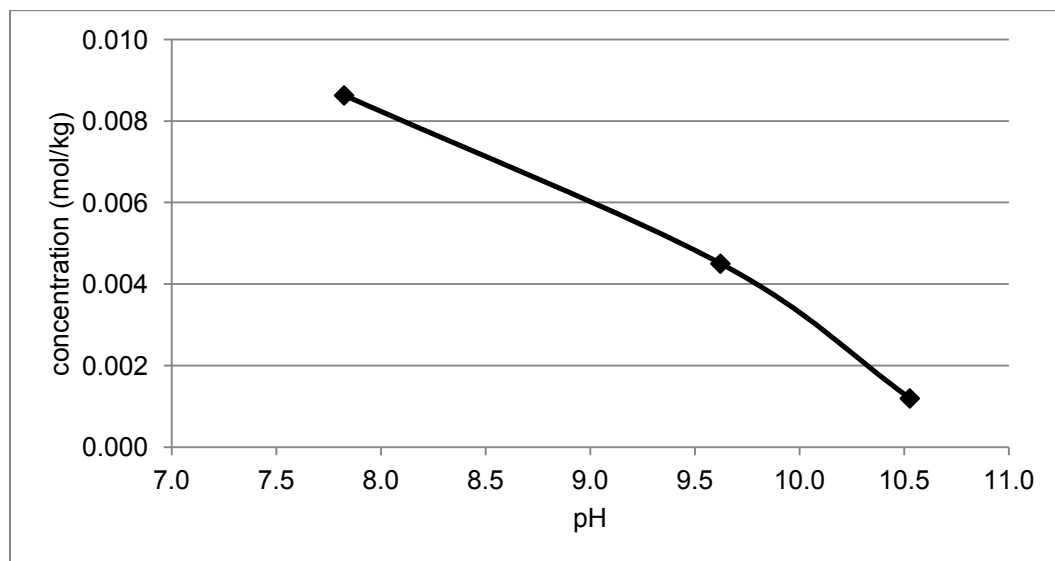


Figure 3.16. $\text{CX}_{\text{Mono}+}$ concentration (solid line) as a function of pH in solutions containing 0.07 mol kg^{-1} $\text{Na}_2^{13}\text{CO}_3$ and 3.0 mol kg^{-1} xylitol at 25°C .

C. Sugar acids

Figure 3.17 shows the ^{13}C NMR spectrum of a solution containing $0.056 \text{ mol kg}^{-1}$ $\text{Na}_2^{13}\text{CO}_3$ and 2.0 mol kg^{-1} gluconic acid at pH 9.6. The triplet resonance at 159.8 ppm corresponds to mono-ester complex $\text{CGA}_{\text{Mono6}\uparrow}$ (Table 3.8), where carbonic acid is linked to the C_6 hydroxyl group of gluconic acid. The four doublet signals between 158.3 and 158.8 ppm correspond to mono-ester complexes $\text{CGA}_{\text{Mono2}\uparrow} - \text{CGA}_{\text{Mono5}\uparrow}$, formed by carbonic acid binding at each of the other hydroxyl groups. An additional signal appears approximately 0.1 ppm up-frequency of the free carbonic acid signal (Figure 3.18), for which no fine coupling was resolved. As it was not observed for the solutions containing non-acid polyols, we suspect that it corresponds to complexes in which carbonic acid is bound directly at the ligand carboxylate group.

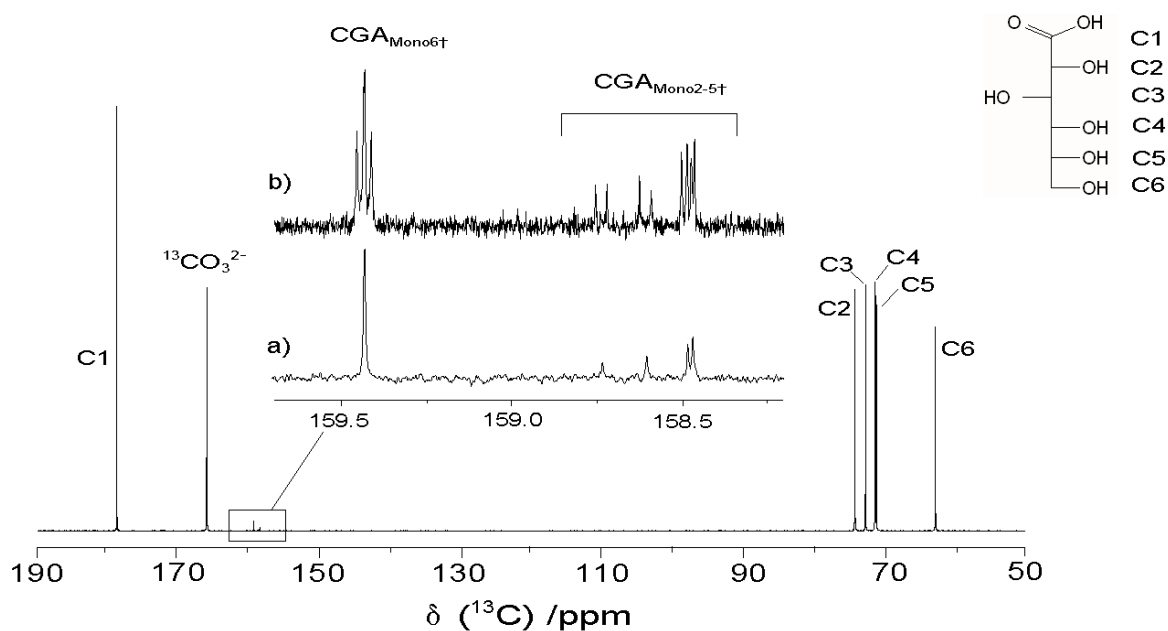


Figure 3.17. Carbon-13 NMR spectrum of an aqueous solution containing $0.056 \text{ mol kg}^{-1}$ $\text{Na}_2^{13}\text{CO}_3$ and 2.0 mol kg^{-1} gluconic acid at pH 9.6 and $25 \text{ }^\circ\text{C}$. The expanded region is shown a) with and b) without gated ^1H decoupling.

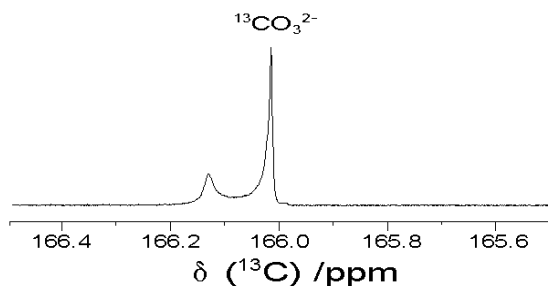


Figure 3.18. Expansion of the high frequency spectral region of Figure 3.17, with gated ^1H -decoupling.

Figure 3.19 shows the ^{13}C NMR spectrum of a solution containing 0.25 mol kg^{-1} $\text{Na}_2^{13}\text{CO}_3$ and 1.5 mol kg^{-1} glucoheptonic acid at pH 10.4. The six signals ranging from 158.0 to 160.0 ppm correspond to mono-ester complexes $\text{CGH}_{\text{Mono}2\uparrow}$ through $\text{CGH}_{\text{Mono}7\uparrow}$ (Table 3.8), analogous to the carbonate-gluconate species. The weak signal at 163.9 ppm has been tentatively assigned to the CGH_{Mono} di-ester complex (Table 3.8) owing to its relative spectral position. Since no scalar coupling could be resolved, the location of the di-ester linkages remains unknown. No evidence was observed of carbonic acid binding directly at the ligand carboxylate group in this solution. When the ligand-to-carbonic acid ratio was increased four-fold, however, new signals overlapping with the free carbonic acid signal were present (Figure 3.20) which we tentatively assign to such species.

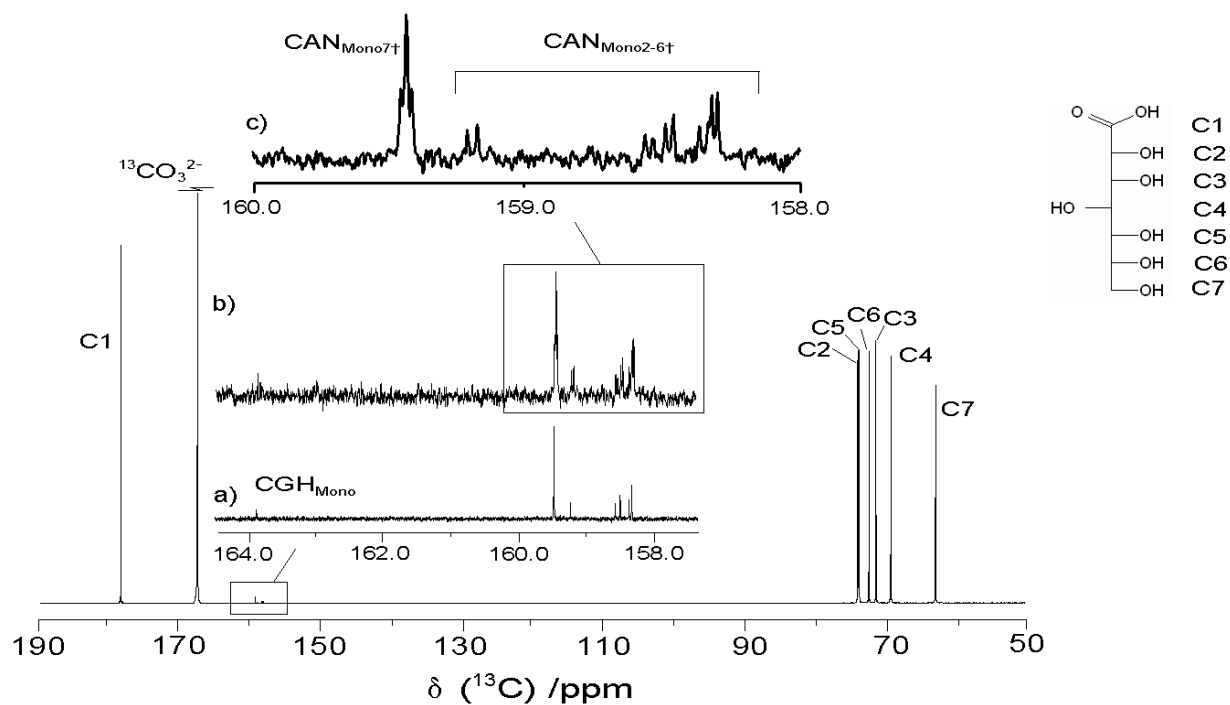


Figure 3.19. Carbon-13 NMR spectrum of an aqueous solution containing $0.25 \text{ mol kg}^{-1} \text{ Na}_2^{13}\text{CO}_3$ and 1.5 mol kg^{-1} glucoheptonic acid at pH 10.4 and 25°C . The expanded region is shown a) with and b) without gated ^1H decoupling, with another expansion (c) of the resolved coupling.

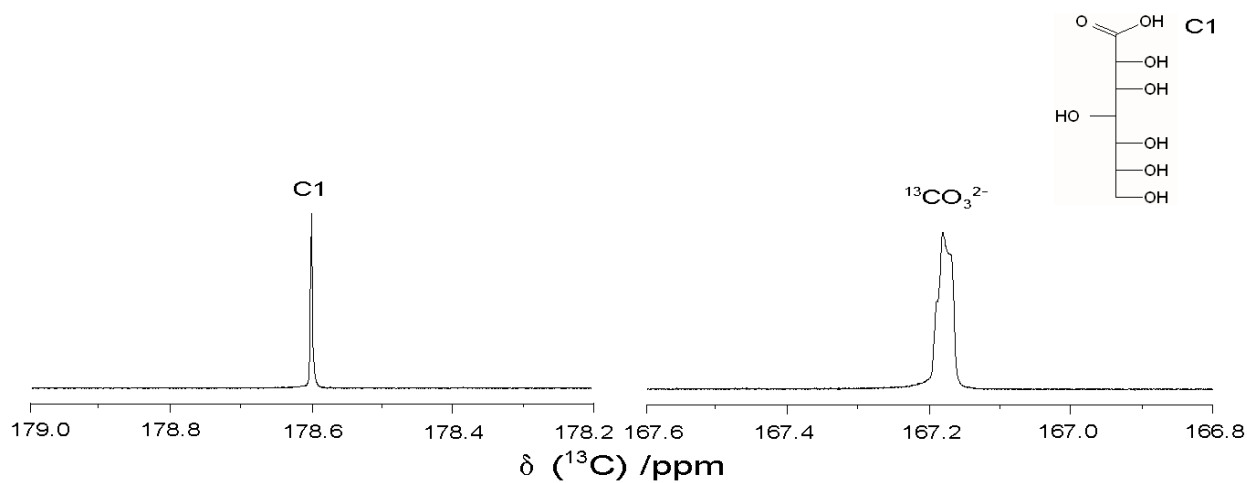


Figure 3.20. Carbon-13 NMR spectrum of an aqueous solution containing $0.057 \text{ mol kg}^{-1} \text{ Na}_2^{13}\text{CO}_3$ and 1.4 mol kg^{-1} glucoheptonic acid at pH 10.1 and 25°C with gated ^1H -decoupling.

The ^{13}C NMR spectrum of a solution containing $0.050 \text{ mol kg}^{-1} \text{ Na}_2^{13}\text{CO}_3$ and 2.3 mol kg^{-1} L-tartaric acid at pH 10.3 is shown in Figure 3.21. The signal down-frequency of the free carbonic acid signal corresponds to mono-ester complex $\text{CTA}_{\text{Mono}2\text{T}}$ (Table 3.8) in which carbonic acid is bound to the C_2 hydroxyl group on the sugar acid. As with the aldonic acids, the additional signal up-frequency to that of free carbonic acid has been tentatively assigned to a complex in which carbonic acid is linked to the ligand carboxylate group.

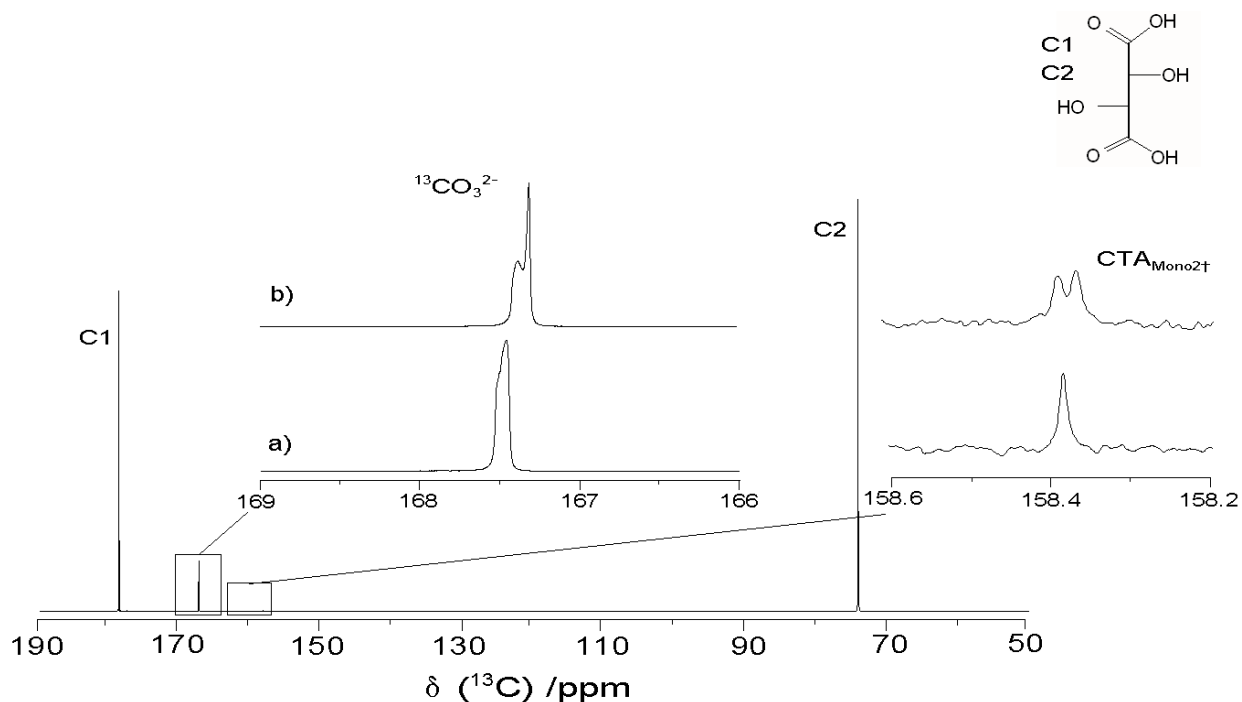
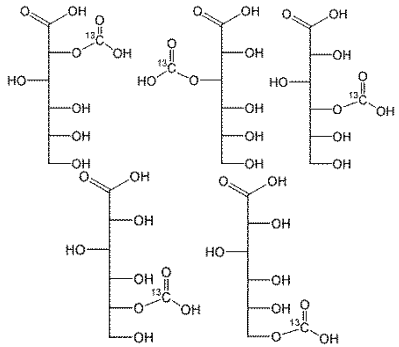
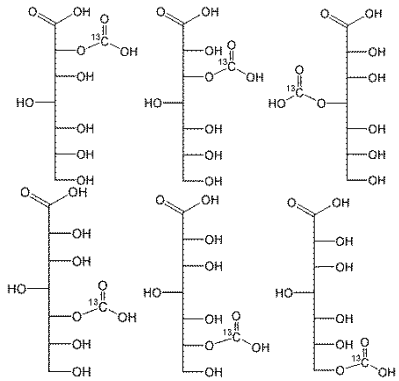
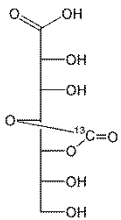
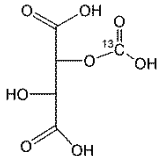


Figure 3.21. Carbon-13 NMR spectrum of an aqueous solution containing $0.050 \text{ mol kg}^{-1} \text{ Na}_2^{13}\text{CO}_3$ and 2.3 mol kg^{-1} L-tartaric acid at pH 10.3 and $25 \text{ }^\circ\text{C}$. The expanded region is shown a) with and b) without gated ^1H decoupling.

Table 3.8. Representative ^{13}C NMR peak assignments for carbonate complexes of sugar acids^a

Sugar acid	Structure	Notation ^b	$^3J(^{13}\text{C}, ^1\text{H})$ coupling of ^{13}C NMR carbonate signal (/Hz) ^c
gluconic acid		CGA_{Mono2†} through CGA_{Mono6†}	2.7 (t) 2.7-4.3 (d)
glucoheptonic acid		CGH_{Mono2†} through CGH_{Mono7†}	2.6 (t) 2.7-4.5 (d)
		CGH_{Mono}	nr
tartaric acid		CTA_{Mono2†}	2.8 (d)

^a Representative chemical shifts were not included due to their large dependency on pH ^b The symbol † denotes a mono-ester linkage between the carbonate centre and ligand. GA = gluconic acid, GH = glucoheptonic acid, and TA = tartaric acid. ^c Multiplicity is represented by t (triplet) or d (doublet). nr = not resolved. ^d Tentative structure, as the location of the di-ester linkage is unknown.

D. Furanoidic vicinal *cis*-diols

We continued this study by investigating the interactions between carbonic acid and furanoidic vicinal *cis*-diols that are structurally analogous to THMF. As with all the hydroxyl-containing molecules investigated thus far, we detected a number of novel carbonate-furanoidic *cis*-diol complexes, as shown in Table 3.9.

Figure 3.22 shows the ^{13}C NMR spectrum of a solution containing $0.042 \text{ mol kg}^{-1}$ $\text{Na}_2^{13}\text{CO}_3$ and 1.5 mol kg^{-1} *cis*-1,2-cyclopentanediol at pH 10.5. The signal down-frequency of the free carbonic acid signal corresponds to mono-ester complex $\text{CC}_{\text{Mono}1\uparrow}$ (Table 3.9). The signal is split into a doublet from long distance scalar coupling to the ligand $-\text{CH}-$ proton.

The ^{13}C NMR spectrum of a solution containing 0.27 mol kg^{-1} $\text{Na}_2^{13}\text{CO}_3$ and 4.0 mol kg^{-1} 1,4-anhydroerythritol is shown in Figure 3.23. The signal at 158.1 ppm corresponds to mono-ester complex $\text{CAN}_{\text{Mono}1\uparrow}$ (Table 3.9), which is analogous to that observed with *cis*-1,2-cyclopentanediol. There is an additional signal up-frequency of the mono-ester complex signal. It is split into a triplet from the ligand protons and represents the first conclusive evidence of a di-ester complex forming with carbonic acid, denoted as CAN_{Mono} . The up-frequency shift of this signal from those of the other carbonate complexes supports the assignment of the di-ester species with glucoheptonic acid, as its signal has a similar up-frequency shift. Additionally, we demonstrated that the carbonate-S-THMF complex proposed by McKenzie *et al.* (Figure 1.5) is certainly viable, except that the carbonate centre would have a three-fold coordination (Figure 3.24) and that the mono-ester complex is more abundant in bulk solution.

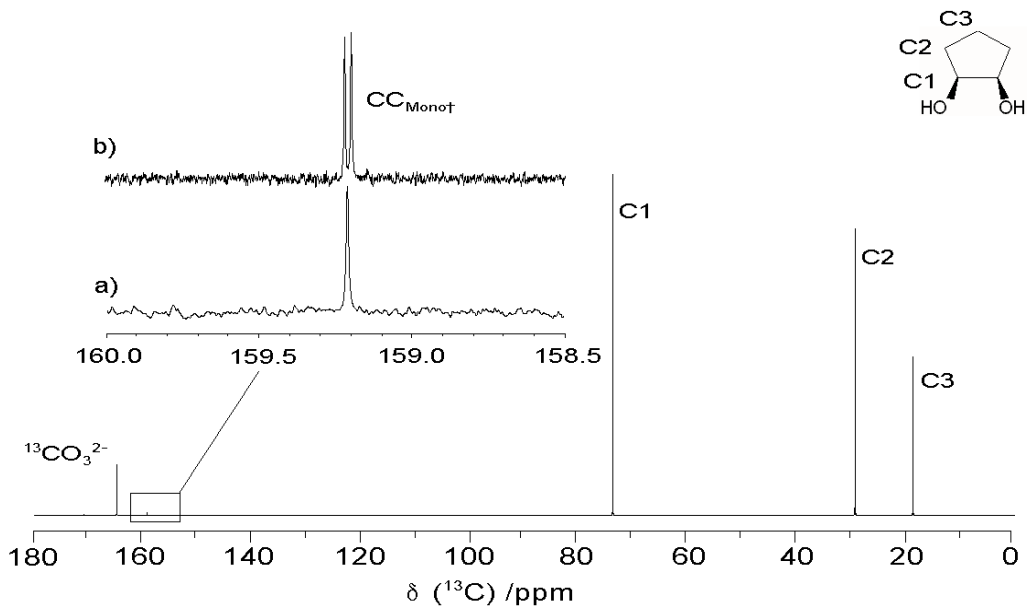


Figure 3.22. Carbon-13 NMR spectrum of an aqueous solution containing $0.042 \text{ mol kg}^{-1}$ $\text{Na}_2^{13}\text{CO}_3$ and 1.5 mol kg^{-1} *cis*-1,2-cyclopentanediol at pH 10.5 and $25 \text{ }^\circ\text{C}$. The expanded region is shown a) with and b) without gated ^1H decoupling.

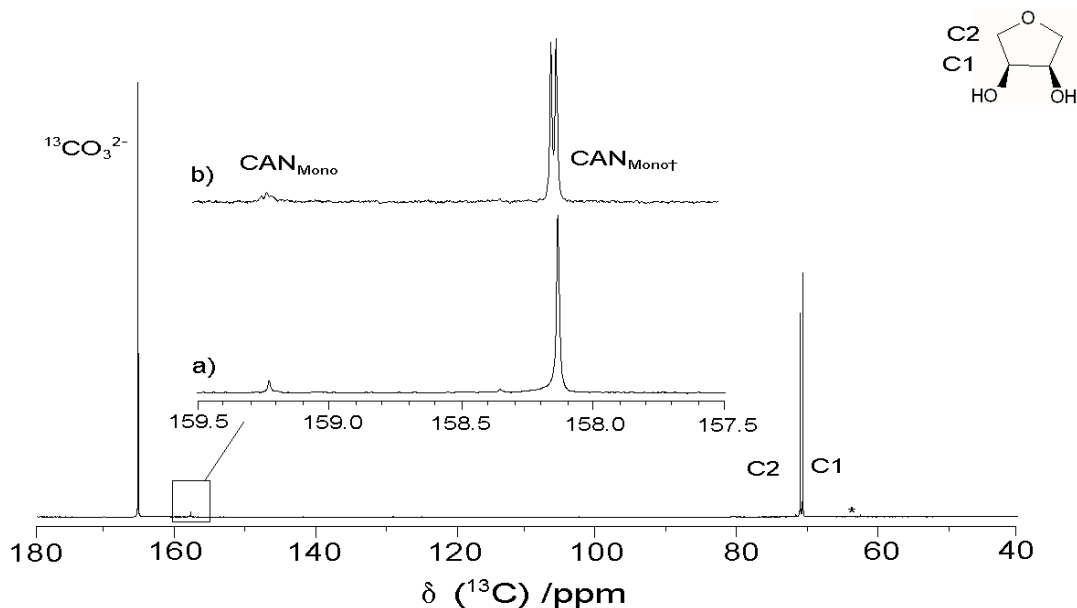


Figure 3.23. Carbon-13 NMR spectrum of an aqueous solution containing 0.27 mol kg^{-1} $\text{Na}_2^{13}\text{CO}_3$ and 4.0 mol kg^{-1} 1,4-anhydroerythritol at $5 \text{ }^\circ\text{C}$. The expanded region is shown a) with and b) without gated ^1H decoupling. The asterisk denotes an impurity.

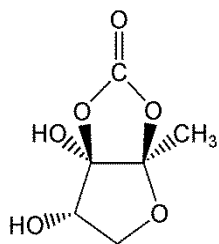


Figure 3.24. A revised version of the carbonate-THMF complex proposed by McKenzie *et al.*^[14] to account for enhanced AI-2 quorum sensing in *V. harveyi*.

Figure 3.25 shows the ^{13}C NMR spectrum of a solution containing $0.044 \text{ mol kg}^{-1}$ $\text{Na}_2^{13}\text{CO}_3$ and 0.72 mol kg^{-1} cytidine at pH 9.1. There are four signals corresponding to carbonate-cytidine complexes present. The signal at 158.5 ppm is split into a triplet from the long distance scalar coupling to the ligand protons and therefore corresponds either to a mono-ester complex in which carbonate is bound through the C_5 hydroxyl group or a di-ester complex in which carbonate is bound through the C_2 and C_3 hydroxyl groups. Adenosine triphosphate (ATP), which contains a phosphate group blocking the C_5 hydroxyl position, was employed to determine the identity of this signal. Figure 3.26 shows the ^{13}C NMR spectrum of a solution containing $0.030 \text{ mol kg}^{-1}$ $\text{Na}_2^{13}\text{CO}_3$ and 0.88 mol kg^{-1} ATP at pH 7.2. No carbonate-ATP complexes were detected. As the most dominant ester-linked complex was no longer present when a phosphate group blocked the C_5 position, the carbonate-cytidine signal at 158.5 ppm likely corresponds to the mono-ester complex $\text{CCY}_{\text{Mono5}\ddagger}$ (Table 3.9). The two signals at 157.3 and 156.8 ppm in Figure 3.25 have been assigned to mono-ester complexes, denoted as $\text{CCY}_{\text{Mono2}\ddagger}$ and $\text{CCY}_{\text{Mono3}\ddagger}$, in which carbonic acid is bound to the ligand C_2 or C_3 hydroxyl groups. Only the coupling of the signal at 157.5 ppm could be resolved (split into a doublet), as the signal at 156.8 ppm overlaps with that corresponding to the C_6 carbon on cytidine. However, its close proximity to the signal at 157.5 ppm would suggest that it is also a mono-ester complex. The signal at 165.20 ppm has been assigned to di-ester complex CCY_{Mono} . The scalar coupling could not be resolved, but with the lack of other binding sites available and the up-frequency shift from the signals corresponding to the mono-ester complexes, it likely corresponds to a di-ester complex. It is highly probable that the di-ester linkage occurs at the C_2 and C_3 hydroxyl groups, analogous to the di-ester complex formed with 1,4-anhydroerythritol.

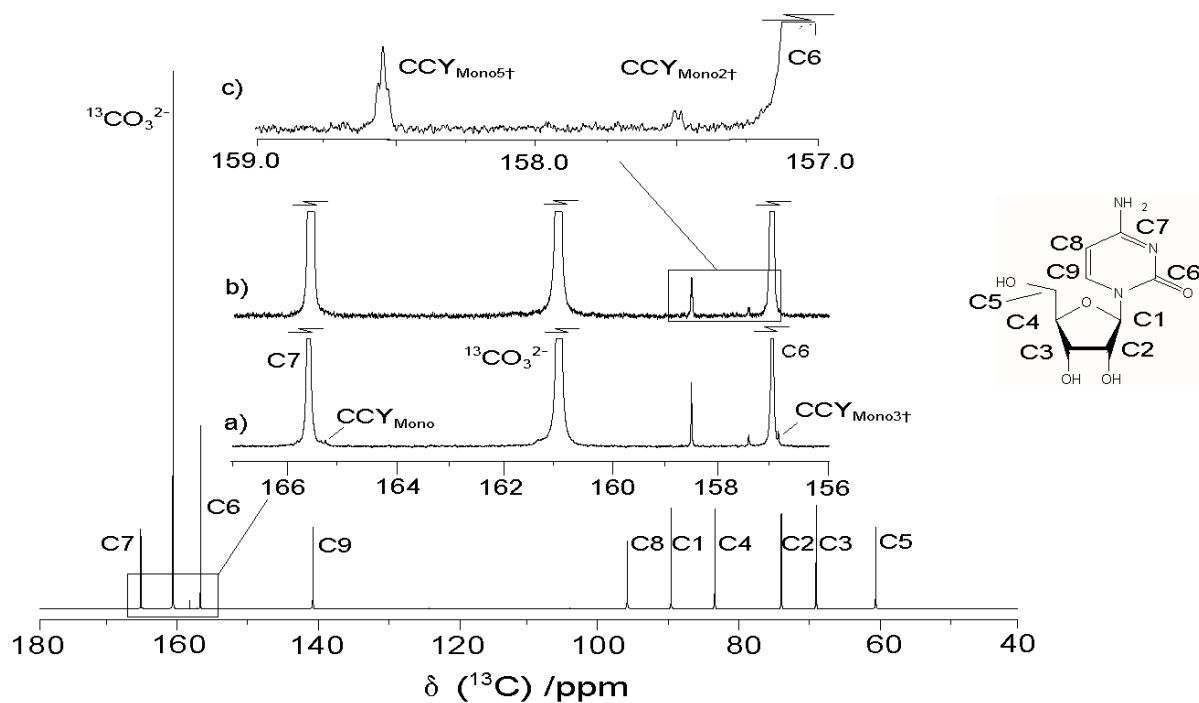


Figure 3.25. Carbon-13 NMR spectrum of an aqueous solution containing $0.044 \text{ mol kg}^{-1}$ $\text{Na}_2^{13}\text{CO}_3$ and 0.72 mol kg^{-1} cytidine at pH 9.1 and 5°C . The expanded region is shown a) with and b) without gated ^1H decoupling, with another expansion (c) of the resolved coupling.

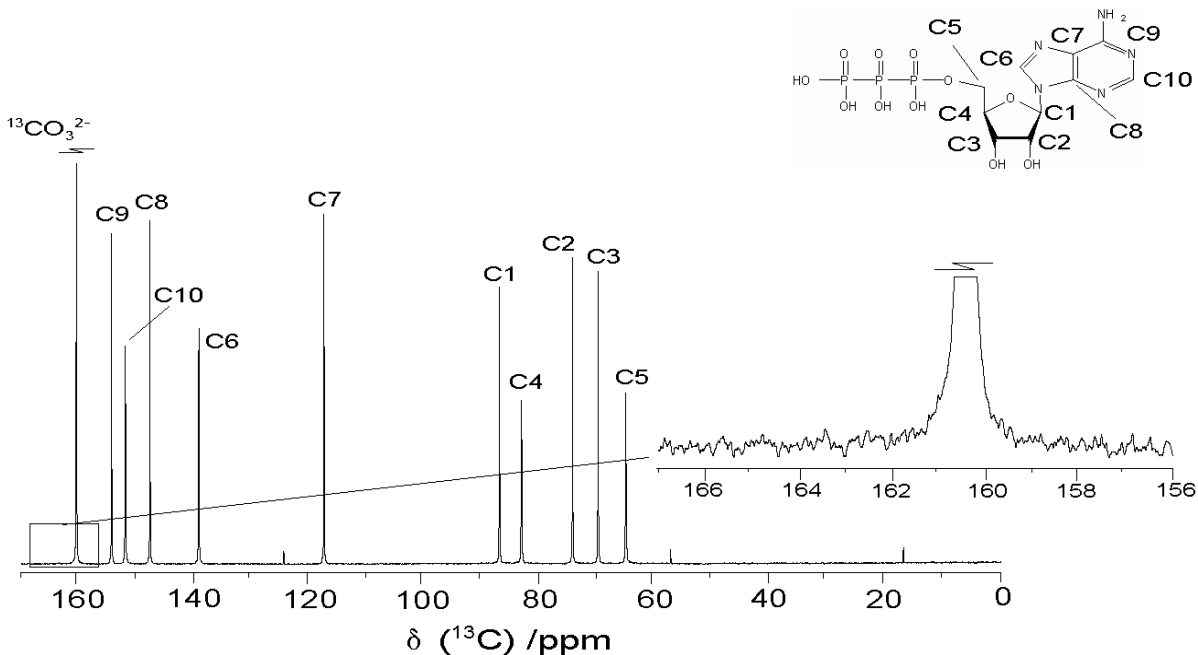


Figure 3.26. Carbon-13 NMR spectrum of an aqueous solution containing $0.030 \text{ mol kg}^{-1}$ $\text{Na}_2^{13}\text{CO}_3$ and 0.88 mol kg^{-1} adenosine triphosphate at pH 7.2 and 25°C . The signals at 57.3 and 16.8 ppm correspond to impurities as they were present in the ^{13}C NMR spectrum of a neat ATP solution.

Table 3.9. Representative ^{13}C NMR peak assignments for carbonate complexes of furanoidic vicinal *cis*-diols^a

furanoidic vicinal <i>cis</i> -diol	Structure	Notation ^b	$^3J(^{13}\text{C}, ^1\text{H})$ coupling of ^{13}C NMR carbonate signal (/Hz) ^c
<i>cis</i> -1,2-cyclopentanediol		$\text{CC}_{\text{Mono1}\dagger}$	2.7 (d)
1,4-anhydroerythritol		$\text{CAN}_{\text{Mono1}\dagger}$ CAN_{Mono}	2.6 (d) 2.5 (t)
cytidine		$\text{CCY}_{\text{Mono2}\dagger}$ $\text{CCY}_{\text{Mono3}\dagger}$ $\text{CCY}_{\text{Mono5}\dagger}$ CCY_{Mono}	2.8 (d) nr 2.5 (t) nr

^a Representative chemical shifts were not included due to their large dependency on pH ^b The symbol † denotes a mono-ester linkage between the carbonate centre and ligand. C = *cis*-1,2-cyclopentanediol, AN = 1,4-anhydroerythritol and CY = cytidine. ^c Multiplicity is represented by t (triplet) or d (doublet). nr = not resolved.

We next investigated complexation by D-ribose and D-fructose, which share two additional characteristics of S-DPD: a) each occurs in solution as a family of interconverting molecules, containing multiple binding sites for carbonic acid; and b) each decomposes in alkaline solution. Figures 3.27 and 3.28 show ^{13}C NMR spectra for solutions respectively containing: $0.24 \text{ mol kg}^{-1} \text{ Na}_2^{13}\text{CO}_3$ and 4.0 mol kg^{-1} D-ribose at pH 7.0; and $0.044 \text{ mol kg}^{-1} \text{ Na}_2^{13}\text{CO}_3$ and 2.0 mol kg^{-1} D-fructose at pH 9.6. Many signals appear down-frequency of the

free carbonic acid signal in each spectrum, indicating the formation of multiple carbonate-saccharide complexes. Doublet resonances correspond to mono-ester complexes and triplets to either mono-ester complexes bound through a terminal hydroxyl group or di-ester complexes bound through adjacent hydroxyl groups. The structures of individual complexes could not be identified, however, owing to the co-existence of different isomeric forms of the saccharide (acyclic, furanoidic and pyranoidic), all of which are capable of binding carbonic acid.

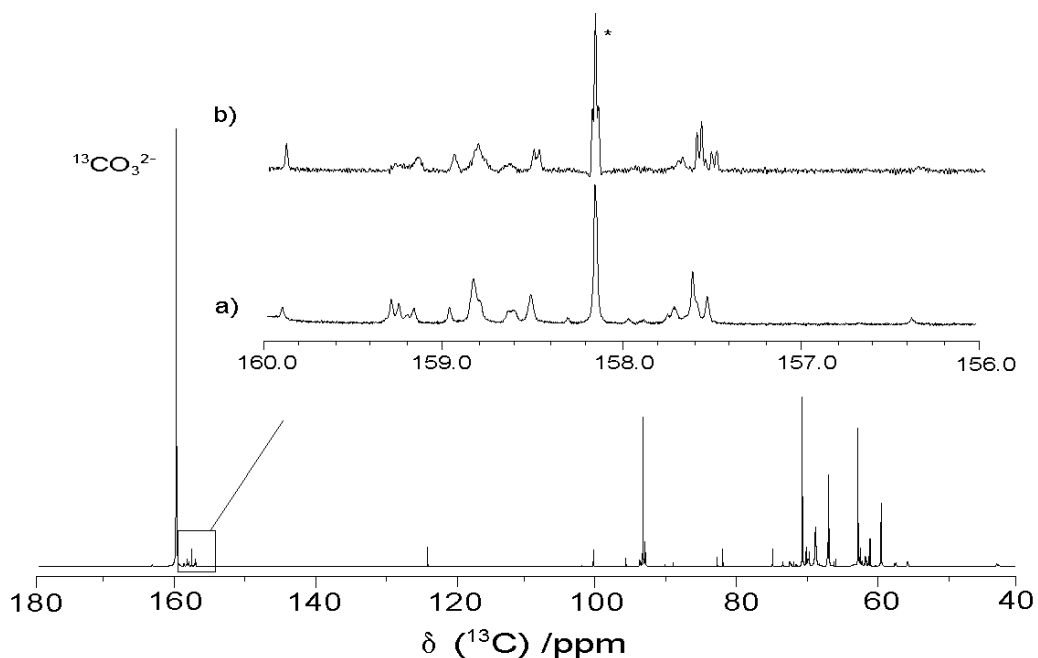


Figure 3.27. Carbon-13 NMR spectrum of an aqueous solution containing $0.24 \text{ mol kg}^{-1} \text{ Na}_2^{13}\text{CO}_3$, 0.96 mol kg^{-1} tris buffer and 4.0 mol kg^{-1} D-ribose at pH 7 and 5°C . The expanded region is shown a) with and b) without gated ^1H decoupling. The signal at 158.2 ppm (marked with an asterisk) corresponds to carbonate-tris buffer complex (Appendix I). (A Lorentzian-Gaussian function was employed with $\text{LB} = -2.5 \text{ Hz}$ and $\text{GB} = 0.35 \text{ Hz}$.)

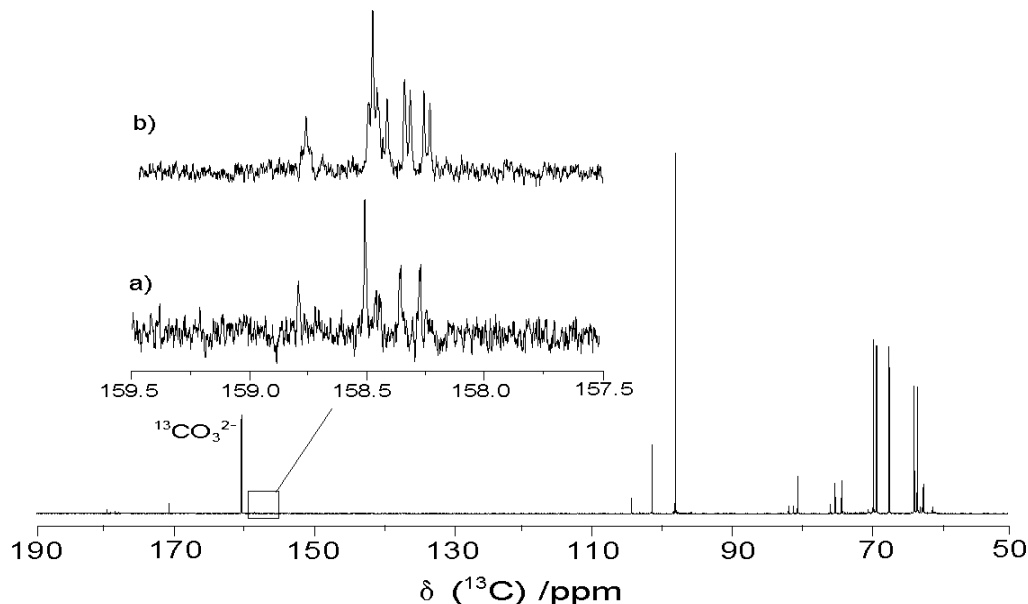


Figure 3.28. Carbon-13 NMR spectrum of an aqueous solution containing $0.044 \text{ mol kg}^{-1}$ $\text{Na}_2^{13}\text{CO}_3$ and 2.0 mol kg^{-1} D-fructose at pH 9.6 and 5°C . The expanded region is shown a) with and b) without gated ^1H decoupling.

Synthetic S-DPD is commercially available (OMM Scientific) at 4 mM concentration in a pH 2 solution.^[99] At higher concentrations or in an alkaline environment the stability of the compound decreases significantly.^[24, 39] Using ribose as a proxy for DPD, we set out to determine whether it would be possible to obtain ^{13}C NMR spectroscopic evidence of carbonate complexation under such dilute conditions. Figure 3.29 shows the ^1H -decoupled ^{13}C NMR spectrum of a pH 7.0 solution containing $0.051 \text{ mol kg}^{-1}$ $\text{Na}_2^{13}\text{CO}_3$ and 4 mmol kg^{-1} D-ribose. Even though the preceding results make it virtually certain that a large number of different carbonate-ribose complexes exist in solution, all were present at concentrations below the detection limit. This is not surprising. Not only were the saccharide concentrations in the preceding examples orders of magnitude higher, a smaller number of different complexes were formed. In the case of DPD, we estimate that at least 14 different mono-ester complexes and 4 different di-ester complexes can exist in solution. Thus, no single species would be concentrated enough to be detectable by ^{13}C NMR spectroscopy. Nonetheless, the extensive evidence provided above of carbonate-saccharide complexes spontaneously forming at physiological pHs enables us to be confident that many if not all of these species do indeed exist.

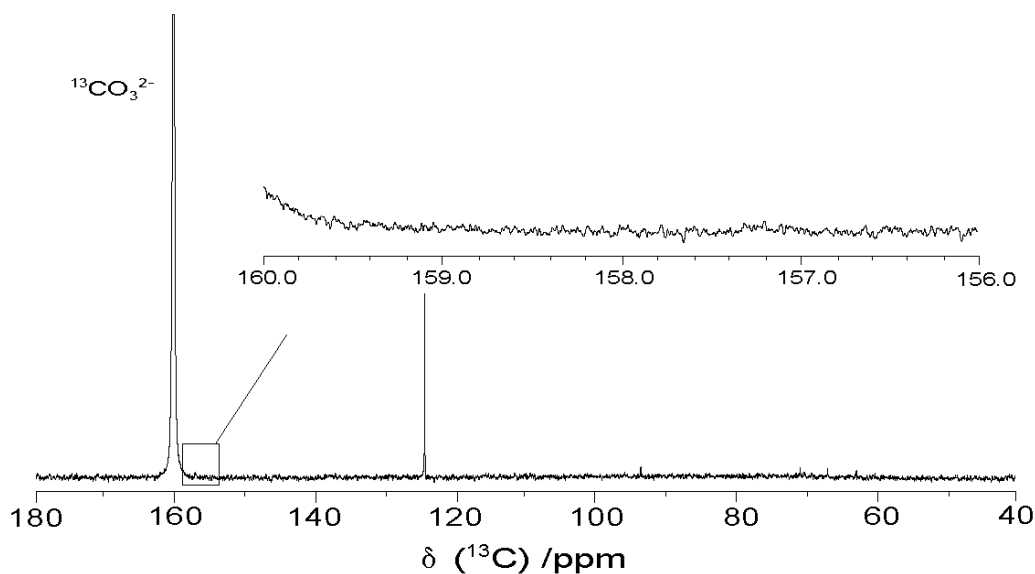
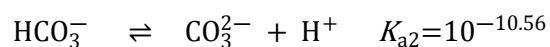
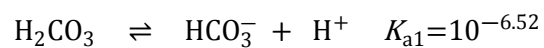


Figure 3.29. Carbon-13 NMR spectrum of an aqueous solution containing $0.051 \text{ mol kg}^{-1}$ $\text{Na}_2^{13}\text{CO}_3$ and $3.9 \times 10^{-3} \text{ mol kg}^{-1}$ D-ribose at pH 7.0 and 5°C . The inset spectrum corresponds to the region where ester linked carbonic acid-ribose complexes have been shown to resonate. The spectrum was acquired using 7180 $\pi/2$ pulses, a 4 s inter-pulse delay and gated ^1H decoupling. The signal at 124.3 ppm corresponds to $\text{CO}_{2(\text{aq})}$.

E. Formation constants of the carbonate-saccharide complexes

Formation constants were determined for the select carbonate-ligand complexes. The representative polyols and furanoidic vicinal cis-diols that were used in determining borate formation constants were also employed here. As with the other oxoacids, we represent the complexation commencing through fully protonated carbonic acid.

Carbonic acid undergoes deprotonation as pH is increased



and, thus,

$$[\text{H}_2\text{CO}_3] = \frac{C_T [\text{H}^+]^2}{[\text{H}^+]^2 + [\text{H}^+]K_{a1} + K_{a1}K_{a2}}$$

where

$$C_T = [\text{H}_2\text{CO}_3] + [\text{HCO}_3^-] + [\text{CO}_3^{2-}]$$

Formation constants for carbonate-saccharide complexes are therefore given by:

$$\begin{aligned} \text{H}_2\text{CO}_3 + \text{L} &\rightleftharpoons \text{HOOC-L} + \text{H}_2\text{O} \\ c\beta_{\text{Mono}\dagger} &= \frac{[\text{HOOC-L}]}{[\text{H}_2\text{CO}_3][\text{L}]} = \frac{[\text{HOOC-L}]([\text{H}^+]^2 + [\text{H}^+]K_{a1} + K_{a1}K_{a2})}{[\text{L}]C_T [\text{H}^+]^2} \end{aligned}$$

$$\begin{aligned} \text{H}_2\text{CO}_3 + \text{L} &\rightleftharpoons \text{OC=L} + 2\text{H}_2\text{O} \\ c\beta_{\text{Mono}} &= \frac{[\text{OC=L}]}{[\text{H}_2\text{CO}_3][\text{L}]} = \frac{[\text{OC=L}]([\text{H}^+]^2 + [\text{H}^+]K_{a1} + K_{a1}K_{a2})}{[\text{L}]C_T [\text{H}^+]^2} \end{aligned}$$

where L represents saccharide, $K_w = [\text{H}^+][\text{OH}^-]$ and “-L” & “=L” represent mono- and di-ester saccharide linkages, respectively.

Carbonic acid ionization constants were directly taken from Nakayama^[100] ($pK_{a1} = 6.36$ at 25 °C and 6.52 at 5 °C; $pK_{a2} = 10.33$ at 25 °C and 10.56 at 5 °C). The concentrations of carbonic acid (C_T), the two carbonate complexes ((HO)OC-L, OC=L) and free ligand (L) were determined through integration of the ¹H-decoupled ¹³C NMR spectra, and the concentration of H⁺ was obtained from pH measurements. The precision of formation constants reported in this section is necessarily limited because of the relatively small number of solutions that were used to generate them (Appendix VII). Nonetheless, the solutions covered a pH ranging from 8 to 11.5 and therefore should reliably extrapolate down to physiological conditions.

Table 3.10 shows the formation constants for carbonate-furanoidic *cis*-diol complexes at 5 and 25 °C. Initially, we set out to determine constants only at 5 °C, but the solubility of 1,4-

anhydroerythritol at that temperature was too low for the di-ester complex to be detected. Therefore, all measurements were repeated at 25 °C. There is no significant difference in formation constants between the ligands, as the uncertainty associated with these values is very high. However, only ligands containing an oxygen heteroatom ring (1,4-anhydroerythritol, cytidine) were determined to form di-ester complexes with carbonic acid, which would suggest that ligands with electron withdrawing heteroatoms have a greater binding affinity than ligands lacking these heteroatoms. The formation constants for D-fructose were not included since whether the complexes were mono- or di-ester species could not be determined (discussed in Section 3.2.2D).

Table 3.11 shows the formation constants for the carbonate-polyol complexes. The mono-ester complex formation constants with the polyols were slightly larger than those of the furanoidic *cis*-diol, which we suspect is due to the increased number of hydroxyl groups, and therefore carbonate binding sites, on the polyols. However, the number of hydroxyl groups on the polyols, *i.e.*, threitol vs. xylitol, had no effect on the formation constants. Similarly, the dihydroxy functionality of the ligand *i.e.*, *threo* vs. *erythro*, did not change its binding affinity towards carbonic acid.

Table 3.10. Formation constants for carbonate-furanoidic *cis*-diol complexes at 5 and 25 °C

		<i>cis</i> -1,2-cyclopentanediol	1,4-anhydroerythritol	cytidine
$\log {}^c\beta_{\text{Mono}\dagger}$	5 °C	0.5 ± 1.5	0.3 ± 1.2	1.0 ± 1.5
	25 °C	0.5 ± 1.0	1.2 ± 1.0	3.2 ± 1.4
$\log {}^c\beta_{\text{Mono}}$	5 °C	nd	nd	0.3 ± 1.5
	25 °C	nd	0.4 ± 1.0	0.2 ± 1.0

nd = not detectable.

Table 3.11. Formation constants for carbonate-polyol complexes at 5 °C.

	threitol	erythritol	xylitol	adonitol
$\log {}^C\beta_{\text{Mono}\dagger}$	2.7 ± 1.0	2.7 ± 1.2	2.5 ± 1.5	2.6 ± 1.6
$\log {}^C\beta_{\text{Mono}}$	nd	nd	nd	nd

nd = not detectable.

3.2.3 Silicate-saccharide complexes

Previous studies indicate that silicic acid silicon would indeed be capable of binding both *S*- and *R*-THMF (likely forming *bis*-ligand silicate complexes in which silicon has five-fold coordination).^[15, 16] We had initially hoped to obtain direct ²⁹Si NMR spectroscopic evidence of these complexes, but the instability of *S*-DPD derivatives in an alkaline environment and the low solubility of silicic at pH < 10 make it unlikely that silicate-THMF species would be detectable by ²⁹Si or ¹³C NMR spectroscopy. We adjusted solution conditions in an attempt to either increase stability of the *S*-DPD derivatives or to create a “cell-like” environment in the NMR tube (Appendix II-IV), but these experiments were either unsuccessful or involved preparation processes which would result in ligand decomposition.

Alternatively, we performed experiments to obtain silicate-saccharide formation constants which could be compared to those we have reported above for analogous borate and carbonate complexes. The general structure and chemical shifts of the silicate-saccharide species investigated in this study are found in Table 3.12 and a sample ²⁹Si NMR spectrum is found in Figure 3.30.

Table 3.12. Representative silicate complexes with polyhydroxy molecules and the corresponding ^{29}Si NMR chemical shift ranges.

Notation	Structure	^{29}Si NMR chemical shift range /ppm ^a
silicate <i>mono</i> -saccharide mono-ester complex (SiS_{Mono})		-0.2 to -2.5
silicate <i>bis</i> -saccharide complex (SiS_{Bis})		-25 to -36
silicate <i>tris</i> -saccharide complex (SiS_{Tris})		-60 to -80

^a Referencing to $\text{Si}(\text{OH})_4$ to 0 ppm.

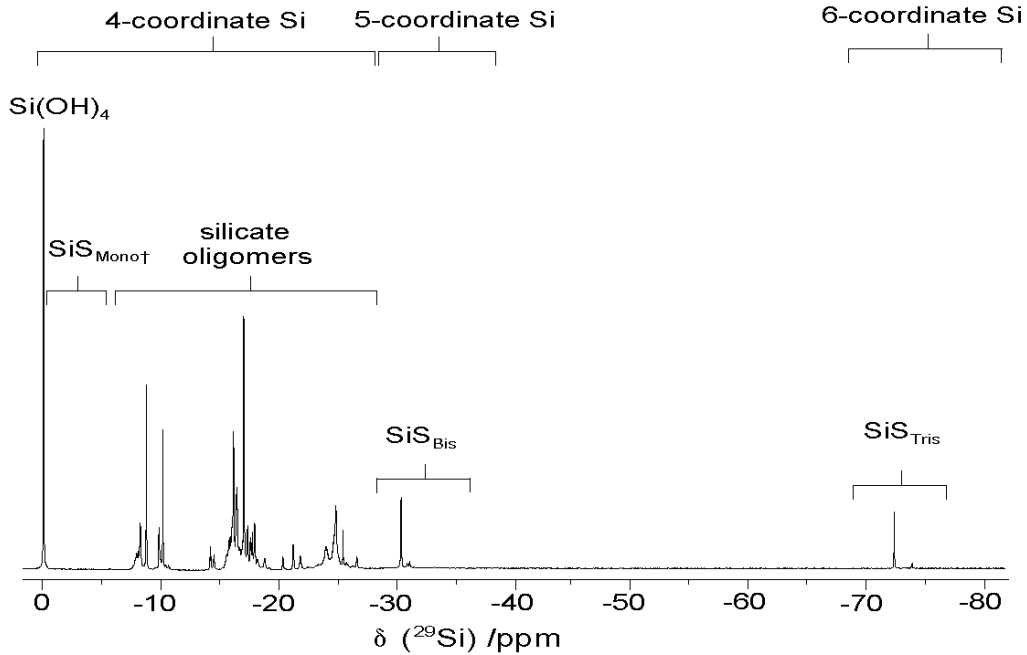
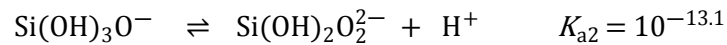
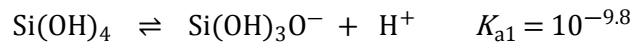


Figure 3.30. Silicon-29 NMR spectrum (99.28 MHz) of an aqueous solution containing 1.0 mol kg⁻¹ ²⁹SiO₂, 1.7 mol kg⁻¹ KOH and 1.7 mol kg⁻¹ mannitol at 5 °C. The regions corresponding to the principal silicate species are shown. (No SiS_{Mono†} species detected).

A. Formation constants of the silicate-saccharide complexes

Silicic acid ionization undergoes deprotonation as pH is increased



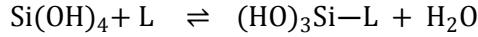
Thus,

$$[\text{Si(OH)}_4] = \frac{[\text{Q}^0][\text{H}^+]^2}{[\text{H}^+]^2 + K_{a1}[\text{H}^+] + K_{a1}K_{a2}}$$

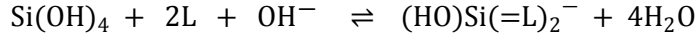
where

$$\text{Q}^0 = [\text{Si(OH)}_4] + [\text{Si(OH)}_3\text{O}^-] + [\text{Si(OH)}_2\text{O}_2^{2-}]$$

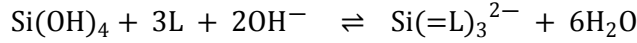
Formation constants for silicate complexes are therefore given by:



$${}^{\text{Si}}\beta_{\text{Mono}^\dagger} = \frac{[(\text{HO})_3\text{Si-L}]}{[\text{Si(OH)}_4][\text{L}]} = \frac{[(\text{HO})_3\text{Si-L}]([\text{H}^+]^2 + K_{a1}[\text{H}^+] + K_{a1}K_{a2})}{[Q^0][\text{L}]}$$



$${}^{\text{Si}}\beta_{\text{Bis}} = \frac{[(\text{HO})\text{Si(=L)}_2^-]}{[\text{Si(OH)}_4][\text{L}]^2[\text{OH}^-]} = \frac{[(\text{HO})\text{Si(=L)}_2^-]([\text{H}^+]^2 + K_{a1}[\text{H}^+] + K_{a1}K_{a2})}{[Q^0][\text{L}]^2 K_w [\text{H}^+]}$$



$${}^{\text{Si}}\beta_{\text{Tris}} = \frac{[\text{Si(=L)}_3^{2-}]}{[\text{Si(OH)}_4][\text{L}]^3[\text{OH}^-]^2} = \frac{[\text{Si(=L)}_3^{2-}]([\text{H}^+]^2 + K_{a1}[\text{H}^+] + K_{a1}K_{a2})}{[Q^0][\text{L}]^3 (K_w [\text{H}^+])^2}$$

where L represents a saccharide, $K_w = [\text{H}^+][\text{OH}^-]$, and “-L” and “=L” represent mono- and di-ester saccharide linkages, respectively.

The appropriate ionization constants at 5 °C and $I = 1$ for silicic acid (pK_{a1} , pK_{a2}) and water (pK_w) were interpolated from data reported by Sjöberg, Busey and Hawkes:^[91, 101, 102] $pK_{a1} = 9.8 \pm 0.1$; $pK_{a2} = 13.1 \pm 0.2$; and $pK_w = 14.6 \pm 0.1$. The uncertainty surrounding the ionization constants (from the interpolation) had had little effect on the formation constants as the values remained well within experimental uncertainties.

The concentration of the various silicate containing species were determined through integration of the ^1H -decoupled ^{29}Si NMR spectra. Knowing the L:Si ratio for each of the silicate complexes, the free saccharide could also be determined through integration of ^{29}Si NMR spectra. The concentration of H^+ was determined through pH measurements. A minimum of three solutions (unless otherwise stated), with varying compositions were used to determine the formation constants (Appendix VIII). Because they were limited to a pH range of 11.8 to 14, the accuracy of these constants physiological conditions are probably qualitative at best.

Table 3.13 shows the formation constants for the silicate-furanoidic *cis*-diol complexes. The formation constants for the *bis*-ligand complexes with ligands containing an oxygen heteroatom (1,4-anhydroerythritol) and electron withdrawing functional groups (D-fructose and cytidine) were larger (ca. 1 order of magnitude) than that for the ligand lacking these properties (*cis*-1,2-cyclopentanediol). There is increased uncertainty when comparing these formation constants, however, as some were determined at 2 °C (compared to 5 °C). The *tris*-ligand complexes with *cis*-1,2-cyclopentanediol and 1,4-anhydroerythritol were not detected in the NMR spectrum. However, the formation constants for these complexes with D-fructose and cytidine were greater than those of the *bis*-ligand complexes.

Table 3.14 shows the formation constants for the silicate-polyols complexes at 5 °C. The formation constants for the polyols were generally smaller than those for the furanoidic *cis*-diols, although some of the larger polyols (xylitol, mannitol) had similar values. The formation constants for the polyols with *threo*-dihydroxy functionality were roughly one order of magnitude greater than those for the polyols lacking this functionality. There was also an increase in binding affinity when the chain length of the polyol was increased. The formation constants for the silicate-xylitol complexes were greater than those of the other polyols. We suspect the increase in binding affinity arises from the two sets of dihydroxy groups with *threo*-functionality on xylitol, whereas other ligands have one or none at all (except iditol). Likewise, a ligand with three sets of *threo*-dihydroxy functional groups (iditol) was also found to bind Si very strongly, so greatly that it forms six-coordinate silicate *bis*-ligand complexes.^[64] As with the furanoidic *cis*-diols, the formation constants for the *tris*-ligand species with polyols containing *threo*-dihydroxy functionality exceeded those of the *bis*-ligand complexes. No *tris*-ligand species were detected with polyols lacking *threo*-dihydroxy functionality.

Table 3.13. Formation constants for silicate-furanoidic *cis*-diol complexes at 5 °C.

	<i>cis</i> -1,2-cyclopentanediol ^a	1,4-anhydroerythritol ^a	D-fructose	cytidine
$\log \beta_{\text{Bis}}^{\text{Si}}$	3.5	5.8	5.3 ± 0.8	5.9 ± 0.8
$\log \beta_{\text{tris}}^{\text{Si}}$	nd	nd	7.9 ± 1.5	7.7 ± 0.9

nd = not detectable. ^a Determined at 2 °C, recalculated from Wen.^[65]

Table 3.14. Formation constants for silicate-polyol complexes at 5 °C.

	threitol ^a	erythritol ^a	xylitol	arabitol ^a	adonitol ^a	mannitol ^a	iditol ^a	allitol
$\log \beta_{\text{Mono}}^{\text{Si}}$	nd	1.4 ± 0.5	nd	nd	2.7 ± 1.2	nd	nd	nd
$\log \beta_{\text{Bis}}^{\text{Si}}$	3.9 ± 0.9	3.0 ± 0.5	5.6 ± 0.5	4.7 ± 0.3	3.5 ± 0.6	4.8 ± 0.5	4.9 ± 0.4 7.2 ± 0.7 ^b	5.0 ± 0.8 ^c
$\log \beta_{\text{Tris}}^{\text{Si}}$	4.4 ± 0.9	nd	7.7 ± 1.2	5.7 ± 1.0	nd	6.8 ± 0.8	nd	nd

nd = not detectable. ^a Recalculated values from Vis.^[64] ^b Six-coordinated silicon *bis*-ligand complex. ^c Only generated using two different solution compositions.

The biological data reported by Noroozi indicates that silicic acid increases the bioluminescence activity of *V. harveyi*.^[17] The data would suggest that silicic acid is modulating AI-2 quorum sensing in a fashion similar to that of boric acid and carbonic acid. The structure of the potential oxoacid bound form of the S-DPD derivative is unknown.

3.2.4 Stannate-saccharide complexes

The only evidence to support stannic acid being complexed by polyhydroxy hydrocarbons in aqueous solution was reported by Mbabazi.^[70-73] Using conductimetry, they determined that di-ester mono-ligand complexes between stannic acid and polyhydroxy molecules, including mannitol and D-fructose, formed in solution at pH 11. However, nothing was revealed about the structure of the resulting complexes. An experimental difficulty encountered in their work was the low stability of Sn(IV) at elevated pH and in the present of alkali metals. Therefore, we used tetramethylammonium hydroxide in place of alkali metal hydroxide, since organic cations have been shown to stabilize stannate in alkaline solutions.^[75] The ¹¹⁹Sn NMR spectrum of an alkaline stannate solution yields two signals which correspond to a six-coordinate stannic acid monomer (Sn(OH)₆²⁻ at -590.8 ppm)^[103] and a tentatively

proposed stannate dimer ($\text{Sn}_2(\text{OH})_{10}^{2-}$ at -536.7 ppm).^[104] Here we report the first structural characterization of organostannate complexes formed in aqueous solution with a wide variety of different alcohol and saccharide molecules.

A. Complexes of simple alcohols.

Figure 3.31 shows the ^{119}Sn NMR spectrum of a solution containing 0.22 mol kg^{-1} Sn and 3.39 mol kg^{-1} methanol. The quartet signal at -596.9 ppm exhibits $J(^{119}\text{Sn}, ^1\text{H}) = 48$ Hz, which is consistent with three bond scalar coupling reported for various organotin complexes.^[105, 106] Given that the hydroxyl protons on stannic acid rapidly exchange with water, the splitting must arise from coupling with the methyl protons. This signal corresponds to a novel mono-ester complex between stannic acid and methanol, denoted in Table 3.15 as **SnM_{Monot}**. Its close proximity to the stannic acid signal would suggest that the stannate centre maintains six-fold coordination in this complex. Indeed, ^{119}Sn chemical shifts reported for organotin compounds in which Sn is four- or five-coordinate are above -230 ppm, whereas those for which Sn is six-coordinate are below -360 ppm.^[107, 108]

Figure 3.32 shows the ^1H -decoupled ^{119}Sn NMR spectrum of a stannate solution containing 0.21 mol kg^{-1} Sn and 6.6 mol kg^{-1} ethanol. One new signal is evident at -599.4 ppm. Owing to the similarity in chemical shift, it can reasonably be assumed to correspond to a complex analogous to the stannate-methanol complex and is denoted as **SnEt_{Monot}** (Table 3.15).

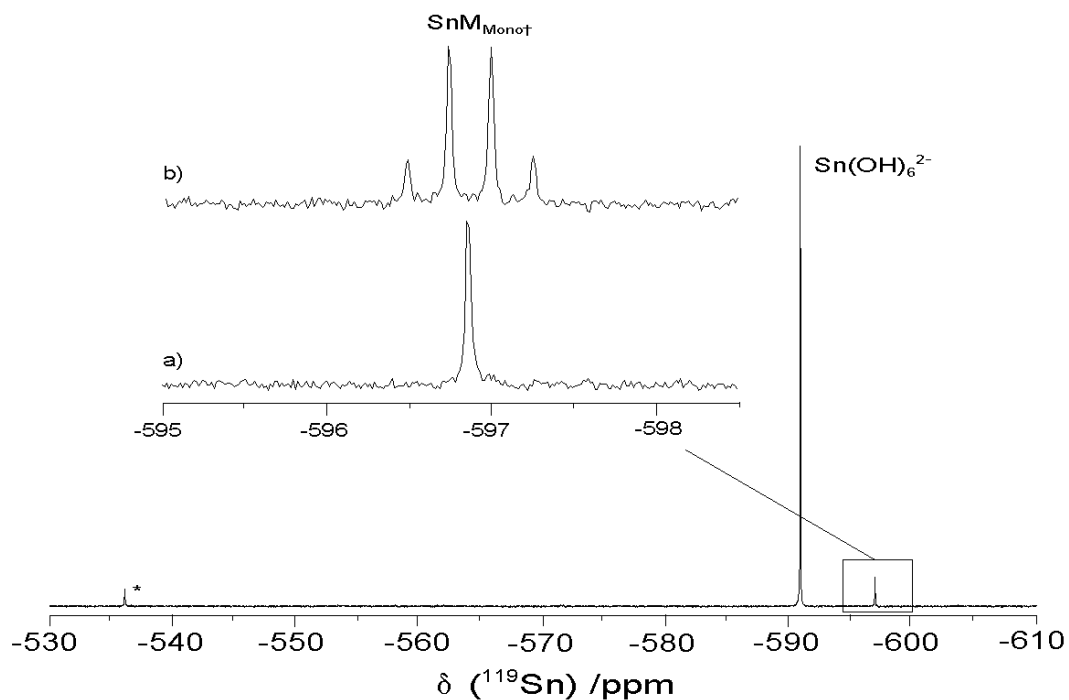


Figure 3.31. Tin-119 NMR spectra (186.35 MHz) of an aqueous solution containing $0.22 \text{ mol kg}^{-1} \text{ Sn}$, 3.4 mol kg^{-1} methanol, 3.1 mol kg^{-1} TMAOH and 0.83 mol kg^{-1} HCl at 5°C . The expanded region is shown a) with and b) without gated ^1H -decoupling. The signal corresponding to the proposed stannic acid dimer is marked with an asterisk.

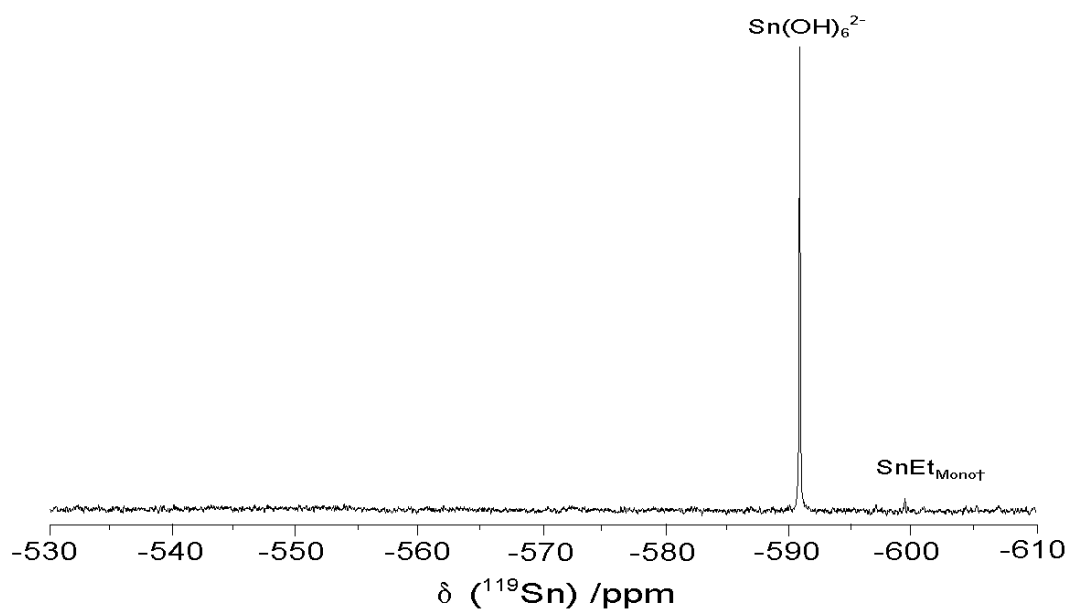
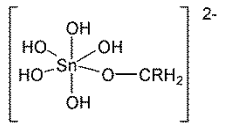
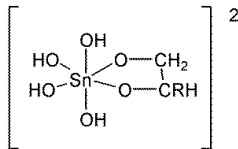
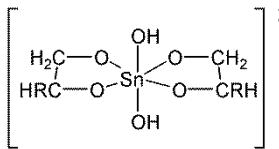
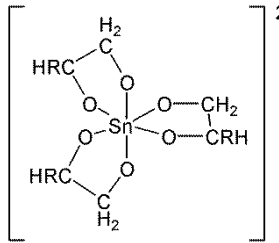
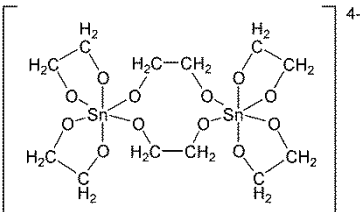
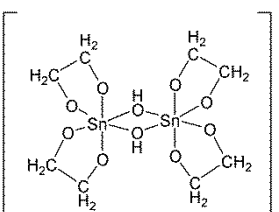


Figure 3.32. $^{119}\text{Sn} \{^1\text{H}\}$ NMR spectrum of an aqueous solution containing $0.21 \text{ mol kg}^{-1} \text{ Sn}$, 6.6 mol kg^{-1} ethanol, 2.9 mol kg^{-1} TMAOH and 0.77 mol kg^{-1} HCl at 5°C .

Table 3.15. Stannate complexes with simple alcohols.

Ligand	Structure	Notation ^a	¹¹⁹ Sn NMR chemical shift /ppm ^{b,c} (multiplicity, ³ J(¹¹⁹ Sn, ¹ H) /Hz)
Simple alcohols methanol (R = H) ethanol (R = CH ₃)		SnM_{Mono†} SnEt_{Mono†}	-596.9 (q, 48) -599.4 (nr)
		SnG_{Mono} SnP_{Mono}	-558.1 (p, 56) -554.9 (nr)
		SnG_{Bis} SnP_{Bis}	-526.3 (n, 54) -518 to -522 (nr)
1,2-alkyldiols ethane-1,2-diol (R = H) propane-1,2-diol (R = CH ₃)		SnG_{Tris} SnP_{Tris}	-494.7 (nr) -484 to -498 (nr)
		Sn₂G_{Tris}	-499.8 (nr)
		Sn₂G_{Bis}	-466.9 (nr)

^a The symbol † denotes a mono-ester linkage between the stannate centre and ligand, M = methanol, Et = ethanol, G = ethane-1,2-diol and P = propane-1,2-diol ^b Multiplicity = q (quartet), p (pentet), n (nonet) or nr = not resolved ^c Chemical shifts are only representative as they vary with solution conditions.

Figure 3.33 shows ^1H -decoupled ^{119}Sn NMR spectra of aqueous stannate solutions with added ethane-1,2-diol. As the concentration of alcohol was increased, the equilibrium shifted towards species corresponding to the signals at higher frequency, which would suggest that these species have a larger ligand:stannate ratio than the species corresponding to the signals at lower frequency. There is a uniform up-frequency shift (approximately 32 ppm) from the stannic acid monomer signal to those corresponding to the stannate-ethane-1,2-diol complexes, which would suggest that there is a uniform increase in ligands attached to the stannate centre. It is evident that the additional hydroxyl group on ethane-1,2-diol shifts the equilibrium from the formation of mono-ester complexes towards the formation of many di-ester complexes.

The signal at -558.1 ppm is split into a pentet by three bond coupling to the ligand $-\text{CH}_2-$ protons (Figure 3.34). As *bis*-ligand stannate complexes were not detected with methanol or ethanol, an analogous complex would likely not form with ethane-1,2-diol. Therefore, this signal has been assigned to a *mono*-ligand di-ester complex, denoted as SnG_{Mono} (Table 3.15), in which the Sn centre retains six-fold coordination.

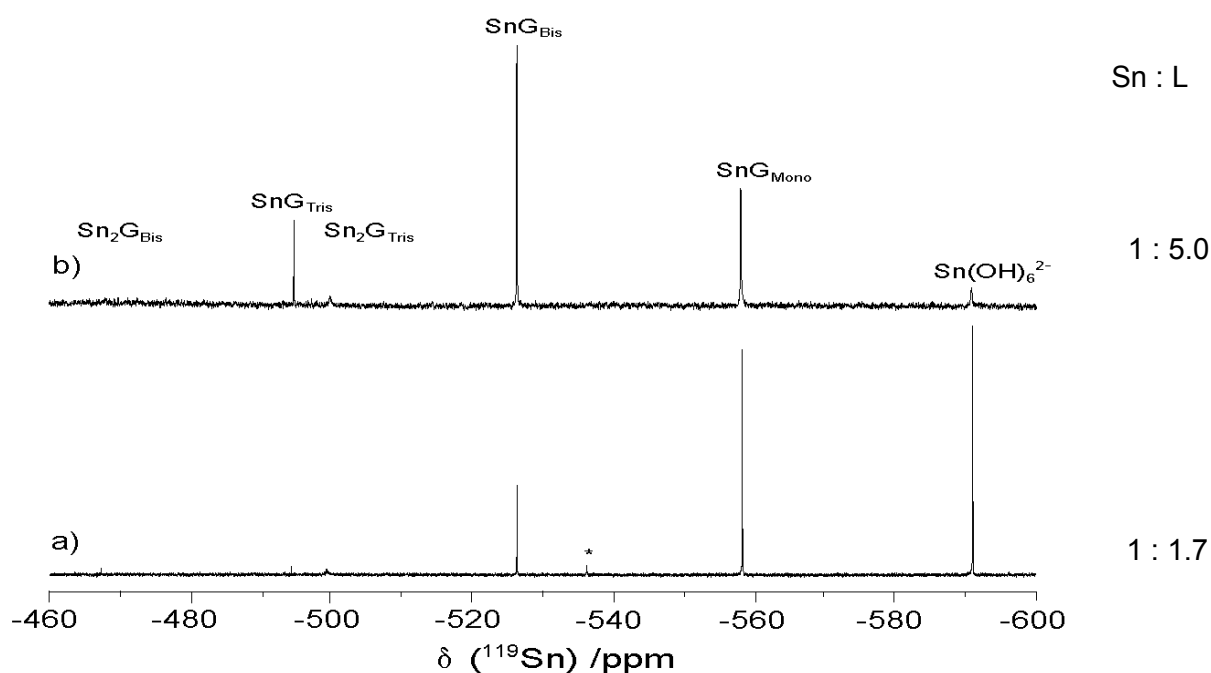


Figure 3.33. ^{119}Sn $\{^1\text{H}\}$ NMR spectra at 21°C of the aqueous solutions containing a) 0.18 mol kg^{-1} Sn, 0.31 mol kg^{-1} ethane-1,2-diol, 2.3 mol kg^{-1} TMAOH and 1.8 mol kg^{-1} HCl at 5°C , and b) 0.19 mol kg^{-1} Sn, 0.95 mol kg^{-1} ethane-1,2-diol, 2.4 mol kg^{-1} TMAOH and 2.2 mol kg^{-1} HCl. (The signal corresponding to the proposed stannic acid dimer is marked with an asterisk.)

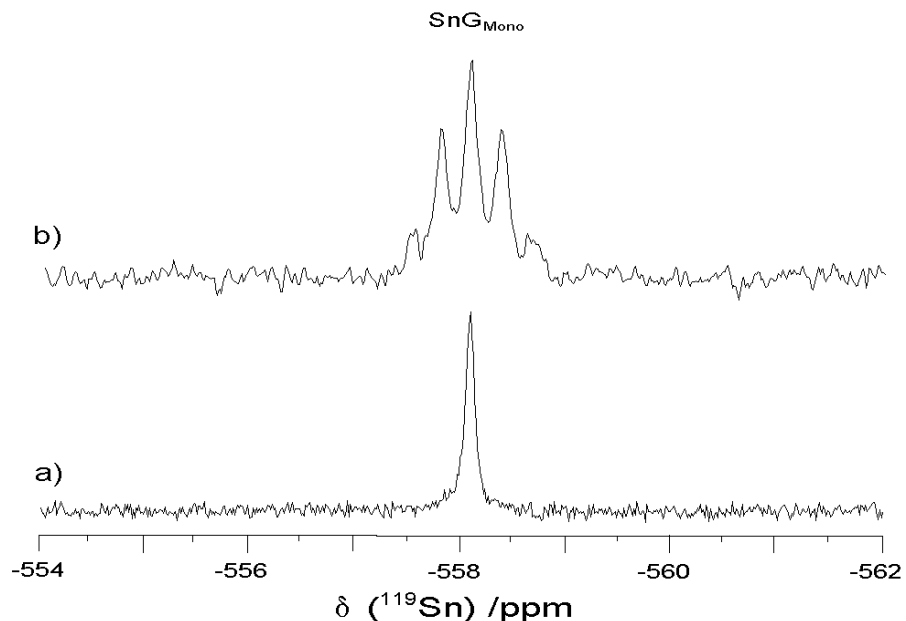


Figure 3.34. ^{119}Sn NMR spectrum of the ethane-1,2-diol containing solution represented in Figure 3.33b, a) with and b) without gated ^1H -decoupling.

The signal at -525.3 split into a simple first order binomial nonet (Figure 3.35) which we therefore assigned to a *bis*-ligand di-ester complex, denoted in Table 3.15 as **SnG_{Bis}**. The chemical shift would suggest that Sn maintains a six-fold coordination.^[107, 108] The presence of only one signal in this region, however, could suggest that the stannate centre has either four- or five-fold coordination as six-fold Sn coordination can form two possible diastereomers of this complex (hence two signals) whereas four- or five-fold coordination only can form one. We investigated the formation of analogous complexes with propane-1,2-diol (**SnP_{Bis}**) to determine whether the Sn centre in this complex retains a six-fold coordination. The theoretical number of diastereomers of the *bis*-ligand complex that can be formed with racemic propane-1,2-diol are: 12 for six-fold Sn coordination, 9 for five-fold Sn coordination and 6 for four-fold Sn coordination. Figure 3.36 shows the ^{119}Sn NMR spectrum of a solution containing 0.22 mol kg^{-1} Sn and 0.65 mol kg^{-1} propane-1,2-diol. The region corresponding to the *bis*-ligand complexes contains at least 10 signals which proves that the stannate centre retains six-fold coordination in the *bis*-ligand complex. We suspect that only one of the diastereomers of stannate-ethane-1,2-diol complex (**SG_{Bis}**, Table 3.15) is forming.

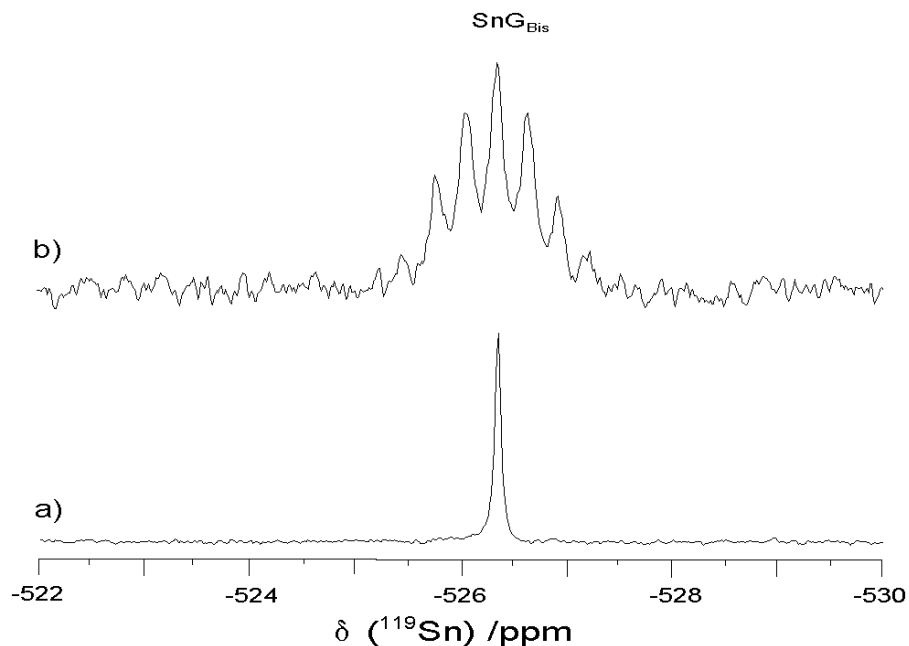


Figure 3.35. ^{119}Sn NMR spectrum of the ethane-1,2-diol containing solution represented in Figure 3.33b, a) with and b) without gated ^1H -decoupling.

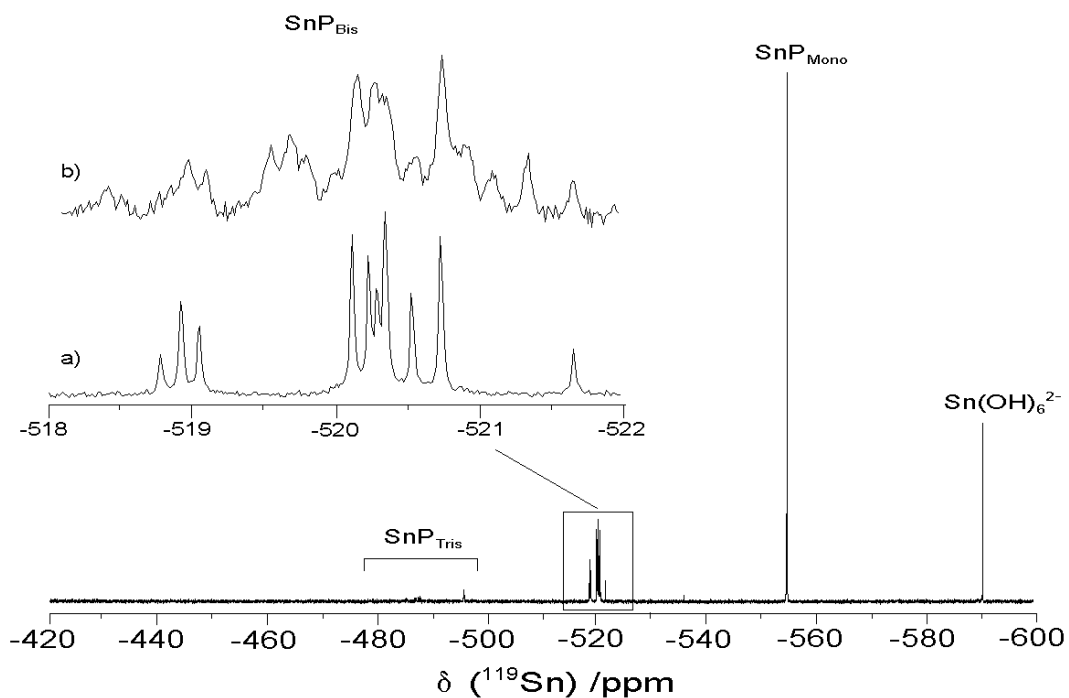


Figure 3.36. ^{119}Sn $\{^1\text{H}\}$ NMR spectrum of an aqueous solution containing 0.22 mol kg^{-1} Sn, 0.65 mol kg^{-1} propane-1,2-diol, 3.1 mol kg^{-1} TMAOH and 0.82 mol kg^{-1} HCl at 5°C . The expanded region is shown with a) with and b) without gated ^1H -decoupling.

The proton coupling of the stannate-ethane-1,2-diol signals at ca. -500 ppm could not be resolved (Figure 3.37). As the chemical shift of the signal at -494.7 ppm from the *bis*-ligand complex signal is similar to the up-frequency shift from the *bis*- to the *mono*-ligand complex signals (approximately 32 ppm), it has been assigned to *tris*-ligand complex SnG_{Tris} (Table 3.15). Since there is only one diastereomer of this complex, the signal at -499.8 ppm is suspected to correspond to a multimeric stannate species, *i.e.*, a complex containing more than one stannate centre. It has been tentatively assigned to a complex in which two ligands are bridging between two stannate centres, denoted as $\text{Sn}_2\text{G}_{\text{Tris}}$. The assignments of previous two signals are in agreement of their respective linewidths, as a species containing multiple stannate centres would likely be more broadened than a monomeric stannate species.

There is an additional signal at -466.90 ppm that was only present in solutions containing a relatively low concentration of ethane-1,2-diol (Figure 3.33a). As this signal disappears at higher ligand to Sn ratios, it has been tentatively assigned to a multimeric stannate species in which the stannate centres are bound through two oxygen linkages, denoted in Table 3.15 as $\text{Sn}_2\text{G}_{\text{Bis}}$. The 59 ppm up-frequency shift of this signal from the SnG_{Bis} complex signal is similar to the shift of between the oxygen bridged $\text{Sn}_2(\text{OH})_{10}^{2-}$ species signal and the $\text{Sn}(\text{OH})_6^{2-}$ signal (55 ppm).

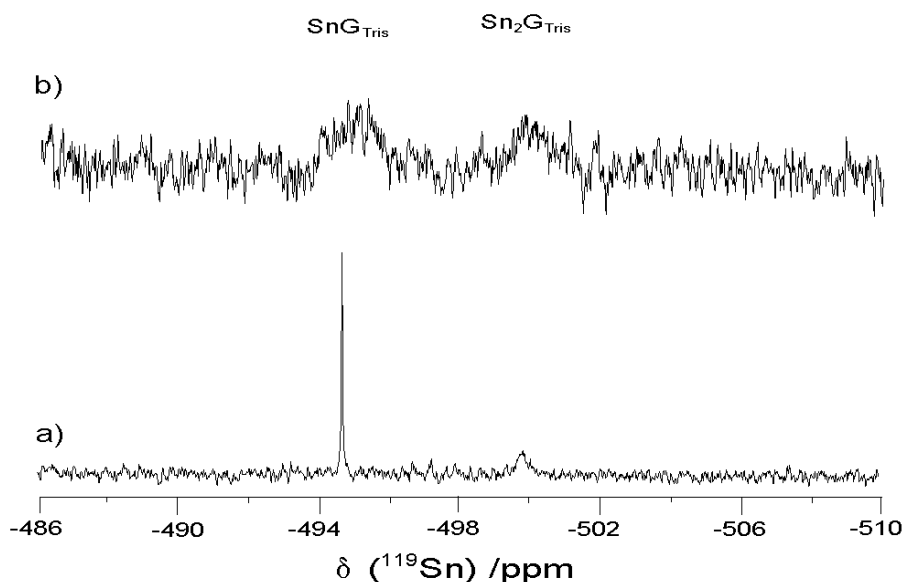


Figure 3.37. ^{119}Sn NMR spectrum of the ethane-1,2-diol solution represented in Figure 3.33b a) with and b) without gated ^1H -decoupling.

B. Complexes of furanoidic vicinal *cis*-diols.

As above, the addition of furanoidic vicinal *cis*-diols to an alkaline stannate solution resulted in many new ^{119}Sn NMR signals. Figure 3.38, for example, shows the ^1H -decoupled ^{119}Sn NMR spectra of alkaline stannate solutions with added *cis*-1,2-cyclopentanediol. The overall peak distribution is analogous to that observed for the stannate-ethane-1,2-diol complex signals (Figure 3.33), in which there is a consistent up-frequency shift (ca. 41 ppm) with the addition of a ligand to the stannate centre.

The signal at -547.5 ppm is split into a triplet of pentets from long distance scalar coupling (Figure 3.39) and has been assigned to the *mono*-ligand complex SnC_{Mono} (Table 3.16). Three-bond coupling ($^3J = 48$ Hz) arises from the ligand protons on C_1 and C_2 and the four-bond coupling arises ($^4J = 9$ Hz) from the C_3 and C_5 protons.

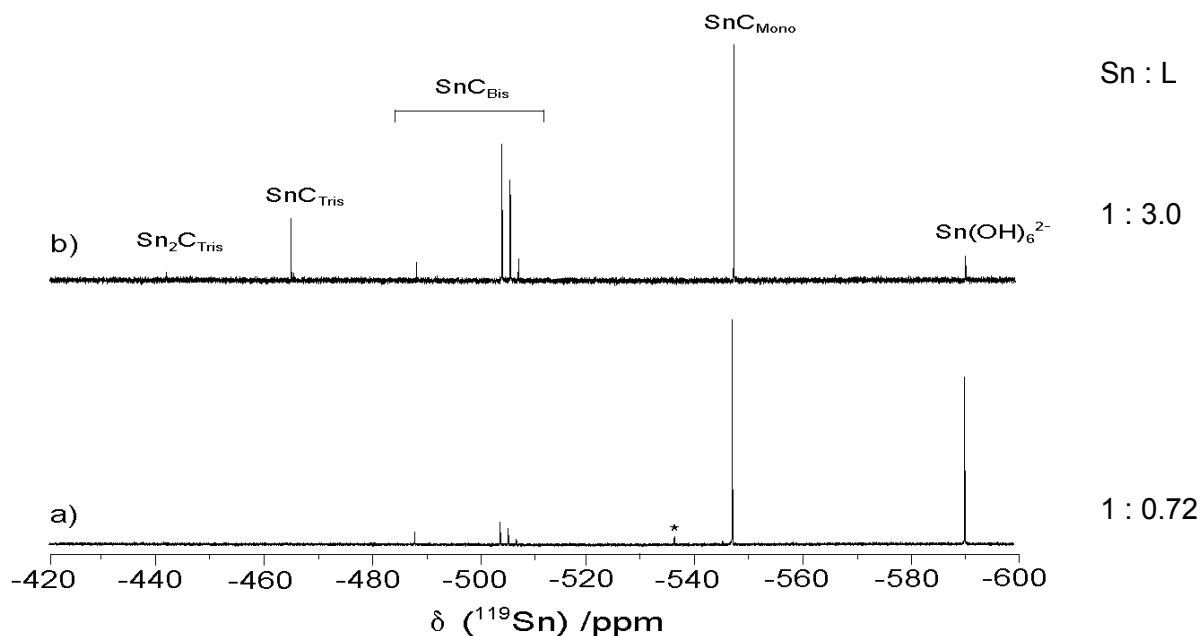


Figure 3.38. ^{119}Sn $\{^1\text{H}\}$ NMR spectra at 21°C of aqueous solutions containing a) 0.18 mol kg^{-1} Sn, 0.13 mol kg^{-1} *cis*-1,2-cyclopentanediol, 2.2 mol kg^{-1} TMAOH and 0.67 mol kg^{-1} HCl, and b) 0.23 mol kg^{-1} Sn, 0.68 mol kg^{-1} *cis*-1,2-cyclopentanediol, 2.1 mol kg^{-1} TMAOH and 0.89 mol kg^{-1} HCl. (The signal corresponding to the proposed stannic acid dimer is marked with an asterisk.)

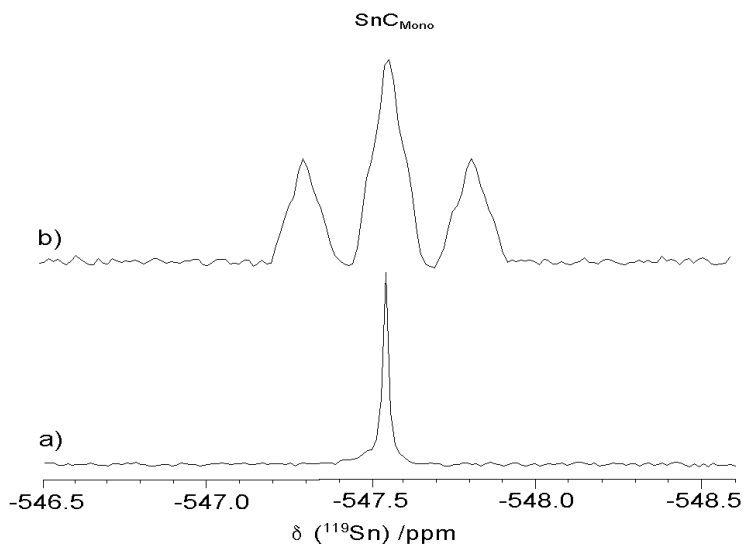


Figure 3.39. ^{119}Sn NMR spectrum of the cyclopentanediol containing solution represented in Figure 3.38b, a) with and b) without gated ^1H -decoupling. (a Lorentzian-Gaussian function was employed with $\text{LB} = -4$ Hz and $\text{GB} = 0.2$)

Four signals between -488 and -508 ppm (Figure 3.40) exhibit pentet splitting patterns from three-bond coupling ($^3J = 41\text{-}47$ Hz) to the C_1 and C_2 protons on the ligand. (Refer to inset structure in Figure 3.25.) Comparison of the ^{13}C and ^{119}Sn NMR spectra shows that the stannate:ligand ratio of the complexes corresponding to these signals is 1:2. Rudimentary modeling indicates that there are 4 diastereomers for a monomeric Sn *bis*-ligand complex in which Sn has six-fold coordination, as shown in Figure 3.41. However, the large separation between the signal at -488.4 ppm and the three resonances would suggest that it does not correspond to a diastereomer of the *bis*-ligand complex, but potentially a bridged stannate species ($\text{Sn}_2\text{C}_{\text{BIS}}$, Table 3.16), somewhat similar to that observed with ethane-1,2-diol ($\text{Sn}_2\text{G}_{\text{TRIS}}$). With limited experimental evidence, we have tentatively assigned the signals ranging from -504 to -508 ppm to three diastereomers of the monomeric stannate *bis*-ligand complex and the signal at -488.4 ppm to a bridged stannate species.

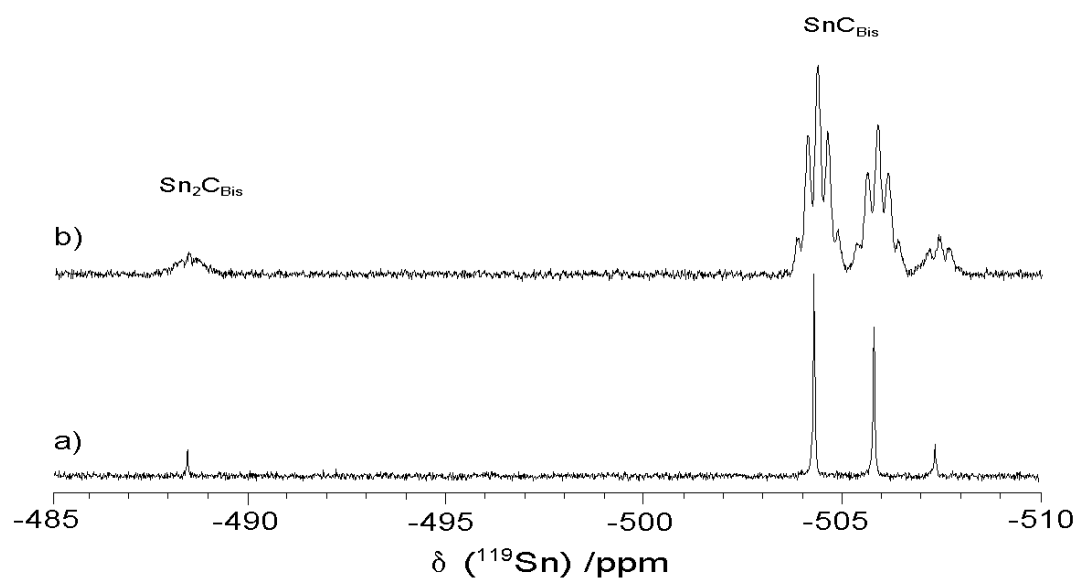


Figure 3.40. ^{119}Sn NMR spectrum of the cyclopentane diol containing solution represented in Figure 3.38b, a) with and b) without gated ^1H -decoupling.

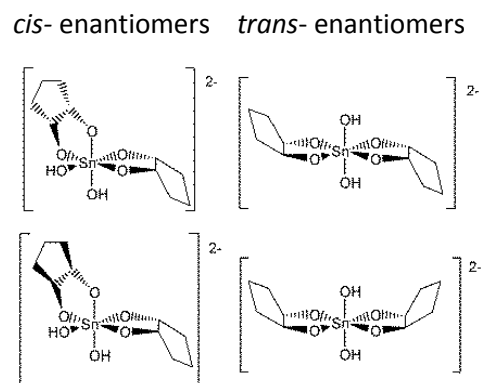
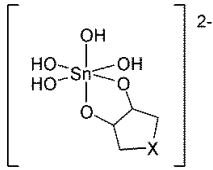
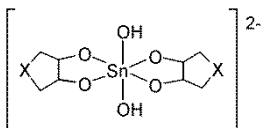
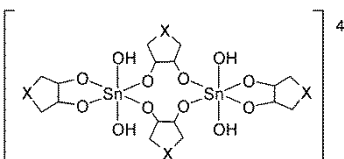
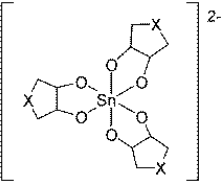
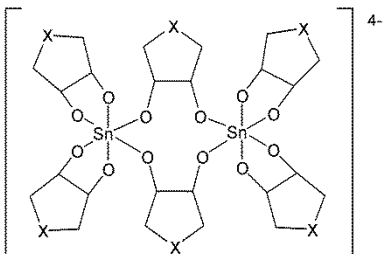
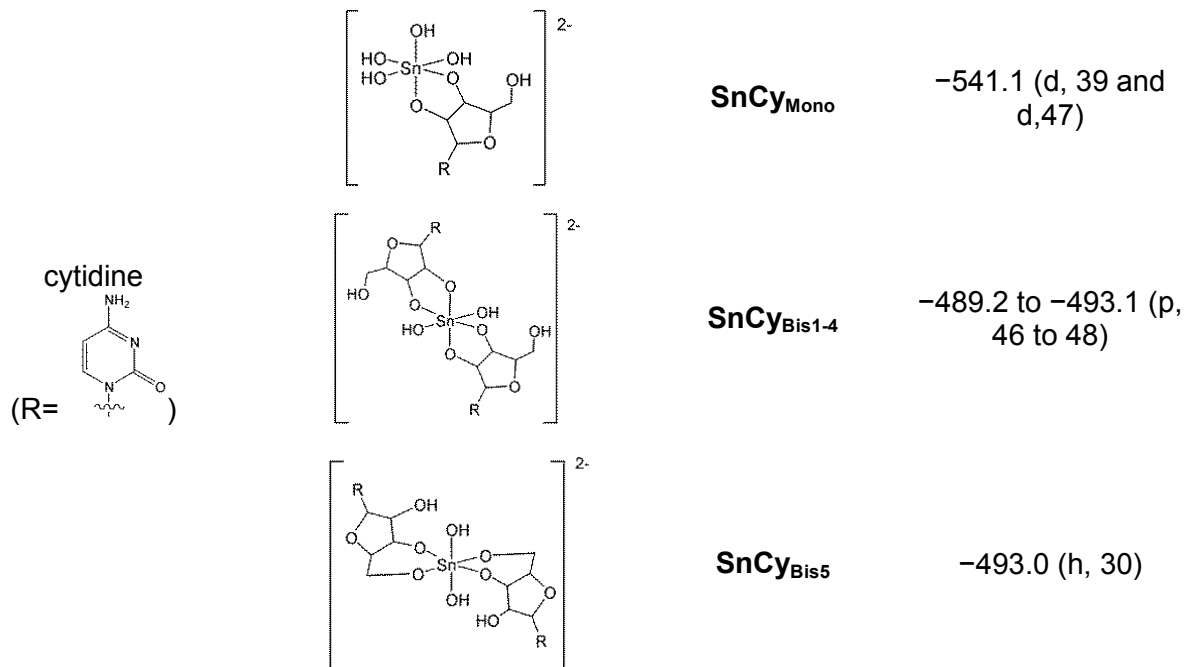


Figure 3.41. The four possible diastereomers of the *bis*-ligand complex between stannic acid and *cis*-1,2-cyclopentane diol.

Table 3.16. Stannate complexes with furanoidic vicinal *cis*-diols (*cis*-1,2-cyclopentanediol, 1,4-anhydroerythritol, cytidine)

saccharide	Structure	Notation ^a	¹¹⁹ Sn NMR chemical shift /ppm (multiplicity, ³ J(¹¹⁹ Sn, ¹ H) /Hz) ^{b,c}
		SnC_{Mono} SnA_{Mono}	-547.5 (t, 48) (p, 9) ^d -541.5 (t, 46) (p, 9) ^d
		SnC_{Bis} SnA_{Bis}	-504 to -508 (p, 41 to 49) -491 to -494 (p, 44 to 47)
Furanoidic <i>cis</i>-diol <i>cis</i> -1,2-cyclopentanediol (X = CH ₂)		Sn₂C_{Bis} Sn₂A_{Bis}	-488.4 (p, 41) -482 (p, 46)
1,4-anhydroerythritol (X = O)		SnC_{Tris} SnA_{Tris}	-465.0 to -465.5 (hp, 50/nr) -441.8 to -442.0 (nr)
		Sn₂C_{Tris} Sn₂A_{Tris}	-441.6 (nr) -426.7 (nr)



^a C = *cis*-1,2-cyclopentanediol, A = 1,4-anhydroerythritol and Cy= cytidine ^b Multiplicity = d (doublet), t (triplet), q (quartet), p (pentet), h (hextet), hp (heptet), n (nonet) or nr = not resolved
^c Chemical shifts are only representative as they vary with solution conditions ^d four bond coupling multiplicity, ⁴J(¹¹⁹Sn, ¹H) /Hz

The signal -465.0 ppm is split into a heptet from long distance scalar coupling (Figure 3.42). This signal has been assigned to the *tris*-ligand complex in which the ligands are all oriented in the same direction (as shown in Figure 3.43a, previously represented as L_δL_δL_δ).^[65] The signal at -465.5 ppm, with unresolved proton coupling, has been assigned to a diastereomer of this complex, in which one of the ligands is oriented in the opposite direction of the other two (L_δL_δL_λ, Figure 3.43b). Analogous to the *tris*-ligand silicate complexes,^[65] there is more steric interactions in the latter complex resulting in a lesser concentration than the former complex. These species are collectively denoted as **SnC_{Tris}**.

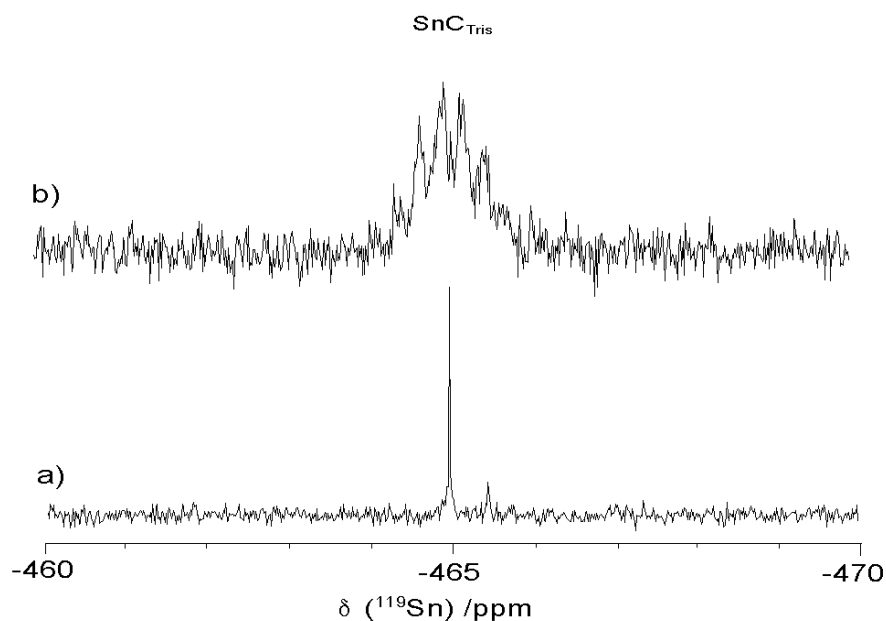


Figure 3.42. ^{119}Sn NMR spectrum of the cyclopentanediol containing solution represented in Figure 3.38b, a) with and b) without gated ^1H -decoupling.

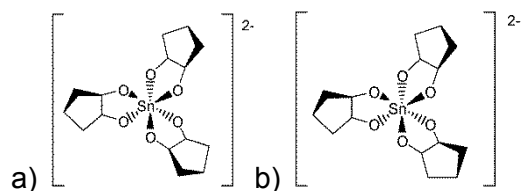


Figure 3.43. The two possible diastereomers of the *tris*-ligand complex between stannic acid and *cis*-1,2-cyclopentanediol.

The proton coupling of the signal at -441.6 ppm could not be resolved (Figure 3.44). It has been tentatively assigned to a complex analogous to the multimeric stannate species between stannic acid and ethane-1,2-diol, in which the stannate centres are bridged by ligands, denoted in Table 3.16 as $\text{Sn}_2\text{C}_{\text{Tris}}$. We suspect that ligands are bridging the stannate centres as this complex is only detected at high ligand concentrations.

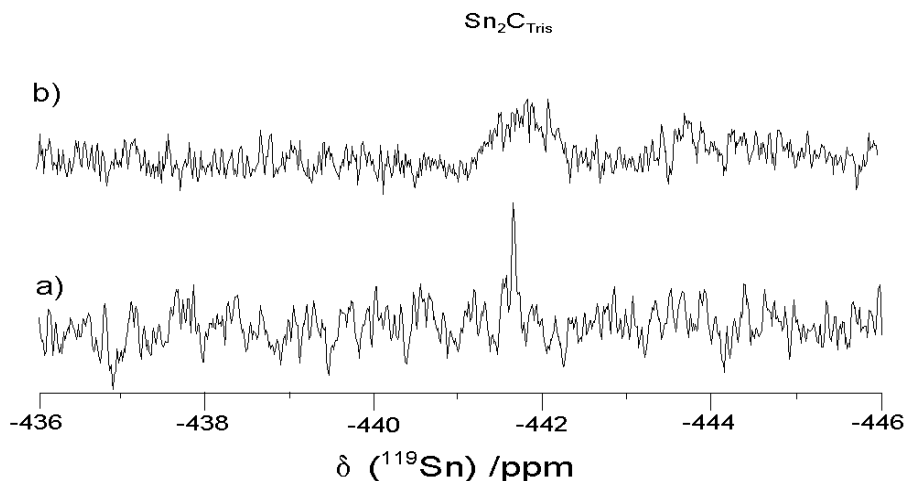


Figure 3.44. ^{119}Sn NMR spectrum of the cyclopentenediol containing solution represented in Figure 3.38b, a) with and b) without gated ^1H -decoupling.

The ^{119}Sn NMR spectrum of an analogous TMA stannate solution, but containing 1,4-anhydroerythritol instead of *cis*-1,2-cyclopentenediol, revealed a similar distribution of resonances (Figures 3.45-3.48) and, hence, organostannate complexes (Table 3.16). There is an *ca.* 50 ppm chemical shift with each di-ester 1,4-anhydroerythritol linkage, which is slightly greater than that of *cis*-1,2-cyclopentenediol (*ca.* 41 ppm). The scalar coupling from 1,4-anhydroerythritol was more resolved than the coupling from *cis*-1,2-cyclopentenediol, most noticeable in the SnA_{Mono} complex (Figure 3.46). As 1,4-anhydroerythritol was found to precipitate within 24 hrs of preparation, the spectra were acquired immediately after solution preparation.

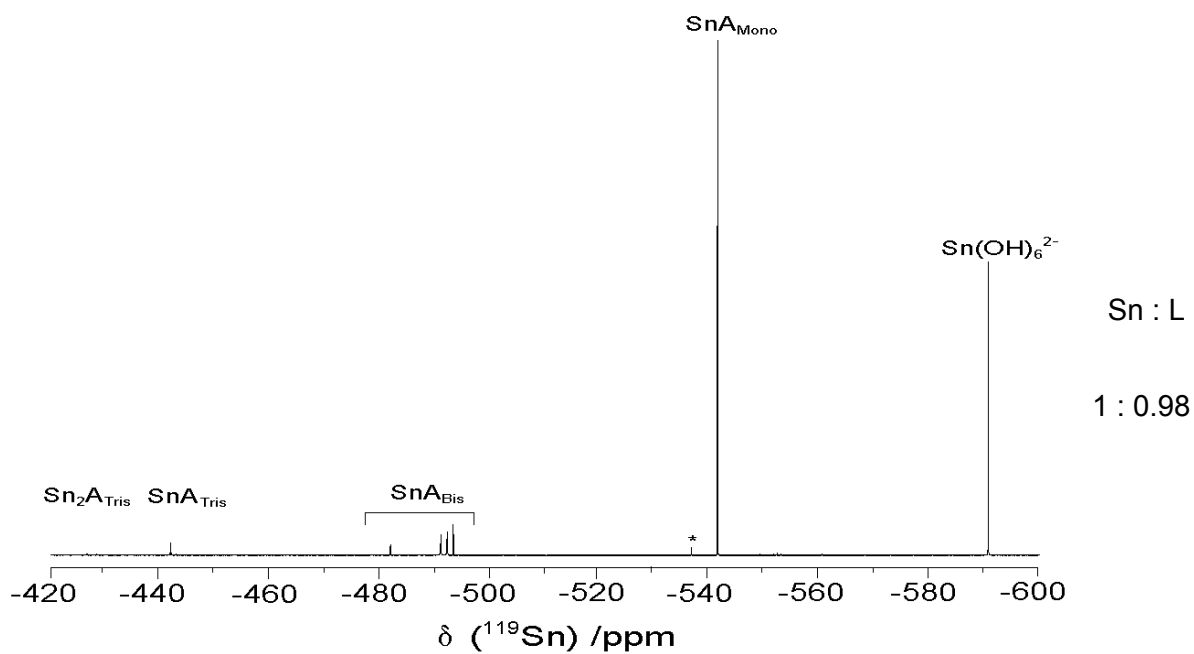


Figure 3.45. $^{119}\text{Sn} \{^1\text{H}\}$ NMR spectrum at 21 °C of an aqueous solution containing 0.41 mol kg^{-1} Sn, 0.40 mol kg^{-1} 1,4-anhydroerythritol, 3.8 mol kg^{-1} TMAOH and 1.6 mol kg^{-1} HCl. The stannate dimer is denoted by the asterisk.

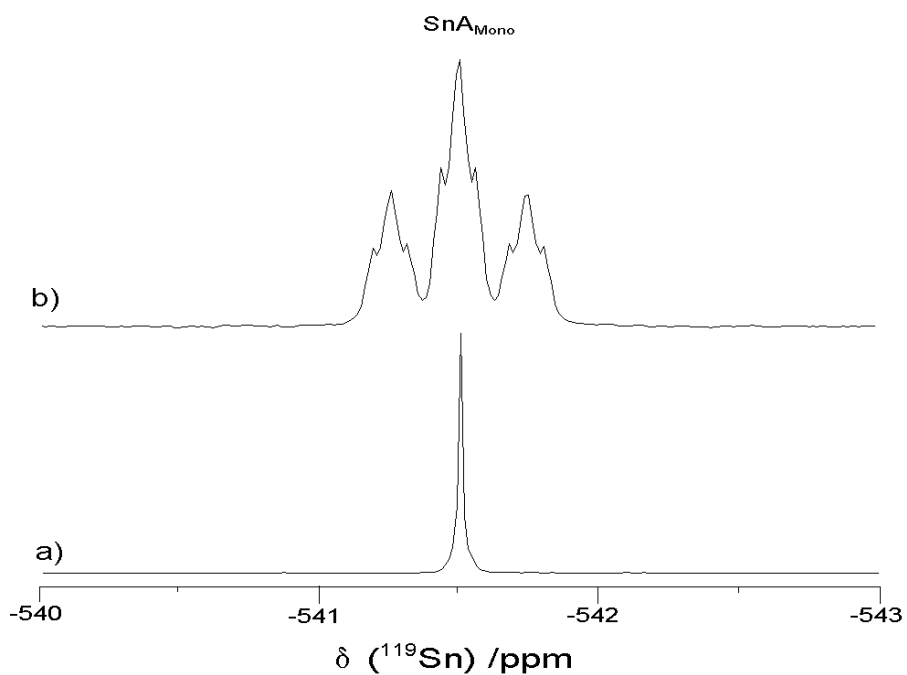


Figure 3.46. ^{119}Sn NMR spectrum of the 1,4-anhydroerythritol containing solution represented in Figure 3.45 a) with and b) without gated ^1H -decoupling.

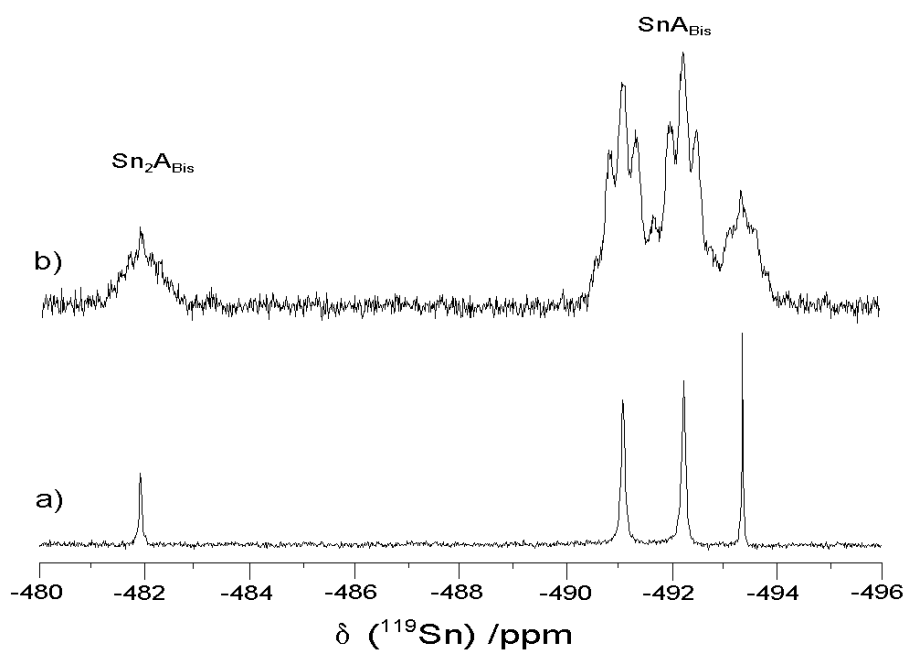


Figure 3.47. ^{119}Sn NMR spectrum of the 1,4-anhydroerythritol containing solution represented in Figure 3.45 a) with and b) without gated ^1H -decoupling.

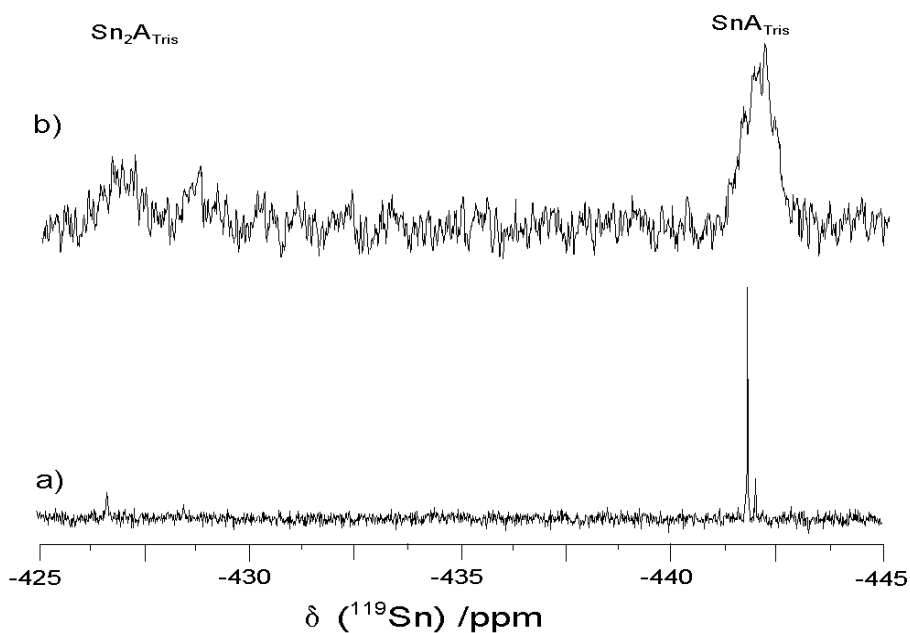


Figure 3.48. ^{119}Sn NMR spectrum of the 1,4-anhydroerythritol containing solution represented in Figure 3.45 a) with and b) without gated ^1H -decoupling.

The ^{119}Sn NMR spectrum of a solution containing 0.22 mol kg^{-1} Sn and 0.43 mol kg^{-1} cytidine (Figure 3.49) also gave a similar signal distribution to that of *cis*-1,2-cyclopentanediol and 1,4-anhydroerythritol. However, there were additional signals in each region of the spectrum and, at a relatively low stannate:ligand ratio, the stannate dimer was not detected. As with 1,4-anhydroerythritol, there is an *ca.* 50 ppm chemical shift with each di-ester ligand linkage.

The signal at -541.1 ppm (Figure 3.50) is split into a doublet of doublets from three bond coupling ($^3J = 39$ and 47 Hz) to the ligand C_2 and C_3 protons. (Refer to inset structure in Figure 3.25.) It has been assigned to the *mono*-ligand complex $\text{SnCy}_{\text{Mono}}$ (Table 3.16). There was no evidence of an ester linkage between stannic acid and the C_5 hydroxymethyl group.

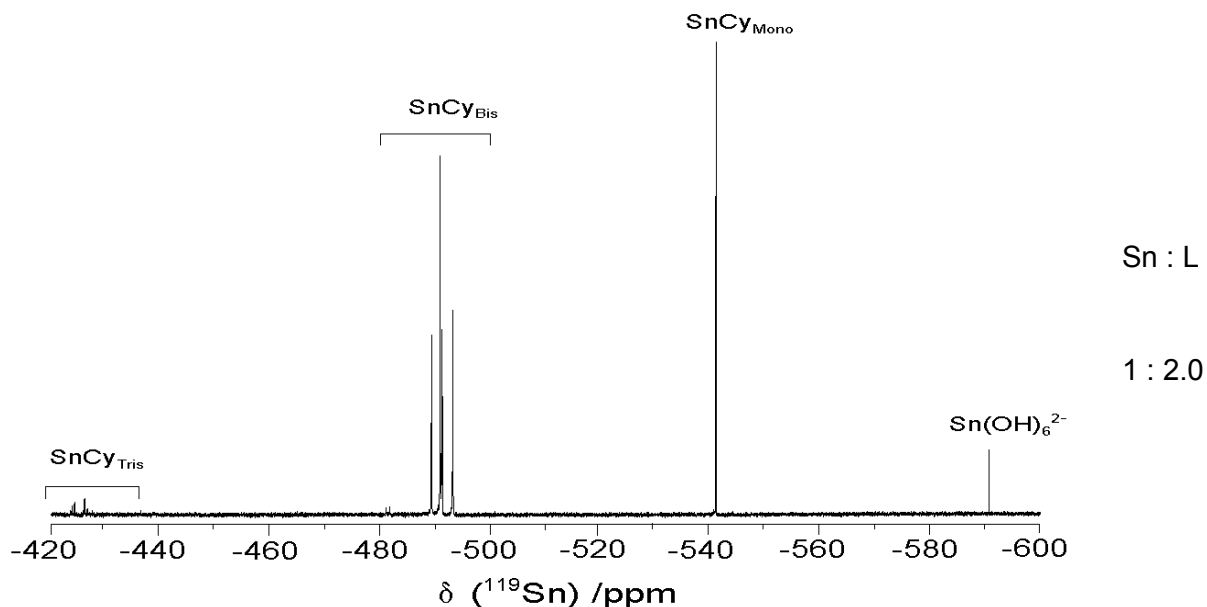


Figure 3.49. ^{119}Sn $\{^1\text{H}\}$ NMR spectrum at 5°C of an aqueous solution containing 0.22 mol kg^{-1} Sn, 0.43 mol kg^{-1} cytidine, 3.1 mol kg^{-1} TMAOH and 0.83 mol kg^{-1} HCl.

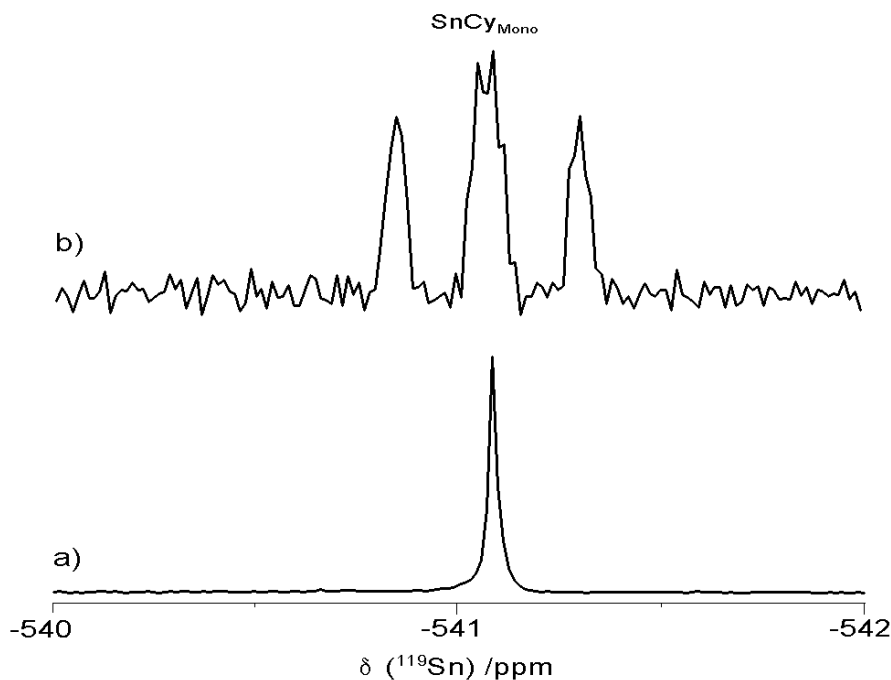


Figure 3.50. ^{119}Sn NMR spectrum of the cytidine containing solution represented in Figure 3.49 a) with and b) without gated ^1H -decoupling. (Lorentzian-Gaussian function was employed with $\text{LB} = -4$ Hz and a $\text{GB} = 0.4$.)

The signal at -489.2 ppm was split into a pentet from the three-bond proton coupling ($^3J = 46$ Hz) to the C_2 and C_3 ligand protons and it corresponds to one diastereomer of a *bis*-ligand complex (Figure 3.51, Table 3.16). The three signals ranging from -490.5 to -491.5 ppm have been assigned to three other diastereomers of this complex. The signal at -493.1 ppm has been assigned to a *bis*-ligand complex, denoted in Table 3.16 as **SnCy_{Bis5}**, in which stannic acid is binding cytidine through a hydroxyl group on the ribose ring (likely C_3) and the C_5 hydroxymethyl group. This signal is split into a heptet from long distance scalar coupling ($^3J = 46$ Hz) to the ligand protons. The proton coupling of the signals between -480 and -485 ppm (not shown in expansion) could not be resolved. However, due to the similar up-frequency shift of these signals from the signals corresponding to the *bis*-ligand species, we have assigned them to bridged di-stannate complex analogous to those observed for *cis*-1,2-cyclopentanediol and 1,4-anhydroerythritol (**Sn₂C_{Bis}**, **Sn₂A_{Bis}**).

The signals between -422 and -428 ppm have been assigned to *tris*-ligand stannate complexes (Figure 3.52). As the three bond proton coupling of these signals could not be resolved, the signal assignments were made through the chemical shift. The large number of signals would suggest that stannate is complexing the ligand through both the C_2/C_3 and the C_3/C_5 binding sites.

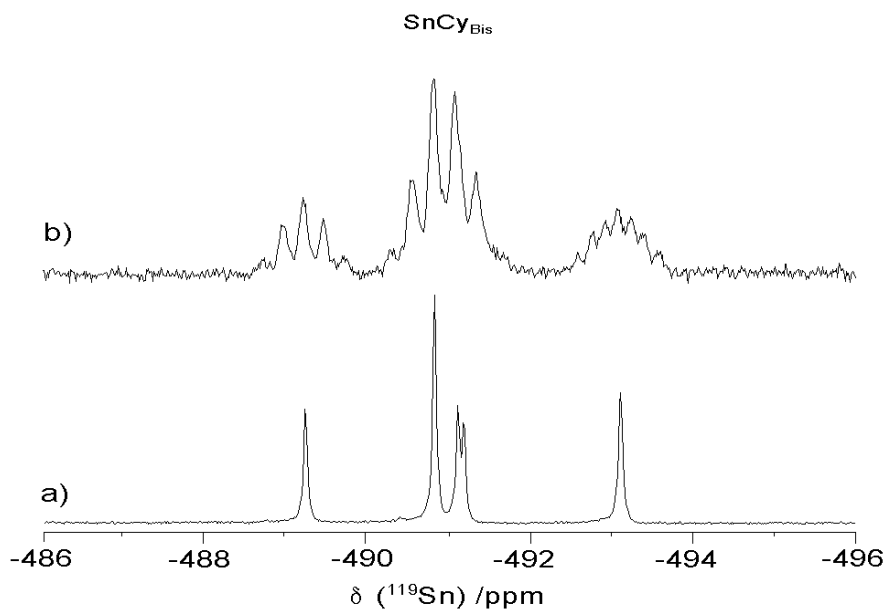


Figure 3.51. ^{119}Sn NMR spectrum of the cytidine containing solution represented in Figure 3.49 a) with and b) without gated ^1H -decoupling.

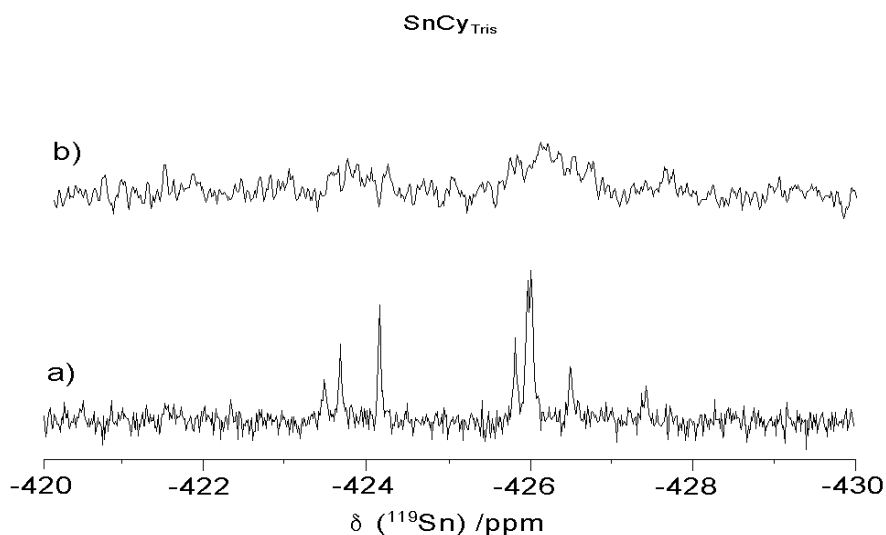


Figure 3.52. ^{119}Sn NMR spectrum of the cytidine containing solution represented in Figure 3.49 a) with and b) without gated ^1H -decoupling.

C. Complexes of acyclic polyols.

The addition of a polyol to an alkaline stannate solution results in many new signals in the ^{119}Sn NMR spectrum. Figure 3.53, for example, shows the ^{119}Sn NMR spectra of TMA stannate solutions with added L-threitol. The overall signal distribution is similar to those of ethane-1,2-diol and the furanoidic *cis*-diols, but the number of signals in each region is greatly increased.

The signal at -561.0 ppm is split into a doublet of triplets from three-bond proton coupling and appears to be split further by weak four bond coupling which could not be resolved (Figure 3.54). It has been assigned to the *mono*-ligand complex $\text{SnT}_{\text{Mono}13}$ (Table 3.17) in which stannic acid is bound through the C_1 and C_3 hydroxyl groups of threitol.

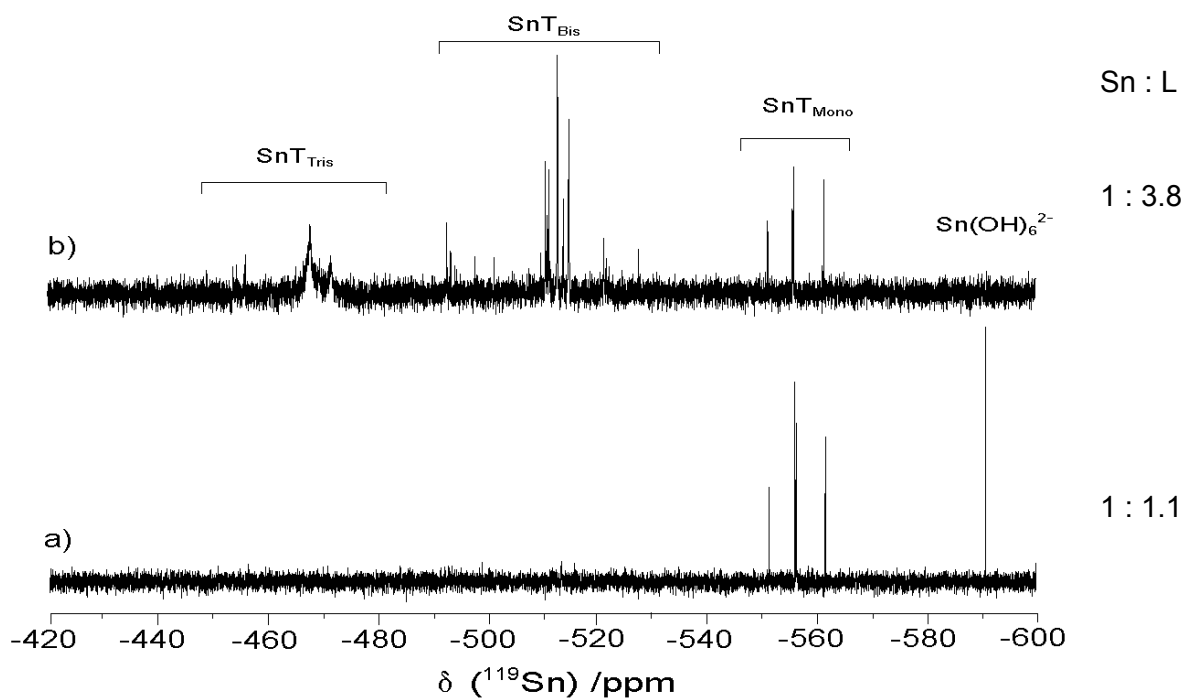


Figure 3.53. ^{119}Sn $\{^1\text{H}\}$ NMR spectra at 5°C of the aqueous solutions containing a) 0.20 mol kg^{-1} Sn, 0.21 mol kg^{-1} L-threitol, 2.5 mol kg^{-1} TMAOH and 0.76 mol kg^{-1} HCl, and b) 0.21 mol kg^{-1} Sn, 0.79 mol kg^{-1} L-threitol, 2.7 mol kg^{-1} mol kg^{-1} TMAOH and 0.80 mol kg^{-1} HCl.

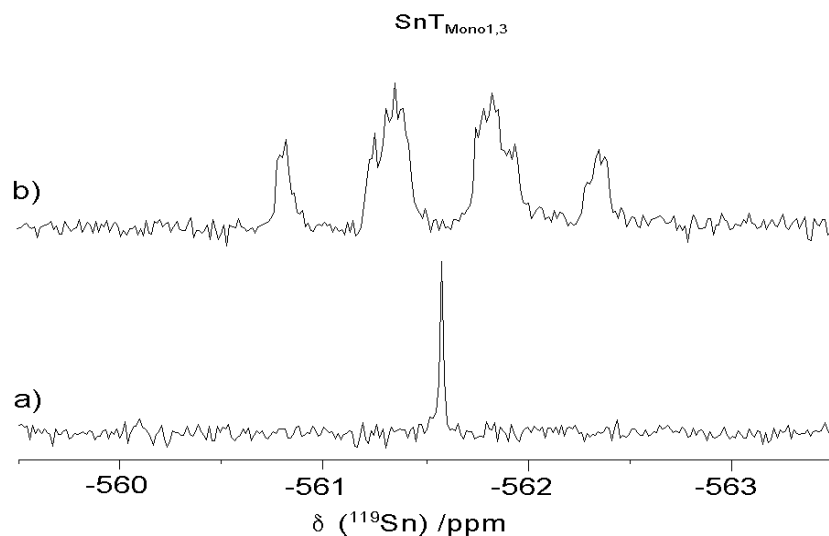


Figure 3.54. ^{119}Sn NMR spectrum of the threitol containing solution represented in Figure 3.53a, a) with and b) without gated ^1H -decoupling.

The signal at -556.0 ppm is split into a doublet of triplets from three-bond proton coupling to the saccharide and was further split into a doublet by four-bond coupling (Figure 3.55). This signal has been assigned to the *mono*-ligand complex $\text{SnT}_{\text{Mono12}}$ (Table 3.17) in which stannic acid is binding the ligand C_1 and C_2 hydroxyl groups. The signal at -556.3 ppm was split into a triplet from long distance scalar coupling and has been assigned to a *mono*-ligand complex, denoted as $\text{SnT}_{\text{Mono23}}$, in which Sn is bound to the C_2 and C_3 hydroxyl groups on threitol.

The signal at -551.3 ppm is split into three sets of doublets from long distance scalar coupling (Figure 3.56). This signal has been tentatively assigned to a *mono*-ligand tri-ester stannate complex, denoted as $\text{SnT}_{\text{Mono123}}$ (Table 3.17). The small up-frequency shift of this signal from those corresponding to mono-ligand di-ester complexes is consistent with this assignment.

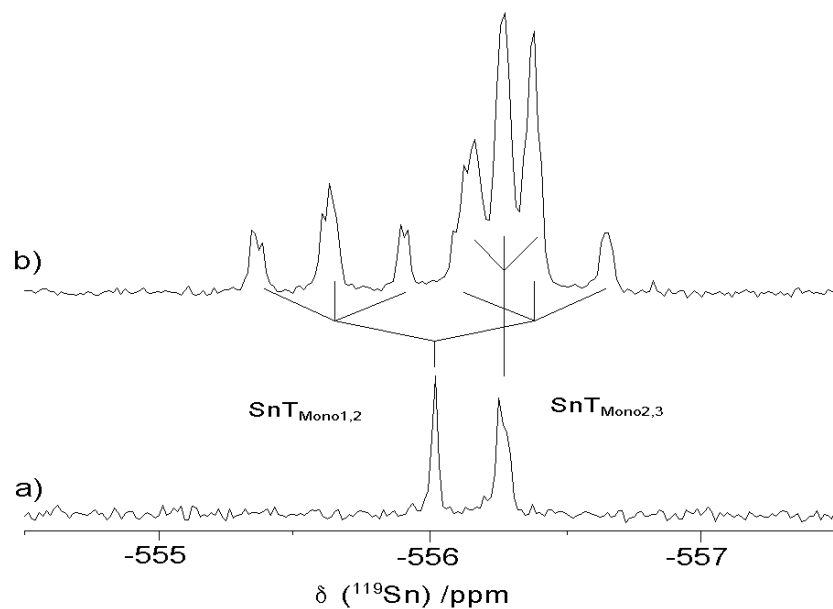


Figure 3.55. ^{119}Sn NMR spectrum of the threitol containing solution represented in Figure 3.53a, a) with and b) without gated ^1H -decoupling.

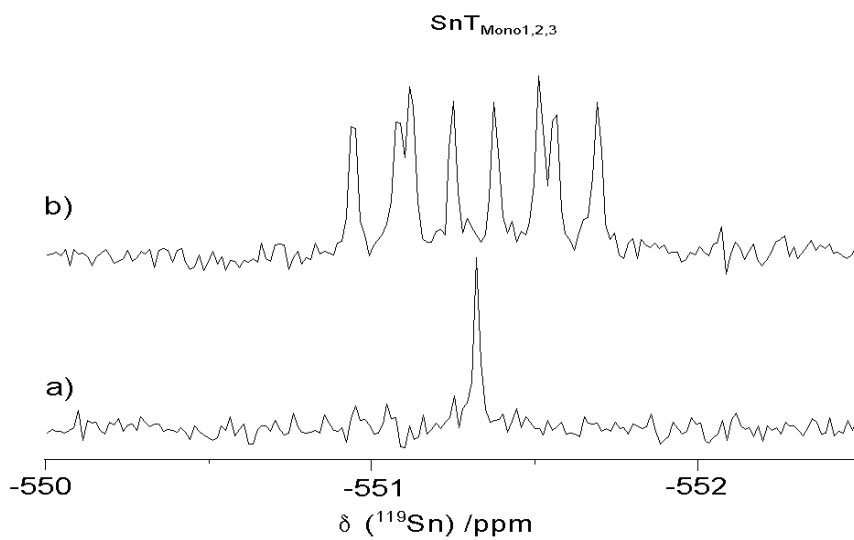


Figure 3.56. ^{119}Sn NMR spectrum of the threitol containing solution represented in Figure 3.53a, a) with and b) without gated ^1H -decoupling.

Only the three bond proton coupling of the signals at -513 and -515 ppm could be resolved between -490 and -540 ppm, both of which are split into pentets (Figure 3.57). These signals have been assigned to two diastereomers of a *bis*-ligand complex in which the stannate centre is bound through the C_2 and C_3 hydroxyl groups on threitol, denoted in Table 3.17 as **SnT_{Bis}**. The other signals in this region correspond to multiple *bis*-ligand complexes. The large number of complexes arises from multiple binding sites on threitol (as shown with the *mono*-ligand complexes) and the combinations of these binding sites (as there are two ligands binding the Sn centre).

The long distance scalar coupling of the signals between -445 and 480 ppm could not be resolved but, from the chemical shifts, the signals have been assigned to *tris*-ligand complexes (Figure 3.58). As with the *bis*-ligand stannate complexes, the large number of combinations of the binding sites on threitol led to the formation of numerous species.

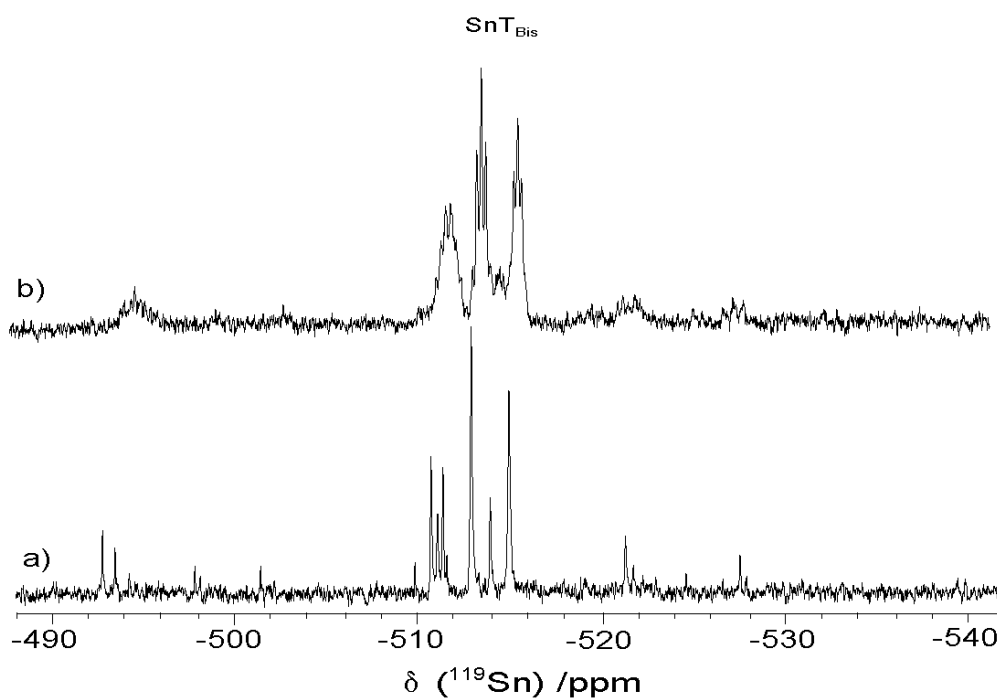


Figure 3.57. ^{119}Sn NMR spectrum of the threitol containing solution represented in Figure 3.53a, a) with and b) without gated ^1H -decoupling.

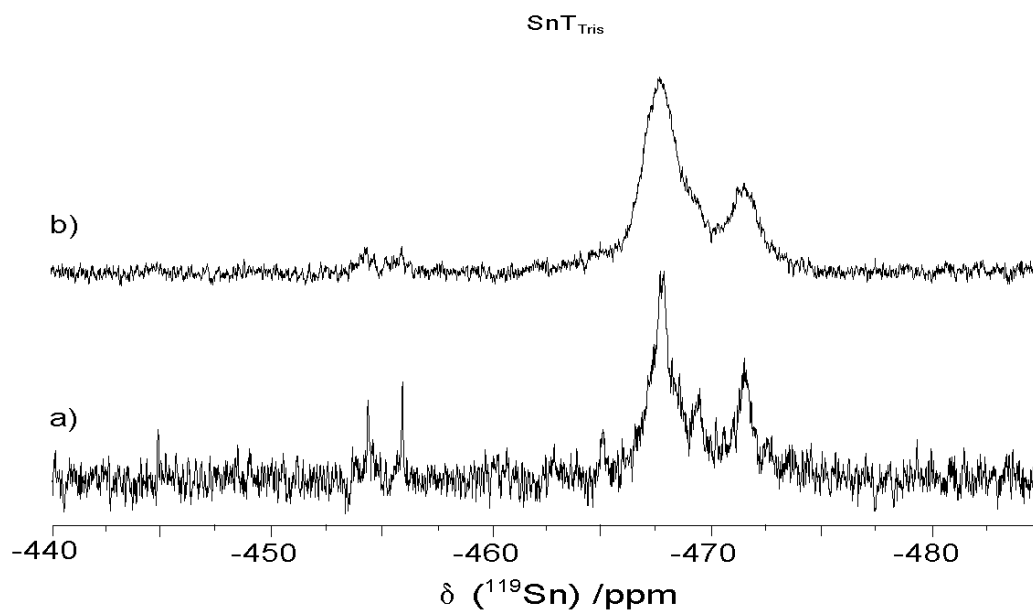
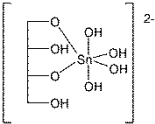
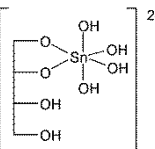
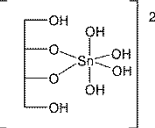
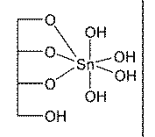
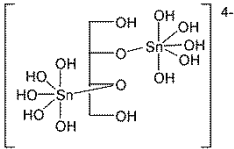
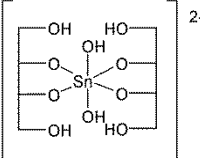


Figure 3.58. ^{119}Sn NMR spectrum of the threitol containing solution represented in Figure 3.53a, a) with and b) without gated ^1H -decoupling.

Table 3.17. Stannate complexes with aliphatic polyhydroxy molecules (threitol, erythritol, xylitol, adonitol, mannitol)

polyol	Structure ^d	Notation	¹¹⁹ Sn NMR chemical shift /ppm (multiplicity, ³ J(¹¹⁹ Sn, ¹ H) /Hz)
threitol erythritol		SnT_{Mono13} SnE_{Mono13}	-561.0 (d, 94 and t, 94) -560.1 (d, 97 and t, 97)
		SnT_{Mono12}	-556.0 (d, 140 and t, 51)(d, 6)
		SnT_{Mono23} SnE_{Mono23}	-556.3 (t, 20) -553.0 (t, 49)
		SnT_{Mono123} SnE_{Mono123}	-551.3 (d, 82 and d, 33 and d, 25) -552.2 (d, 90 and d, 28 and d, 21)
		SnE_{Mono†}	-551.5 (d, 115)
		SnT_{Bis1} SnT_{Bis2}	-513 (p, 47) -515 (p, 43)

^a T = threitol, E = erythritol ^b Multiplicity = d (doublet), t (triplet), p (pentet) or nr = not resolved ^c Chemical shifts are only representative as they vary with solution conditions ^d no stereochemistry is implied in the structures of the polyols

To determine whether the dihydroxy functionality of the polyols changes the binding affinity towards stannate, the interactions between stannic acid and erythritol were compared with threitol. Figure 3.59 shows the ^{119}Sn NMR spectra of solutions containing *meso*-erythritol and stannic acid.

The signal at -560.1 ppm was split into a doublet of triplets from three-bond proton coupling (Figure 3.60). Evidence of four bond proton coupling was present but could not be resolved. This signal has been assigned to *mono*-ligand complex $\text{SnE}_{\text{Mono}13}$ (Table 3.17), in which stannic acid is bound to the C_1 and C_3 hydroxyl groups of erythritol, analogous to the stannate-threitol complex ($\text{SnT}_{\text{Mono}13}$).

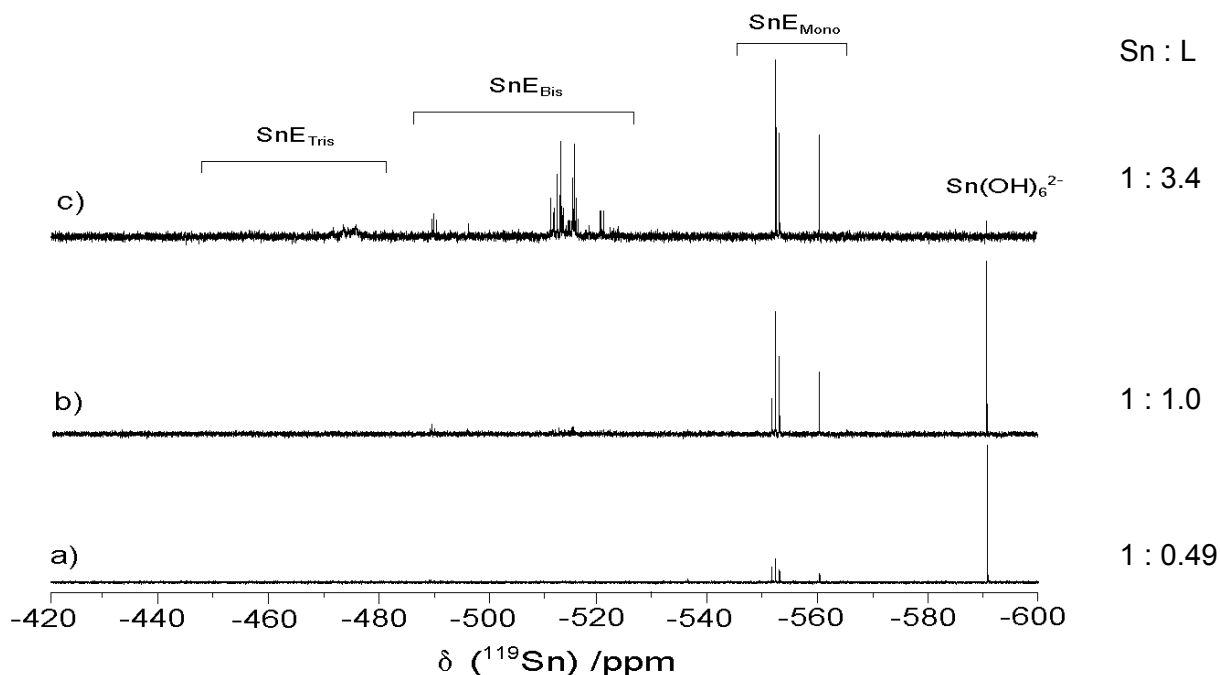


Figure 3.59. ^{119}Sn $\{^1\text{H}\}$ NMR spectra at 5°C of aqueous solutions containing 0.23 mol kg^{-1} Sn, 2.9 mol kg^{-1} TMAOH and 0.9 mol kg^{-1} HCl and a) 0.11 mol kg^{-1} erythritol, b) 0.24 mol kg^{-1} erythritol or c) 0.79 mol kg^{-1} erythritol.

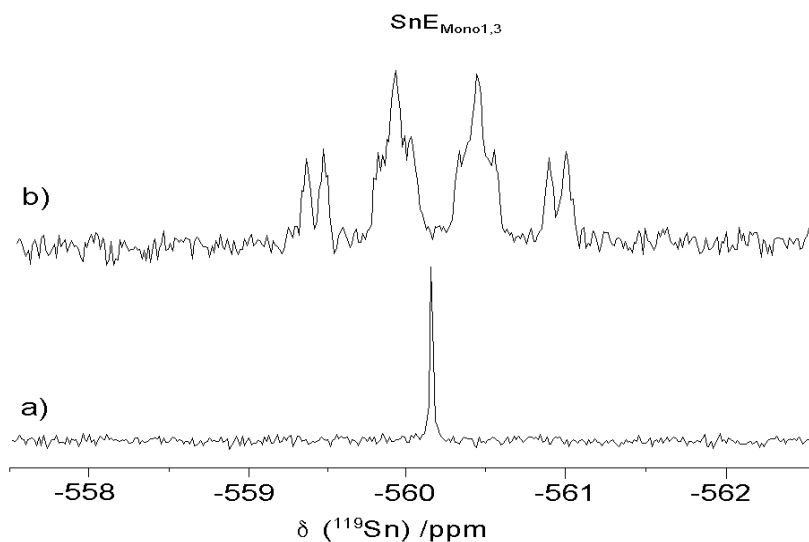


Figure 3.60. ^{119}Sn NMR spectrum of the erythritol containing solution represented in Figure 3.59b, a) with and b) without gated ^1H -decoupling.

The signal at -552.2 ppm is split into three sets of doublets from long distance scalar coupling (Figure 3.61) and has been tentatively assigned to a *mono*-ligand tri-ester complex $\text{SnE}_{\text{Mono}123}$ (Table 3.17). The signal at -553.0 ppm is split into a triplet from proton coupling and corresponds to *mono*-ligand complex $\text{SnE}_{\text{Mono}23}$, in which the stannic acid is binding the C_2 and C_3 hydroxyl groups on erythritol. The relative concentration of this complex with respect to the other *mono*-ligand complexes is less than that of threitol, $\text{SnT}_{\text{Mono}23}$, in the same solution conditions. As the internal hydroxyl groups on erythritol are oriented away from one another, the binding affinity to these hydroxyl groups decreases from that of threitol, which has been demonstrated with borate- and silicate-polyol complexes.^[36, 64] The complex corresponding to the signal at -552.8 ppm could not be identified. This signal is split into a doublet of doublets and a plausible complex that has two non-equivalent protons coupling to the stannate centre could not be determined. The signal at -551.5 ppm is split into a doublet from three bond proton coupling. This signal disappears when the ligand concentration is increased above an equimolar stannate-saccharide composition (Figure 3.62). It has been assigned to a dimeric stannate complex, denoted as $\text{Sn}_2\text{E}_{\text{Mono}}$, in which the stannate centres are bound through the C_2 or C_3 hydroxyl group on erythritol. It is not present in the solutions containing threitol as the C_2 and C_3 hydroxyl groups are oriented towards the same side of the ligand preventing the two stannate groups from accessing these hydroxyl groups simultaneously.

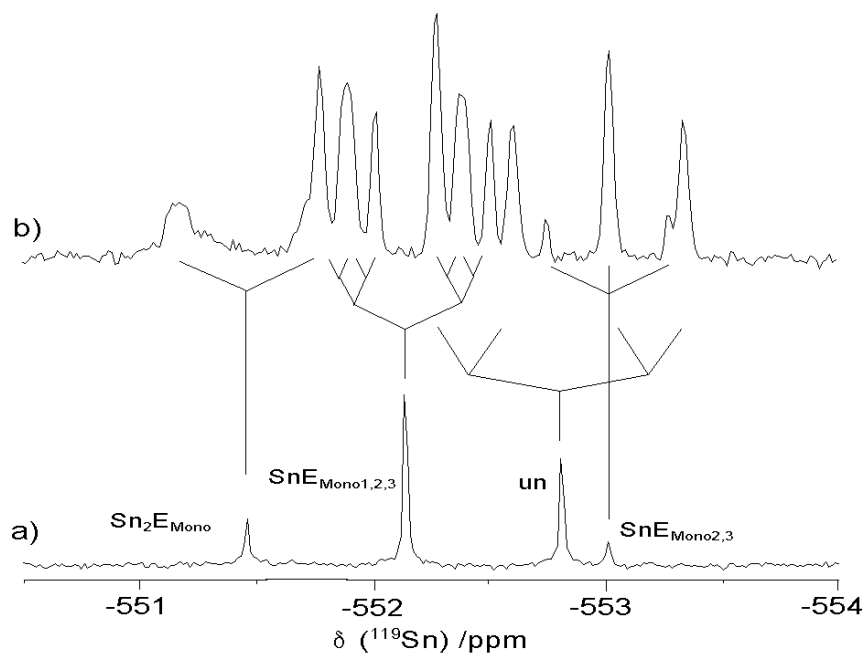


Figure 3.61. ^{119}Sn NMR spectrum of the erythritol containing solution represented in Figure 3.59b, a) with and b) without gated ^1H -decoupling.

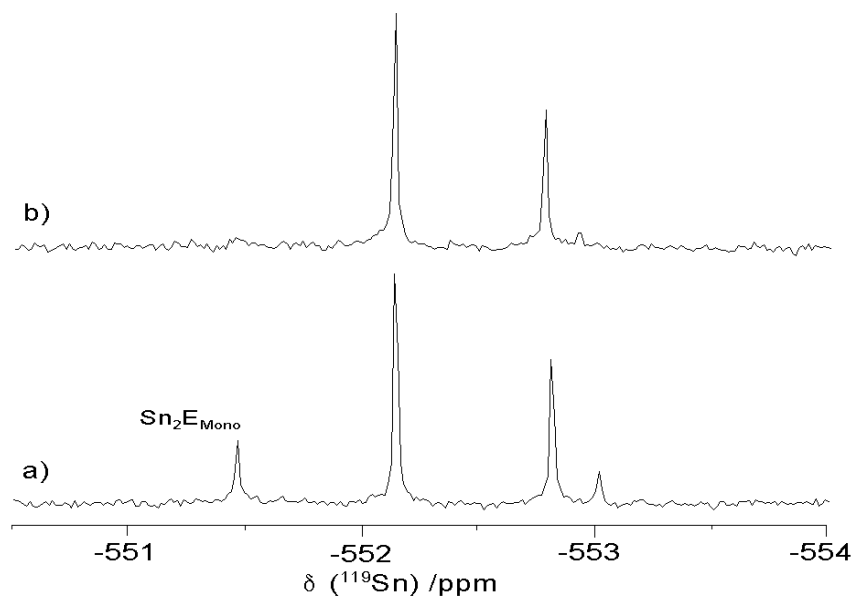


Figure 3.62. ^{119}Sn $\{^1\text{H}\}$ NMR spectra of the erythritol containing solutions represented in Figure 3.59 b and c.

The long distance scalar coupling of the signals between -485 and -530 could not be resolved but, through the chemical shifts, they have been assigned to *bis*-ligand complexes (Figure 3.63). Similarly, the signals ranging between -440 and -480 ppm have been assigned to *tris*-ligand complexes though their chemical shifts (Figure 3.64). The large number of signals results from the numerous binding sites on erythritol.

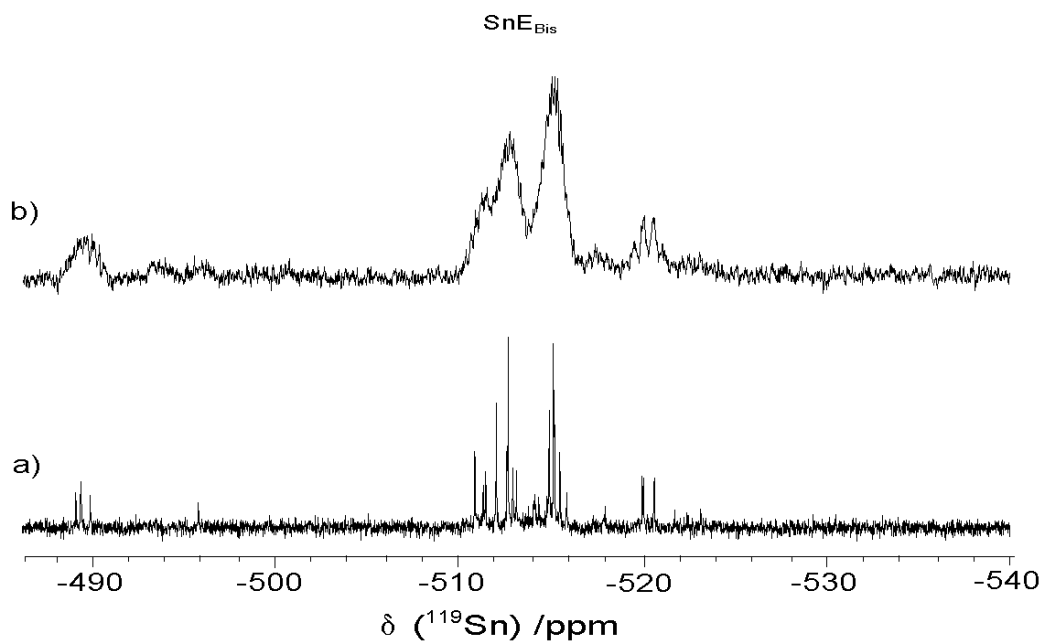


Figure 3.63. ^{119}Sn NMR spectrum of the erythritol containing solution represented in Figure 3.59a, a) with and b) without gated ^1H -decoupling.

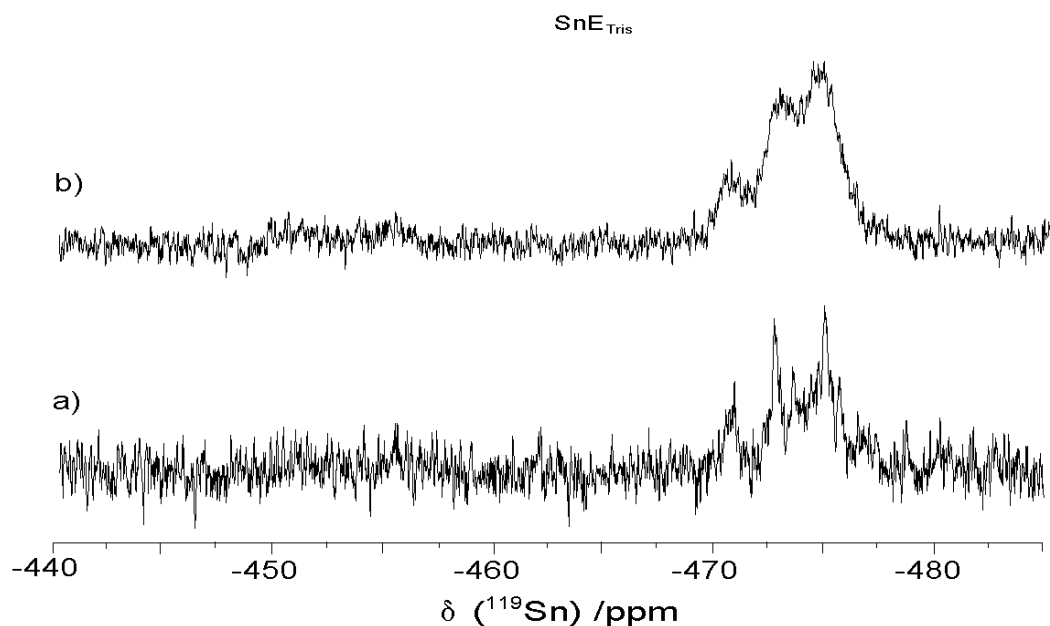


Figure 3.64. ^{119}Sn NMR spectrum of the erythritol containing solution represented in Figure 3.59a, a) with and b) without gated ^1H -decoupling.

The ^{119}Sn NMR spectra increased in complexity when longer chain saccharides were added to stannate solutions. Figure 3.65 shows the ^{119}Sn NMR spectra of alkaline solutions containing stannic acid along with adonitol, xylitol or mannitol. With all of these polyols, Sn formed *mono*-, *bis*- and *tris*-ligand complexes, but the number of isomers of each species exceeded that of the ligands previously analyzed. Due to the large number of signals, we did not attempt to characterize the any of the complexes. Mannitol was included as it has been previously demonstrated to bind stannic acid, forming proposed di-ester *mono*-ligand complexes.^[72, 73] Here, we indicate that there are 7 signals ranging from -540 to -570 ppm (Figure 3.65c) that correspond to *mono*-ligand stannate-mannitol complexes. The exact identities of these signals are still unknown.

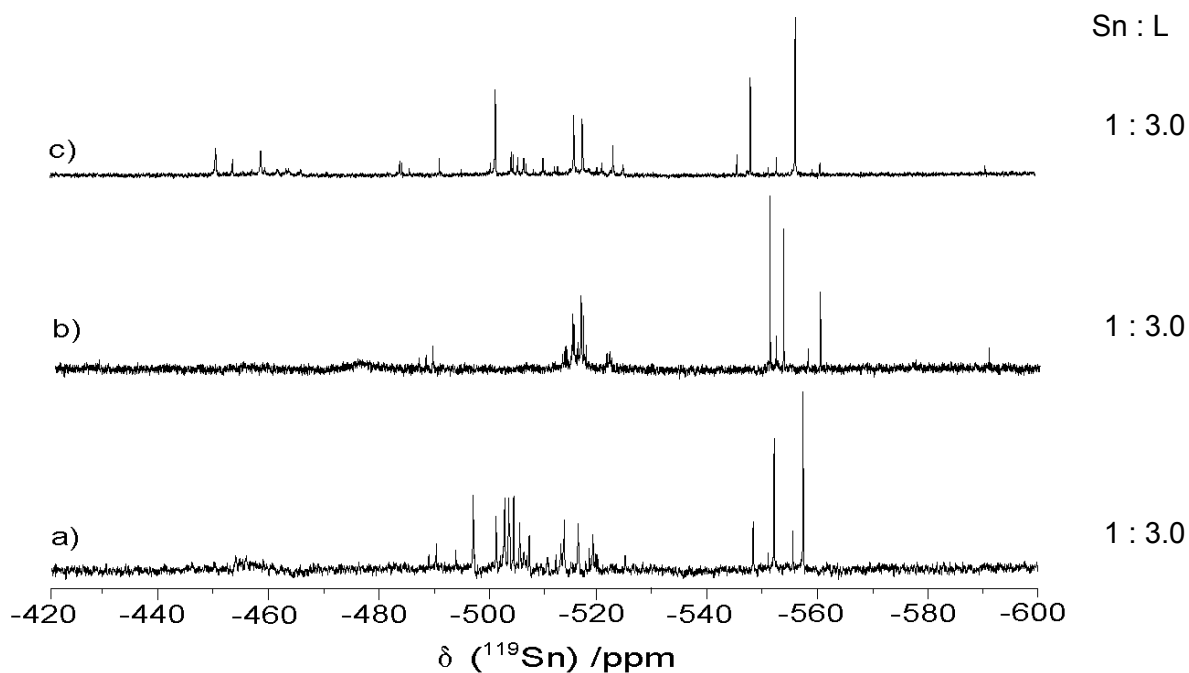
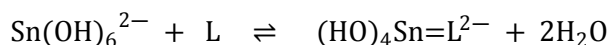


Figure 3.65. $^{119}\text{Sn} \{^1\text{H}\}$ NMR spectra at 5 °C of aqueous solutions containing 0.2 mol kg⁻¹ Sn, 3 mol kg⁻¹ TMAOH, 0.8 mol kg⁻¹ HCl and 0.6 mol kg⁻¹ xylitol (a), adonitol (b) or mannitol (c).

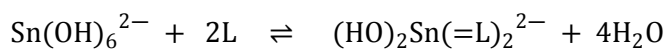
Here, we demonstrated the ability of hydroxyl containing molecules to bind stannic acid. We provided insight towards the structure of these complexes and demonstrated that *mono*-, *bis*- and *tris*-ligand complexes form in solution. All of the saccharides containing 2 or more hydroxyl groups investigated were found to complex stannic acid very strongly. The conditions used in this study were extremely harsh (pH > 14), and attempts at lowering the alkalinity of these solutions all resulted in sample precipitation. Therefore, it is unclear whether these results can be applied to any biological systems.

D. Formation constants of stannate-saccharide complexes

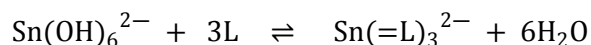
The very high alkalinity of the stannate solutions (pH > 14) precluded accurate pH measurement. We were therefore unable to analyse the stannate complexation equilibria using an analogous reaction scheme to that used for the other oxoacids, that is, employing neutral stannic acid as the starting reactant. Instead, the following scheme was considered:



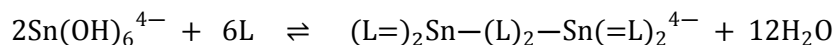
$$\beta_{\text{Mono}}^{\text{Sn}} = \frac{[(\text{HO})_4\text{Sn}=\text{L}^{2-}]}{[\text{Sn(OH)}_6^{2-}][\text{L}]}$$



$$\beta_{\text{B}}^{\text{Sn}} = \frac{[(\text{HO})_2\text{Sn}(=\text{L})_2^{2-}]}{[\text{Sn(OH)}_6^{2-}][\text{L}]^2}$$



$$\beta_{\text{Tris}}^{\text{Sn}} = \frac{[\text{Sn}(=\text{L})_3^{2-}]}{[\text{Sn(OH)}_6^{2-}][\text{L}]^3}$$



$$\beta_{\text{Tris}\ddagger}^{\text{Sn}} = \frac{[(\text{L}=\text{O})_2\text{Sn}-(\text{L})_2-\text{Sn}(=\text{L})_2^{4-}]}{[\text{Sn(OH)}_6^{2-}]^2[\text{L}]^6}$$

where L represents saccharide, and “-L” & “=L” represent mono- and di-ester saccharide linkages, respectively.

The concentrations of the various stannate species and, indirectly (having already established the L:Sn ratio of each species), the free saccharide were determined through the integration of the ^1H -decoupled ^{119}Sn NMR spectra. The solutions used in this study contained high saccharide concentrations to avoid formation of mono-ligand complexes containing more than one stannate centre. The description of the solutions used for the determination of the formation constants can be found in Appendix IX.

The formation constants for the stannate-furanoidic *cis*-diol complexes are shown in Table 3.18. With the exception of cytidine, there was no difference in the formation constants between the ligands. An oxygen heteroatom in the ligand ring did not increase the binding affinity towards stannic acid, as it did with boric and silicic acids. The reason the formation constants for cytidine are greater than the other ligands is unknown.

Table 3.19 shows the formation constants for stannate-polyol complexes at 5 °C. The dihydroxy functionality of the polyol had no effect on the binding affinity towards the stannic acid. Similarly, there was no significant difference between the polyol chain length and the binding coefficients.

Table 3.18. Formation constants for stannate-furanoidic *cis*-diol complexes at 5 °C.^a

	<i>cis</i> -1,2-cyclopentanediol	1,4-anhydroerythritol ^b	D-fructose	cytidine
$\log {}^{\text{Sn}}\beta_{\text{Mono}}$	1.7	2.0	1.8	2.7
$\log {}^{\text{Sn}}\beta_{\text{Bis}}$	3.0	3.8	3.0	5.2
$\log {}^{\text{Sn}}\beta_{\text{Tris}}$	2.7	4.2	3.1	5.7
$\log {}^{\text{Sn}}\beta_{\text{Tris}\ddagger}$	6.7	10.8	nd	nd

^a All values have an experimental uncertainty of approximately ± 1.5 . ^b Formation constants determined at 21 °C. nd = not detectable.

Table 3.19. Formation constants for stannate-polyol complexes at 5 °C. ^a

	threitol	erythritol	xylitol	adonitol	mannitol
$\log {}^{\text{Sn}}\beta_{\text{Mono}}$	2.3	2.0	2.3	1.9	2.3
$\log {}^{\text{Sn}}\beta_{\text{Bis}}$	3.7	3.0	3.6	2.9	3.7
$\log {}^{\text{Sn}}\beta_{\text{Tris}}$	4.3	3.3	3.3	3.3	3.9

^a All values have an experimental uncertainty of approximately ± 1.5 .

Table 3.20 shows a comparison between formation constants for the mono-ligand complexes reported in the literature^[73] and those determined here. The values were similar (within our experimental uncertainty) despite the different solution conditions (pH 11 vs. pH > 14).

Table 3.20. Comparison of the formation constants from the literature and this study. Literature results for stannate-saccharide formation constants at 25.2 °C at pH 11.0 determined using a conductimetric technique. K_{C1} represents formation constants for *mono*-ligand di-ester stannate complexes.^[73]

	Literature values		This study ^a	
	Mannitol	D-fructose	Mannitol	D-fructose
$\log K_{C1}$	1.96	1.37	2.3	1.8

^a Values from this study have an experimental uncertainty of approximately ± 1.5 .

3.2.5 Comparison of saccharide complex formation constants for boric acid, carbonic acid and silicic acid

Here, representative formation constants for the oxoacid-ligand complexes are compared. The relative binding affinities to ligands which are structurally analogous to S-DPD derivatives (specifically cytidine) will indicate the potential ability of these oxoacids to affect AI-2 quorum sensing activity. The formation constants for the stannate-ligand complexes were excluded as complexation was represented differently than the other oxoacids.

A. *Mono*-ligand mono-ester complexes.

Only carbonic acid and silicic acid formed mono-ester complexes with the representative ligands used for determining the formation constants. For silicic acid, only the polyols with *erythro*-dihydroxy functionality formed these complexes, which was initially reported in the previous work conducted in this laboratory.^[64] We suspect that these species do not form with other representative ligands as the equilibrium is shifted significantly towards the formation of the di-ester complexes. Carbonic acid, on the other hand, was found to form mono-ester complexes with every hydroxyl-containing ligand investigated here. Table 3.21 shows representative formation constants for the mono-ester complexes with silicic acid and carbonic acid. The formation constant for the silicate-adonitol complex was similar to that of carbonate, while the silicate-erythritol complex formed less readily than the carbonate-erythritol complex. Presumably, the other silicate-saccharide complexes (specifically the *bis*-ligand complex) shift the equilibrium away from these uni-dentate species. As a result, the formation constants for these silicate-saccharide complexes are similar or slightly lower than those of carbonate. The coordination of the oxoacid centre in these species is different, that is, Si is four-coordinated and C is three-coordinated.

Table 3.21. Representative formation constants for mono-ester complexes with carbonic acid and silicic acid at 5 °C

	H ₂ CO ₃		H ₄ SiO ₄	
	erythritol	adonitol	erythritol	adonitol
log $\beta_{\text{Mono}\dagger}$	2.7 ± 1.2	2.6 ± 1.6	1.4 ± 0.5	2.4 ± 1.2

B. *Mono*-ligand di-ester complexes.

Only boric acid and carbonic acid were found to form *mono*-ligand di-ester complexes with the representative ligands. Table 3.22 shows select formation constants of these complexes. The formation constants for the borate-cytidine complexes are significantly greater than those of carbonate. Similarly, the formation constant for the borate-xylitol di-ester complexes were greater than those of carbonate, as there was no evidence of carbonate-polyol di-ester complexes forming. We note that the coordination of borate and carbonate are different in these complexes, *i.e.*, B has a four-fold coordination while C has a three-fold coordination.

McKenzie *et al.* demonstrated that carbonic acid increases the Al-2 activity in *V. harveyi*, but the increase in activity by boric acid was greater than that of carbonic acid.^[14] The formation constants we report for cytidine show a similar trend, that is, boric acid binds this particular THMF structural analogue far more readily (roughly 8 orders of magnitude) than carbonic acid.

Table 3.22. Representative formation constants for di-ester *mono*-ligand complexes with boric acid and carbonic acid at 5 °C

	H ₃ BO ₃		H ₂ CO ₃	
	xylitol	cytidine	xylitol	cytidine
log β_{Mono}	8.4 ± 0.5	8.5 ± 0.4	nd	0.4 ± 1.0

C. *Bis*-ligand oxoacid complexes.

Only boric acid and silicic acid were determined to form *bis*-ligand complexes with the representative ligands. The oxoacids in these complexes have different geometries, in which B has a four-fold coordination and Si has a five-fold coordination. Table 3.23 shows representative formation constants of the *bis*-ligand complexes for boric acid and silicic acid. The formation constants for borate complexes were approximately five orders of magnitude larger than those of silicate for all three ligands. For both oxoacids, the binding affinities of the ligands with *threo*-dihydroxy functionality were greater (*ca.* two orders of magnitude) than those lacking this functionality.

Table 3.23. Representative formation constants for di-ester *bis*-ligand complexes with boric acid and silicic acid at 5 °C

	H ₃ BO ₃			H ₄ SiO ₄		
	xylitol	adonitol	cytidine	xylitol	adonitol	cytidine
log β_{Bis}	10.9 ± 0.3	8.8 ± 0.6	10.7 ± 0.2	5.6 ± 0.5	3.5 ± 0.6	5.9 ± 0.8

Conclusions

Although we did not demonstrate that inorganic oxoacids can regulate AI-2 quorum sensing activity, we established that it is chemically possible for H_2CO_3 and H_4SiO_4 to bind S-DPD derivatives. We identified the first ever ester-linked complexes spontaneously forming in solution between carbonic acid and hydroxyl containing molecules, including alcohols, polyols and furanoidic vicinal *cis*-diols. The carbon centres in these novel mono- and di-ester species were found to maintain a three-fold coordination. With this information, we demonstrated that the carbonate-S-THMF complex proposed by McKenzie *et al.* is in fact viable, but the carbonate centre would have three-coordination.^[14]

We also determined formation constants for oxoacid complexes involving ligands structurally analogous to S-DPD derivatives. The formation constants are applicable over a wide pH range including physiological conditions. The general binding affinities of the oxoacids to the representative saccharides are: **B > Si > C**. As the binding affinity of silicic acid to the saccharides falls in between that of boric and carbonic acids (both of which found to up-regulate regulate AI-2 quorum sensing activity), it is very plausible that silicic acid can bind THMF and regulate AI-2 quorum sensing activity in bacteria native to silicic acid rich environments.

Additionally, we provided the first ever structural characterization of complexes spontaneously forming in aqueous solution between stannic acid and polyhydroxy hydrocarbons. Stannic acid was found to form *mono*-, *bis*- and *tris*-ligand complexes with ligands containing vicinal diols. Ligands lacking two or more hydroxyl groups, *e.g.*, alcohols, were found to form dilute mono-ester complexes with stannic acid. The Sn centre in all of these complexes was found have six-fold coordination.

Future work

Here, we indicated that both carbonic acid and silicic acid can bind the THMF derivative of S-DPD but *in vivo* studies of the AI-2 quorum sensing activity are still required to confirm our hypothesis that oxoacid modulate quorum sensing. As oxoacids-saccharide complexes have now been indentified for boric, carbonic, silicic and stannic acids, the lifetimes of these complexes should now be determined.

References

- [1] J. M. Henke, B. L. Bassler, *Trends in Cell Biology* **2004**, *14*, 648.
- [2] A. Eberhard, *Journal of Bacteriology* **1972**, *109*, 1101.
- [3] A. Eberhard, A. L. Burlingame, C. Eberhard, G. L. Kenyon, K. H. Nealson, N. J. Oppenheimer, *Biochemistry* **1981**, *20*, 2444.
- [4] K. H. Nealson, T. Platt, J. Woodland Hastings, *Journal of Bacteriology* **1970**, *104*, 313.
- [5] B. L. Bassler, M. Wright, R. E. Showalter, M. R. Silverman, *Molecular Microbiology* **1993**, *9*, 773.
- [6] B. L. Bassler, M. Wright, M. R. Silverman, *Molecular Microbiology* **1994**, *13*, 273.
- [7] X. Chen, S. Schauder, N. Potier, A. Van Dorsselaer, I. Pelczer, B. L. Bassler, F. M. Hughson, *Nature* **2002**, *415*, 545.
- [8] S. Schauder, K. Shokat, M. G. Surette, B. L. Bassler, *Molecular Microbiology* **2001**, *41*, 463.
- [9] K. B. Xavier, B. L. Bassler, *Current Opinion in Microbiology* **2003**, *6*, 191.
- [10] R. McNab, S. K. Ford, A. El-Sabaeny, B. Barbieri, G. S. Cook, R. J. Lamont, *Journal of Bacteriology* **2003**, *185*, 274.
- [11] S. T. Miller, K. B. Xavier, S. R. Campagna, M. E. Taga, M. F. Semmelhack, B. L. Bassler, F. M. Hughson, *Molecular Cell* **2004**, *15*, 677.
- [12] W. Galloway, J. T. Hodgkinson, S. D. Bowden, M. Welch, D. R. Spring, *Chemical Reviews* **2011**, *111*, 28.
- [13] D. S. Blehert, R. J. Palmer, J. B. Xavier, J. S. Almeida, P. E. Kolenbrander, *Journal of Bacteriology* **2003**, *185*, 4851.
- [14] K. M. McKenzie, M. M. Meijler, C. A. Lowery, G. E. Boldt, K. D. Janda, *Chemical Communications* **2005**, 4863.
- [15] S. D. Kinrade, R. J. Balec, A. S. Schach, J. P. Wang, C. T. G. Knight, *Dalton Transactions* **2004**, 3241.
- [16] S. D. Kinrade, E. W. Deguns, A. M. E. Gillson, C. T. G. Knight, *Dalton Transactions* **2003**, 3713.
- [17] M. Noroozi, HBSc thesis, Lakehead University (Thunder Bay, ON), **2010**.
- [18] E. Laasik, L. Andresen, A. Mae, *Fems Microbiology Letters* **2006**, *258*, 227.
- [19] S. J. Coulthurst, K. S. Lilley, G. P. C. Salmond, *Molecular Plant Pathology* **2006**, *7*, 31.
- [20] W. A. Dew, G. G. Pyle, S. D. Kinrade, *Unpublished* **2009**.
- [21] B. N. Lilley, B. L. Bassler, *Molecular Microbiology* **2000**, *36*, 940.
- [22] M. F. Semmelhack, S. R. Campagna, C. Hwa, M. J. Federle, B. L. Bassler, *Organic Letters* **2004**, *6*, 2635.
- [23] J. A. I. Smith, J. X. Wang, S. M. Nguyen-Mau, V. Lee, H. O. Sintim, *Chemical Communications* **2009**, 7033.
- [24] M. M. Meijler, L. G. Hom, G. F. Kaufmann, K. M. McKenzie, C. Z. Sun, J. A. Moss, M. Matsushita, K. D. Janda, *Angewandte Chemie-International Edition* **2004**, *43*, 2106.
- [25] C. A. Lowery, K. M. McKenzie, L. W. Qi, M. M. Meijler, K. D. Janda, *Bioorganic & Medicinal Chemistry Letters* **2005**, *15*, 2395.
- [26] J. A. Freeman, B. L. Bassler, *Molecular Microbiology* **1999**, *31*, 665.
- [27] W. S. Dodds, L. F. Stutzman, B. J. Sollami, *Industrial and Engineering Chemistry* **1956**, *1*, 92.
- [28] Z. T. Wen, R. A. Burne, *Journal of Bacteriology* **2004**, *186*, 2682.
- [29] Z. T. Wen, A. H. Nguyen, J. P. Bitoun, J. Abranches, H. V. Baker, R. A. Burne, *Molecular Oral Microbiology* **2011**, *26*, 2.
- [30] Z. T. Wen, R. A. Burne, *Applied and Environmental Microbiology* **2002**, *68*, 1196.
- [31] M. A. O'Neill, T. Ishii, P. Albersheim, A. G. Darvill, *Annual Review of Plant Biology* **2004**, *55*, 109.

- [32] C. D. Hunt, *Journal of Trace Elements in Experimental Medicine* **2003**, *16*, 291.
- [33] H. N. Hu, S. G. Penn, C. B. Lebrilla, P. H. Brown, *Plant Physiology* **1997**, *113*, 649.
- [34] R. van den berg, J. A. Peters, H. Vanbakkum, *Carbohydrate Research* **1994**, *253*, 1.
- [35] M. Vanduin, J. A. Peters, A. P. G. Kieboom, H. Vanbakkum, *Tetrahedron* **1985**, *41*, 3411.
- [36] M. Makkee, A. P. G. Kieboom, H. Vanbakkum, *Recueil Des Travaux Chimiques Des Pays-Bas- Journal of the Royal Netherlands Chemical Society* **1985**, *104*, 230.
- [37] K. Ishihara, Y. Mouri, S. Funahashi, M. Tanaka, *Inorganic Chemistry* **1991**, *30*, 2356.
- [38] P. P. Power, W. G. Woods, *Plant and Soil* **1997**, *193*, 1.
- [39] M. F. Semmelhack, S. R. Campagna, M. J. Federle, B. L. Bassler, *Organic Letters* **2005**, *7*, 569.
- [40] M. Winter, *Vol. 2012*, WebElement Ltd. UK, **1993-2012**.
- [41] N. W. Rakestraw, H. E. Mahncke, *Ind. Eng. Chem. Anal. Ed.* **1935**, *7*, 425.
- [42] C. R. Parker, *Water analysis by atomic absorption*, Varian Techtron Pty. Ltd., Springvale, Australia, **1972**.
- [43] M. Tariq, C. J. B. Mott, *Journal of Agronomy* **2007**, *6*, 1.
- [44] M. Burguera, J. L. Burguera, C. Rondon, P. Carrero, *Spectrochimica Acta Part B-Atomic Spectroscopy* **2001**, *56*, 1845.
- [45] S. Kempe, *The Global Carbon Cycle*, Scientific Committee on Problems of the Environment, **1979**.
- [46] R. Zeebe, *Vol. 2012*, The Encyclopedia of Earth, **2009**.
- [47] W. J. Cai, M. H. Dai, Y. C. Wang, W. D. Zhai, T. Huang, S. T. Chen, F. Zhang, Z. Z. Chen, Z. H. Wang, *Continental Shelf Research* **2004**, *24*, 1301.
- [48] M. B. David, G. F. Vance, *Environmental Science & Technology* **1989**, *23*, 1021.
- [49] C. Geers, G. Gros, *Physiological Reviews* **2000**, *80*, 681.
- [50] M. Sommer, D. Kaczorek, Y. Kuzyakov, J. Breuer, *Journal of Plant Nutrition and Soil Science-Zeitschrift Fur Pflanzenernahrung Und Bodenkunde* **2006**, *169*, 310.
- [51] R. Jugdaohsingh, *Journal of Nutrition Health & Aging* **2007**, *11*, 99.
- [52] G. Weber, *Fresenius Zeitschrift Fur Analytische Chemie* **1985**, *321*, 217.
- [53] J. F. Ma, *Soil Science and Plant Nutrition* **2004**, *50*, 11.
- [54] G. Heine, G. Tikum, W. J. Horst, *Journal of Plant Nutrition and Soil Science-Zeitschrift Fur Pflanzenernahrung Und Bodenkunde* **2005**, *168*, 600.
- [55] E. Eneji, S. Inanaga, S. Muranaka, J. Li, P. An, T. Hattori, W. Tsuji, *Grass and Forage Science* **2005**, *60*, 393.
- [56] D. W. Rains, E. Epstein, R. J. Zasoski, M. Aslam, *Plant and Soil* **2006**, *280*, 223.
- [57] M. J. Hodson, P. J. White, A. Mead, M. R. Broadley, *Annals of Botany* **2005**, *96*, 1027.
- [58] N. Mitani, J. F. Ma, T. Iwashita, *Plant and Cell Physiology* **2005**, *46*, 279.
- [59] J. F. Ma, K. Tamai, N. Yamaji, N. Mitani, S. Konishi, M. Katsuhara, M. Ishiguro, Y. Murata, M. Yano, *Nature* **2006**, *440*, 688.
- [60] R. K. Iler, *The chemistry of silica*, Wiley, **1979**.
- [61] S. D. Kinrade, K. J. Maa, A. S. Schach, T. A. Sloan, C. T. G. Knight, *Journal of the Chemical Society-Dalton Transactions* **1999**, 3149.
- [62] S. D. Kinrade, J. W. Del Nin, A. S. Schach, T. A. Sloan, K. L. Wilson, C. T. G. Knight, *Science* **1999**, *285*, 1542.
- [63] S. D. Kinrade, R. J. Hamilton, A. S. Schach, C. T. G. Knight, *Journal of the Chemical Society-Dalton Transactions* **2001**, 961.
- [64] B. Vis, HBSc thesis, Lakehead University (Thunder Bay, ON), **2010**.
- [65] J. Wen, MSc thesis, Lakehead University (Thunder Bay, ON), **2006**.
- [66] J. B. Lambert, G. Lu, S. R. Singer, V. M. Kolb, *Journal of the American Chemical Society* **2004**, *126*, 9611.
- [67] S. D. Kinrade, A. S. Schach, R. J. Hamilton, C. T. G. Knight, *Chemical Communications* **2001**, 1564.

- [68] K. Schwarz, D. B. Milne, V. Vinyard, *Biochemical and Biophysical Research Communications* **1970**, *40*, 23.
- [69] J. F. Lascourreges, P. Caumette, O. F. X. Donard, *Applied Organometallic Chemistry* **2000**, *14*, 98.
- [70] J. Mbabazi, M. Ntale, J. Kwetegyeka, G. Mulongo, H. Twinomuhwezi, P. Nnamuyomba, *Research Journal of Chemical Sciences* **2011**, *1*, 30.
- [71] J. Mbabazi, *Carbohydrate Research* **1985**, *140*, 151.
- [72] J. Mbabazi, *Polyhedron* **1985**, *4*, 75.
- [73] J. Mbabazi, J. Wasswa, M. Ntale, *Bulletin of the Chemical Society of Ethiopia* **2010**, *24*, 447.
- [74] R. Boncukcuoglu, A. E. Yilmaz, M. M. Kocakerim, M. Copur, *Desalination* **2004**, *160*, 159.
- [75] S. D. Kinrade, R. T. Syvitski, K. Marat, C. T. G. Knight, *Journal of the American Chemical Society* **1996**, *118*, 4196.
- [76] J. G. Cao, Z. Y. Wei, E. A. Meighen, *Biochemical Journal* **1995**, *312*, 439.
- [77] H. Sztajer, A. Lemme, R. Vilchez, S. Schulz, R. Geffers, C. Y. Y. Yip, C. M. Levesque, D. G. Cvitkovitch, I. Wagner-Dobler, *Journal of Bacteriology* **2008**, *190*, 401.
- [78] M. M. Hossain, S. Tsuyumu, *Journal of General Plant Pathology* **2006**, *72*, 34.
- [79] P. Chomczynski, N. Sacchi, *Analytical Biochemistry* **1987**, *162*, 156.
- [80] C. A. Heid, J. Stevens, K. J. Livak, P. M. Williams, *Genome Research* **1996**, *6*, 986.
- [81] Z. E. Nackerdien, A. Keynan, B. L. Bassler, J. Lederberg, D. S. Thaler, *Plos One* **2008**, *3*.
- [82] F. Devreux, A. Ledieu, P. Barboux, Y. Minet, *Journal of Non-Crystalline Solids* **2004**, *343*, 13.
- [83] A. Ledieu, F. Devreux, P. Barboux, L. Sicard, O. Spalla, *Journal of Non-Crystalline Solids* **2004**, *343*, 3.
- [84] A. Davis, J. H. Golden, *Journal of the Chemistry Society B: Physical Organic* **1968**, 45.
- [85] N. Guarrotxena, L. Audouin, J. Verdu, *Angewandte Makromolekulare Chemie* **1997**, *247*, 73.
- [86] D. M. Mowery, R. L. Clough, R. A. Assink, *Macromolecules* **2007**, *40*, 3615.
- [87] G. R. McDonald, A. L. Hudson, S. M. J. Dunn, H. T. You, G. B. Baker, R. M. Whittal, J. W. Martin, A. Jha, D. E. Edmondson, A. Holt, *Science* **2008**, *322*, 917.
- [88] A. E. Yilmaz, R. Boncukcuoglu, M. T. Yilmaz, M. M. Kocakerim, *Journal of Hazardous Materials* **2005**, *117*, 221.
- [89] M. Ozdemir, I. Kipcak, *Environmental Progress* **2007**, *26*, 375.
- [90] M. D. D. Garcia-Soto, E. M. Camacho, *Solvent Extraction and Ion Exchange* **2005**, *23*, 741.
- [91] S. J. Hawkes, *Journal of Chemical Education* **1995**, *72*, 799.
- [92] S. D. f. O. C. SDBS, *Vol. 2012*, National Institute of Advanced Industrial Science and Technology.
- [93] C. B. Kim, M. A. Park, B. Song, K. Park, *Bulletin of the Korean Chemical Society* **2003**, *24*, 1371.
- [94] S. Komatsu, T. Takata, T. Endo, *Macromolecules* **1993**, *26*, 875.
- [95] S. Komatsu, T. Takata, T. Endo, *Macromolecules* **1992**, *25*, 7286.
- [96] J. W. Stansbury, *Journal of Dental Research* **1992**, *71*, 1408.
- [97] V. Exarchou, A. Troganis, I. P. Gerotheranassis, M. Tsimidou, D. Boskou, *Tetrahedron* **2002**, *58*, 7423.
- [98] G. Ruderman, E. R. Caffarena, I. G. Mogilner, E. J. Tolosa, *Journal of Solution Chemistry* **1998**, *27*, 935.
- [99] OMM Scientific, **2012**.
- [100] F. S. Nakayama, *Journal of Inorganic and Nuclear Chemistry* **1971**, *33*, 1287.
- [101] S. Sjoberg, Y. Hagglund, A. Nordin, N. Ingri, *Marine Chemistry* **1983**, *13*, 35.
- [102] R. H. Busey, R. E. Mesmer, *Inorganic Chemistry* **1977**, *16*, 2444.
- [103] M. J. Taylor, J. M. Coddington, *Polyhedron* **1992**, *11*, 1531.
- [104] S. D. Kinrade, R. J. Balec, *Unpublished* **2004**.
- [105] J. C. Meurice, J. G. Duboudin, M. Ratier, M. Petraud, R. Willem, M. Biesemans, *Organometallics* **1999**, *18*, 1699.

- [106] G. Casella, F. Ferrante, G. Saielli, *Organic & Biomolecular Chemistry* **2010**, *8*, 2711.
- [107] R. Hani, R. A. Geanangel, *Coordination Chemistry Reviews* **1982**, *44*, 229.
- [108] K. Benner, J. Ihringer, P. Klufers, D. Marinov, *Angewandte Chemie-International Edition* **2006**, *45*, 5818.
- [109] N. P. Wen, M. H. Brooker, *Journal of Physical Chemistry* **1995**, *99*, 359.
- [110] J. Y. Park, S. J. Yoon, H. Lee, *Environmental Science & Technology* **2003**, *37*, 1670.
- [111] A. Ricardo, M. A. Carrigan, A. N. Olcott, S. A. Benner, *Science* **2004**, *303*, 196.
- [112] G. Springsteen, G. F. Joyce, *Journal of the American Chemical Society* **2004**, *126*, 9578.
- [113] P. Ball, *Chemical Reviews* **2008**, *108*, 74.
- [114] G. Engelhardt, D. Hoebbel, W. Wieker, H. Jancke, *Zeitschrift Fur Chemie* **1974**, *14*, 109.
- [115] R. C. Mawhinney, R. C. Merchant, *Unpublished* **2010**.

Appendix I. A study of the interactions between carbonic acid and amine buffers

Introduction

Primary amines have been found to bind $\text{CO}_{2(l)}$ through carbon-nitrogen linkages and are therefore used to remove atmospheric carbon dioxide.^[109] The formation of carbon-nitrogen bonds, referred to as carbamide linkages, have been well characterized using UV-Vis and NMR spectroscopy.^[109, 110] Here, we characterize the complexes that form between carbonic acid and two amine buffers.

Methods

Carbonate solutions were prepared by dissolving $\text{Na}_2^{13}\text{CO}_3$ into solutions buffered with tris (2-amino-2-hydroxymethyl-propane-1,3-diol) or ammonium. Carbon-13 NMR spectra were acquired at 125.67 MHz with a 90° pulse angle and a 4 s recycle time. Chemical shifts were internally referenced to the solvent.

Results and Discussion

Figure A1 shows the ^{13}C NMR spectrum of a solution containing $0.069 \text{ mol kg}^{-1}$ $\text{Na}_2^{13}\text{CO}_3$ and $0.744 \text{ mol kg}^{-1}$ tris at pH 7.02. The signals at 158.50, 163.87 and 163.91 ppm correspond to carbonate-tris complexes. The signal at 158.50 ppm was split into a triplet from three-bond scalar coupling to the ligand $-\text{CH}_2-$ protons. It corresponds to the ester-linked complex **CTR_{Monot}** (Table A1) which is analogous to those in Section 3.2.2. The signals at 163.87 and 163.91 ppm have been assigned to carbonate-tris complexes bound through carbamide linkages, denoted as **CTR_{C+}** (Table A1). No proton coupling was detected. A carbamide linkage between aqueous carbon dioxide and tris has been previously reported.^[110] However, only one signal in this range was present in the ^{13}C NMR spectrum. Investigations were conducted to identify the complex that corresponds to the additional signal.

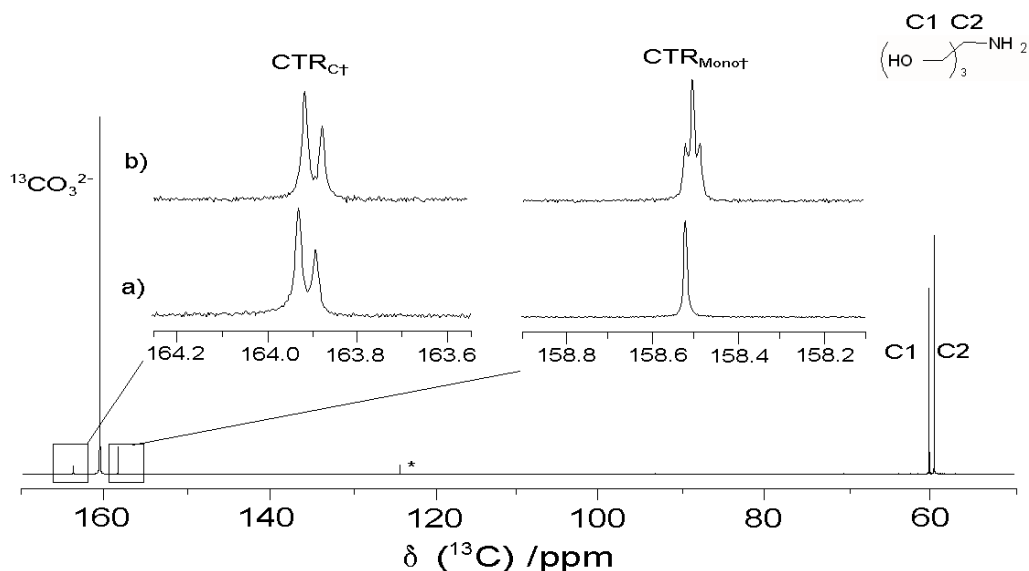


Figure A1. Carbon-13 NMR spectrum of an aqueous solution containing $0.069 \text{ mol kg}^{-1}$ $\text{Na}_2^{13}\text{CO}_3$ and $0.744 \text{ mol kg}^{-1}$ tris at pH 7.0 and 5°C . The expanded region is shown a) with and b) without gated ^1H decoupling. (The signal corresponding to $\text{CO}_{2(l)}$ is marked with an asterisk.)

Figure A2 shows expansions of the ^1H -decoupled ^{13}C NMR spectra of solutions containing 0.05 mol kg^{-1} $\text{Na}_2^{13}\text{CO}_3$ and 0.7 mol kg^{-1} tris at pH ranging from 7 to 13. The ratio between the signals at 163.87 and 163.91 ppm decreased upon increasing temperature from 5 to 25°C (Figure A1) but did not change with pH which would suggest that these signals do not correspond to two protonation states of the carbamide linked complex. They are instead suspected to be conformational isomers of the carbamide linked complex.

Figure A3 shows that the combined concentration of the carbamide linked complexes rises to a maximum level between pH 8.5 and 10, approximately correlating to the presence of both mono-deprotonated carbonic acid (HCO_3^-) and neutral amine of tris buffer ($(\text{CH}_2\text{OH})_3\text{CNH}_2$).

The pH dependence of the ester linked complex $\text{CTR}_{\text{Mono}\dagger}$ is shown in Figure A4. The concentration roughly correlates to the abundance of HCO_3^- .

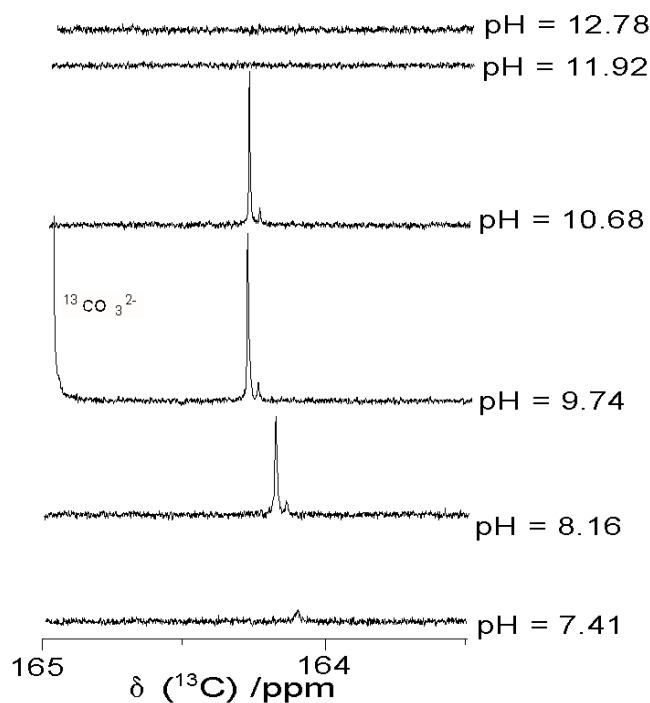


Figure A2. Carbon-13 NMR spectra of aqueous solutions containing $0.05 \text{ mol kg}^{-1} \text{ Na}_2^{13}\text{CO}_3$ and 0.7 mol kg^{-1} tris at different pH values and 25°C .

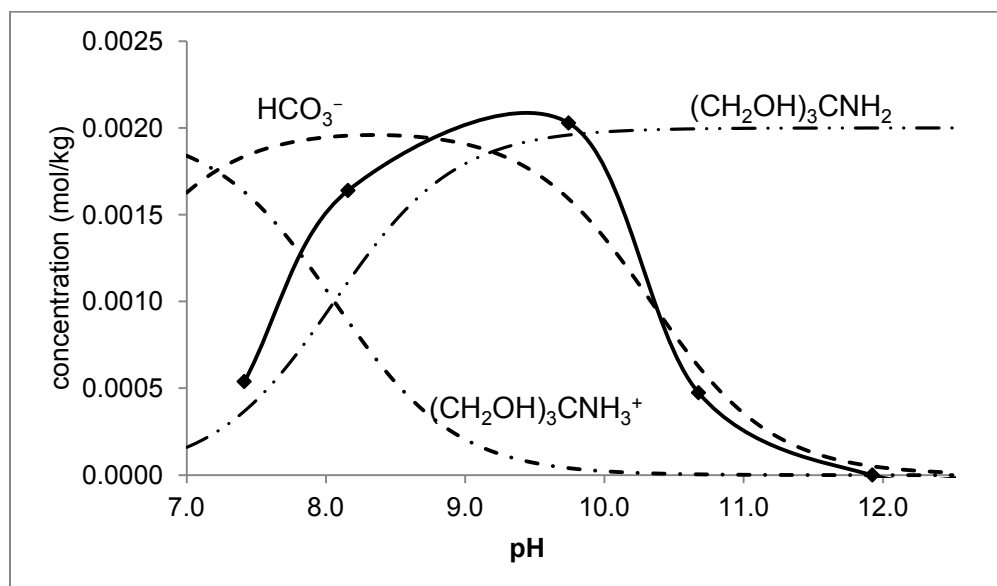


Figure A3. Combined concentration of the two proposed carbamide complexes (solid line) as a function of pH at 25°C for solutions containing $0.05 \text{ mol kg}^{-1} \text{ Na}_2^{13}\text{CO}_3$ and 0.74 mol kg^{-1} tris. The relative concentration of HCO_3^- , $(\text{CH}_2\text{OH})_3\text{CNH}_2$ and $(\text{CH}_2\text{OH})_3\text{CNH}_3^+$ were calculated from their respective pK_a s.

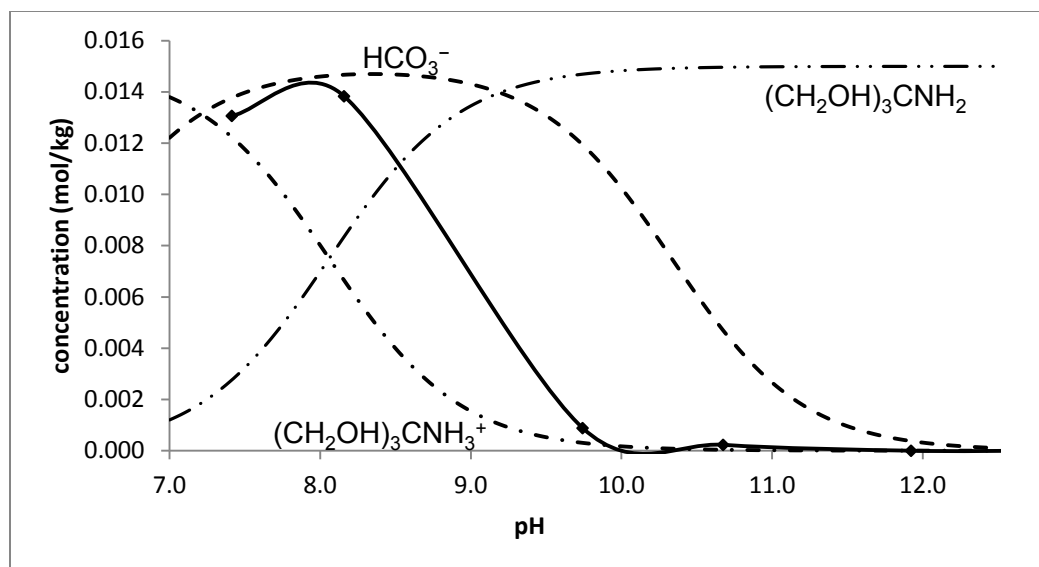


Figure A4. Concentration of the ester linked **CTR_{Mono+}** complex vs pH at 25 °C. The concentration of the complex (solid line) was determined through the quantification of the ¹H-decoupled ¹³C NMR spectra of aqueous solutions containing 0.05 mol kg⁻¹ Na₂¹³CO₃ and 0.744 mol kg⁻¹ tris. The relative concentration of HCO₃⁻, (CH₂OH)₃CNH₂ and (CH₂OH)₃CNH₃⁺ were determined according to their respective pK_a values at 25 °C.

Figure A5 shows the ¹³C NMR spectrum of a solution containing 0.073 mol kg⁻¹ Na₂¹³CO₃ and 1.007 mol kg⁻¹ ammonium chloride at pH 9.98. At 25 °C, there was an additional signal overlapping with the signal corresponding to free carbonic acid (Figure A5b). Upon cooling the solution to 5 °C, the separation between these two signals increased (Figure A5a). In both the ¹H-coupled and ¹H-decoupled ¹³C NMR spectra, the signal at 165.51 ppm was split into a triplet (Figure A5c,d) and has been assigned to a carbamide-linked complex between ammonia and carbonic acid, denoted as **CAM_{c+}** (Table A1). This complex is analogous to that previously characterized by Wen *et al.* between carbon dioxide and ammonia, which they assigned to a carbamide ion complex (NH₂COO⁻).^[109]

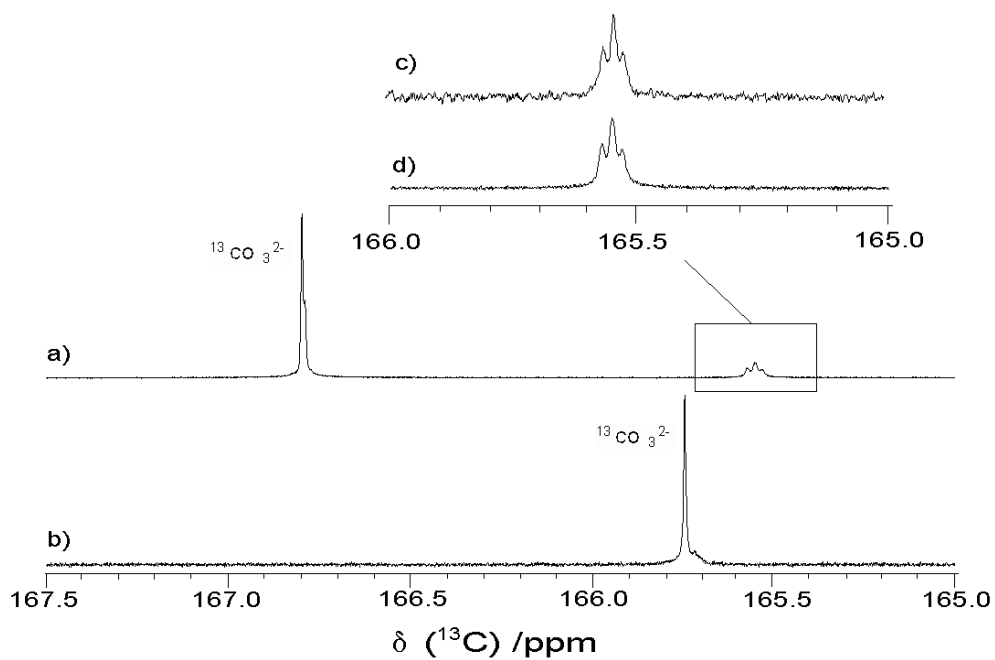
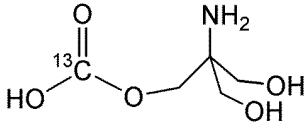
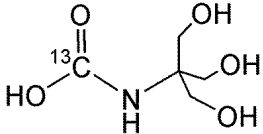
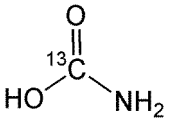


Figure A5. Carbon-13 NMR spectrum (125.67 MHz) of an aqueous solution containing $0.073 \text{ mol kg}^{-1} \text{ Na}_2^{13}\text{CO}_3$ and $1.007 \text{ mol kg}^{-1}$ ammonium chloride at pH 9.98, acquired at a) $5 \text{ }^\circ\text{C}$ and b) $21 \text{ }^\circ\text{C}$. The expanded region is shown c) with and d) without gated ^1H decoupling at $5 \text{ }^\circ\text{C}$.

Table A1. Representative ^{13}C NMR peak assignment of carbonate complexes with amine buffers.

Amine	Structure	Notation ^a	$^3J(^{13}\text{C}, ^1\text{H})$ coupling of ^{13}C NMR carbonate signal (/Hz) ^b
tris		CTR_{Monot}	2.2 (t)
		CTR_{C†}	nr
ammonia		CAM_{C†}	2.5 (t) ^c

^a The “C” subscript in the notation system represents a carbamide linkage, the symbol † denotes a mono-ester complex, TR = tris and AM = ammonium ^b Multiplicity represented by t (triplet). ^c Suspected $^1J(^{13}\text{C}, ^{14}\text{N})$.

Conclusions

Here, we determined complexes forming between common biological buffers and carbonic acid. Therefore, these buffers were not used in the investigation of the complexes between carbonic acid and hydroxyl-contain molecules (in Section 3.2.2).

Appendix II. A study of the use of boric acid to stabilize aqueous *S*-DPD in alkaline environments.

Introduction

In aqueous solution, *S*-DPD and its derivatives undergo rapid decomposition, except at low concentrations (ca. 4 mmol kg⁻¹) and in acidic conditions (pH < 2).^[24, 99] Thus, it is unlikely to survive the long periods that are necessary to acquire a ¹³C or a ²⁹Si NMR spectrum of the corresponding silicate complexes. Boric acid stabilizes *S*-DPD derivatives at pH 8,^[39] just as it has been shown to stabilize ribose from hydrolysis under alkaline conditions.^[111] Our objective was to determine whether boric acid can be used for increase the stability of *S*-DPD under alkaline conditions in the presence of excess silicic acid.

Methods

Solutions were prepared by adding freshly prepared ribose solution (ca. 10 mmol kg⁻¹) and an alkaline borate solution (ca. 10 mmol kg⁻¹) to a previously prepared alkaline silicate solution (ca. 1 mol kg⁻¹, Section 2.1). Hydrogen-1 NMR spectra were acquired at 499.97 MHz with a 90° pulse angle and a 10 s recycle time, using a presaturation pulse sequence to suppress the water signal. Chemical shifts were internally referenced to the solvent.

Results and Discussion

Figure A6 shows the ¹H NMR spectra of a 1 mol kg⁻¹ silicate solution containing 4 mmol kg⁻¹ ribose (*S*-DPD derivative analogue) and 4 mmol kg⁻¹ boric acid. The signals at 4.9 ppm and 3.5 ppm are from C₁ and C₂ hydrogens of β-pyranose.^[112] These signals were not present in Figure A6 as ribose is bound to boron or silicon resulting in a frequency shift. We therefore used the ¹H NMR spectrum at 0 days to represent intact ribose. After 5 and 12 days the ¹H NMR spectra changed significantly, suggesting that ribose is decomposing over time. We suspect that the silicic acid is prevented boric acid from binding and stabilizing ribose. Similar results were observed upon decreasing silicic acid concentration and increasing the boric acid concentration. Therefore, it is unlikely that boric acid can stabilize the *S*-DPD derivatives for the long periods necessary to acquire a ¹³C or a ²⁹Si NMR spectrum of the corresponding silicate complexes.

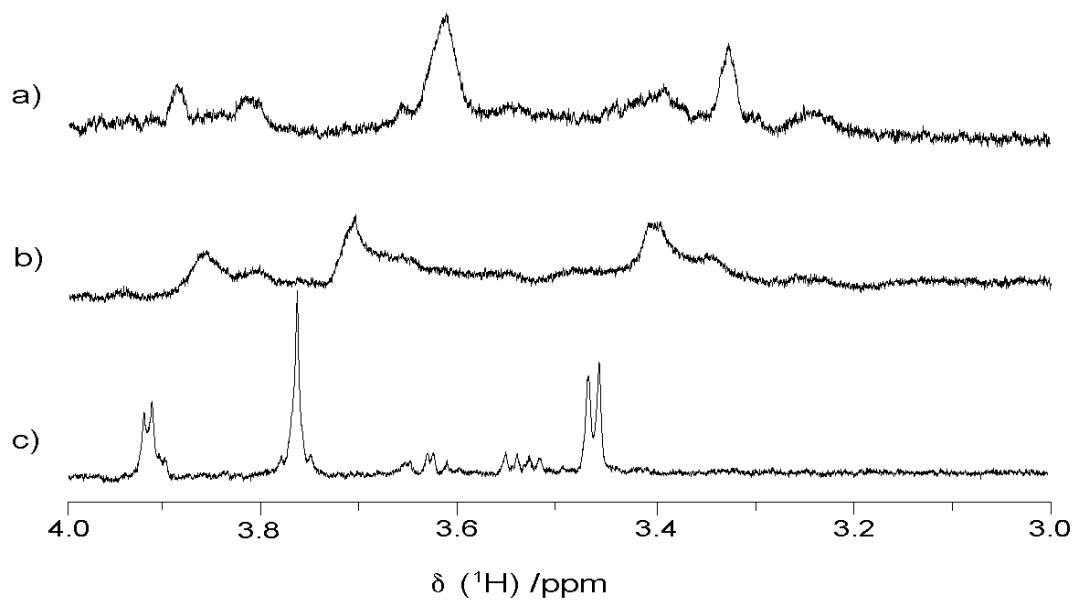


Figure A6. Expanded regions of ^1H NMR spectra of a sample containing 1 mol kg^{-1} Si, 4 mmol kg^{-1} B and 4 mmol kg^{-1} D-ribose at a) 0 days, b) 5 days and c) 12 days.

Conclusion

Boric acid in the presence of excess silicic acid does not increase the stability of D-ribose.

Appendix III. Silicon-polyol interaction in a polysaccharide artificial cell environment

Introduction

Previous investigations of aqueous silicate-saccharide interactions were conducted in bulk solution.^[15, 16, 61-63] Although these studies provide insight towards the chemistry of silicon, they may not be directly translatable to processes taking place in a cellular environment where there is little free water.^[113] Here we investigated the speciation of silicic acid in polysaccharide gels as a proxy for the cell environment.

For this study we employed the nomenclature system that was previously developed for silicate species.^[62, 114] The symbol Q represents each a quadrifunctional silicon centre and its degree of connectivity (number of siloxane linkages) is represented by a superscript. For example, monomeric silicic acid is denoted by Q⁰ and dimeric silicic acid (H₆Si₂O₇) by Q¹Q¹ or Q¹₂, where the subscript represents the number of equivalent Si centres in the species. Pentaosilicon *bis*-(diolato)-hydroxo and hexaosilicon *tris*-(diolato) complexes are denoted as PL₂ and HL₃, respectively, where P and H represent 5- and 6-coordinate silicate centres and L represents saccharide ligand. The regions corresponding to the complexes are defined in Figure A7.

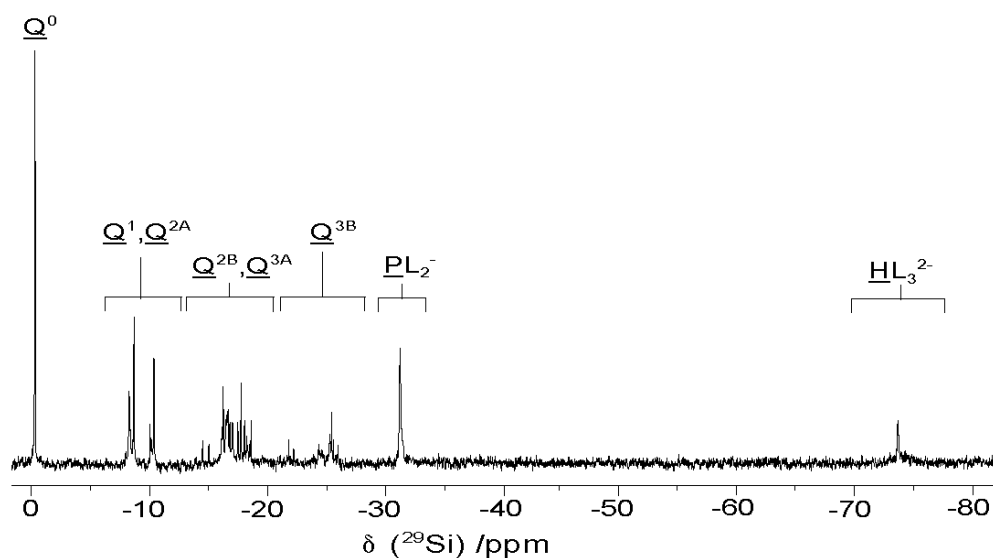


Figure A7. Silicon-29 NMR spectrum (99.28 MHz) of a sample containing 1.54 mol kg⁻¹ Si, 1.54 mol kg⁻¹ OH, 1.62 mol kg⁻¹ arabitol and 7.57 wt% n-propanol. The signals are labeled as described above.

Methods

To create the gel matrix, solid polysaccharide powder (polyethylene oxide, polyvinyl alcohol, polyethylene glycol, agarose, and gelatin) was added directly to an alkaline silicate solution with or without xylitol, in a FEP NMR tube liner (8 mm I.D.). The tube was placed in boiling water for 10 min and allowed to cool to room temperature. Silicon-29 NMR spectra were acquired using a 90° pulse angle and a 40 s recycle time. Chemical shifts were reported relative to the silicic acid monomer signal, set to 0 ppm.

Results and Discussion

Polyethylene oxide, polyvinyl alcohol, polyethylene glycol and gelatin all resulted in the formation of multiphase mixtures and were not investigated further. Only agarose was found to form a single phase gel in the presence of silicic acid. There was no evidence of a direct

interaction between silicic acid and the gel. Table A2 shows the distribution of \underline{Q} -centres in a silicate solution as a function of agarose content. The concentrations of the larger silicate oligomers (\underline{Q}^{3B}) increased by 30-50% in the gel, while the concentration of the other oligomers (\underline{Q}^0 , \underline{Q}^1 , \underline{Q}^{2A} , \underline{Q}^{2B} and \underline{Q}^{3A}) decreased or remained the same. As silicate oligomerization occurs through condensation reactions and as agarose decreases the amount of available water, the concentration of the \underline{Q}^{3B} species increases in the gel matrix.

Cytoplasm can contain up to 400 g L^{-1} of macromolecules.^[113] Some of the sugar alcohols in a typical cellular environment have been demonstrated to bind silicic acid in bulk solution.^[16, 62, 63] Here, the interactions between silicic acid and xylitol in an agarose gel were investigated to mimic a cellular environment. Table A3 shows the concentrations of the silicate species with and without agarose gel. The concentration of smaller silicate oligomers (\underline{Q}^0 and \underline{Q}^1 , \underline{Q}^{2A}) decreased while the concentration of the larger silicate oligomers (\underline{Q}^{2B} - \underline{Q}^{3A} and \underline{Q}^{3B}) and silicate-xylitol complexes (\underline{PL}_2 and \underline{HL}_3) increased in the gel samples. Specifically, the concentration of the \underline{PL}_2^- and \underline{HL}_3^{2-} complexes increased by 50 to 100% in the gels. Silicon-saccharide complexation, which also occurs through condensation reactions, increases as the amount of available water decreased.

Table A2. The concentration of \underline{Q} -centres in silicate solutions mixtures containing 1.01 mol kg^{-1} Si, $1.01 \text{ mol kg}^{-1} \text{ OH}^-$ and 0 to 9.1 wt% agarose.

components		species concentration / mol kg^{-1}			
Si / mol kg^{-1}	agarose / wt%	\underline{Q}^0	\underline{Q}^1 , \underline{Q}^{2A}	\underline{Q}^{2B} , \underline{Q}^{3A}	\underline{Q}^{3B}
1.06	0	0.17	0.27	0.44	0.12
	1	0.15	0.24	0.46	0.16
	4.8	0.14	0.26	0.45	0.15
	9.1	0.15	0.26	0.43	0.17

Table A3. The concentration of silicate species present in silicate mixtures containing 1.01 mol kg⁻¹ Si, 1.01 mol kg⁻¹ OH⁻, 0.51 mol kg⁻¹ xylitol and 0 to 9.1 wt% agarose.

Si / mol kg ⁻¹	components		species concentrations / mol kg ⁻¹					
	xylitol / mol kg ⁻¹	agarose wt%	<u>Q</u> ⁰	<u>Q</u> ¹ , <u>Q</u> ²	<u>Q</u> ² , <u>Q</u> ³	<u>Q</u> ³	<u>PL</u> ₂ ⁻	<u>HL</u> ₃ ²⁻
1.06	0.51	0	0.134	0.279	0.444	0.118	0.014	0.016
		1	0.145	0.244	0.422	0.149	0.029	0.017
		4.8	0.101	0.229	0.464	0.167	0.025	0.020
		9.1	0.120	0.222	0.441	0.173	0.037	0.014

Conclusion

As expected, the concentration of the larger silicate oligomers and the silicate-saccharide complexes increased in the gel environment from that in bulk solution. Hence, the formation constants reported in Section 3.2 would likely be larger in a cellular environment.

Appendix IV. Silicate speciation in the presence of co-solvent.

Introduction

Here, we investigated the effect that co-solvents have on silicate speciation. The nomenclature system described in Appendix III was used.

Method

Methanol, ethanol or *n*-propanol was added to a silicate solution containing a saccharide ligand directly in the FEP NMR tube liner, followed by extensive mixing. Silicon-29 NMR spectra were acquired using a 90° pulse angle and a 40 s recycle time. Chemical shifts were reported relative to the silicic acid monomer signal, set to 0 ppm.

Results and discussion

Precipitation occurred immediately upon the addition of small volumes of methanol or ethanol to a silicate-saccharide solution. There was no visible precipitation, however, upon addition of similar volumes of *n*-propanol. Table A4 shows the concentration of silicate species as a function of *n*-propanol addition. The concentration of smaller silicate oligomers (\underline{Q}^0 , \underline{Q}^1 and \underline{Q}^{2A}) decreased while those of the larger silicate oligomers (\underline{Q}^{2B} , \underline{Q}^{3A} and \underline{Q}^{3B}) and silicate-arabitol complexes (\underline{PL}_2^- and \underline{HL}_3^{2-}) increased. More specifically, the concentration of the \underline{Q}^{3B} oligomers increased by ca. 35% and the concentration of the \underline{PL}_2 and the \underline{HL}_3 complexes increased by ca. 17% and 9%, respectively. Silicate oligomers and silicate-saccharide complexes form through condensation reactions and, as *n*-propanol decreases the amount of available water, the equilibrium shifts towards these species.

Table A4. The concentration of silicate species present in silicate mixtures containing 1.54 mol kg⁻¹ Si, 1.54 mol kg⁻¹ OH, 1.62 mol kg⁻¹ arabitol and 0 to 7.57 wt% n-propanol

Si / mol kg ⁻¹	components		species concentrations / mol kg ⁻¹					
	arabitol / mol kg ⁻¹	n-propanol / wt%	\underline{Q}^0	$\underline{Q}^1, \underline{Q}^{2A}$	$\underline{Q}^{2B}, \underline{Q}^{3A}$	\underline{Q}^{3B}	\underline{PL}_2^-	\underline{HL}_3^{2-}
1.54	1.62	0	0.30	0.38	0.51	0.11	0.21	0.10
		7.57	0.24	0.33	0.53	0.15	0.24	0.11

Conclusion

The concentration of the larger silicate oligomers and silicate-saccharide complexes increases in the presence of the co-solvent due to the decreased amount of available water.

Appendix V. Complexation of silicic acid by furanoidic vicinal *trans*-diols

Introduction

Previous studies have shown that silicic acid is unable to form di-ester linked complexes with furanoidic vicinal-diol molecules if the hydroxyl groups are in *trans* configuration.^[15, 16, 66] Aliphatic polyhydroxy molecules lacking *threo*-dihydroxy functionality were similarly thought to be unable to bind Si through such linkages, but recent computational and high sensitivity ²⁹Si NMR spectroscopic analysis have shown that di-ester linked complexes involving such ligands may indeed occur, albeit at very low concentration.^[62, 64, 115] Here, we employ similar spectroscopic techniques to test the principle that silicic acid does not form di-ester linkages with vicinal *trans*-diols.

Methods

Solutions were prepared by dissolving ²⁹SiO₂ (Isotonics, 99.35 atom% ²⁹Si) in aqueous KOH in a PTFE-lined pressure vessel at 170 °C for a minimum of 24 h. *Trans*-1,2-cyclopentane-1,2-diol was added to the resulting solution without heat. Silicon-29 NMR spectra were acquired using a 90° pulse angle and a 40 s recycle time. Chemical shifts were reported relative to the silicic acid monomer signal, set to 0 ppm

Results and discussion

Figure A8 shows the ¹H-decoupled ²⁹Si NMR spectrum of a solution containing ²⁹SiO₂ and *trans*-1,2-cyclopentane-1,2-diol. As suggested previously, there is no evidence of a di-ester linkage between Si and *trans*-1,2-cyclopentane-1,2-diol. There was, however, an additional signal just down-frequency from the silicic acid monomer signal corresponding to a mono-ester tetraoxosilicon complex, analogous to the alkoxy substituted silicate complexes with alcohols.^[61]

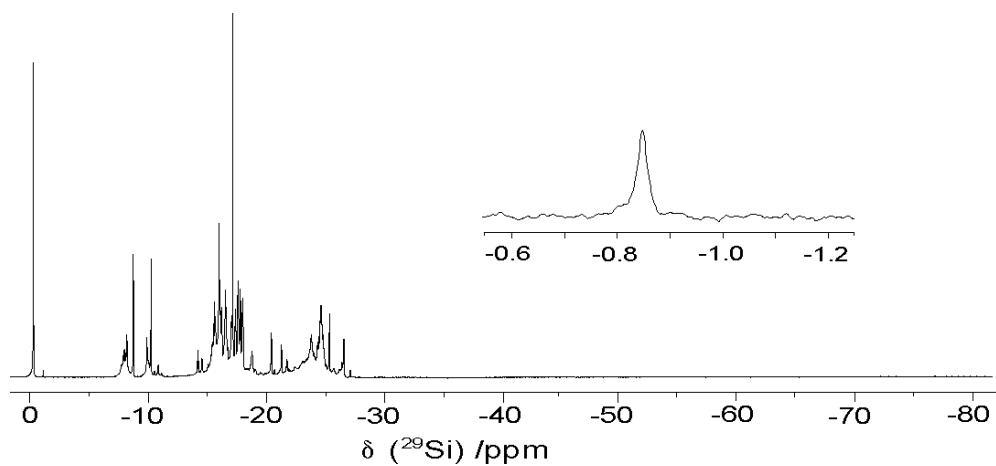


Figure A8. Silicon-29 NMR spectrum (99.28 MHz) of a solution containing $1.04 \text{ mol kg}^{-1} \text{ }^{29}\text{Si}$, $1.04 \text{ mol kg}^{-1} \text{ OH}^-$ and $3.06 \text{ mol kg}^{-1} \text{ trans-1,2-cyclopentane-1,2-diol}$. The inset spectrum is an expansion of the signal corresponding to a tetraoxosilicon mono-ester *trans*-1,2-cyclopentane-1,2-diol complex.

Conclusion

Despite using high resolution spectroscopic techniques, no di-ester linkages between silicic acid *trans*-1,2-cyclopentane-1,2-diol were detected.

Appendix VI. Composition of solutions used in determining the formation constants of the borate-ligand complexes

A. Solutions used for the determination of the formation constants for borate-furanoidic *cis*-diol complexes at 25 °C.

L= *cis*-1,2-cyclopentanediol

T = 25 °C

Solution number	Initial solution composition (mol/kg)		Concentration of B in the each species (determined through integration of ^{11}B NMR spectrum, mol/kg)		Concentration of L in borate complexes (mol/kg)	
bv.12.276	[H ₃ BO ₃]	0.099	[H ₃ BO ₃]	0.049	(HO) ₂ B=L ⁻	nd
	[L]	0.252	(HO) ₂ B=L ⁻	nd	B(=L) ₂ ⁻	0.100
	[K ₂ HPO ₄]	0.475	B(=L) ₂ ⁻	0.050	total bound ligand	
	pH of resulting solution 6.9				0.100	
				free ligand		0.152
bv.12.277	[H ₃ BO ₃]	0.095	[H ₃ BO ₃]	0.039	(HO) ₂ B=L ⁻	nd
	[L]	0.201	(HO) ₂ B=L ⁻	nd	B(=L) ₂ ⁻	0.111
	[K ₂ HPO ₄]	0.477	B(=L) ₂ ⁻	0.055	total bound ligand	
	pH of resulting solution 7.3				0.111	
				free ligand		0.090
bv.12.278	[H ₃ BO ₃]	0.092	[H ₃ BO ₃]	0.042	(HO) ₂ B=L	0.001
	[L]	0.168	(HO) ₂ B=L ⁻	0.001	B(=L) ₂ ⁻	0.097
	[K ₂ HPO ₄]	0.490	B(=L) ₂ ⁻	0.048	total bound ligand	
	pH of resulting solution 7.8				0.098	
				free ligand		0.070

L= 1,4-anhydroerythritol

T = 25 °C

Solution number	Initial solution composition (mol/kg)		Concentration of B in the each species (determined through integration of ^{11}B NMR spectrum, mol/kg)		Concentration of L in borate complexes (mol/kg)	
bv.12.279	$[\text{H}_3\text{BO}_3]$	0.099	$[\text{H}_3\text{BO}_3]$	0.020	$(\text{HO})_2\text{B}=\text{L}^-$	0.003
	$[\text{L}]$	0.198	$(\text{HO})_2\text{B}=\text{L}^-$	0.003	$\text{B}(=\text{L})_2^-$	0.154
	$[\text{K}_2\text{HPO}_4]$	0.475	$\text{B}(=\text{L})_2^-$	0.077	total bound ligand	
	pH of resulting solution 6.8				0.156	
						free ligand 0.042
bv.12.280	$[\text{H}_3\text{BO}_3]$	0.095	$[\text{H}_3\text{BO}_3]$	0.007	$(\text{HO})_2\text{B}=\text{L}^-$	0.005
	$[\text{L}]$	0.229	$(\text{HO})_2\text{B}=\text{L}^-$	0.005	$\text{B}(=\text{L})_2^-$	0.165
	$[\text{K}_2\text{HPO}_4]$	0.477	$\text{B}(=\text{L})_2^-$	0.082	total bound ligand	
	pH of resulting solution 7.1				0.170	
						free ligand 0.059
bv.12.281	$[\text{H}_3\text{BO}_3]$	0.092	$[\text{H}_3\text{BO}_3]$	0.020	$(\text{HO})_2\text{B}=\text{L}^-$	0.010
	$[\text{L}]$	0.159	$(\text{HO})_2\text{B}=\text{L}^-$	0.010	$\text{B}(=\text{L})_2^-$	0.123
	$[\text{K}_2\text{HPO}_4]$	0.490	$\text{B}(=\text{L})_2^-$	0.061	total bound ligand	
	pH of resulting solution 7.4				0.133	
						free ligand 0.026

L= D-fructose

T = 25 °C

Solution number	Initial solution composition (mol/kg)		Concentration of B in the each species (determined through integration of ^{11}B NMR spectrum, mol/kg)		Concentration of L in borate complexes (mol/kg)	
bv.12.282	$[\text{H}_3\text{BO}_3]$	0.099	$[\text{H}_3\text{BO}_3]$	0.025	$(\text{HO})_2\text{B}=\text{L}^-$	0.010
	[L]	0.202	$(\text{HO})_2\text{B}=\text{L}^-$	0.010	$\text{B}(=\text{L})_2^-$	0.127
	$[\text{K}_2\text{HPO}_4]$	0.475	$\text{B}(=\text{L})_2^-$	0.064	total bound ligand	
	pH of resulting solution 6.8				0.137	
				free ligand 0.065		
bv.12.283	$[\text{H}_3\text{BO}_3]$	0.095	$[\text{H}_3\text{BO}_3]$	0.010	$(\text{HO})_2\text{B}=\text{L}^-$	0.010
	[L]	0.252	$(\text{HO})_2\text{B}=\text{L}^-$	0.010	$\text{B}(=\text{L})_2^-$	0.149
	$[\text{K}_2\text{HPO}_4]$	0.477	$\text{B}(=\text{L})_2^-$	0.075	total bound ligand	
	pH of resulting solution 7.1				0.159	
				free ligand 0.093		
bv.12.284	$[\text{H}_3\text{BO}_3]$	0.092	$[\text{H}_3\text{BO}_3]$	0.008	$(\text{HO})_2\text{B}=\text{L}^-$	0.011
	[L]	0.233	$(\text{HO})_2\text{B}=\text{L}^-$	0.011	$\text{B}(=\text{L})_2^-$	0.146
	$[\text{K}_2\text{HPO}_4]$	0.490	$\text{B}(=\text{L})_2^-$	0.073	total bound ligand	
	pH of resulting solution 7.3				0.157	
				free ligand 0.077		

L= cytidine

T = 25 °C

Solution number	Initial solution composition (mol/kg)		Concentration of B in the each species (determined through integration of ^{11}B NMR spectrum, mol/kg)		Concentration of L in borate complexes (mol/kg)	
bv.12.285	$[\text{H}_3\text{BO}_3]$	0.099	$[\text{H}_3\text{BO}_3]$	0.018	$(\text{HO})_2\text{B}=\text{L}^-$	0.004
	$[\text{L}]$	0.269	$(\text{HO})_2\text{B}=\text{L}^-$	0.004	$\text{B}(=\text{L})_2^-$	0.153
	$[\text{K}_2\text{HPO}_4]$	0.475	$\text{B}(=\text{L})_2^-$	0.077	total bound ligand	
	pH of resulting solution 6.8				0.157	
				free ligand 0.111		
bv.12.286	$[\text{H}_3\text{BO}_3]$	0.095	$[\text{H}_3\text{BO}_3]$	0.019	$(\text{HO})_2\text{B}=\text{L}^-$	0.005
	$[\text{L}]$	0.216	$(\text{HO})_2\text{B}=\text{L}^-$	0.005	$\text{B}(=\text{L})_2^-$	0.141
	$[\text{K}_2\text{HPO}_4]$	0.477	$\text{B}(=\text{L})_2^-$	0.071	total bound ligand	
	pH of resulting solution 7.2				0.147	
				free ligand 0.070		
bv.12.287	$[\text{H}_3\text{BO}_3]$	0.092	$[\text{H}_3\text{BO}_3]$	0.010	$(\text{HO})_2\text{B}=\text{L}^-$	0.009
	$[\text{L}]$	0.229	$(\text{HO})_2\text{B}=\text{L}^-$	0.009	$\text{B}(=\text{L})_2^-$	0.145
	$[\text{K}_2\text{HPO}_4]$	0.490	$\text{B}(=\text{L})_2^-$	0.073	total bound ligand	
	pH of resulting solution 7.4				0.154	
				free ligand 0.075		

L = S-DPD derivatives

T = 25 °C

Solution number	Initial solution composition (mol/kg)		Concentration of B in the each species (determined through integration of ^{11}B NMR spectrum, mol/kg)		Concentration of L in borate complexes (mol/kg)	
Semmelhack	$[\text{H}_3\text{BO}_3]$	0.005	$[\text{H}_3\text{BO}_3]$	0.001	$(\text{HO})_2\text{B}=\text{L}^-$	0.001
	$[\text{L}]$	0.015	$(\text{HO})_2\text{B}=\text{L}^-$	0.001	$\text{B}(=\text{L})_2^-$	0.005
	$[\text{Na}_2\text{CO}_3]$	sat	$\text{B}(=\text{L})_2^-$	0.002	total bound ligand	
	pH of resulting solution 7.8				0.006	
				free ligand		0.009
Semmelhack	$[\text{H}_3\text{BO}_3]$	0.015	$[\text{H}_3\text{BO}_3]$	0.006	$(\text{HO})_2\text{B}=\text{L}^-$	0.004
	$[\text{L}]$	0.015	$(\text{HO})_2\text{B}=\text{L}^-$	0.004	$\text{B}(=\text{L})_2^-$	0.011
	$[\text{Na}_2\text{CO}_3]$	sat	$\text{B}(=\text{L})_2^-$	0.005	total bound ligand	
	pH of resulting solution 7.8				0.015	
				free ligand		0.0003

B. Solutions used for the determination of the formation constants for borate-furanoidic *cis*-diol complexes at 5 °C.

L = *cis*-1,2-cyclopentanediol

T = 5 °C

Solution number	Initial solution composition (mol/kg)		Concentration of B in the each species (determined through integration of ^{11}B NMR spectrum, mol/kg)		Concentration of L in borate complexes (mol/kg)	
bv.12.276	$[\text{H}_3\text{BO}_3]$	0.099	$[\text{H}_3\text{BO}_3]$	0.033	$(\text{HO})_2\text{B}=\text{L}^-$	nd
	$[\text{L}]$	0.252	$(\text{HO})_2\text{B}=\text{L}^-$	nd	$\text{B}(=\text{L})_2^-$	0.132
	$[\text{K}_2\text{HPO}_4]$	0.475	$\text{B}(=\text{L})_2^-$	0.066	total bound ligand	
	pH of resulting solution 6.9				0.132	
				free ligand		0.119

bv.12.277	[H ₃ BO ₃]	0.095	[H ₃ BO ₃]	0.029	(HO) ₂ B=L ⁻	0.002				
	[L]	0.201	(HO) ₂ B=L ⁻	0.002	B(=L) ₂ ⁻	0.127				
	[K ₂ HPO ₄]	0.477	B(=L) ₂ ⁻	0.064	<table border="1"> <tr> <td>total bound ligand</td> </tr> <tr> <td>0.129</td> </tr> <tr> <td>free ligand</td> </tr> <tr> <td>0.072</td> </tr> </table>		total bound ligand	0.129	free ligand	0.072
	total bound ligand									
0.129										
free ligand										
0.072										
pH of resulting solution		7.4								

bv.12.278	[H ₃ BO ₃]	0.092	[H ₃ BO ₃]	0.032	(HO) ₂ B=L ⁻	0.005				
	[L]	0.168	(HO) ₂ B=L ⁻	0.005	B(=L) ₂ ⁻	0.108				
	[K ₂ HPO ₄]	0.490	B(=L) ₂ ⁻	0.054	<table border="1"> <tr> <td>total bound ligand</td> </tr> <tr> <td>0.113</td> </tr> <tr> <td>free ligand</td> </tr> <tr> <td>0.054</td> </tr> </table>		total bound ligand	0.113	free ligand	0.054
	total bound ligand									
0.113										
free ligand										
0.054										
pH of resulting solution		7.8								

L = 1,4-anhydroerythritol

T = 5 °C

Solution number	Initial solution composition (mol/kg)		Concentration of B in the each species (determined through integration of ¹¹ B NMR spectrum, mol/kg)		Concentration of L in borate complexes (mol/kg)					
	[H ₃ BO ₃]	[L]	[H ₃ BO ₃]	(HO) ₂ B=L ⁻	(HO) ₂ B=L ⁻	B(=L) ₂ ⁻				
bv.12.279	[H ₃ BO ₃]	0.099	[H ₃ BO ₃]	0.015	(HO) ₂ B=L ⁻	0.0053				
	[L]	0.198	(HO) ₂ B=L ⁻	0.005	B(=L) ₂ ⁻	0.1572				
	[K ₂ HPO ₄]	0.475	B(=L) ₂ ⁻	0.079	<table border="1"> <tr> <td>total bound ligand</td> </tr> <tr> <td>0.163</td> </tr> <tr> <td>free ligand</td> </tr> <tr> <td>0.035</td> </tr> </table>		total bound ligand	0.163	free ligand	0.035
	total bound ligand									
0.163										
free ligand										
0.035										
pH of resulting solution		6.8								
bv.12.280	[H ₃ BO ₃]	0.095	[H ₃ BO ₃]	0.003	(HO) ₂ B=L ⁻	0.0052				
	[L]	0.229	(HO) ₂ B=L ⁻	0.005	B(=L) ₂ ⁻	0.1722				
	[K ₂ HPO ₄]	0.477	B(=L) ₂ ⁻	0.086	<table border="1"> <tr> <td>total bound ligand</td> </tr> <tr> <td>0.177</td> </tr> <tr> <td>free ligand</td> </tr> <tr> <td>0.051</td> </tr> </table>		total bound ligand	0.177	free ligand	0.051
	total bound ligand									
0.177										
free ligand										
0.051										
pH of resulting solution		7.2								

bv.12.281	[H ₃ BO ₃]	0.092	[H ₃ BO ₃]	0.017	(HO) ₂ B=L ⁻	0.0092
	[L]	0.159	(HO) ₂ B=L ⁻	0.009	B(=L) ₂ ⁻	0.1311
	[K ₂ HPO ₄]	0.490	B(=L) ₂ ⁻	0.066	total bound ligand 0.140	
	pH of resulting solution 7.4					
					free ligand 0.018	

L = D-fructose

T = 5 °C

Solution number	Initial solution composition (mol/kg)		Concentration of B in the each species (determined through integration of ¹¹ B NMR spectrum, mol/kg)		Concentration of L in borate complexes (mol/kg)	
bv.12.282	[H ₃ BO ₃]	0.099	[H ₃ BO ₃]	0.020	(HO) ₂ B=L ⁻	0.0102
	[L]	0.202	(HO) ₂ B=L ⁻	0.010	B(=L) ₂ ⁻	0.1385
	[K ₂ HPO ₄]	0.475	B(=L) ₂ ⁻	0.069	total bound ligand 0.149	
	pH of resulting solution 6.8					
					free ligand 0.053	
bv.12.283	[H ₃ BO ₃]	0.095	[H ₃ BO ₃]	0.005	(HO) ₂ B=L ⁻	0.0094
	[L]	0.252	(HO) ₂ B=L ⁻	0.009	B(=L) ₂ ⁻	0.1603
	[K ₂ HPO ₄]	0.477	B(=L) ₂ ⁻	0.080	total bound ligand 0.170	
	pH of resulting solution 7.2					
					free ligand 0.082	
bv.12.284	[H ₃ BO ₃]	0.092	[H ₃ BO ₃]	0.004	(HO) ₂ B=L ⁻	0.0107
	[L]	0.233	(HO) ₂ B=L ⁻	0.011	B(=L) ₂ ⁻	0.1528
	[K ₂ HPO ₄]	0.490	B(=L) ₂ ⁻	0.076	total bound ligand 0.163	
	pH of resulting solution 7.4					
					free ligand 0.070	

L = cytidine

T = 5 °C

Solution number	Initial solution composition (mol/kg)		Concentration of B in each species (determined through integration of ¹¹ B NMR spectrum, mol/kg)		Concentration of L in borate complexes (mol/kg)	
bv.12.285	[H ₃ BO ₃]	0.099	[H ₃ BO ₃]	0.011	(HO) ₂ B=L ⁻	0.0044
	[L]	0.269	(HO) ₂ B=L ⁻	0.004	B(=L) ₂ ⁻	0.1679
	[K ₂ HPO ₄]	0.475	B(=L) ₂ ⁻	0.084		
	pH of resulting solution					
6.8						
				total bound ligand		
				0.172		
				free ligand		
				0.096		
bv.12.286	[H ₃ BO ₃]	0.095	[H ₃ BO ₃]	0.011	(HO) ₂ B=L ⁻	0.01
	[L]	0.216	(HO) ₂ B=L ⁻	0.010	B(=L) ₂ ⁻	0.1471
	[K ₂ HPO ₄]	0.477	B(=L) ₂ ⁻	0.074		
	pH of resulting solution					
7.3						
				total bound ligand		
				0.157		
				free ligand		
				0.059		
bv.12.287	[H ₃ BO ₃]	0.092	[H ₃ BO ₃]	0.005	(HO) ₂ B=L ⁻	0.0074
	[L]	0.229	(HO) ₂ B=L ⁻	0.007	B(=L) ₂ ⁻	0.1586
	[K ₂ HPO ₄]	0.490	B(=L) ₂ ⁻	0.079		
	pH of resulting solution					
7.4						
				total bound ligand		
				0.166		
				free ligand		
				0.063		

C. Solutions used for the determination of the formation constants for borate-polyol complexes at 25 °C.

L= threitol

T = 25 °C

Solution number	Initial solution composition (mol/kg)		Concentration of B in the each species (determined through integration of ^{11}B NMR spectrum, mol/kg)		Concentration of L in borate complexes (mol/kg)	
bv.12.313	$[\text{H}_3\text{BO}_3]$	0.095	$[\text{H}_3\text{BO}_3]$	0.060	$(\text{HO})_2\text{B}=\text{L}^-$	0.001
	$[\text{L}]$	0.208	$(\text{HO})_2\text{B}=\text{L}^-$	0.001	$\text{B}(=\text{L})_2^-$	0.067
	$[\text{K}_2\text{HPO}_4]$	0.477	$\text{B}(=\text{L})_2^-$	0.034	total bound ligand	
	pH of resulting solution				0.068	
7.5				free ligand		
0.140						
bv.12.314	$[\text{H}_3\text{BO}_3]$	0.094	$[\text{H}_3\text{BO}_3]$	0.040	$(\text{HO})_2\text{B}=\text{L}^-$	0.011
	$[\text{L}]$	0.179	$(\text{HO})_2\text{B}=\text{L}^-$	0.011	$\text{B}(=\text{L})_2^-$	0.085
	$[\text{K}_2\text{HPO}_4]$	0.475	$\text{B}(=\text{L})_2^-$	0.043	total bound ligand	
	pH of resulting solution				0.096	
8.2				free ligand		
0.083						

L= erythritol

T = 25 °C

Solution number	Initial solution composition (mol/kg)		Concentration of B in the each species (determined through integration of ^{11}B NMR spectrum, mol/kg)		Concentration of L in borate complexes (mol/kg)	
bv.12.302	$[\text{H}_3\text{BO}_3]$	0.099	$[\text{H}_3\text{BO}_3]$	0.0948	$(\text{HO})_2\text{B}=\text{L}^-$	nd
	$[\text{L}]$	0.193	$(\text{HO})_2\text{B}=\text{L}^-$	nd	$\text{B}(=\text{L})_2^-$	0.0084
	$[\text{K}_2\text{HPO}_4]$	0.475	$\text{B}(=\text{L})_2^-$	0.0042	total bound ligand	
	pH of resulting solution				0.008	
7.1				free ligand		
0.185						

bv.12.303	[H ₃ BO ₃]	0.095	[H ₃ BO ₃]	0.0815	(HO) ₂ B=L ⁻	0.0005	
	[L]	0.187	(HO) ₂ B=L ⁻	0.0005	B(=L) ₂ ⁻	0.0252	
	[K ₂ HPO ₄]	0.475	B(=L) ₂ ⁻	0.0126	total bound ligand		
	pH of resulting solution		7.6		0.026		
						free ligand	0.161

L= adonitol

T = 25 °C

Solution number	Initial solution composition (mol/kg)		Concentration of B in the each species (determined through integration of ¹¹ B NMR spectrum, mol/kg)		Concentration of L in borate complexes (mol/kg)		
bv.12.300	[H ₃ BO ₃]	0.099	[H ₃ BO ₃]	0.077	(HO) ₂ B=L ⁻	0.010	
	[L]	0.198	(HO) ₂ B=L ⁻	0.010	B(=L) ₂ ⁻	0.024	
	[K ₂ HPO ₄]	0.475	B(=L) ₂ ⁻	0.012	total bound ligand		
	pH of resulting solution		7.0		0.034		
						free ligand	0.164
bv.12.301	[H ₃ BO ₃]	0.095	[H ₃ BO ₃]	0.057	(HO) ₂ B=L ⁻	0.023	
	[L]	0.196	(HO) ₂ B=L ⁻	0.023	B(=L) ₂ ⁻	0.030	
	[K ₂ HPO ₄]	0.477	B(=L) ₂ ⁻	0.015	total bound ligand		
	pH of resulting solution		7.4		0.053		
						free ligand	0.144

L= xylitol

T = 25 °C

Solution number	Initial solution composition (mol/kg)		Concentration of B in the each species (determined through integration of ^{11}B NMR spectrum, mol/kg)		Concentration of L in borate complexes (mol/kg)	
			Species	Concentration	Species	Concentration
bv.12.298	[H ₃ BO ₃]	0.099	[H ₃ BO ₃]	0.025	(HO) ₂ B=L ⁻	nd
	[L]	0.200	(HO) ₂ B=L ⁻	nd	B(=L) ₂ ⁻	0.148
	[K ₂ HPO ₄]	0.475	B(=L) ₂ ⁻	0.074	total bound ligand 0.148	
	pH of resulting solution 6.9					
				free ligand 0.051		
bv.12.299	[H ₃ BO ₃]	0.095	[H ₃ BO ₃]	0.017	(HO) ₂ B=L ⁻	0.003
	[L]	0.205	(HO) ₂ B=L ⁻	0.003	B(=L) ₂ ⁻	0.150
	[K ₂ HPO ₄]	0.477	B(=L) ₂ ⁻	0.075	total bound ligand 0.153	
	pH of resulting solution 7.3					
				free ligand 0.052		

D. Solutions used for the determination of the formation constants for borate-polyol complexes at 5 °C.

L= threitol

T = 5 °C

Solution number	Initial solution composition (mol/kg)		Concentration of B in the each species (determined through integration of ^{11}B NMR spectrum, mol/kg)		Concentration of L in borate complexes (mol/kg)	
			Species	Concentration	Species	Concentration
bv.12.313	[H ₃ BO ₃]	0.095	[H ₃ BO ₃]	0.053	(HO) ₂ B=L ⁻	0.003
	[L]	0.208	(HO) ₂ B=L ⁻	0.003	B(=L) ₂ ⁻	0.0765
	[K ₂ HPO ₄]	0.477	B(=L) ₂ ⁻	0.038	total bound ligand 0.068	
	pH of resulting solution 7.5					
				free ligand 0.079		

bv.12.314	[H ₃ BO ₃]	0.094	[H ₃ BO ₃]	0.049	(HO) ₂ B=L ⁻	0.009
	[L]	0.179	(HO) ₂ B=L ⁻	0.009	B(=L) ₂ ⁻	0.0715
	[K ₂ HPO ₄]	0.475	B(=L) ₂ ⁻	0.036	total bound ligand	
	pH of resulting solution		0.081			
		8.2				
		free ligand				
		0.083				

L= erythritol

T = 5 °C

Solution number	Initial solution composition (mol/kg)	Concentration of B in the each species (determined through integration of ¹¹ B NMR spectrum, mol/kg)	Concentration of L in borate complexes (mol/kg)			
bv.12.302	[H ₃ BO ₃]	0.099	[H ₃ BO ₃]	0.091	(HO) ₂ B=L ⁻	nd
	[L]	0.193	(HO) ₂ B=L ⁻	nd	B(=L) ₂ ⁻	0.016
	[K ₂ HPO ₄]	0.475	B(=L) ₂ ⁻	0.008	total bound ligand	
	pH of resulting solution		0.016			
		7.1				
		free ligand				
		0.177				
bv.12.303	[H ₃ BO ₃]	0.095	[H ₃ BO ₃]	0.071	(HO) ₂ B=L ⁻	0.004
	[L]	0.187	(HO) ₂ B=L ⁻	0.004	B(=L) ₂ ⁻	0.039
	[K ₂ HPO ₄]	0.475	B(=L) ₂ ⁻	0.020	total bound ligand	
	pH of resulting solution		0.044			
		7.6				
		free ligand				
		0.143				

L= adonitol

T = 5 °C

Solution number	Initial solution composition (mol/kg)		Concentration of B in the each species (determined through integration of ^{11}B NMR spectrum, mol/kg)		Concentration of L in borate complexes (mol/kg)	
bv.12.300	$[\text{H}_3\text{BO}_3]$	0.099	$[\text{H}_3\text{BO}_3]$	0.071	$(\text{HO})_2\text{B}=\text{L}^-$	0.013
	$[\text{L}]$	0.198	$(\text{HO})_2\text{B}=\text{L}^-$	0.013	$\text{B}(=\text{L})_2^-$	0.030
	$[\text{K}_2\text{HPO}_4]$	0.475	$\text{B}(=\text{L})_2^-$	0.015	total bound ligand	
	pH of resulting solution				0.043	
	7.0				free ligand	
					0.156	
bv.12.301	$[\text{H}_3\text{BO}_3]$	0.095	$[\text{H}_3\text{BO}_3]$	0.041	$(\text{HO})_2\text{B}=\text{L}^-$	0.024
	$[\text{L}]$	0.196	$(\text{HO})_2\text{B}=\text{L}^-$	0.024	$\text{B}(=\text{L})_2^-$	0.059
	$[\text{K}_2\text{HPO}_4]$	0.477	$\text{B}(=\text{L})_2^-$	0.030	total bound ligand	
	pH of resulting solution				0.083	
	7.4				free ligand	
					0.113	

L= xylitol

T = 5 °C

Solution number	Initial solution composition (mol/kg)		Concentration of B in the each species (determined through integration of ^{11}B NMR spectrum, mol/kg)		Concentration of L in borate complexes (mol/kg)	
bv.12.298	$[\text{H}_3\text{BO}_3]$	0.099	$[\text{H}_3\text{BO}_3]$	0.023	$(\text{HO})_2\text{B}=\text{L}^-$	nd
	$[\text{L}]$	0.200	$(\text{HO})_2\text{B}=\text{L}^-$	nd	$\text{B}(=\text{L})_2^-$	0.152
	$[\text{K}_2\text{HPO}_4]$	0.475	$\text{B}(=\text{L})_2^-$	0.076	total bound ligand	
	pH of resulting solution				0.152	
	6.9				free ligand	
					0.048	
bv.12.299	$[\text{H}_3\text{BO}_3]$	0.095	$[\text{H}_3\text{BO}_3]$	0.012	$(\text{HO})_2\text{B}=\text{L}^-$	0.006
	$[\text{L}]$	0.205	$(\text{HO})_2\text{B}=\text{L}^-$	0.006	$\text{B}(=\text{L})_2^-$	0.153
	$[\text{K}_2\text{HPO}_4]$	0.477	$\text{B}(=\text{L})_2^-$	0.077	total bound ligand	
	pH of resulting solution				0.160	
	7.2				free ligand	
					0.046	

Appendix VII. Composition of solutions used in determining the formation constants of the carbonate-ligand complexes

A. Solutions used for the determination of the formation constants for carbonate-furanoidic *cis*-diol complexes at 25 °C.

L = *cis*-1,2-cyclopentanediol T = 25 °C

Solution number	Initial solution composition (mol/kg)		Concentration of C in the each species (determined through integration of ¹³ C NMR spectrum, mol/kg)		Concentration of L in carbonate complexes (mol/kg)		Calculated concentration of fully protonated oxoacid (mol/kg)	
	[Na ₂ ¹³ CO ₃]	[L]	C _T	(HO)OC-L	(HO)OC-L	OC=L	H ₂ CO ₃	
bv.12.304	0.044	0.891	0.0438	0.0003	0.0003	nd	1.1E-04	
	[K ₂ HPO ₄]	0.513						
	pH of resulting solution				total bound ligand			
	8.9				0.0003			
					free ligand			
					0.891			

L = 1,4-anhydroerythritol T = 25 °C

Solution number	Initial solution composition (mol/kg)		Concentration of C in the each species (determined through integration of ¹³ C NMR spectrum, mol/kg)		Concentration of L in carbonate complexes (mol/kg)		Calculated concentration of fully protonated oxoacid (mol/kg)	
	[Na ₂ ¹³ CO ₃]	[L]	C _T	(HO)OC-L	(HO)OC-L	OC=L	H ₂ CO ₃	
bv.11.646	0.111	3.821	0.1081	0.0023	0.0023	0.0003	3.4E-05	
	[K ₂ HPO ₄]	-						
	pH of resulting solution				total bound ligand			
	9.8				0.003			
					free ligand			
					3.818			

L = cytidine

T = 25 °C

Solution number	Initial solution composition (mol/kg)		Concentration of C in each species (determined through integration of ¹³ C NMR spectrum, mol/kg)		Concentration of L in carbonate complexes (mol/kg)		Calculated concentration of fully protonated oxoacid (mol/kg)	
	[Na ₂ ¹³ CO ₃]	[L]	C _T	(HO)OC-L	(HO)OC-L	OC=L	H ₂ CO ₃	
bv.12.227	[Na ₂ ¹³ CO ₃]	0.036	C _T	0.0359	(HO)OC-L	0.0002	H ₂ CO ₃	6.4E-08
	[L]	0.847	(HO)OC-L	0.0002	OC=L	0.0001		
	[K ₂ HPO ₄]	0.350	OC=L	0.0001	total bound ligand			
	pH of resulting solution 11.2				0.0002			
					free ligand			
					0.847			
bv.12.228	[Na ₂ ¹³ CO ₃]	0.011	C _T	0.0095	(HO)OC-L	0.0007	H ₂ CO ₃	4.4E-04
	[L]	0.789	(HO)OC-L	0.0007	OC=L	0.0005		
	[K ₂ HPO ₄]	0.502	OC=L	0.0005	total bound ligand			
	pH of resulting solution 7.7				0.0012			
					free ligand			
					0.788			

B. Solutions used for the determination of the formation constants for carbonate-furanoidic *cis*-diol complexes at 5 °C.

L = *cis*-1,2-cyclopentanediol

T = 5 °C

Solution number	Initial solution composition (mol/kg)		Concentration of C in each species (determined through integration of ¹³ C NMR spectrum, mol/kg)		Concentration of L in carbonate complexes (mol/kg)		Calculated concentration of fully protonated oxoacid (mol/kg)	
	[Na ₂ ¹³ CO ₃]	[L]	C _T	(HO)OC-L	(HO)OC-L	OC=L	H ₂ CO ₃	
bv.12.55	[Na ₂ ¹³ CO ₃]	0.044	C _T	0.043	(HO)OC-L	0.0007	H ₂ CO ₃	2.0E-04
	[L]	1.099	(HO)OC-L	0.0007	OC=L	nd		
	[K ₂ HPO ₄]	0.513	OC=L	nd	total bound ligand			
	pH of resulting solution 8.9				0.0007			
					free ligand			
					1.099			

L = 1,4-anhydroerythritol

T = 5 °C

Solution number	Initial solution composition (mol/kg)		Concentration of C in the each species (determined through integration of ^{13}C NMR spectrum, mol/kg)		Concentration of L in carbonate complexes (mol/kg)		Calculated concentration of fully protonated oxoacid (mol/kg)	
							H_2CO_3	
bv.12.56	$[\text{Na}_2^{13}\text{CO}_3]$	0.044	C_T	0.0438	(HO)OC-L	0.0003	H_2CO_3	9.8E-04
	[L]	1.201	(HO)OC-L	0.0003	OC=L	nd		
	$[\text{K}_2\text{HPO}_4]$	0.513	OC=L	nd	total bound ligand			
	pH of resulting solution				0.0003			
						free ligand		
						1.201		
bv.12.153	$[\text{Na}_2^{13}\text{CO}_3]$	0.044	C_T	0.0434	(HO)OC-L	0.0002	H_2CO_3	6.6E-05
	[L]	0.856	(HO)OC-L	0.0002	OC=L	nd		
	$[\text{K}_2\text{HPO}_4]$	0.480	OC=L	nd	total bound ligand			
	pH of resulting solution				0.0002			
						free ligand		
						0.856		

L = cytidine

T = 5 °C

Solution number	Initial solution composition (mol/kg)		Concentration of C in the each species (determined through integration of ^{13}C NMR spectrum, mol/kg)		Concentration of L in carbonate complexes (mol/kg)		Calculated concentration of fully protonated oxoacid (mol/kg)	
							H_2CO_3	
bv.12.308	$[\text{Na}_2^{13}\text{CO}_3]$	0.044	C_T	0.0431	(HO)OC-L	0.0008	H_2CO_3	1.1E-04
	[L]	0.715	(HO)OC-L	0.0008	OC=L	0.0002		
	$[\text{K}_2\text{HPO}_4]$	0.513	OC=L	0.0002	total bound ligand			
	pH of resulting solution				0.001			
						free ligand		
						0.714		

C. Solutions used for the determination of the formation constants for carbonate-polyol complexes at 5 °C.

L = L-threitol

T = 5 °C

Solution number	Initial solution composition (mol/kg)		Concentration of C in the each species (determined through integration of ¹³ C NMR spectrum, mol/kg)		Concentration of L in carbonate complexes (mol/kg)		Calculated concentration of fully protonated oxoacid (mol/kg)	
	[Na ₂ ¹³ CO ₃]	[L]	C _T	(HO)OC-L	(HO)OC-L	OC=L	H ₂ CO ₃	
bv.12.20	[Na ₂ ¹³ CO ₃]	0.044	C _T	0.0421	(HO)OC-L	0.0015	H ₂ CO ₃	1.0E-05
	[L]	1.637	(HO)OC-L	0.0015	OC=L	nd		
	[K ₂ HPO ₄]	0.480	OC=L	nd	total bound ligand			
	pH of resulting solution				0.0015			
		10.0			free ligand			
					1.635			
bv.12.21	[Na ₂ ¹³ CO ₃]	0.043	C _T	0.0431	(HO)OC-L	0.0001	H ₂ CO ₃	6.4E-08
	[L]	1.487	(HO)OC-L	0.0001	OC=L	nd		
	[K ₂ HPO ₄]	0.419	OC=L	nd	total bound ligand			
	pH of resulting solution				0.0001			
		11.4			free ligand			
					1.487			
bv.11.615	[Na ₂ ¹³ CO ₃]	0.124	C _T	0.1235	(HO)OC-L	0.0007	H ₂ CO ₃	4.4E-07
	[L]	1.468	(HO)OC-L	0.0007	OC=L	nd		
	[K ₂ HPO ₄]	-	OC=L	nd	total bound ligand			
	pH of resulting solution				0.0007			
		11.2			free ligand			
					1.467			
bv.12.58	[Na ₂ ¹³ CO ₃]	0.044	C _T	0.0410	(HO)OC-L	0.0031	H ₂ CO ₃	2.2E-04
	[L]	1.414	(HO)OC-L	0.0031	OC=L	nd		
	[K ₂ HPO ₄]	0.513	OC=L	nd	total bound ligand			
	pH of resulting solution				0.0031			
		8.8			free ligand			
					1.411			

L = meso-erythritol

T = 5 °C

Solution number	Initial solution composition (mol/kg)		Concentration of C in the each species (determined through integration of ^{13}C NMR spectrum, mol/kg)		Concentration of L in carbonate complexes (mol/kg)		Calculated concentration of fully protonated oxoacid (mol/kg)	
bv.12.18	$[\text{Na}_2^{13}\text{CO}_3]$	0.044	C_T	0.0422	(HO)OC-L	0.0014	H_2CO_3	8.7E-06
	[L]	1.591	(HO)OC-L	0.0014	OC=L	nd		
	$[\text{K}_2\text{HPO}_4]$	0.480	OC=L	nd	total bound ligand			
	pH of resulting solution 10.1				0.0014			
				free ligand				
				1.589				
bv.12.19	$[\text{Na}_2^{13}\text{CO}_3]$	0.043	C_T	0.0431	(HO)OC-L	0.0001	H_2CO_3	6.7E-08
	[L]	1.523	(HO)OC-L	0.0001	OC=L	nd		
	$[\text{K}_2\text{HPO}_4]$	0.419	OC=L	nd	total bound ligand			
	pH of resulting solution 11.4				0.0001			
				free ligand				
				1.523				
bv.12.614	$[\text{Na}_2^{13}\text{CO}_3]$	0.125	C_T	0.1241	(HO)OC-L	0.0005	H_2CO_3	5.6E-07
	[L]	1.461	(HO)OC-L	0.0005	OC=L	nd		
	$[\text{K}_2\text{HPO}_4]$	-	OC=L	nd	total bound ligand			
	pH of resulting solution 8.7				0.0005			
				free ligand				
				1.460				
bv.12.57	$[\text{Na}_2^{13}\text{CO}_3]$	0.044	C_T	0.0405	(HO)OC-L	0.0036	H_2CO_3	2.4E-04
	[L]	1.890	(HO)OC-L	0.0036	OC=L	nd		
	$[\text{K}_2\text{HPO}_4]$	0.513	OC=L	nd	total bound ligand			
	pH of resulting solution 11.2				0.0036			
				free ligand				
				1.886				

L = xylitol

T = 5 °C

Solution number	Initial solution composition (mol/kg)		Concentration of C in the each species (determined through integration of ^{13}C NMR spectrum, mol/kg)		Concentration of L in carbonate complexes (mol/kg)		Calculated concentration of fully protonated oxoacid (mol/kg)	
bv.12.24	[Na ₂ ¹³ CO ₃]	0.044	C _T	0.0419	(HO)OC-L	0.0017	H ₂ CO ₃	1.2E-05
	[L]	1.838	(HO)OC-L	0.0017	OC=L	nd		
	[K ₂ HPO ₄]	0.480	OC=L	nd	total bound ligand			
	pH of resulting solution				0.0017			
		10.0			free ligand			
					1.836			
bv.12.25	[Na ₂ ¹³ CO ₃]	0.043	C _T	0.0431	(HO)OC-L	0.0001	H ₂ CO ₃	9.9E-08
	[L]	1.666	(HO)OC-L	0.0001	OC=L	nd		
	[K ₂ HPO ₄]	0.419	OC=L	nd	total bound ligand			
	pH of resulting solution				0.0001			
		11.3			free ligand			
					1.666			
bv.12.61	[Na ₂ ¹³ CO ₃]	0.044	C _T	0.0390	(HO)OC-L	0.0051	H ₂ CO ₃	2.0E-04
	[L]	2.865	(HO)OC-L	0.0051	OC=L	nd		
	[K ₂ HPO ₄]	0.513	OC=L	nd	total bound ligand			
	pH of resulting solution				0.0051			
		8.8			free ligand			
					3.860			

L = adontiol

T = 5 °C

Solution number	Initial solution composition (mol/kg)		Concentration of C in the each species (determined through integration of ¹³ C NMR spectrum, mol/kg)		Concentration of L in carbonate complexes (mol/kg)		Calculated concentration of fully protonated oxoacid (mol/kg)	
bv.12.22	[Na ₂ ¹³ CO ₃]	0.044	C _T	0.0422	(HO)OC-L	0.0014	H ₂ CO ₃	1.2E-05
	[L]	1.597	(HO)OC-L	0.0014	OC=L	nd		
	[K ₂ HPO ₄]	0.480	OC=L	nd	total bound ligand			
	pH of resulting solution				0.0014			
						free ligand		
						1.596		
bv.12.23	[Na ₂ ¹³ CO ₃]	0.0432	C _T	0.0430	(HO)OC-L	0.0002	H ₂ CO ₃	1.0E-07
	[L]	1.5947	(HO)OC-L	0.0002	OC=L	nd		
	[K ₂ HPO ₄]	0.419	OC=L	nd	total bound ligand			
	pH of resulting solution				0.0002			
						free ligand		
						1.595		
bv.12.59	[Na ₂ ¹³ CO ₃]	0.0441	C _T	0.0406	(HO)OC-L	0.0035	H ₂ CO ₃	2.7E-04
	[L]	1.8339	(HO)OC-L	0.0035	OC=L	nd		
	[K ₂ HPO ₄]	0.513	OC=L	nd	total bound ligand			
	pH of resulting solution				0.0035			
						free ligand		
						1.830		

Appendix VIII. Composition of solutions used in determining the formation constants of the silicate-ligand complexes

A. Solutions used for the determination of the formation constants for silicate-furanoidic *cis*-diol complexes at 5 °C. (Data for *cis*-1,2-cyclopentanediol and 1,4-anhydroerythritol were determined by Wen *et al.*^[65])

L= D-fructose

T = 5 °C

Solution number	Initial solution composition (mol/kg)		Concentration of Si in the each species (determined through integration of ²⁹ Si NMR spectrum, mol/kg)		Concentration of L in silicate complexes (mol/kg)		Calculated concentration of fully protonated oxoacid (mol/kg)						
	[SiO ₂]	[L]	[KOH]	pH of resulting solution	Q ⁰	Q ¹ -Q ³	(HO) ₃ Si-L	(HO)Si(=L) ₂ ⁻	Si(=L) ₃ ²⁻	total bound ligand	free ligand	Si(OH) ₄	
bv.12.147	1.283	1.139	1.283	12.7	0.071	1.118	nd	0.187	nd	0.187	0.944	6.6E-05	
bv.12.208	1.27	0.97	1.27	12.8	0.082	1.131	nd	0.110	nd	0.110	0.860	5.8E-05	

bv.12.209	[SiO ₂]	0.717	Q ⁰	0.077	(HO) ₃ Si-L	nd	Si(OH) ₄	1.6E-04
	[L]	0.991	Q ¹ -Q ³	0.457	(HO)Si(=L) ₂ ⁻	0.215 9		
	[KOH]	0.717	(HO) ₃ Si-L	nd	Si(=L) ₃ ²⁻	0.224 4		
	pH of resulting solution 12.4		(HO)Si(=L) ₂ ⁻	0.108	total bound ligand			
		Si(=L) ₃ ²⁻	0.075	free ligand		0.535		

L = cytidine

T = 5 °C

Solution number	Initial solution composition (mol/kg)	Concentration of Si in the each species (determined through integration of ²⁹ Si NMR spectrum, mol/kg)	Concentration of L in silicate complexes (mol/kg)	Calculated concentration of fully protonated oxoacid (mol/kg)				
bv.12.210	[SiO ₂]	1.268	Q ⁰	0.083	(HO) ₃ Si-L	nd	Si(OH) ₄	5.7E-06
	[L]	0.723	Q ¹ -Q ³	1.076	(HO)Si(=L) ₂ ⁻	0.071		
	[KOH]	1.268	(HO) ₃ Si-L	nd	Si(=L) ₃ ²⁻	0.219		
	pH of resulting solution 13.4		(HO)Si(=L) ₂ ⁻	0.035	total bound ligand			
		Si(=L) ₃ ²⁻	0.073	free ligand		0.425		
bv.12.211	[SiO ₂]	1.234	Q ⁰	0.115	(HO) ₃ Si-L	nd	Si(OH) ₄	3.07E-06
	[L]	0.826	Q ¹ -Q ³	1.011	(HO)Si(=L) ₂ ⁻	0.066		
	[KOH]	1.434	(HO) ₃ Si-L	nd	Si(=L) ₃ ²⁻	0.225		
	pH of resulting solution 13.7		(HO)Si(=L) ₂ ⁻	0.033	total bound ligand			
		Si(=L) ₃ ²⁻	0.075	free ligand		0.526		
bv.12.212	[SiO ₂]	0.774	Q ⁰	0.072	(HO) ₃ Si-L	nd	Si(OH) ₄	2.46E-05
	[L]	0.915	Q ¹ -Q ³	0.486	(HO)Si(=L) ₂ ⁻	0.270		
	[KOH]	0.775	(HO) ₃ Si-L	nd	Si(=L) ₃ ²⁻	0.244		
	pH of resulting solution 13.0		(HO)Si(=L) ₂ ⁻	0.135	total bound ligand			
		Si(=L) ₃ ²⁻	0.081	free ligand		0.385		

L = *cis*-1,2-cyclopentanediol T = 2 °C

Solution number	Initial solution composition (mol/kg)		Concentration of Si in the each species (determined through integration of ²⁹ Si NMR spectrum, mol/kg)		Concentration of L in silicate complexes (mol/kg)		Calculated concentration of fully protonated oxoacid (mol/kg)	
			Species	Concentration	Species	Concentration	Species	Concentration
ji.04.42	[SiO ₂]	0.906	Q ⁰	0.093	(HO) ₃ Si-L	nd	Si(OH) ₄	3.5E-04
	[L]	2.352	Q ¹ -Q ³	0.873	(HO)Si(=L) ₂ ⁻	0.028		
	[NaOH]	0.999	(HO) ₃ Si-L	nd	Si(=L) ₃ ²⁻	nd		
	pH of resulting solution 12.2		(HO)Si(=L) ₂ ⁻	0.014	total bound ligand			
			Si(=L) ₃ ²⁻	nd	0.028			
				free ligand				
				2.322				

L = 1,4-anhydroerthritol T = 2 °C

Solution number	Initial solution composition (mol/kg)		Concentration of Si in the each species (determined through integration of ²⁹ Si NMR spectrum, mol/kg)		Concentration of L in silicate complexes (mol/kg)		Calculated concentration of fully protonated oxoacid (mol/kg)	
			Species	Concentration	Species	Concentration	Species	Concentration
ji.04.38	[SiO ₂]	0.961	Q ⁰	0.054	(HO) ₃ Si-L	nd	Si(OH) ₄	2.0E-04
	[L]	2.454	Q ¹ -Q ³	0.433	(HO)Si(=L) ₂ ⁻	0.965		
	[NaOH]	0.999	(HO) ₃ Si-L	nd	Si(=L) ₃ ²⁻	nd		
	pH of resulting solution 12.2		(HO)Si(=L) ₂ ⁻	0.483	total bound ligand			
			Si(=L) ₃ ²⁻	nd	0.965			
				free ligand				
				1.407				

B. Solutions used for the determination of the formation constants for silicate-polyol complexes at 5 °C. (Data for L-threitol, erythritol, arabitol, adonitol, iditol and mannitol were determined by Vis *et al.*^[64])

L = L-threitol

T = 5 °C

Solution number	Initial solution composition (mol/kg)		Concentration of Si in each species (determined through integration of ²⁹ Si NMR spectrum, mol/kg)		Concentration of L in silicate complexes (mol/kg)		Calculated concentration of fully protonated oxoacid (mol/kg)	
bv.09.253	[SiO ₂]	0.989	Q ⁰	0.078	(HO) ₃ Si-L	nd	Si(OH) ₄	2.4E-05
	[L]	2.163	Q ¹ -Q ³	0.876	(HO)Si(=L) ₂ ⁻	0.069		
	[NaOH]	1.065	(HO) ₃ Si-L	nd	Si(=L) ₃ ²⁻	nd		
	pH of resulting solution 13.0		(HO)Si(=L) ₂ ⁻	0.035	total bound ligand			
			Si(=L) ₃ ²⁻	nd	0.069			
					free ligand			
				2.089				
bv.09.261	[SiO ₂]	0.929	Q ⁰	0.160	(HO) ₃ Si-L	nd	Si(OH) ₄	6.3E-05
	[L]	2.032	Q ¹ -Q ³	0.748	(HO)Si(=L) ₂ ⁻	0.041		
	[NaOH]	1.595	(HO) ₃ Si-L	nd	Si(=L) ₃ ²⁻	nd		
	pH of resulting solution 12.9		(HO)Si(=L) ₂ ⁻	0.020	total bound ligand			
			Si(=L) ₃ ²⁻	nd	0.041			
					free ligand			
				1.988				
bv.09.264	[SiO ₂]	0.887	Q ⁰	0.157	(HO) ₃ Si-L	nd	Si(OH) ₄	2.9E-05
	[L]	4.150	Q ¹ -Q ³	0.585	(HO)Si(=L) ₂ ⁻	0.185		
	[NaOH]	1.968	(HO) ₃ Si-L	nd	Si(=L) ₃ ²⁻	0.155		
	pH of resulting solution 13.2		(HO)Si(=L) ₂ ⁻	0.093	total bound ligand			
			Si(=L) ₃ ²⁻	0.052	0.340			
					free ligand			
				3.760				

bv.10.16	[SiO ₂]	0.862	Q ⁰	0.311	(HO) ₃ Si-L	nd	Si(OH) ₄	3.4E-05	
	[L]	4.036	Q ¹ -Q ³	0.470	(HO)Si(=L) ₂ ⁻	0.063			
	[NaOH]	2.599	(HO) ₃ Si-L	nd	Si(=L) ₃ ²⁻	0.152			
	pH of resulting solution		13.3	(HO)Si(=L) ₂ ⁻	0.031	total bound ligand			0.215
				Si(=L) ₃ ²⁻	0.051	free ligand			3.791
bv.10.78	[SiO ₂]	0.951	Q ⁰	0.313 3	(HO) ₃ Si-L	nd	Si(OH) ₄	6.0E-06	
	[L]	1.507	Q ¹ -Q ³	0.628 9	(HO)Si(=L) ₂ ⁻	0.010			
	[NaOH]	2.567	(HO) ₃ Si-L	nd	Si(=L) ₃ ²⁻	0.009			
	pH of resulting solution		13.8	(HO)Si(=L) ₂ ⁻	0.005 2	total bound ligand			0.020
				Si(=L) ₃ ²⁻	0.003 2	free ligand			1.486
bv.10.81	[SiO ₂]	1.017	Q ⁰	0.070 3	(HO) ₃ Si-L	nd	Si(OH) ₄	2.5E-05	
	[L]	1.780	Q ¹ -Q ³	0.913 2	(HO)Si(=L) ₂ ⁻	0.059			
	[KOH]	1.018	(HO) ₃ Si-L	nd	Si(=L) ₃ ²⁻	0.012			
	pH of resulting solution		13.0	(HO)Si(=L) ₂ ⁻	0.029 3	total bound ligand			0.070
				Si(=L) ₃ ²⁻	0.003 9	free ligand			1.705

L = meso-erythritol

T = 5 °C

Solution number	Initial solution composition (mol/kg)	Concentration of Si in the each species (determined through integration of ²⁹ Si NMR spectrum, mol/kg)	Concentration of L in silicate complexes (mol/kg)	Calculated concentration of fully protonated oxoacid (mol/kg)					
bv.10.80	[SiO ₂]	1.073	Q ⁰	0.075	(HO) ₃ Si-L	nd	Si(OH) ₄	8.5E-06	
	[L]	1.394	Q ¹ -Q ³	0.997	(HO)Si(=L) ₂ ⁻	0.002			
	[KOH]	1.075	(HO) ₃ Si-L	nd	Si(=L) ₃ ²⁻	nd			
	pH of resulting solution		13.3	(HO)Si(=L) ₂ ⁻	0.001	total bound ligand			0.002
				Si(=L) ₃ ²⁻	nd	free ligand			1.392

bv.10.82	[SiO ₂]	0.998	Q ⁰	0.068	(HO) ₃ Si-L	0.004	Si(OH) ₄	5.6E-05	
	[L]	1.815	Q ¹ -Q ³	0.923	(HO)Si(=L) ₂ ⁻	0.006			
	[KOH]	0.999	(HO) ₃ Si-L	0.004	Si(=L) ₃ ²⁻	nd			
	pH of resulting solution		12.7	(HO)Si(=L) ₂ ⁻	0.003	total bound ligand			
				Si(=L) ₃ ²⁻	nd	0.010			
					free ligand				
					1.805				

bv.10.89	[SiO ₂]	0.944	Q ⁰	0.128	(HO) ₃ Si-L	0.0002	Si(OH) ₄	5.0E-06	
	[L]	1.721	Q ¹ -Q ³	0.815	(HO)Si(=L) ₂ ⁻	0.002			
	[KOH]	1.329	(HO) ₃ Si-L	0.0002	Si(=L) ₃ ²⁻	nd			
	pH of resulting solution		13.6	(HO)Si(=L) ₂ ⁻	0.001	total bound ligand			
				Si(=L) ₃ ²⁻	nd	0.0022			
					free ligand				
					1.719				

L = D-arabitol

T = 5 °C

Solution number	Initial solution composition (mol/kg)	Concentration of Si in the each species (determined through integration of ²⁹ Si NMR spectrum, mol/kg)	Concentration of L in silicate complexes (mol/kg)	Calculated concentration of fully protonated oxoacid (mol/kg)					
bv.09.231	[SiO ₂]	0.696	Q ⁰	0.035	(HO) ₃ Si-L	nd	Si(OH) ₄	9.3E-05	
	[L]	6.530	Q ¹ -Q ³	0.010	(HO)Si(=L) ₂ ⁻	1.165			
	[NaOH]	0.774	(HO) ₃ Si-L	nd	Si(=L) ₃ ²⁻	0.206			
	pH of resulting solution		12.3	(HO)Si(=L) ₂ ⁻	0.583	total bound ligand			
				Si(=L) ₃ ²⁻	0.069	1.372			
					free ligand				
					4.851				
bv.09.237	[SiO ₂]	0.696	Q ⁰	0.028	(HO) ₃ Si-L	nd	Si(OH) ₄	7.1E-05	
	[L]	7.336	Q ¹ -Q ³	nd	(HO)Si(=L) ₂ ⁻	1.147			
	[NaOH]	0.774	(HO) ₃ Si-L	nd	Si(=L) ₃ ²⁻	0.284			
	pH of resulting solution		12.3	(HO)Si(=L) ₂ ⁻	0.574	total bound ligand			
				Si(=L) ₃ ²⁻	0.095	1.432			
					free ligand				
					5.545				

bv.09.238	[SiO ₂]	0.697	Q ⁰	0.030	(HO) ₃ Si-L	nd	Si(OH) ₄	9.0E-05	
	[L]	7.114	Q ¹ -Q ³	nd	(HO)Si(=L) ₂ ⁻	1.183			
	[NaOH]	0.774	(HO) ₃ Si-L	nd	Si(=L) ₃ ²⁻	0.226			
	pH of resulting solution		12.2	(HO)Si(=L) ₂ ⁻	0.591	total bound ligand			
				Si(=L) ₃ ²⁻	0.075	1.408			
					free ligand				
					5.362				
bv.09.239	[SiO ₂]	0.696	Q ⁰	0.032	(HO) ₃ Si-L	nd	Si(OH) ₄	9.5E-05	
	[L]	6.954	Q ¹ -Q ³	0.009	(HO)Si(=L) ₂ ⁻	1.180			
	[NaOH]	0.776	(HO) ₃ Si-L	nd	Si(=L) ₃ ²⁻	0.197			
	pH of resulting solution		12.2	(HO)Si(=L) ₂ ⁻	0.590	total bound ligand			
				Si(=L) ₃ ²⁻	0.066	1.377			
					free ligand				
					5.248				
bv.09.244	[SiO ₂]	1.007	Q ⁰	0.087	(HO) ₃ Si-L	nd	Si(OH) ₄	5.8E-05	
	[L]	1.458	Q ¹ -Q ³	0.838	(HO)Si(=L) ₂ ⁻	0.141			
	[NaOH]	1.008	(HO) ₃ Si-L	nd	Si(=L) ₃ ²⁻	0.036			
	pH of resulting solution		12.8	(HO)Si(=L) ₂ ⁻	0.070	total bound ligand			
				Si(=L) ₃ ²⁻	0.012	0.177			
					free ligand				
					1.272				
bv.09.245	[SiO ₂]	1.007	Q ⁰	0.056	(HO) ₃ Si-L	nd	Si(OH) ₄	1.5E-04	
	[L]	3.409	Q ¹ -Q ³	0.648	(HO)Si(=L) ₂ ⁻	0.537			
	[NaOH]	1.008	(HO) ₃ Si-L	nd	Si(=L) ₃ ²⁻	0.104			
	pH of resulting solution		12.3	(HO)Si(=L) ₂ ⁻	0.269	total bound ligand			
				Si(=L) ₃ ²⁻	0.035	0.641			
					free ligand				
					2.691				

bv.09.246	[SiO ₂]	1.007	Q ⁰	0.038	(HO) ₃ Si-L	nd	Si(OH) ₄	2.4E-04	
	[L]	5.726	Q ¹ -Q ³	0.432	(HO)Si(=L) ₂ ⁻	1.003			
	[NaOH]	1.008	(HO) ₃ Si-L	nd	Si(=L) ₃ ²⁻	0.108			
	pH of resulting solution			(HO)Si(=L) ₂ ⁻	0.501	total bound ligand			
	11.9			Si(=L) ₃ ²⁻	0.036	1.111			
					free ligand				
					4.395				
bv.09.247	[SiO ₂]	1.007	Q ⁰	0.056	(HO) ₃ Si-L	nd	Si(OH) ₄	2.6E-04	
	[L]	4.922	Q ¹ -Q ³	0.444	(HO)Si(=L) ₂ ⁻	0.927			
	[NaOH]	1.008	(HO) ₃ Si-L	nd	Si(=L) ₃ ²⁻	0.131			
	pH of resulting solution			(HO)Si(=L) ₂ ⁻	0.464	total bound ligand			
	12.0			Si(=L) ₃ ²⁻	0.044	1.058			
					free ligand				
					3.683				
bv.10.37	[SiO ₂]	0.870	Q ⁰	0.136	(HO) ₃ Si-L	nd	Si(OH) ₄	6.4E-04	
	[L]	4.977	Q ¹ -Q ³	0.185	(HO)Si(=L) ₂ ⁻	0.372			
	[NaOH]	2.226	(HO) ₃ Si-L	nd	Si(=L) ₃ ²⁻	1.090			
	pH of resulting solution			(HO)Si(=L) ₂ ⁻	0.186	total bound ligand			
	13.1			Si(=L) ₃ ²⁻	0.363	1.462			
					free ligand				
					3.267				

L = adonitol

T = 5 °C

Solution number	Initial solution composition (mol/kg)	Concentration of Si in the each species (determined through integration of ²⁹ Si NMR spectrum, mol/kg)	Concentration of L in silicate complexes (mol/kg)	Calculated concentration of fully protonated oxoacid (mol/kg)					
bv.10.84	[SiO ₂]	1.032	Q ⁰	0.063	(HO) ₃ Si-L	0.006	Si(OH) ₄	1.5E-04	
	[L]	4.148	Q ¹ -Q ³	0.935	(HO)Si(=L) ₂ ⁻	0.056			
	[KOH]	1.033	(HO) ₃ Si-L	0.006	Si(=L) ₃ ²⁻	nd			
	pH of resulting solution			(HO)Si(=L) ₂ ⁻	0.028	total bound ligand			
	12.3			Si(=L) ₃ ²⁻	nd	0.062			
					free ligand				
					4.077				

bv.10.88	[SiO ₂]	0.990	Q ⁰	0.077	(HO) ₃ Si-L	0.009	Si(OH) ₄	2.8E-06	
	[L]	3.982	Q ¹ -Q ³	0.882	(HO)Si(=L) ₂ ⁻	0.045			
	[KOH]	1.276	(HO) ₃ Si-L	0.009	Si(=L) ₃ ²⁻	nd			
	pH of resulting solution			(HO)Si(=L) ₂ ⁻	0.023	total bound ligand			
	13.6			Si(=L) ₃ ²⁻	nd	0.054			
						free ligand			
						3.921			

bv.10.90	[SiO ₂]	0.929	Q ⁰	0.124	(HO) ₃ Si-L	0.002	Si(OH) ₄	6.5E-06	
	[L]	3.735	Q ¹ -Q ³	0.787	(HO)Si(=L) ₂ ⁻	0.032			
	[KOH]	1.896	(HO) ₃ Si-L	0.002	Si(=L) ₃ ²⁻	nd			
	pH of resulting solution			(HO)Si(=L) ₂ ⁻	0.016	total bound ligand			
	13.5			Si(=L) ₃ ²⁻	nd	0.034			
						free ligand			
						3.697			

L = xylitol

T = 5 °C

Solution number	Initial solution composition (mol/kg)	Concentration of Si in the each species (determined through integration of ²⁹ Si NMR spectrum, mol/kg)			Concentration of L in silicate complexes (mol/kg)		Calculated concentration of fully protonated oxoacid (mol/kg)		
bv.12.63	[SiO ₂]	1.030	Q ⁰	0.015	(HO) ₃ Si-L	nd	Si(OH) ₄	3.4E-04	
	[L]	5.055	Q ¹ -Q ³	0.000	(HO)Si(=L) ₂ ⁻	1.533			
	[KOH]	1.031	(HO) ₃ Si-L	nd	Si(=L) ₃ ²⁻	0.746			
	pH of resulting solution			(HO)Si(=L) ₂ ⁻	0.766	total bound ligand			
	11.4			Si(=L) ₃ ²⁻	0.249	2.279			
						free ligand			
						2.392			
bv.12.136	[SiO ₂]	1.225	Q ⁰	0.092	(HO) ₃ Si-L	nd	Si(OH) ₄	2.9E-06	
	[L]	2.454	Q ¹ -Q ³	0.461	(HO)Si(=L) ₂ ⁻	0.180			
	[KOH]	1.605	(HO) ₃ Si-L	nd	Si(=L) ₃ ²⁻	1.744			
	pH of resulting solution			(HO)Si(=L) ₂ ⁻	0.090	total bound ligand			
	13.6			Si(=L) ₃ ²⁻	0.581	1.924			
						free ligand			
						0.371			

bv.12.137	[SiO ₂]	0.880	Q ⁰	0.230	(HO) ₃ Si-L	nd	Si(OH) ₄	1.1E-07	
	[L]	1.873	Q ¹ -Q ³	0.270	(HO)Si(=L) ₂ ⁻	0.044			
	[KOH]	2.128	(HO) ₃ Si-L	nd	Si(=L) ₃ ²⁻	1.072			
	pH of resulting solution		14.6	(HO)Si(=L) ₂ ⁻	0.022	total bound ligand			
				Si(=L) ₃ ²⁻	0.357	1.116			
					free ligand				
					0.685				
bv.12.138	[SiO ₂]	1.215	Q ⁰	0.107	(HO) ₃ Si-L	nd	Si(OH) ₄	7.1E-06	
	[L]	1.200	Q ¹ -Q ³	0.870	(HO)Si(=L) ₂ ⁻	0.105			
	[KOH]	1.215	(HO) ₃ Si-L	nd	Si(=L) ₃ ²⁻	0.557			
	pH of resulting solution		13.4	(HO)Si(=L) ₂ ⁻	0.052	total bound ligand			
				Si(=L) ₃ ²⁻	0.186	0.662			
					free ligand				
					0.511				
bv.12.150	[SiO ₂]	1.269	Q ⁰	0.154	(HO) ₃ Si-L	nd	Si(OH) ₄	1.5E-06	
	[L]	0.374	Q ¹ -Q ³	1.092	(HO)Si(=L) ₂ ⁻	0.008			
	[KOH]	1.269	(HO) ₃ Si-L	nd	Si(=L) ₃ ²⁻	0.055			
	pH of resulting solution		13.9	(HO)Si(=L) ₂ ⁻	0.004	total bound ligand			
				Si(=L) ₃ ²⁻	0.018	0.064			
					free ligand				
					0.310				

L = D-mannitol

T = 5 °C

Solution number	Initial solution composition (mol/kg)	Concentration of Si in the each species (determined through integration of ²⁹ Si NMR spectrum, mol/kg)			Concentration of L in silicate complexes (mol/kg)		Calculated concentration of fully protonated oxoacid (mol/kg)		
bv.09.242	[SiO ₂]	1.007	Q ⁰	0.075	(HO) ₃ Si-L	nd	Si(OH) ₄	1.9E-04	
	[L]	1.277	Q ¹ -Q ³	0.842	(HO)Si(=L) ₂ ⁻	0.103			
	[NaOH]	1.008	(HO) ₃ Si-L	nd	Si(=L) ₃ ²⁻	0.116			
	pH of resulting solution		12.3	(HO)Si(=L) ₂ ⁻	0.052	total bound ligand			
				Si(=L) ₃ ²⁻	0.039	0.219			
					free ligand				
					1.049				

bv.09.255	[SiO ₂]	0.938	Q ⁰	0.143	(HO) ₃ Si-L	nd	Si(OH) ₄	1.9E-05	
	[L]	1.280	Q ¹ -Q ³	0.661	(HO)Si(=L) ₂ ⁻	0.043			
	[NaOH]	1.518	(HO) ₃ Si-L	nd	Si(=L) ₃ ²⁻	0.338			
	pH of resulting solution		13.3	(HO)Si(=L) ₂ ⁻	0.021	total bound ligand			
				Si(=L) ₃ ²⁻	0.113	0.380			
					free ligand				
					0.882				
bv.10.17	[SiO ₂]	0.875	Q ⁰	0.255	(HO) ₃ Si-L	nd	Si(OH) ₄	8.5E-06	
	[L]	1.177	Q ¹ -Q ³	0.463	(HO)Si(=L) ₂ ⁻	0.025			
	[NaOH]	2.073	(HO) ₃ Si-L	nd	Si(=L) ₃ ²⁻	0.436			
	pH of resulting solution		13.6	(HO)Si(=L) ₂ ⁻	0.012	total bound ligand			
				Si(=L) ₃ ²⁻	0.145	0.461			
					free ligand				
					0.697				
bv.10.75	[SiO ₂]	1.030	Q ⁰	0.363	(HO) ₃ Si-L	nd	Si(OH) ₄	2.0E-05	
	[L]	1.717	Q ¹ -Q ³	0.280	(HO)Si(=L) ₂ ⁻	0.108			
	[NaOH]	1.742	(HO) ₃ Si-L	nd	Si(=L) ₃ ²⁻	0.996			
	pH of resulting solution		13.5	(HO)Si(=L) ₂ ⁻	0.054	total bound ligand			
				Si(=L) ₃ ²⁻	0.332	1.104			
					free ligand				
					0.547				
bv.10.85	[SiO ₂]	0.504	Q ⁰	0.055	(HO) ₃ Si-L	nd	Si(OH) ₄	4.9E-05	
	[L]	0.754	Q ¹ -Q ³	0.420	(HO)Si(=L) ₂ ⁻	0.034			
	[KOH]	0.505	(HO) ₃ Si-L	nd	Si(=L) ₃ ²⁻	0.030			
	pH of resulting solution		12.7	(HO)Si(=L) ₂ ⁻	0.017	total bound ligand			
				Si(=L) ₃ ²⁻	0.010	0.066			
					free ligand				
					0.687				
bv.10.87	[SiO ₂]	0.466	Q ⁰	0.127	(HO) ₃ Si-L	nd	Si(OH) ₄	1.2E-06	
	[L]	0.696	Q ¹ -Q ³	0.314	(HO)Si(=L) ₂ ⁻	0.0116			
	[KOH]	1.007	(HO) ₃ Si-L	nd	Si(=L) ₃ ²⁻	0.0572			
	pH of resulting solution		13.9	(HO)Si(=L) ₂ ⁻	0.006	total bound ligand			
				Si(=L) ₃ ²⁻	0.019	0.069			
					free ligand				
					0.626				

L = iditol

T = 5 °C

Solution number	Initial solution composition (mol/kg)		Concentration of Si in the each species (determined through integration of ^{29}Si NMR spectrum, mol/kg)		Concentration of L in silicate complexes (mol/kg)		Calculated concentration of fully protonated oxoacid (mol/kg)	
bv.09.250	[SiO ₂]	0.885	Q ⁰	0.068	(HO) ₃ Si-L	nd	Si(OH) ₄	1.6E-04
	[L]	0.436	Q ¹ -Q ³	0.728	(HO)Si(=L) ₂ ⁻	0.028		
	[NaOH]	0.886	(HO) ₃ Si-L	nd	Si(≡L) ₂ ²⁻	0.151		
	pH of resulting solution 13.2		(HO)Si(=L) ₂ ⁻	0.014	total bound ligand			
			Si(≡L) ₂ ²⁻	0.075	0.179			
					free ligand			
				0.253				
bv.09.259	[SiO ₂]	0.849	Q ⁰	0.164	(HO) ₃ Si-L	nd	Si(OH) ₄	2.8E-05
	[L]	0.418	Q ¹ -Q ³	0.600	(HO)Si(=L) ₂ ⁻	0.025		
	[NaOH]	1.254	(HO) ₃ Si-L	nd	Si(≡L) ₂ ²⁻	0.145		
	pH of resulting solution 13.7		(HO)Si(=L) ₂ ⁻	0.012	total bound ligand			
			Si(≡L) ₂ ²⁻	0.072	0.169			
					free ligand			
				0.245				
bv.10.19	[SiO ₂]	0.790	Q ⁰	0.273	(HO) ₃ Si-L	nd	Si(OH) ₄	2.0E-05
	[L]	0.389	Q ¹ -Q ³	0.397	(HO)Si(=L) ₂ ⁻	0.006		
	[NaOH]	1.844	(HO) ₃ Si-L	nd	Si(≡L) ₂ ²⁻	0.235		
	pH of resulting solution 13.7		(HO)Si(=L) ₂ ⁻	0.003	total bound ligand			
			Si(≡L) ₂ ²⁻	0.118	0.241			
					free ligand			
				0.144				
bv.10.31	[SiO ₂]	0.716	Q ⁰	0.128	(HO) ₃ Si-L	nd	Si(OH) ₄	1.5E-04
	[L]	0.353	Q ¹ -Q ³	0.494	(HO)Si(=L) ₂ ⁻	0.028		
	[NaOH]	1.140	(HO) ₃ Si-L	nd	Si(≡L) ₂ ²⁻	0.162		
	pH of resulting solution 13.2		(HO)Si(=L) ₂ ⁻	0.014	total bound ligand			
			Si(≡L) ₂ ²⁻	0.081	0.190			
					free ligand			
				0.159				

L = allitol

T = 5 °C

Solution number	Initial solution composition (mol/kg)	Concentration of Si in each species (determined through integration of ^{29}Si NMR spectrum, mol/kg)	Concentration of L in silicate complexes (mol/kg)	Calculated concentration of fully protonated oxoacid (mol/kg)
bv.11.266	[SiO ₂] 1.002	Q ⁰ 0.069	(HO) ₃ Si-L nd	Si(OH) ₄ 1.7E-06
	[L] 0.247	Q ¹ -Q ³ 0.932	(HO)Si(=L) ₂ ⁻ 0.002	
	[KOH] 1.003	(HO) ₃ Si-L nd	Si(=L) ₃ ²⁻ nd	
	pH of resulting solution 13.7	(HO)Si(=L) ₂ ⁻ 0.001	total bound ligand 0.002	
		Si(=L) ₃ ²⁻ nd	free ligand 0.245	
bv.10.381	[SiO ₂] 0.563	Q ⁰ 0.056	(HO) ₃ Si-L nd	Si(OH) ₄ 2.1E-06
	[L] 0.235	Q ¹ -Q ³ 0.505	(HO)Si(=L) ₂ ⁻ 0.002	
	[KOH] 0.563	(HO) ₃ Si-L nd	Si(=L) ₃ ²⁻ nd	
	pH of resulting solution 13.6	(HO)Si(=L) ₂ ⁻ 0.001	total bound ligand 0.002	
		Si(=L) ₃ ²⁻ nd	free ligand 0.232	

Appendix IX. Composition of solutions used in determining the formation constants of the stannate-ligand complexes

A. Solutions used for the determination of the formation constants for stannate-furanoidic *cis*-diol complexes at 5 °C

L= *cis*-1,2-cyclopentanediol

T = 5 °C

Solution number	Initial solution composition (mol/kg)	Concentration of Sn in the each species (determined through integration of ^{119}Sn NMR spectrum, mol/kg)	Concentration of L in stannate complexes (mol/kg)
bv.11.580	[Sn]	0.225	$\text{Sn}(\text{OH})_6^{2-}$ 0.003
	[L]	0.680	$(\text{HO})_4\text{Sn}-(\text{OH})_2-\text{Sn}(\text{OH})_4^{2-}$ nd
	[TMAOH]	2.09	$(\text{HO})_4\text{Sn}=\text{L}^{2-}$ 0.034
	[HCl]	0.892	$(\text{HO})_2\text{Sn}=(\text{L})_2^{2-}$ 0.160
			$\text{Sn}=(\text{L})_3^{2-}$ 0.021
			$(\text{L})_2\text{Sn}-(\text{L})_2-\text{Sn}=(\text{L})_2^{4-}$ 0.007
			$(\text{HO})_4\text{Sn}=\text{L}^{2-}$ 0.034
			$(\text{HO})_2\text{Sn}=(\text{L})_2^{2-}$ 0.320
			$\text{Sn}=(\text{L})_3^{2-}$ 0.062
			$(\text{L})_2\text{Sn}-(\text{L})_2-\text{Sn}=(\text{L})_2^{4-}$ 0.022
			total bound ligand 0.438
			free ligand 0.231

L= 1,4-anhydroerythritol

T = 5 °C

Solution number	Initial solution composition (mol/kg)	Concentration of Sn in the each species (determined through integration of ^{119}Sn NMR spectrum, mol/kg)	Concentration of L in stannate complexes (mol/kg)
bv.11.572	[Sn]	0.409	$\text{Sn}(\text{OH})_6^{2-}$ 0.132
	[L]	0.404	$(\text{HO})_4\text{Sn}-(\text{OH})_2-\text{Sn}(\text{OH})_4^{2-}$ 0.003
	[TMAOH]	3.80	$(\text{HO})_4\text{Sn}=\text{L}^{2-}$ 0.167
	[HCl]	1.62	$(\text{HO})_2\text{Sn}=(\text{L})_2^{2-}$ 0.100
			$\text{Sn}=(\text{L})_3^{2-}$ 0.003
			$(\text{L})_2\text{Sn}-(\text{L})_2-\text{Sn}=(\text{L})_2^{4-}$ 0.003
			$(\text{HO})_4\text{Sn}=\text{L}^{2-}$ 0.167
			$(\text{HO})_2\text{Sn}=(\text{L})_2^{2-}$ 0.201
			$\text{Sn}=(\text{L})_3^{2-}$ 0.010
			$(\text{L})_2\text{Sn}-(\text{L})_2-\text{Sn}=(\text{L})_2^{4-}$ 0.008
			total bound ligand 0.387
			free ligand 0.012

L= D-fructose

T = 5 °C

Solution number	Initial solution composition (mol/kg)		Concentration of Sn in the each species (determined through integration of ^{119}Sn NMR spectrum, mol/kg)		Concentration of L in stannate complexes (mol/kg)					
bv.12.335	[Sn]	0.213	$\text{Sn}(\text{OH})_6^{2-}$	0.004	$(\text{HO})_4\text{Sn}=\text{L}^{2-}$	0.048				
	[L]	0.609	$(\text{HO})_4\text{Sn}-(\text{OH})_2-\text{Sn}(\text{OH})_4^{2-}$	nd	$(\text{HO})_2\text{Sn}(\text{=L})_2^{2-}$	0.252				
	[TMAOH]	3.01	$(\text{HO})_4\text{Sn}=\text{L}^{2-}$	0.048	$\text{Sn}(\text{=L})_3^{2-}$	0.106				
	[HCl]	0.801	$(\text{HO})_2\text{Sn}(\text{=L})_2^{2-}$	0.126	$(\text{L})_2\text{Sn}-(\text{L})_2-\text{Sn}(\text{=L})_2^{4-}$	nd				
			$\text{Sn}(\text{=L})_3^{2-}$	0.035	<table border="1"> <tr> <td>total bound ligand</td> <td>0.406</td> </tr> <tr> <td>free ligand</td> <td>0.195</td> </tr> </table>		total bound ligand	0.406	free ligand	0.195
	total bound ligand	0.406								
free ligand	0.195									
		$(\text{L})_2\text{Sn}-(\text{L})_2-\text{Sn}(\text{=L})_2^{4-}$	nd							

L= cytidine

T = 5 °C

Solution number	Initial solution composition (mol/kg)		Concentration of Sn in the each species (determined through integration of ^{119}Sn NMR spectrum, mol/kg)		Concentration of L in stannate complexes (mol/kg)					
bv.12.323	[Sn]	0.220	$\text{Sn}(\text{OH})_6^{2-}$	0.004	$(\text{HO})_4\text{Sn}=\text{L}^{2-}$	0.033				
	[L]	0.431	$(\text{HO})_4\text{Sn}-(\text{OH})_2-\text{Sn}(\text{OH})_4^{2-}$	nd	$(\text{HO})_2\text{Sn}(\text{=L})_2^{2-}$	0.349				
	[TMAOH]	3.11	$(\text{HO})_4\text{Sn}=\text{L}^{2-}$	0.033	$\text{Sn}(\text{=L})_3^{2-}$	0.027				
	[HCl]	0.828	$(\text{HO})_2\text{Sn}(\text{=L})_2^{2-}$	0.174	$(\text{L})_2\text{Sn}-(\text{L})_2-\text{Sn}(\text{=L})_2^{4-}$	nd				
			$\text{Sn}(\text{=L})_3^{2-}$	0.009	<table border="1"> <tr> <td>total bound ligand</td> <td>0.409</td> </tr> <tr> <td>free ligand</td> <td>0.016</td> </tr> </table>		total bound ligand	0.409	free ligand	0.016
	total bound ligand	0.409								
free ligand	0.016									
		$(\text{L})_2\text{Sn}-(\text{L})_2-\text{Sn}(\text{=L})_2^{4-}$	nd							

B. Solutions used for the determination of the formation constants for stannate-polyol complexes at 5 °C

L= threitol

T = 5 °C

Solution number	Initial solution composition (mol/kg)		Concentration of Sn in the each species (determined through integration of ^{119}Sn NMR spectrum, mol/kg)		Concentration of L in stannate complexes (mol/kg)	
bv.11.617	[Sn]	0.213	$\text{Sn}(\text{OH})_6^{2-}$	0.0003	$(\text{HO})_4\text{Sn}=\text{L}^{2-}$	0.015
	[L]	0.787	$(\text{HO})_4\text{Sn}-(\text{OH})_2-\text{Sn}(\text{OH})_4^{2-}$	nd	$(\text{HO})_2\text{Sn}(=\text{L})_2^{2-}$	0.200
	[TMAOH]	2.66	$(\text{HO})_4\text{Sn}=\text{L}^{2-}$	0.015	$\text{Sn}(=\text{L})_3^{2-}$	0.291
	[HCl]	0.799	$(\text{HO})_2\text{Sn}(=\text{L})_2^{2-}$	0.100	$(\text{L})_2\text{Sn}-(\text{L})_2-\text{Sn}(=\text{L})_2^{4-}$	nd
			$\text{Sn}(=\text{L})_3^{2-}$	0.097	total bound ligand	
			$(\text{L})_2\text{Sn}-(\text{L})_2-\text{Sn}(=\text{L})_2^{4-}$	nd	0.506	
					free ligand	
					0.267	

L= erythritol

T = 5 °C

Solution number	Initial solution composition (mol/kg)		Concentration of Sn in the each species (determined through integration of ^{119}Sn NMR spectrum, mol/kg)		Concentration of L in stannate complexes (mol/kg)	
bv.11.616	[Sn]	0.213	$\text{Sn}(\text{OH})_6^{2-}$	0.001	$(\text{HO})_4\text{Sn}=\text{L}^{2-}$	0.040
	[L]	0.787	$(\text{HO})_4\text{Sn}-(\text{OH})_2-\text{Sn}(\text{OH})_4^{2-}$	nd	$(\text{HO})_2\text{Sn}(=\text{L})_2^{2-}$	0.227
	[TMAOH]	2.79	$(\text{HO})_4\text{Sn}=\text{L}^{2-}$	0.040	$\text{Sn}(=\text{L})_3^{2-}$	0.206
	[HCl]	0.840	$(\text{HO})_2\text{Sn}(=\text{L})_2^{2-}$	0.114	$(\text{L})_2\text{Sn}-(\text{L})_2-\text{Sn}(=\text{L})_2^{4-}$	nd
			$\text{Sn}(=\text{L})_3^{2-}$	0.069	total bound ligand	
			$(\text{L})_2\text{Sn}-(\text{L})_2-\text{Sn}(=\text{L})_2^{4-}$	nd	0.473	
					free ligand	
					0.302	

L= xylitol

T = 5 °C

Solution number	Initial solution composition (mol/kg)		Concentration of Sn in the each species (determined through integration of ^{119}Sn NMR spectrum, mol/kg)		Concentration of L in stannate complexes (mol/kg)	
bv.11.309	[Sn]	0.208	$\text{Sn}(\text{OH})_6^{2-}$	0.001	$(\text{HO})_4\text{Sn}=\text{L}^{2-}$	0.045
	[L]	0.556	$(\text{HO})_4\text{Sn}-(\text{OH})_2-\text{Sn}(\text{OH})_4^{2-}$	nd	$(\text{HO})_2\text{Sn}(=\text{L})_2^{2-}$	0.300
	[TMAOH]	2.94	$(\text{HO})_4\text{Sn}=\text{L}^{2-}$	0.045	$\text{Sn}(=\text{L})_3^{2-}$	0.036
	[HCl]	0.784	$(\text{HO})_2\text{Sn}(=\text{L})_2^{2-}$	0.150	$(\text{L})_2\text{Sn}-(\text{L})_2-\text{Sn}(=\text{L})_2^{4-}$	nd
			$\text{Sn}(=\text{L})_3^{2-}$	0.012		
			$(\text{L})_2\text{Sn}-(\text{L})_2-\text{Sn}(=\text{L})_2^{4-}$	nd		
					total bound ligand	
					0.381	
					free ligand	
					0.167	

L= adonitol

T = 5 °C

Solution number	Initial solution composition (mol/kg)		Concentration of Sn in the each species (determined through integration of ^{119}Sn NMR spectrum, mol/kg)		Concentration of L in stannate complexes (mol/kg)	
bv.11.310	[Sn]	0.179	$\text{Sn}(\text{OH})_6^{2-}$	0.002	$(\text{HO})_4\text{Sn}=\text{L}^{2-}$	0.037
	[L]	0.583	$(\text{HO})_4\text{Sn}-(\text{OH})_2-\text{Sn}(\text{OH})_4^{2-}$	nd	$(\text{HO})_2\text{Sn}(=\text{L})_2^{2-}$	0.187
	[TMAOH]	2.54	$(\text{HO})_4\text{Sn}=\text{L}^{2-}$	0.037	$\text{Sn}(=\text{L})_3^{2-}$	0.138
	[HCl]	0.674	$(\text{HO})_2\text{Sn}(=\text{L})_2^{2-}$	0.094	$(\text{L})_2\text{Sn}-(\text{L})_2-\text{Sn}(=\text{L})_2^{4-}$	nd
			$\text{Sn}(=\text{L})_3^{2-}$	0.046		
			$(\text{L})_2\text{Sn}-(\text{L})_2-\text{Sn}(=\text{L})_2^{4-}$	nd		
					total bound ligand	
					0.362	
					free ligand	
					0.213	

L= mannitol

T = 5 °C

Solution number	Initial solution composition (mol/kg)		Concentration of Sn in the each species (determined through integration of ^{119}Sn NMR spectrum, mol/kg)		Concentration of L in stannate complexes (mol/kg)	
bv.11.269	[Sn]	0.214	$\text{Sn}(\text{OH})_6^{2-}$	0.001	$(\text{HO})_4\text{Sn}=\text{L}^{2-}$	0.038
	[L]	0.597	$(\text{HO})_4\text{Sn}-(\text{OH})_2-\text{Sn}(\text{OH})_4^{2-}$	nd	$(\text{HO})_2\text{Sn}(=\text{L})_2^{2-}$	0.269
	[TMAOH]	3.02	$(\text{HO})_4\text{Sn}=\text{L}^{2-}$	0.038	$\text{Sn}(=\text{L})_3^{2-}$	0.121
	[HCl]	0.804	$(\text{HO})_2\text{Sn}(=\text{L})_2^{2-}$	0.134	$(\text{L})_2\text{Sn}-(\text{L})_2-\text{Sn}(=\text{L})_2^{4-}$	nd
			$\text{Sn}(=\text{L})_3^{2-}$	0.040		
			$(\text{L})_2\text{Sn}-(\text{L})_2-\text{Sn}(=\text{L})_2^{4-}$	nd		
					total bound ligand	
					0.428	
					free ligand	
					0.161	